

Aus dem Institut für Landnutzung
der Agrar- und Umweltwissenschaftlichen Fakultät

**WATER QUALITY MONITORING OF THE KETTLE HOLES BY
MEANS OF HYPERSPECTRAL REMOTE SENSING IN
MECKLENBURG-VORPOMMERN STATE, GERMANY**

Dissertation

zur

Erlangung des akademischen Grades

Doktor der Ingenieurwissenschaften (Dr.-Ing.)

an der Agrar- und Umweltwissenschaftlichen Fakultät

der Universität Rostock

vorgelegt von

Dipl. Ing. Rahmatulla M. Igamberdiev, geb. am 01.03.1978 in Osh, Kirgisien

wohnhaft in Rostock

Rostock, den 09.02.2010

urn:nbn:de:gbv:28-diss2010-0121-7

Gutachter:

Prof. Dr. Bernd Lennartz (Universität Rostock)

Prof. Dr. Jiaguo Qi (Michigan State University, East Lansing, MI, USA)

Prof. Dr. Ralf Bill (Universität Rostock)

Frau Dr. Carolin Wloczyk (Deutsches Zentrum Luft- und Raumfahrt – DLR, Neustrelitz)

Verteidigt am: 25. Juli 2010

Table of Contents

Table of Contents	iii
List of Figures	v
List of Tables	ix
List of frequently used abbreviations	x
Summary	xi
Zusammenfassung	xiv
Acknowledgement	xvii
1 Introduction	1
1.1 Motivation	1
1.2 Water quality and eutrophication	2
1.3 The concept of remote sensing	4
1.4 Remote Sensing and Water Quality	4
1.5 Hyperspectral remote sensing.....	5
1.5.1 Spectral data characteristics.....	6
1.5.2 Hyperspectral data volume	7
1.6 Research objectives	8
2 Literature review	9
2.1 Spectral response of water bodies	9
2.2 Spectral characteristics of chlorophyll	12
2.3 Spectral characteristics of suspended sediments	16
2.4 Water depth estimation using a remote sensing signal.....	19
2.5 Spectral range selection methods	21
2.5.1 Most sensitive spectral ranges	21
2.5.2 Spectral derivative analysis	22
2.5.2 Spectral Band Ratio method.....	23
2.5.3 Multivariate statistical methods.....	25
3 Experimental design	27
3.1 Study area	27
3.1.1 Geology and physiography	27
3.1.2 Land use and climate	28
3.1.3 Selection of kettle holes.....	29
3.1.4 Kettle holes' hydro-morphological characteristics.....	30
3.2 Remote sensing data acquisition	30
3.2.1 Hand-held analytical spectral device (ASD)	31
3.2.2 Reflective optics system imaging spectrometer (ROSIS)	32
3.2.3 Hyperspectral Mapper (HyMap)	33
3.2.4 Pre-processing of the airborne data	35
3.3 Laboratory analytical methods for water quality parameters	36
3.3.1 Water samples collection.....	36
3.3.2 Chlorophyll.....	37
3.3.3 Total suspended sediments	37
3.3.4 Water samples absorption at 750nm.....	38
3.4 Methods for analysis of hand-held spectral data	38

3.4.1 Data pre-processing	38
3.4.2 Field spectra air-water correction	41
3.4.3 Reflectance filtering techniques	45
3.4.4 Spectral algebra	49
3.4.5 Spectral derivative analysis	51
3.5 Methods for analysis of airborne images.....	53
3.5.1 De-noising of image spectra	53
3.5.2 Retrieval of water bodies from the airborne data	54
3.5.3 Derivative analysis of image spectra	56
4 Results and discussions	58
4.1 Analysis of handheld spectra.....	58
4.1.1 Spectral signatures of kettle holes	58
4.1.2 Seasonal and cross-seasonal spectral response.....	61
4.1.3 Spectral algebra algorithms and biomass concentrations.....	64
4.1.4 Application of spectral algebra algorithms for biomass estimation	65
4.1.5 Analysis of biomass estimation algorithms accuracy.....	87
4.2 Analysis of airborne spectra	90
4.2.1 Analysis of field and airborne spectra	90
4.2.2 Remote sensing data classification approach	92
4.2.3 Chlorophyll content mapping	94
4.2.4 Suspended sediment concentration mapping.....	100
4.2.5 Water depth mapping.....	106
4.3 Optimal spectral ranges	112
5 Conclusions and future research.....	114
5.1 Water quality assessment based on handheld spectra	114
5.2 Water quality assessment based on airborne spectra.....	116
5.3 Future research	119
5.3.1 Water quality parameters mapping as a part of land use/ land cover maps.....	119
5.3.2 Investigation of subsurface spectral properties of kettle holes.....	120
6 References	123
Appendix A.....	133
Kettle holes description	133
Appendix B.....	137
Pigment concentrations data from 2007 and 2008 field campaigns.....	137
Appendix C.....	140
MATLAB routine for reflectance de-noising and graphical visualization.....	140
Appendix D.....	141
Data from a nearby weather station (Greifswald) during sampling	141
Appendix E.....	142
MATLAB routine and subroutine for processing of the hyperspectral imagery to the first derivative dataset	142
Appendix F.....	143
Volume reflectance calculated from field spectra collected on overcast weather.....	143
Selbständigkeitserklärung	144
Curriculum Vitae.....	145
Theses.....	146

List of Figures

Figure 1-1: Hyperspectral “cube” of image data such as that recorded by an imaging spectrometer	7
Figure 2-1: Generalized reflectance spectra for vegetation, soil, and water	10
Figure 2-2: A schematic diagram of the various processes that contribute to the water-leaving radiance as measured by a remote sensor in optically shallow waters	11
Figure 2-3: Absorption and scattering of light in pure water	12
Figure 2-4: Percent reflectance of clear and algae-laden water based on <i>in situ</i> spectrometer measurements	13
Figure 2-5: Spectra reflectance of Frisian waters, measured <i>in situ</i> in August 1995, with Landsat TM bands 1-4 superimposed.....	14
Figure 2-6: Modelled reflectance spectra for chlorophyll concentrations of 1, 10, 50, 100 and 250µg/L, respectively	15
Figure 2-7: Remote sensing reflectance spectra of the water bodies studied in Dall’Olmo and Gitelson (2005)	15
Figure 2-8 Percent reflectance of algae-laden water with various concentrations of suspended sediment ranging from 0 – 500mg/L	17
Figure 2-9: a) <i>In situ</i> spectral reflectance measurements of clear water and clear water with various levels of clayey soil suspended sediment concentrations from 0 – 1,000mg/l. b) <i>In situ</i> spectral reflectance measurements of clear water and clear water with various levels of silty soil suspended sediment concentrations	18
Figure 2-10: Conceptual model for de-correlating colour band data from depth.....	19
Figure 2-11: Reflectance spectra of water at depths ranging from 0.02 to 15 m	20
Figure 3-1: Relief map from SRTM (SRTM 2009) data overlaid with water bodies shape-file of Mecklenburg– Vorpommern (LUNG-MV 2009).	28
Figure 3-2: True colour composite ROSIS image (15 May 2008) of test area (close to the village Schmarsow, Demmin suburbs - FRG) with kettle holes numeration.	29
Figure 3-4: Central wavelengths of ROSIS and HyMap sensors in comparison with eutrophic water spectrum of K4 taken on 15 May 2008	35
Figure 3-5: Spectral analytical procedure for field and airborne spectral data in the form of flow diagrams	39
Figure 3-6: De-noised spectral signatures of kettle holes influenced by different biophysical dominants	40

Figure 3-7: Schematic diagram of radiative transfer influenced by surface, phytoplankton, gelbstoff, suspended matter, and water molecules, as well as different bottom types that contribute to the signal as measured by a remote sensor in shallow water	41
Figure 3-8: Spectra from K6.....	44
Figure 3-9: Comparison between remote sensing reflectance R_{rs} and subsurface volume reflectance $R(0-)$ from two kettle holes.	45
Figure 3-10: De-noised spectra taken from kettle hole K4 at 29.07.2008.....	47
Figure 3-11: Noise removal filters comparison over volumetric reflectance as observed for K4 taken on 24.10.2007.....	48
Figure 3-12: Semi-empirical algorithms for spectral signatures analysis	50
Figure 3-13: Spectral signatures of investigated kettle holes from ROSIS image on 15 May 2008	54
Figure 3-14: An image mask of water bodies created on band 23 of HyMap using ‘Raster\Fill’ and AOI tools of ERDAS Imagine Viewer.....	55
Figure 3-15: Original reflectance (a) and calculated first derivative (b) spectra on ROSIS image from kettle hole K6.....	57
Figure 4-1: Kettle holes’ volume reflectance collected in 2007 and 2008.....	61
Figure 4-2: First derivative spectra of kettle hole K1 calculated from volume reflectance for 2007 and 2008 datasets	66
Figure 4-3: Pearson’s correlation coefficients (R) for kettle hole K1 between volume reflectance, derivative spectra and biomass concentrations for seasonal (2007 and 2008) and cross-seasonal data (CHL and TCHL for 2007-08).....	67
Figure 4-4: Received correlations between various algorithms and biomass concentration for kettle hole K1	69
Figure 4-5: First derivative spectra of kettle hole K2 in the 2007 season.....	70
Figure 4-6: Pearson’s correlation coefficients (R) between volume reflectance, derivative spectra and CHL, TCHL concentration in the 2007 season for kettle hole K2.	71
Figure 4-7: Received correlations between various algorithms and biomass concentration for kettle hole K2.....	72
Figure 4-8: First derivative spectra of kettle hole K4 calculated from volume reflectance for 2007 and 2008 datasets	73
Figure 4-9: Pearson’s correlation coefficients (R) for kettle hole K4 between volume reflectance, derivative spectra and biomass concentrations for seasonal (2007 and 2008) and cross-seasonal data (CHL and TCHL for 2007-08).....	74

Figure 4-10: Received correlations between various algorithms and biomass concentration for kettle hole K4.....	76
Figure 4-11: First derivative spectra of kettle hole K5 calculated from volume reflectance for 2007 and 2008 datasets	76
Figure 4-12: Pearson's correlation coefficients (R) for kettle hole K5 between volume reflectance, derivative spectra and biomass concentrations for seasonal (2007 and 2008) and cross-seasonal data (CHL and TCHL for 2007-08).....	77
Figure 4-13: Received correlations between various algorithms and biomass concentrations for kettle hole K5. Note the scale, axes and algorithms differences.	79
Figure 4-14: First derivative spectra of kettle hole K6 calculated from volume reflectance for 2007 and 2008 datasets	80
Figure 4-15: Pearson's correlation coefficients (R) for kettle hole K6 between volume reflectance, derivative spectra and biomass concentrations for seasonal (2007 and 2008) and cross-seasonal data (CHL and TCHL for 2007-08).....	81
Figure 4-17: Received correlations between various algorithms and biomass concentration for kettle hole K6.....	83
Figure 4-18: Pearson's correlation coefficients (R) for kettle hole K7 between volume reflectance, derivative spectra and biomass concentrations for seasonal (2007 and 2008) and cross-seasonal data (CHL and TCHL for 2007-08).....	85
Figure 4-19: Received correlations between various algorithms and biomass concentration for kettle hole K7.....	86
Figure 4-20: Average spectral signatures of kettle holes: handheld field (a), (c), ROSIS (b) and HyMap (d) spectra taken on 15 May 2008 and 29 July 2008 respectively. X-axes of (a) and (c) are fitted for (b) and (d) accordingly	92
Figure 4-21: Observed CHL (bars) and TSS (lines) concentrations of the studied 5 kettle holes on the flight dates	93
Figure 4-22: Continuum-removed average reflectance of kettle holes for ROSIS (a) and HyMap (b) datasets.....	96
Figure 4-23: Chlorophyll spatial variations retrieved from ROSIS (a) and HyMap (b) data with enlargement of kettle holes.....	98
Figure 4-24: Pearson's correlation coefficients (R) between average normalized reflectance, derivative spectra and TSS concentrations from all kettle holes for ROSIS (a) and HyMap datasets	101

Figure 4-25: Received linear regression correlations between TSS concentrations from investigated kettle holes and derivative reflection values at 596nm and 630nm wavelengths from ROSIS and HyMap datasets accordingly	102
Figure 4-26: Suspended sediment concentrations spatial variations retrieved from ROSIS (a) and HyMap (b) data with enlargement of kettle holes	104
Figure 4-27: Observed water depth values of the 5 studied kettle holes on the flight dates	106
Figure 4-28: Pearson's correlation coefficients (R) between average normalized reflectance, derivative spectra and depth from all kettle holes for ROSIS (a) and HyMap datasets	107
Figure 4-29: Received linear regression correlations water depth from investigated kettle holes and derivative reflection values at 530nm wavelength from ROSIS and HyMap datasets	108
Figure 4-30: Water depth spatial variations retrieved from ROSIS (a) and HyMap (b) data with enlargement of kettle holes.....	110

List of Tables

Table 2-1: Summary of wavebands from the literature review	22
Table 3-1: Kettle holes' hydro-morphological characteristics	30
Table 3-2: ROSIS sensor's specifications	33
Table 3-3: HyMap sensor's specifications	34
Table 4-1: Coefficients of determination from linear regression using various methods between normalized volume reflectance and biomass concentration for kettle hole K1	68
Table 4-2: Linear regression coefficients using various methods between normalized volume reflectance and biomass concentration for kettle hole K1 in the season of 2007...	72
Table 4-3: Coefficients of determination from linear regression using various methods between normalized volume reflectance and biomass concentration for kettle hole K4	75
Table 4-4: Coefficients of determination from linear and logarithmic regression using various methods between normalized volume reflectance and biomass concentration for kettle hole K5	78
Table 4-5: Coefficients of determination from linear regression using various methods between normalized volume reflectance and biomass concentration for kettle hole K6 (without data from overcast days)	83
Table 4-6: Coefficients of determination from linear regression using various methods between normalized volume reflectance and biomass concentration for kettle hole K7	86
Table 4-7: Accuracy assessment of the best cross-seasonal algorithms for each kettle hole	88
Table 4-8: Accuracy assessment of CHL mapping from the ROSIS dataset	99
Table 4-9: Accuracy assessment of CHL mapping from the HyMap dataset	99
Table 4-10: Accuracy assessment of TSS mapping from ROSIS dataset	105
Table 4-11: Accuracy assessment of TSS mapping from HyMap dataset	105
Table 4-12: Accuracy assessment of water depth mapping from ROSIS dataset	111
Table 4-13: Accuracy assessment of water depth mapping from HyMap dataset	111
Table 4-14: Identified optimal spectral wavebands for water quality parameters	113

List of frequently used abbreviations

CHL	Chlorophyll- <i>a</i>
TCHL	Total chlorophyll
TSS	Total suspended sediment
ASD	Analytical Spectral Devices
ROSIS	Reflective Optics System Imaging Spectrometer
HyMap	Hyperspectral Mapper
FOV	Field Of View
NIR	Near Infra-Red (range of electromagnetic spectrum)
VIS	Visual (range of electromagnetic spectrum)
DLR	Deutsches Zentrum für Luft- und Raumfahrt e. V. (German Aerospace Centre)
WQ	Water Quality
HRS	Hyperspectral Remote Sensing
DWT	Discrete Wavelet Transformation
DN	Digital Number
ENVI	Environment for Visualizing Images software

Summary

The acquisition of inland water quality (WQ) data is an important but tedious task due to the pronounced spatial and temporal variability of most in-water constituents, especially small shallow water bodies. Small inland waters such as kettle holes are subject to pollution, drainage, and structural alteration by intensive land use practices. Hyperspectral Remote Sensing (HRS) provides data in the contiguous narrow bands which may assist in WQ monitoring campaigns.

This research aims to make a first attempt at presenting the ability of hyperspectral remote sensing (two-years field spectrometry data, HyMap and ROSIS sensors imagery) for kettle holes' water quality parameters (chlorophyll, depth, total suspended sediments) mapping in agricultural young moraine landscapes in North-Eastern Germany. The objectives of this study are to: (1) determine the status of the water quality (trophic state) of several kettle holes (spatial heterogeneity and temporal dynamics); (2) evaluate and assess the applicability of HRS techniques to the water quality of kettle holes (integration of ground truth and RS data, validation of suitable RS approaches, and identification of the optimal spectral bands (ranges) that are most sensitive to water quality indicators for various kettle holes).

The test area is located close to the city of Demmin, about 150 km north of the city of Berlin, and covers approximately 10 km². The first survey (May, 2007) showed that all kettle holes are within agricultural fields and have different shapes, sizes, water table depths, water regimes and trophic states. After the elimination of all kettle holes that were permanently dried or covered by duckweed, the primary monitoring programme included 6 sampling stations. Field data were collected from 6 kettle holes in the period between June and October 2007 (a total of 7 datasets, 5 of which were with spectral data). In summer 2008, kettle hole K2 dried out and it was also excluded from further monitoring. In 2008, ground truth data were collected in 10 field campaigns from 5 kettle holes in the period between May and September 2008.

A multi-temporal database was built including data of the ROSIS (Reflective Optics System Imaging Spectrometer, German Aerospace Centre - DLR) and HyMap ('Hyperspectral Mapper' - HyVista, Australia) airborne hyperspectral sensors. The collected ROSIS image spectra, having a range from 389 to 845nm and an interval of 4nm

in 115 bands, were recorded with full ground coverage at an altitude of about 3500m resulting in a spatial resolution of 2×2 m. HyMap is a whisk-broom scanner with 126 bands between 450 and 2500nm and it provided data sets from an altitude of about 2000m with a 4×4m pixel size and about 15nm bandwidth. Only the first 34 bands between 450 and 920nm relevant for the determination of water constituents were used in this study.

Analysis of handheld spectra revealed that the spectral signatures of the studied ponds are kettle holes' type specific and depend on the agricultural activity and respective nutrient status in a catchment area. The data processing showed that for field spectra, the sequential application of Savitzky-Golay Filter and Discrete Wavelet Transformation produces the best de-noising performance. The study of spectral algebra algorithms showed that in spite of the high variety of hydro-morphological, physical and bio-ecological factors influencing upwelling radiance from the water body, the application of the derivative analysis approach produces good and stable correlations ($R^2=0.60\div0.82$) with chlorophyll concentrations for all types of kettle hole. At the same time, linear regression between chlorophyll and the *Peak Magnitude* algorithm gave a consistent correlation for kettle holes with high algae content. At low algae content, *Peak Magnitude above a Baseline* algorithms gave the best results. The methods based on the reflectance values at specific wavelengths are the most applicable for algae-dominated ponds.

Analysis of hyperspectral airborne ROSIS and HyMap datasets presented an approach to estimate spatial and temporal variation of kettle holes' water quality parameters, such as chlorophyll content, depth (transparency) and total suspended sediments. Field spectra from the height of 30-35cm (i.e. an area of 0.01÷0.015m²) were collected. The investigated field and airborne spectra for almost all kettle holes did not correspond with each other due to differences in the ground sampling distance. Airborne pixels of ROSIS and HyMap imagery had an area of 4m² and 16m² accordingly and their spectra were highly influenced by algae or the bottom properties of kettle holes. The study of airborne spectra revealed that the chlorophyll absorption near 677nm was the same for both datasets. In order to enhance absorption properties, both airborne hyperspectral datasets were normalized by the continuum removal approach. Linear regression algorithms for ROSIS and HyMap datasets were derived using normalized average chlorophyll absorption spectra for each kettle hole. The overall accuracy of biomass mapping for ROSIS data was 71%, and for HyMap it was 64%.

For estimation of depth and total suspended sediments (TSS), the derivative analysis approach was applied to the airborne image datasets. Derivative airborne spectra showed that the best correlation for TSS was at 596nm and at 630nm with overall classification accuracy of 83% and 76% for ROSIS and HyMap datasets accordingly. Correlation between depth and derivative reflectance at 530nm of ROSIS and HyMap hyperspectral imagery revealed high linear regressions coefficients with a classification accuracy of 87% and 80% respectively. Overall, the ROSIS sensor dataset with 2×2m spatial and 4nm spectral resolutions was preferable for small water bodies' biomass concentration mapping compared to the HyMap sensor dataset (4×4m spatial and 13÷15nm spectral resolutions).

The results of this study show that HRS can provide useful information for WQ monitoring in agricultural young moraine landscapes in North-Eastern Germany. The analysis of the remote sensing data showed that the correlation between the spectral signals and the chlorophyll concentration is stable over one season as long as the 'type of kettle hole' does not change. However, the biomass mapping results showed that, depending on the type of kettle hole, the 'packaging effect' and bottom reflection can lead to miscalculation of chlorophyll content.

Zusammenfassung

Die Gewinnung von Daten zur Wasserqualität der Binnengewässer (WQ-Daten) ist eine wichtige, aber durch die ausgeprägte räumliche und zeitliche Variabilität der meisten Wasserinhaltsstoffe langwierige Aufgabe. Dies trifft insbesondere für kleine und flache Gewässer zu. Kleine Binnengewässer wie Sölle unterliegen Verschmutzung, Entwässerung sowie strukturellen Veränderungen durch eine intensive Landnutzung. Die hyperspektrale Fernerkundung (HRS) kann Wasserqualitäts-Monitoringprogramme unterstützen und vereinfachen.

In der vorliegenden Arbeit wird die Eignung der HRS für das Monitoring von Wasserqualitätsparametern von Söllen (Chlorophyll, Tiefe, gelöste Stoffe) in einer intensiv landwirtschaftlich genutzten Jungmoränenlandschaft Nordostdeutschlands anhand von zweijährigen feldspektrometrischen Daten sowie Bilddaten von HyMap- und ROSIS-Sensoren untersucht. Diese Arbeit hat zum Ziel (1) die Wasserqualität (Trophiestatus) mehrerer Sölle zu erfassen (räumliche Variabilität und zeitliche Dynamik); (2) die HRS-Technik im Hinblick auf ihre Anwendbarkeit im Wasserqualitäts-Monitoring von Söllen zu bewerten. Dazu werden Felddaten und HRS-Daten verglichen, geeignete HRS-Ansätze validiert und die spektralen Kanäle identifiziert, die für Wasserqualitätsparameter verschiedener Sölle höchste Empfindlichkeit zeigen.

Das Untersuchungsgebiet befindet sich in der Nähe von Demmin, ca. 150 km nördlich von Berlin und umfasst ca. 10 km².

Die erste Aufnahme im Mai 2007 zeigte, dass alle Sölle in Ackerflächen liegen und sich in Größe, Form, Wassertiefe, Wasserregime und Trophiestatus unterscheiden. Das erste Monitoringprogramm umfasste 6 Probenahmestellen an 6 Söllen, trockene und mit *Lemna minor* bedeckte Sölle wurden nicht berücksichtigt. Felddaten wurden an den 6 Probenahmestellen im Zeitraum von Juni bis Oktober 2007 erfasst (7 Datensätze). An 5 Zeitpunkten erfolgte eine gleichzeitige Erfassung von HRS-Daten. Im Jahr 2008 wurden im Zeitraum von Mai bis September an 10 Zeitpunkten Felddatensätze für jeweils 5 Sölle erfasst. Ein Soll fiel trocken und wurde im weiteren Monitoring nicht mehr berücksichtigt.

Eine multitemporale Datenbasis wurde erstellt, sie enthält Daten der ROSIS- (Reflective Optics System Imaging Spectrometer, Deutsches Zentrum für Luft- und Raumfahrt e. V.)

und HyMap-Sensoren (Hyperspectral Mapper, HyVista, Australien). Der ROSIS-Sensor, der im Wellenlängenbereich von 389 bis 845 nm arbeitet und Bildspektren mit einem Intervall von 4 nm in 115 Kanälen aufzeichnet, wurde in einer Höhe von ungefähr 3500 m geflogen. Die räumliche Auflösung ergibt sich zu 2×2 m. HyMap ist ein Whiskbroom Scanner mit 126 Kanälen zwischen 450 und 2500 nm, er lieferte Datensätze aus einer Höhe von ca. 2000 m mit einer Bodenauflösung von 4×4 m. Die 126 Spektralbänder hatten eine Breite von jeweils 15 nm. Nur die ersten 34 Kanäle zwischen 450 und 920 nm, die für die Bestimmung von Wasserinhaltsstoffen relevant sind, wurden in dieser Arbeit verwendet.

Die Analyse von Feldspektren zeigte, dass die spektralen Signale der untersuchten Wasserkörper spezifisch für die jeweiligen Sölle sind und von der landwirtschaftlichen Aktivität und dem Nährstoffstatus im jeweiligen Einzugsgebiet abhängen. Die Datenanalyse und -verarbeitung zeigte, dass für Feldspektren eine Kombination des Savitzky-Golay-Filters und der Discrete Wavelet Transformation die besten de-noising-Ergebnisse liefert. Die Untersuchung spektraler Algebra-Algorithmen zeigte, dass trotz der großen Anzahl hydro-morphologischer, physikalischer und bioökologischer Faktoren, die die Strahlung der Wasserkörper beeinflussen, der Differentialquotient gute und stabile Korrelationen mit den Chlorophyllkonzentrationen ($R^2 = 0.60 - 0.82$) aller Sölle zeigte. Gleichzeitig ergibt die lineare Regression zwischen Chlorophyllkonzentration und *Peak Magnitude* Algorithmus für Sölle mit hohem Algenwachstum eine konsistente Korrelation. Für Sölle mit geringem Algenwachstum ergaben *Peak Magnitude above a Baseline* Algorithmen die besten Ergebnisse. Zusammengefasst kann man sagen, dass Methoden, die auf dem Reflexionswert spezifischer Wellenlängen basieren, für durch Algen dominierte Sölle am besten geeignet sind.

Mit der Analyse der hyperspektralen ROSIS- und HyMap-Datensätze wird ein Ansatz vorgestellt, die räumliche und zeitliche Variation der Wasserqualitätsparameter von Söllen (Chlorophyllgehalt, Tiefe (Transparenz) und gelöste Stoffe) abzuschätzen. Feldspektren wurden aus einer Höhe von 30-35 cm (d.h. eine Fläche von $0.01 - 0.015 \text{ m}^2$) aufgenommen. Aufgrund von Unterschieden in der Aufnahmehöhe stimmen Feldspektren und Spektren der ROSIS- und HyMap-Sensoren fast aller Sölle nicht vollständig überein. Pixel der ROSIS- und HyMap-Bilder haben eine Fläche von 4 m^2 bzw. 16 m^2 und ihre Spektren sind stark beeinflusst durch Algenwuchs oder Eigenschaften des Untergrunds der Sölle. Die Untersuchung der ROSIS- und HyMap-Spektren zeigte, dass die

Chlorophyllabsorption nahe 677 nm in beiden Datensätzen gleich hoch ist. Um die Absorptionseigenschaften zu verbessern, wurden beide hyperspektrale Spektren mit dem ‘continuum removal’-Ansatz normalisiert. Mit den normalisierten durchschnittlichen Chlorophyllabsorptionsspektren wurden lineare Regressionsgleichungen für ROSIS- und HyMap-Datensätze abgeleitet. Die Gesamtgenauigkeit der Biomasseerfassung liegt bei 71% für die ROSIS-Daten sowie 64% für die HyMap-Daten.

Um Tiefe und Gehalt an suspendierten Stoffen (TSS) abzuschätzen, wurde der Differentialquotient für die ROSIS- und HyMap-Datensätze berechnet. Dabei wurden für TSS bei 596 nm und 630 nm mit einer Gesamtgenauigkeit von 83% bzw. 76% (für ROSIS- bzw. HyMap Datensätze) die besten Korrelationen erreicht. Die lineare Korrelation zwischen Tiefe und der Ableitung der Reflektanzen bei 530 nm der ROSIS- und HyMap-Daten ergibt hohe Bestimmtheitsmaße mit einer Klassifikationsgenauigkeit von 87% und 80%. Insgesamt zeigt sich der ROSIS-Datensatz mit einer räumlichen Auflösung von 2×2 m und einer spektralen Auflösung von 4 nm als geeigneter für das Monitoring der Biomassekonzentration in kleinen Wasserkörpern als der HyMap-Datensatz.

Die Ergebnisse dieser Arbeit zeigen, dass HRS dem Wasserqualitätsmonitoring in der landwirtschaftlich geprägten Jungmoränenlandschaft Nordostdeutschlands nützliche Information liefern kann. Korrelationen zwischen spektralen Signalen und der Chlorophyllkonzentration im Soll bleiben stabil, solange sich der „Solltyp“ nicht ändert. Jedoch zeigen die Ergebnisse auch, dass, abhängig vom “Solltyp”, der Packaging-Effekt des Chlorophylls und Reflexionen vom Untergrund der Sölle zu Fehlern in der Berechnung des Chlorophyllgehalts führen können.

Acknowledgement

The completion of this work came with the assistance from many people whom mentioning each one may not be exhaustive. However, I wish to express my sincere appreciation and gratitude to all the people who contributed towards this work in one way or another. I would like to pay special thanks and appreciation to Allah, the Almighty, who have made it possible to get DAAD scholarship, to come to Germany and complete this work.

I express my sincere gratitude to supervisor Prof. Dr. Dr. Bernd Lennartz for accepting me as a PhD student. He has been always a constant, buoyant source of encouragement and inspiration.

I would like to acknowledge Prof. Dr. Ralf Bill and Dr. Görres Grenzdörffer for their support and advices throughout the study.

I thank also Prof. Dr. Hendrik Schubert for his friendly assistance and permission to work in his laboratory. He brought the main part for biological perspective to this research.

I deeply thank many members of the Institute of Land Use, especially of the working group Soil Physics and Resource Management: Tilo Hartwig, for his support and advices during field trips; Marianne Kietzmann and Helga Weiland, for helping in analyzing of the field samples; Johanna Meincke, for her complete assistance in administrative and logistic issues; Petra Kahle, for clarifying and explaining the basics of Soil Science; Sigrid and Max Kohne, for sharing the office, encouragement during my first year; Johanna Frings for her help during writing this work.

I wish also to express my deep appreciation to DLR (German Aerospace Centre), German Remote Sensing Data Center (DFD), Oberpfaffenhofen, especially to Martin Bachmann and Stefanie Holzwarth for providing the aerial datasets.

My thanks will not be complete without mentioning Jens Kruse, Bärbel Tiemeyer, Manon Janssen and Esayas Alemayehu – you are the great people.

I would like to thank the German Academic Exchange Office (DAAD) for their financial support. My gratitude extends to the Faculty for Agricultural and Environmental Sciences, University of Rostock for the wonderful academic facility.

Finally, my heart is full of thanks and respects to my wife and my children who supported and constantly encouragement me very much during my studies. I also want to thank our neighbour Frau Bachmann for being an “Oma” for my children. I express my deep love and affection to my father, mother and brothers for their love and moral support during my study period.

1 Introduction

1.1 Motivation

Kettle hole (or kettle) – A depression formed when a block of ice from a receding glacier becomes isolated and buried in glacial debris (till). As the block melts the till collapses to form a hollow, which may become filled with water to form a kettle lake or pond (Allaby 2006).

Typically, kettle holes are defined as small digressional lentic waters or wetlands (<1 ha) often glacially shaped within the depressions of catchments. The term “kettle holes” is preferably used in Europe (Kalettka and Rudat 2006; Watznauer 1989), whereas “potholes” is a synonym in Northern America (Mitsch and Gosselink 2007). The term “ponds” is used in a general sense to include non-moraine landscapes. Kettle holes are by nature closed flow systems lacking an integrated drainage network. They are characterized by a high variability of hydro-morphological site conditions, especially of the hydroperiod. Most of the kettle holes undergo severe wet–dry cycles. Especially on arable land, many of them tend towards high water marshy outflows. Therefore, kettle holes have a high potential for both geomorphic structural diversity and biological species diversity (Kalettka and Rudat 2006).

In North-Eastern Germany more than 150,000 kettle holes can be found mostly within arable land and forest (Kalettka *et al.* 2005). They are characterized by a wet-dry cycle, and therefore provide a high potential for structural and species diversity. However, kettle holes are subject to pollution, drainage, and structural alteration by intensive land use practices. The agricultural activity embraces artificial drainage measures which strongly alter the sites’ hydrology including the hydroperiod of the kettle holes. Fertilization and soil tillage additionally impact the kettle holes’ ecology. According to the fertilization scenario and climate conditions, nutrients - potentially enhancing algae growth in water bodies - may reach the kettle holes by surface runoff and groundwater flow. The temporal development of the chlorophyll content of kettle holes somehow reflects the land use patterns and fertilization practice within the respective catchment. Furthermore, shores of kettle holes are a source for enhanced greenhouse gas emissions due to eutrophication (Merbach *et al.* 2002).

In Germany kettle holes are protected by law, but there is still a need to develop effective conservation and management strategies (Kalettka *et al.* 2005). In particular, the fast yet efficient and precise determination of the water quality and the temporal development in kettle holes are required to assess the sustainability of agricultural and conservation measures.

Lakes together with kettle holes are valuable water resources. Tens of thousands of inland lakes have served as crucial resources for drinking water, irrigation, industry, transportation, recreation, fishing, support of biodiversity, and sheer aesthetic enjoyment (Scheffer 1998). A well-documented effect of human activities upon aquatic ecosystems is *eutrophication*, a process whereby water bodies, such as lakes, estuaries, ponds, kettle holes or slow-moving streams receive excess nutrients that stimulate excessive productivity, simplification of biotic communities, and a reduction in the ability of the metabolism of the organisms to adapt to the nutrient loading (Carlson and Simpson 1996). When eutrophication occurs, excessive inputs often exceed the capacity of the ecosystems to be balanced, thus the conditions lead to reduced stability of the ecosystem. In order to effectively maintain the quality of inland waters, it is necessary to monitor humans' utilization of these resources independently in terms of residential, industrial, and agricultural activities (Wetzel 1992). Although the fundamental laws of resource utilization may be recognized by most agencies and industries, they are not being seriously implemented.

Recent research in the Southern Baltic region demonstrated the tight relation between discharge generation and nutrient export (Tiemeyer *et al.* 2006; Tiemeyer *et al.* 2007). Prompted by climate change, raising temperature induces more winter precipitation and subsequently winter discharge which leaches more nutrients to surface water bodies including kettle holes (Kahle *et al.* 2009; Tiemeyer *et al.* 2009; Tiemeyer *et al.* 2008). Therefore, an effective water quality assessment and monitoring techniques are needed to maintain sustainable natural ecosystems, especially for such small water bodies as kettle holes.

1.2 Water quality and eutrophication

There is no single definition of water quality, as it depends on the respective processes and on the intended use of the water (Kneubuehler *et al.* 2005). In this thesis the water quality of kettle holes is defined through process of eutrophication. Trophic state is an important

water quality variable that describes the biological condition of a water body. Eutrophication has many negative effects on aquatic ecosystems. Perhaps the most obvious consequence is the increased growth of algae and aquatic weeds that interfere with the use of the water for fisheries, recreation, industry, agriculture, and drinking water. As the mass of algae in the water grows, the water may become murkier and less aesthetically pleasing. Particularly, when the algae die and decompose, periods of oxygen depletion (hypoxia and anoxia) occur more frequently (Carpenter *et al.* 1998). Even living algae create conditions favourable for some species over others and may cause shifts in the structure of phytoplankton, zooplankton, and bottom-dwelling (benthic) communities (Howarth 2008). Eutrophication brings on ecological changes that decrease the biological diversity – the variety of living organisms – in the ecosystem (Seehausen *et al.* 1997).

A variety of mathematical models have been developed and applied to rivers, lakes, and estuaries to monitor, simulate and control eutrophication (Dall'Olmo *et al.* 2003; Dekker *et al.* 1996; Kloiber *et al.* 2002; Koponen *et al.* 2002; Liu *et al.* 2003; Pozdnyakov *et al.* 1998; Shafique *et al.* 2001). Most water quality models demand comprehensive water quality sampling programmes. In an ideal circumstance, monitoring of water bodies includes the determination of concentrations of water quality variables and the processes that generate their spatial distribution and the temporal variation of those variables (Fisher 1994). However, the conventional measurement of water quality requires *in situ* sampling, and expensive and time-consuming laboratory work (Giardino *et al.* 2001). Therefore, it is usually based on the determination of concentrations at one or only a few fixed stations that are assumed to represent the overall distribution of phytoplankton in a lake, or the spatial interpolation of the concentration from the stations to obtain continuous field maps of the various water quality parameters (Kallio *et al.* 2003). Algal blooms are extremely patchy, both temporally and spatially. Consequently, they often remain unobserved using the traditional sampling methods based on temporally sparse sampling at fixed monitoring stations (Harma *et al.* 2001). Traditional *in situ* sampling methods also do not provide the spatial overview that is necessary for the regional assessment and monitoring of lake water quality (Shafique *et al.* 2001). On the other hand, optical indications of water quality have the potential to enhance the abilities of resource managers to monitor water bodies in a timely and cost-effective manner.

1.3 The concept of remote sensing

Remote sensing (RS) is defined as the acquisition of information about the properties of electromagnetic waves emitted, reflected or diffracted by the sensed objects without being in direct physical contact. Broad scope remote sensing based water quality research has been developed to detect environmental indicators that are useful in assessing, quantifying and monitoring inland water quality. More fundamentally, the absorption and scattering of light by components of the lacustrine water column provide basic information about the substances suspended in the water (Dekker 1993). Although a fairly new method, the development of spectral indices can be a useful and effective tool for the diagnosis of water conditions by water resource managers (Shafique *et al.* 2001).

1.4 Remote Sensing and Water Quality

Remote sensing has been increasingly used for determining and monitoring trophic status of inland water bodies, especially over the past 30 years (Cannizzaro and Carder 2006; Dekker 1993; Doxaran *et al.* 2002a; Duan *et al.* 2009; Giardino *et al.* 2007; Gitelson 1992; Svab *et al.* 2005). Several methodologies are successfully applied toward establishing relationships between the spectral response and water-quality parameters (i.e. inorganic sediment particles, chlorophyll content, coloured dissolved organic material and Secchi disk depth) in many studies (Dall'Olmo *et al.* 2005; Dekker 1993; Doxaran *et al.* 2003; Gitelson *et al.* 2008; Islam *et al.* 2007; Ma *et al.* 2008; Thiemann and Kaufmann 2002). Currently, existing methodologies for remote sensing of water quality parameters mainly include theoretical, empirical and semi-empirical or semi-analytical methods (Ma *et al.* 2006). These algorithms aim to develop linear or nonlinear regression function between water quality parameters and remote sensing data (Liu *et al.* 2003).

For example, estimation of chlorophyll-*a* (CHL) distribution in lakes by remote sensing techniques has included the use of airborne photography (Wrigley and Horne 1974), airborne spectrometry (Attila *et al.* 2008; Thiemann and Kaufmann 2002; Tsai and Philpot 2002; Turdukulov 2003) and satellite sensors (Brando and Dekker 2003; Dall'Olmo *et al.* 2005; Harma *et al.* 2001; Kallio *et al.* 2008; Thiemann and Kaufmann 2000). Results are usually reported in the form of concentration maps (Kallio *et al.* 2003).

Data acquisition by remote sensing is fast (e.g., tens of lakes may be acquired within a day by an airborne sensor or hundreds of lakes by a spaceborne sensor), and large areas can be

surveyed over a short period of time. However, the spectral and spatial configurations of current aquatic satellite sensors are not suitable for inland water quality monitoring. In most cases they are not suitable for phytoplankton monitoring in lakes due to their spectral configuration and poor spatial resolution (typically from *several* hundred metres to 1,000 metres). The low spatial resolution of most satellite data can produce sources of error in the empirical approaches used to assess water quality indicators. For example, a single *in situ* sample may not be representative of an entire pixel area. In most cases, a single pixel is greater than several metres in diameter, and it is rare for a single object or target feature to fill any one pixel. Thus, the characteristics of any pixel can rarely be considered truly homogenous (Lillesand *et al.* 2007). In addition, the accuracy of locating the pixel that corresponds to the *in situ* sample may be uncertain depending on the geo-location method used (Giardino *et al.* 2001).

Spaceborne sensors provide the global coverage of the Earth's surface conditions at different spatial and temporal resolutions, but the efficacy of all current spaceborne remote sensing systems for detailed characterization of water quality parameters is limited by their spatial and spectral resolutions. Sensors with high spatial resolution do not have a sufficient number of narrow spectral bands (e.g., IKONOS, QuickBird, Landsat, and ASTER), while narrowband spaceborne sensors usually have coarse spatial resolution (e.g., MODIS). Satellite sensor systems such as Landsat TM and ETM+, and ASTER currently provide data of sufficient spatial resolution for inland lake applications. However, their spectral resolution is questionable. It is important to recognize that these sensors average the spectral information over the entire width of the spectral band (Dekker 1993; Gitelson *et al.* 1993). Airborne sensors are generally designed to serve as a prototype for future spaceborne sensor systems (Liu *et al.* 2003).

1.5 Hyperspectral remote sensing

Hyperspectral sensors (0.4 μm – 2.5 μm wavelength range) capture the unique spectra (or 'spectral signature') of an object. These signatures can be used to identify and quantify the materials of which it is composed (Lillesand *et al.* 2007). With this principle, hyperspectral data enable the identification of the Earth's surface features with greater thematic accuracy. Airborne imaging spectrometers have been used to assess the trophic status of lakes and to map the spatial distribution of phytoplankton (Bukata *et al.* 1997). The analysis of hyperspectral imagery involves the decomposition of each reflectance pixel into

its biophysical constituents. The identity of these constituents is determined by comparison with ‘library’ spectra of known materials measured in the field or in the laboratory (Richards and Jia 2006).

The previous generations of spaceborne optical imagers are limited to either panchromatic or multispectral devices providing only a few spectral bands and limited resolving power. Numerous effective methods, mostly derived from multivariate statistics, have been developed and applied successfully for spatial or spectral analysis of these data (Tsai and Philpot 1998). Hyperspectral imagers typically collect data in tens to several hundred contiguous, narrow bands in the electromagnetic spectrum. The large numbers of bands that are simultaneously imaged produce vast quantities of information. With higher resolution, spectrally continuous data, researchers have tended to select a subset of suitable bands to optimize the existing algorithms for multispectral data analysis or to generate new algorithms based on traditional multispectral concepts (Dekker *et al.* 1995; Doxaran *et al.* 2002a; Gitelson *et al.* 1993; Penuelas *et al.* 1994).

The new generation of airborne imaging spectrometers, such as the ROSIS (Reflective Optics System Imaging Spectrometer, German Aerospace Centre - DLR) and HyMap (HyVista, Australia), offer considerable advances in terms of radiometric sensitivity and operational flexibility (Gege *et al.* 2008; Igamberdiev *et al.* In press; Turdukulov 2003). The main problems with hyperspectral data are the substantial redundancy of the information, the difficulties in identifying the optical bandwidth and centre wavelength of the bands that maximize the explanation of biophysical attributes, and the system limitations associated with the storage of the image data volumes.

1.5.1 Spectral data characteristics

Given the enormous number of wavebands recorded, the data produced by the imaging spectrometers are different from those of multispectral scanners – leading to the term *hyperspectral*. The data produced for a given geographical area can be viewed as a cube, as shown in Figure 1-1, having three dimensions that represent spatial location (two dimension) and spectral wavelength (the third dimension) (Richards and Jia 2006)

When displaying remotely sensed data on the display device, only three of the spectral bands are usually assigned to the red, green and blue colour elements of the device. Careful band selection ensures the most informative display. This is relatively simple for

multispectral data, such as the six 30 m bands from Landsat, but with hyperspectral data, selecting the three bands to display can be challenging. Choosing the most appropriate three channels to display is not straightforward and, in any case, would lead to substantial loss of the spectral benefits offered by these types of data. However, unless spectral transformations are employed, a set of three bands comparable to those used with multispectral imagery is often adopted (near IR, red, green) for simple display of the data (Richards and Jia 2006).

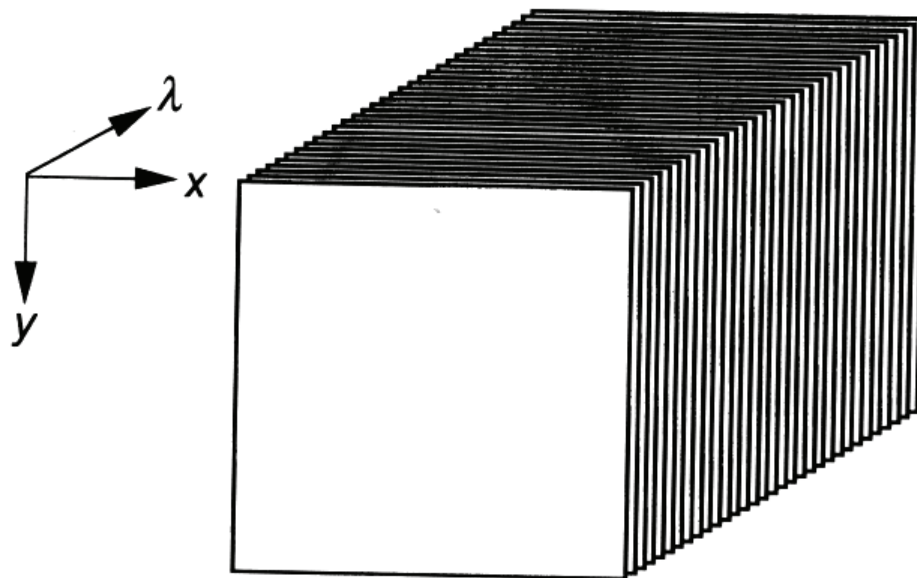


Figure 1-1: Hyperspectral “cube” of image data such as that recorded by an imaging spectrometer (after Richard and Jia, 2006)

1.5.2 Hyperspectral data volume

It is obvious that the major differences between multispectral and hyperspectral data (e.g., Landsat versus AVIRIS) are the number of wavebands (7 versus 224) and the radiometric quantization (8 versus 10 bits per pixel per band). Disregarding differences in spatial resolution, the relative data volume per pixel is 7×8 vs. 224×10 – i.e., 56: 2240 bits per pixel. For each pixel, there are 40 times as many bits for AVIRIS as for TM data. Consequently, storage and transmission of hyperspectral data are issues for consideration (Richards and Jia 2006).

At the same time, 40 times as much data per pixel does not imply that the same amount of information can be extracted about the ground cover types. Even though additional data often enhance the possibility of discovering that information, much of it does not add to the potential information content. Hyperspectral data often contain substantial overlap or

redundancy of information content among the bands of data recorded for a given pixel. Spectral redundancy means that the information content of one band can be fully or partly predicted from the other bands in the data (Richards and Jia 2006).

1.6 Research objectives

Many previous studies relied on the correlation of local *in situ* measurements of chlorophyll content, suspended sediments and depth with the remote sensing data. Recent findings have provided a new semi-analytical model for remote estimation of CHL in turbid waters – three-band and its special case two-band models – based on spectral algebra of two CHL absorption ranges, 658-674nm and 733-780nm, and its reflection peak in 700-735nm range. A new model was successfully applied to the Medium Resolution Imaging Spectrometer (MERIS) and Moderate Resolution Imaging Spectroradiometer (MODIS) datasets to estimate CHL in turbid waters (Gitelson *et al.* 2008). A relatively novel application of remote sensing is investigation of ecological processes on a small spatial scale. Analysis of ecological processes using hyperspectral and hyperspatial data showed that in order to understand large-scale distributions of assemblages, information about small-scale processes is required (Murphy *et al.* 2008). This research aims to make a first attempt to present the ability of hyperspectral remote sensing (two-years field spectrometry data, HyMap and ROSIS sensors imagery) for kettle holes' water quality parameters (chlorophyll, water depth, total suspended sediments) mapping in agricultural young moraine landscape in North-Eastern Germany.

The objectives of this study are to:

1. Determine the status of the water quality (trophic state) of several kettle holes:
 - a. Spatial heterogeneity;
 - b. Temporal dynamics;
2. Evaluate and assess RS techniques applicability to the water quality of kettle holes:
 - a. Ground truth and RS data integration;
 - b. Validate suitable RS approaches;
 - c. Identify the optimal spectral ranges that are most sensitive to water quality indicators for various kettle holes.

2 Literature review

The use of water colour remote sensing for determination of an optical water quality variable was initially developed for the oceans. The optical properties of ocean waters are in general only affected by phytoplankton and its breakdown products. These optically relatively simple waters are known as Case1 waters. All other types of waters, i.e. those whose optical properties are influenced by dissolved organic matter from a terrestrial origin, dead particulate matter, and particulate inorganic matter in addition to phytoplankton, were determined to be Case2 waters. If the bottom reflectance influences the water-leaving radiance signal, water is also considered to be Case2 (Dekker *et al.* 2001a).

Remote sensing techniques have been successfully applied for operational mapping of the biophysical properties of Case1 waters (Sathyendranath 2000). However, Case2 waters continue to represent a challenge to remote sensing techniques. Several remote sensing studies have estimated water quality parameters such as depth, chlorophyll-*a* (CHL), and total suspended sediments (TSS) (Liu *et al.* 2003). Various studies used multispectral remote sensing data to map the general water quality indicator for Secchi depth; however, multispectral data do not provide enough spectral resolution for the detection of algae or accurate assessment of CHL. Other researchers used hyperspectral data to predict suspended sediment concentration, CHL content and harmful blue-green algae in the ocean where concentrations of complicating optical factors (e.g., total suspended sediments and dissolved organic carbon) are very low. Various studies used different analytical techniques, such as principle component analysis (PCA), derivative spectroscopy, and regression techniques, to identify optimal narrow spectral wavebands and develop water quality models. The region-waveband indicators can be more sensitive to changes in biophysical variables and less affected by noise from the atmosphere or the sensor itself than the narrow-band indicators. The literature review presented in this chapter serves as a guideline to what has been done and what can be done to improve water quality assessment algorithms.

2.1 Spectral response of water bodies

Light and other forms of electromagnetic radiation are commonly described in terms of their wavelength. For example, visible light has wavelengths between 400 and 700 nm. A

reflectance spectrum shows the reflectance of a material measured across a range of wavelengths. Most natural earth surface materials have diagnostic absorption features in the 0.4 – 2.5 μm range of the reflected spectrum. The sensor measures reflected surface radiation, which then needs to be calibrated and corrected for atmospheric effects to derive reflectance. Reflectance is subsequently used for spectral signature analysis and comparison to spectral libraries of known substrates (e.g. an individual macrophyte species). An estimate of substrate is then calculated from the strength of the returned signal (Figure 2.1).

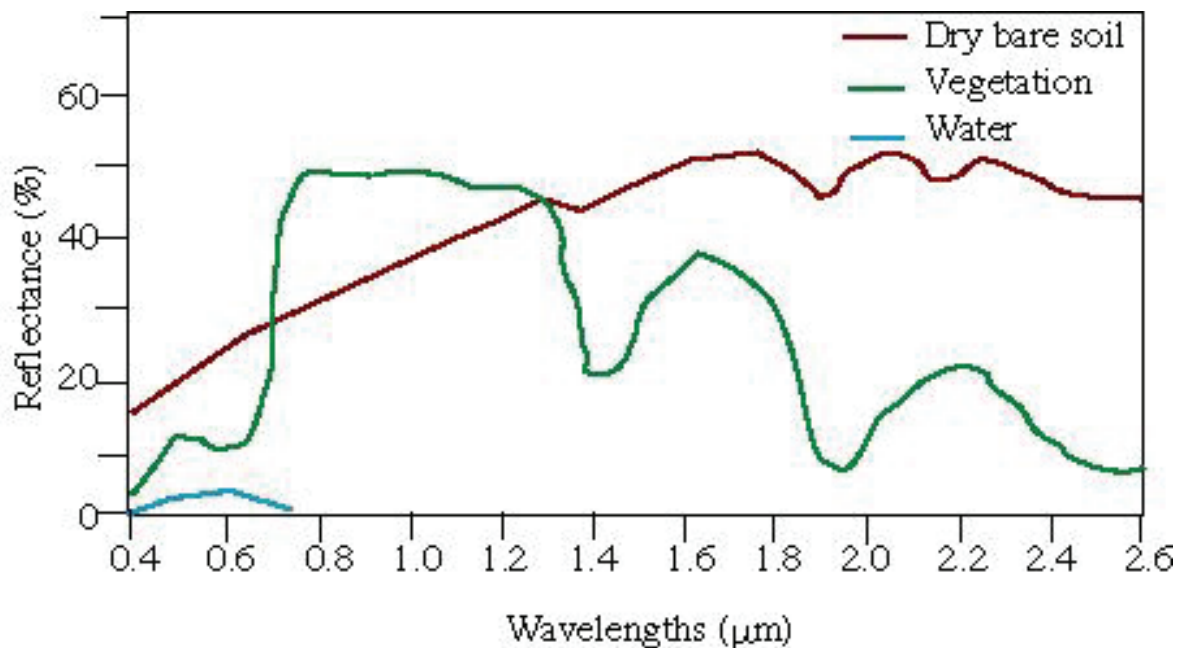


Figure 2-1: Generalized reflectance spectra for vegetation, soil, and water (adapted from Mather 2004)

Remote sensing of water quality is concerned with the behaviour of light in aquatic media. When light penetrates a water body, it will either be absorbed or scattered; these processes attenuate the irradiance and change its spectral composition. Thus, remote sensing techniques aim to quantify the light propagation process in the water environment. Optical properties of inland water bodies are complex features influenced by scattering and absorption processes as well as the water constituents: phytoplankton, suspended matter and yellow substance (see Figure 2-2) (Dekker *et al.* 2001b). When conducting remote sensing investigations on water bodies, it is useful to understand how pure water selectively absorbs and scatters incident solar radiation. Several important relationships

were observed when the absorption and scattering data were graphed, as shown in Figure 2-2 (Jensen 2006).

The blue wavelength region from approximately 400–500nm had the least amount of absorption and scattering of incident light in the water column, with the minimum absorption at 460–480 nm. The wavelengths of violet to light blue light penetrated further than any other range of light into the water column because they had the best transmission (Clark *et al.* 1997). The water column absorbed incoming irradiance in the green and yellow wavelengths from 520 – 580 nm very well with relatively little scattering taking place. Almost all of the incident red and infrared (580 – 3,000 nm) radiance entering deep pure water was absorbed with negligible scattering (Figure 2-3). Consequently, pure water appeared blue to our eyes due to the combined effect of molecular scattering of violet and blue light (< 520 nm) and significant absorption of green and red light (520 – 700 nm) in the same water column. Blue-coloured waters are typically found in pure mid-ocean water and deep non-turbid inland water bodies (Jensen 2006).

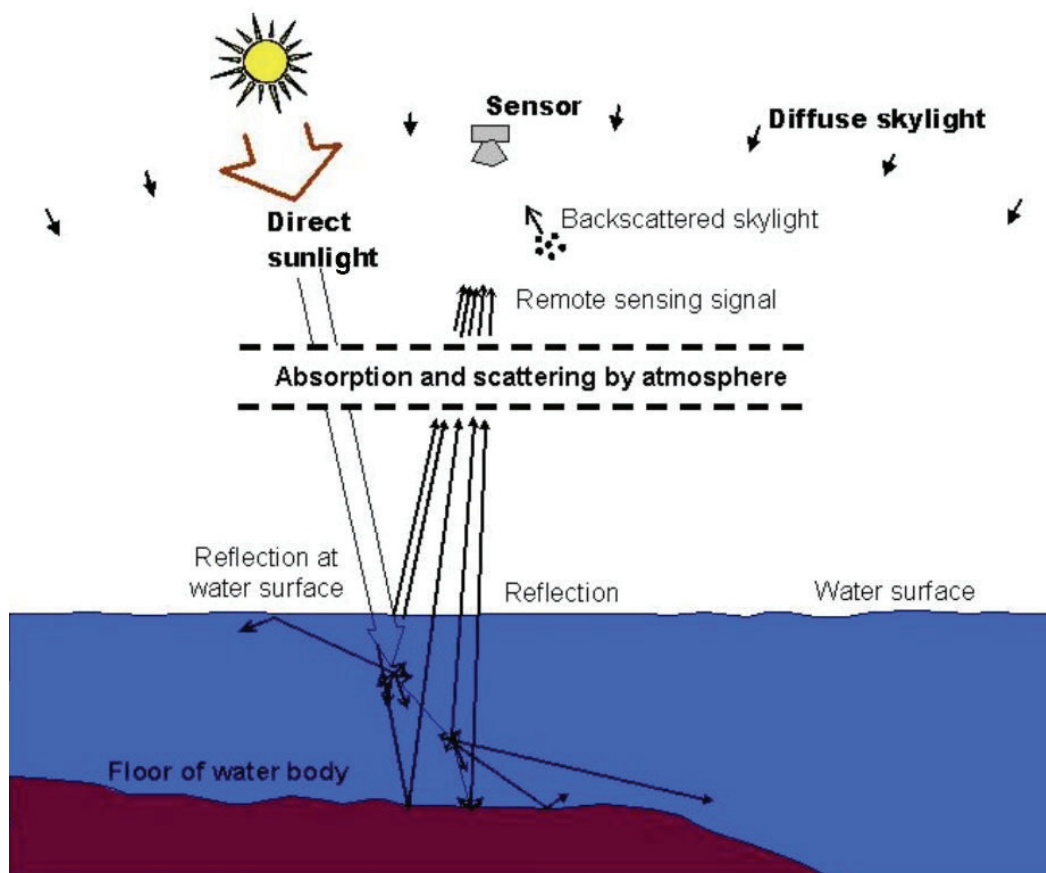


Figure 2-2: A schematic diagram of the various processes that contribute to the water-leaving radiance as measured by a remote sensor in optically shallow waters (after Dekker *et al.* 2001a)

In the natural environment, the spectrum shape characteristics of water from different lakes differed significantly depending on dissolved and suspended constituents within the water. The trophic state of the water strongly influences the spectral signatures (Thiemann and Kaufmann 2000).

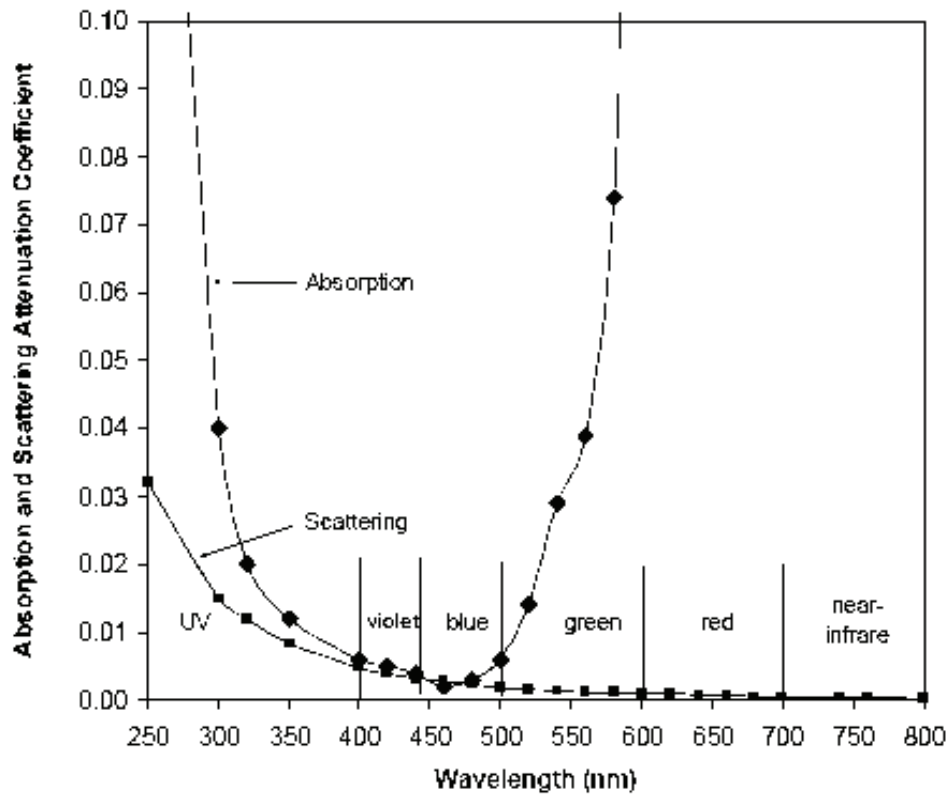


Figure 2-3: Absorption and scattering of light in pure water (after Jensen, 2006)

2.2 Spectral characteristics of chlorophyll

The spectral reflectance characteristics of pure water changed when chlorophyll-*a* was introduced. For example, Figure 2-4 depicted the spectral reflectance characteristics of clear water and the same water laden with algae consisting primarily of chlorophyll-*a* (Han 1997). Basically, as chlorophyll-*a* concentration increased in the water column, the amount of energy reflected in the blue and red wavelengths significantly decreased but increased in the green wavelength. Clear water reflected approximately 2 percent between 400 and 500 nm and dropped gradually to less than 1 percent at wavelengths beyond 710 nm (Jensen 2006). Conversely, the algae-laden water presents four pronounced scattering/absorption features of chlorophyll (Figure 2-4) (Gitelson 1992; Han 1997; Rundquist *et al.* 1996):

- 1) Strong chlorophyll-*a* absorption in the blue region between 400 and 500 nm;
- 2) Maximum reflectance in green wavelengths around 550 nm (green peak) caused by *relatively* lower absorption of green light by algae;
- 3) Strong chlorophyll-*a* absorption in red wavelengths at approximately 675 nm; and
- 4) Prominent reflectance peak between 690 – 700 nm caused by an interaction of algal-cell scattering and a combined effect of minimum pigment and water absorption. The height of this peak above the baseline (absorption trough) has been used to accurately measure the amount of chlorophyll.

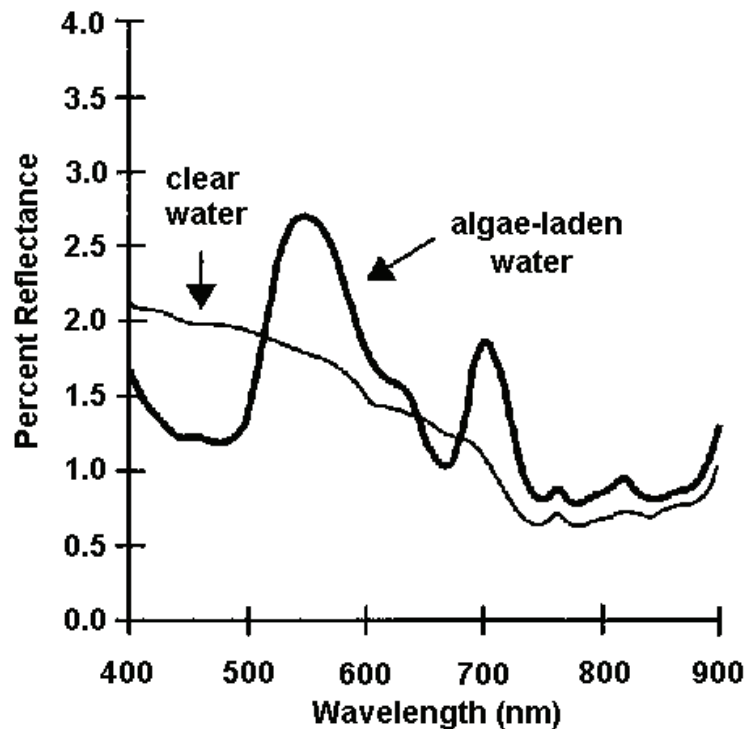


Figure 2-4: Percent reflectance of clear and algae-laden water based on *in situ* spectrometer measurements (after Han 1997)

Dekker *et al.* (2001c) illustrated the key spectral features in lake water signature curves. From their measured reflectance spectra in Figure 2-5, it was obvious that the absorption and scattering of the various constituents created a distinctive reflectance spectrum for each of the water samples. In general, there was little reflectance at shorter wavelengths of 400 – 500 nm, due to the combined effects of absorption by coloured dissolved organic matter (CDOM), inanimate particles (tripton), and phytoplankton pigments. A local maximum in reflectance, caused by a local minimum in the combined absorption effects of

CDOM and tripton absorption (which both exponentially decline with increasing wavelength) and low phytoplankton pigment absorption efficiency, was found at approximately 550 nm – 580 nm. The local minimum in reflectance at 630 nm is caused by the combined effects of cyanophycocyanin absorption and a first shoulder in the absorption of water was noticeable. As this local minimum became more pronounced, the relative contribution of cyanobacteria to the total algal components increased. The local reflectance peak at 650 nm is due to a local minimum in absorption by pigments and an increasingly smaller contribution from CDOM and tripton absorption. A narrow reflectance minimum is centred at 676 nm, which was the *in vivo* chlorophyll-*a* maximum absorption peak. Beyond 680 nm, reflectance increased significantly to a maximum of 14% at 706 nm. In the studied lake there was a vast amount of algae identifiable by the large reflectance at 706 nm, and the major algal pigment absorption at wavelengths from 400 – 680 nm (Figure 2-4).

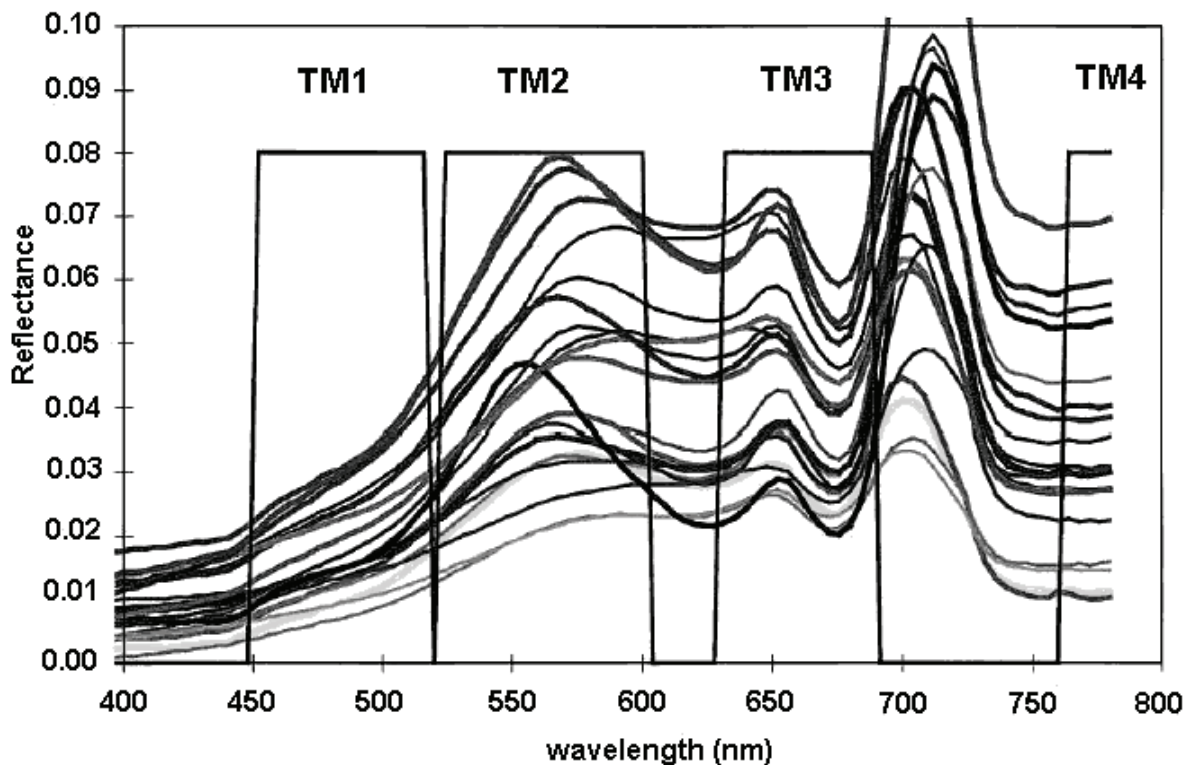


Figure 2-5: Spectra reflectance of Frisian waters, measured *in situ* in August 1995, with Landsat TM bands 1-4 superimposed (after Dekker et al. 2001b)

Over the full spectral range, the shape of the spectral signature for water was broadly determined by the spectral absorption of dissolved organic matter in the blue, and by the absorption of chlorophyll-*a* and water itself in the red and near-infrared (Figure 2-6). Rijkeboer *et al.* (1998) modelled subsurface reflectance $R(0^-)$ for chlorophyll using the averaged constant values for gilvin and tripton absorption and scattering, as obtained for

the shallow lakes (Kirk 1994). With increasing CHL concentration, the first peak decreased and the wavelength changed from 588 nm to 572 nm. Both the peak at about 640 nm and the far-red peak shifted towards longer wavelengths.

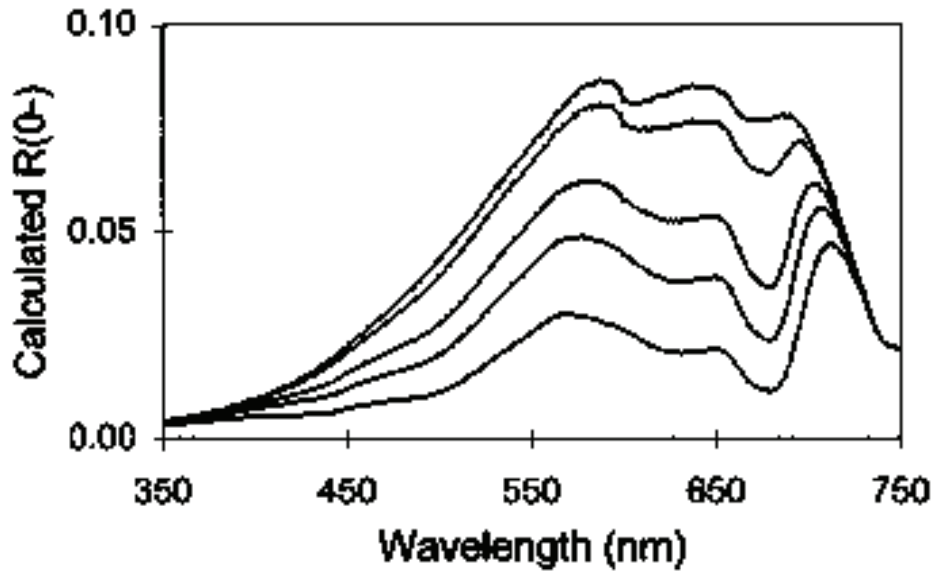


Figure 2-6: Modelled reflectance spectra for chlorophyll concentrations of 1, 10, 50, 100 and 250 µg/L, respectively (after Rijkeboer *et al.* 1998).

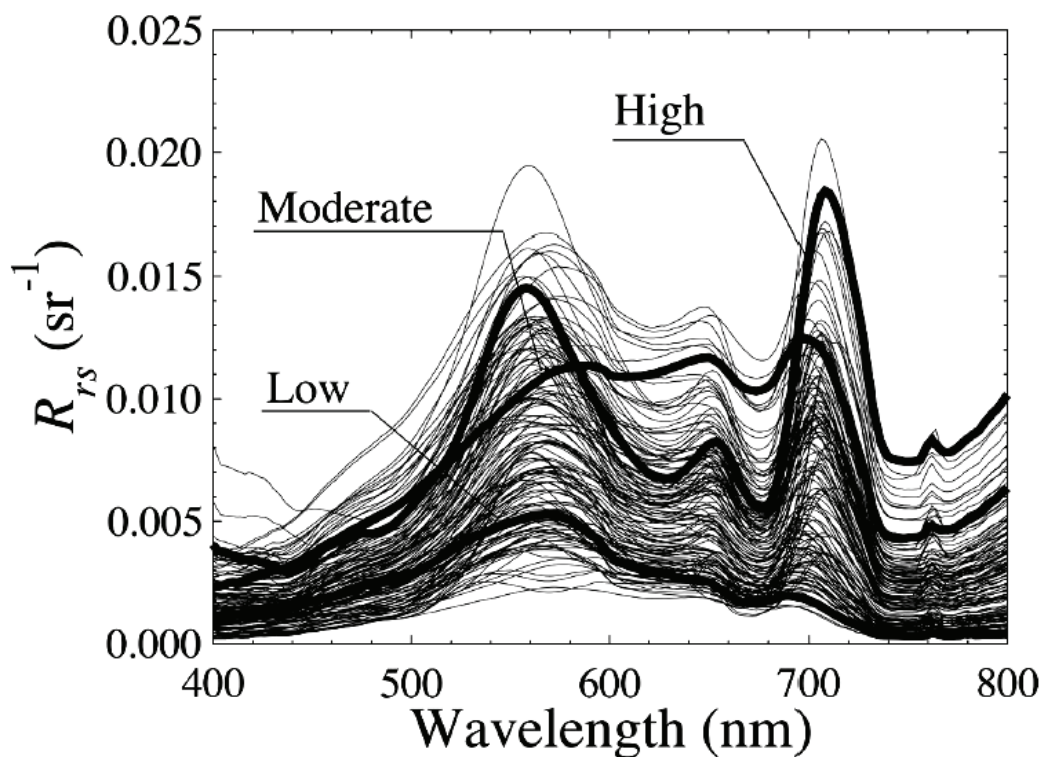


Figure 2-7: Remote sensing reflectance spectra of the water bodies studied in Dall’Olmo and Gitelson (2005). Some examples are highlighted: curve “Low” (Chl-a = 11 µg/L; TSS

= 5mg/L), curve “High” (Chl-a = 89µg/L; TSS = 21mg/L), and curve “Moderate” (Chl-a = 24µg/L; TSS = 55mg/L).

The far-red peak clearly evolved due to an increase in chlorophyll-*a*. This simple way of modelling the reflectance using the inherent optical properties is of paramount importance to analyze shapes of the spectra in dependence of concentrations of the major constituents of the water (Dekker *et al.* 1995). With continued increase in chlorophyll-*a* content, the reflectance peak of water shifted toward longer wavelengths (Figure 2-7; Gitelson, 1992). Thus, the indicator of the chlorophyll-*a* concentration of the water column was related to the shape of the reflectance curve in this region, and not simply the peak height (Dekker 1993).

2.3 Spectral characteristics of suspended sediments

The sediments came from a variety of sources, such as agricultural cropland erosion and urban surface runoff. The particles ranged from fine clay particles (3 – 4µm in diameter), to silt (5 – 40µm), to fine-grain sand (41 – 130µm), and coarse grain sand (131 – 250µm). Most of the suspended mineral sediments were concentrated in the inland and near-shore water bodies (Bukata *et al.* 1995). Thus, suspended mineral concentration was usually of no significance to deep ocean remote sensing studies. On the other hand, inland water bodies might carry a significant load of suspended sediments that could dramatically impact the spectral reflectance characteristics of the water bodies (Jensen 2006; Teodoro *et al.* 2007).

For several reasons, it was important to monitor the type, amount, and spatial distribution of suspended minerals in inland water bodies. First, sediment affected water quality and its suitability for drinking, recreation, and industrial purposes. Second, sediment served as a carrier and storage agent of pesticides, absorbed phosphorus, nitrogen, and organic compounds, and could be an indicator of pollution. Third, photosynthesis by phytoplankton and submerged aquatic vegetation could be significantly impacted as suspended sediments impede the transmission of solar radiation in the water column. These phytoplankton and aquatic vegetation played a vital role in the food chain of the aquatic ecosystem (Jensen 2006).

Fortunately, remote sensing had been used to monitor the suspended mineral concentrations in water bodies. The *in situ* measurements of suspended mineral concentrations were usually required to derive a quantitative relationship with the remote

sensor data. When collecting samples, the remote sensor data and the *in situ* suspended sediment measurements should be collected on days that have little wind because wind-roughened surface water creates specula reflections (Han and Rundquist 1998).

When both suspended mineral sediment and chlorophyll were present in the water body at the same time, a dramatically different spectral response was produced. For example, Figure 2-8 illustrates the spectral response of water as red loam sediment concentrations from 0 – 500mg/L were added to the water that contained algae. For algae-laden water, the green peak reflectance shifted from 547 nm at 0mg/L to 596 nm at 500mg/L (Han 1997).

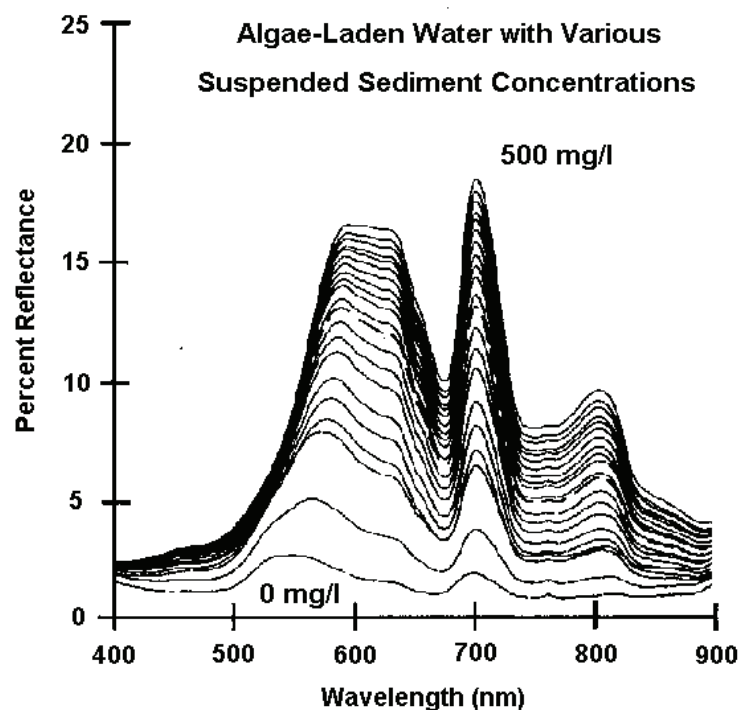


Figure 2-8 Percent reflectance of algae-laden water with various concentrations of suspended sediment ranging from 0 – 500mg/L (after Han, 1997)

Figure 2-9 depicts the spectral reflectance of clear water and water with varying suspended sediment concentrations of two different types of soil: clayey and silty. For deep clear water, spectral reflectance dropped continuously after approximately 580 nm due to increased absorption in the water column. Increases in suspended particulates (either inorganic or organic) were related to increases in overall brightness (Shafique *et al.* 2001). A water body with suspended sediment in it would generally appear brighter in imagery than a water body without any suspended sediment. The clayey soil (Figure 2-9b) had approximately 10 percent lower reflectance at all wavelengths than the light-coloured silty soil because it contained more organic matter and was darker in colour (Figure 2-9a). If the

suspended particulates were organic in nature, the reflectance data indicated a relative increase of about 705 nanometres (Shafique *et al.* 2001). Reflectance increased in the 580–690nm region and in the near-infrared region as more mineral sediments were added to the water bodies. Thus, the peak reflectance shifted toward longer wavelengths in the visible region as suspended sediments increased (Jensen 2006).

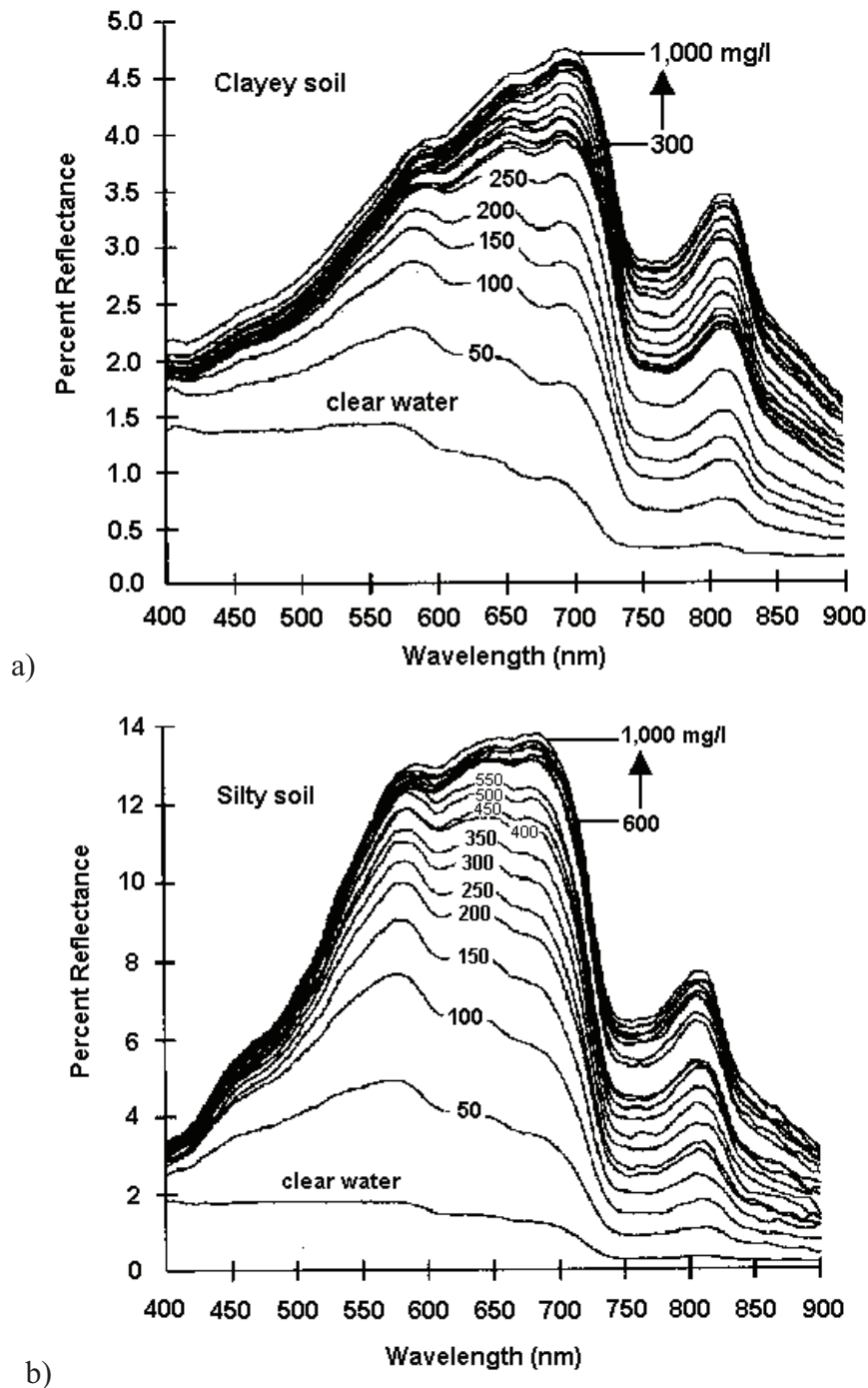


Figure 2-9: a) *In situ* spectral reflectance measurements of clear water and clear water with various levels of clayey soil suspended sediment concentrations from 0 – 1,000mg/l. b) *In situ* spectral reflectance measurements of clear water and clear water with various levels of silty soil suspended sediment concentrations (after Lodhi *et al.*, 1997)

These results suggest that: (1) the *type* of suspended sediments (soil) in waters might be assessed using the visible wavelength range of 580 – 690 nm; and (2) the *amount* of suspended minerals in waters where suspended minerals were the predominant constituent might be estimated using the near-infrared wavelength range of 714 – 880 nm (Lodhi *et al.* 1997).

2.4 Water depth estimation using a remote sensing signal

The remote sensing technique has been employed by many investigators to derive water depth mostly on the coastal zone (Gao 2009). Jerlov (1976) developed a single band model based on the assumption that bottom reflectance and water attenuation are constant throughout the scene. A number of models have been proposed to derive water depth based on a bottom reflection-based remote bathymetric theory (Lyzenga 1978). Ji *et al.* (1992) developed a water column scattering-based remote bathymetric model, which can be applied to turbid and deep coastal waters. Tripathi (2002) introduced the turbidity influence factor (TIF) to correct the errors brought by suspended sediments from the estuary.

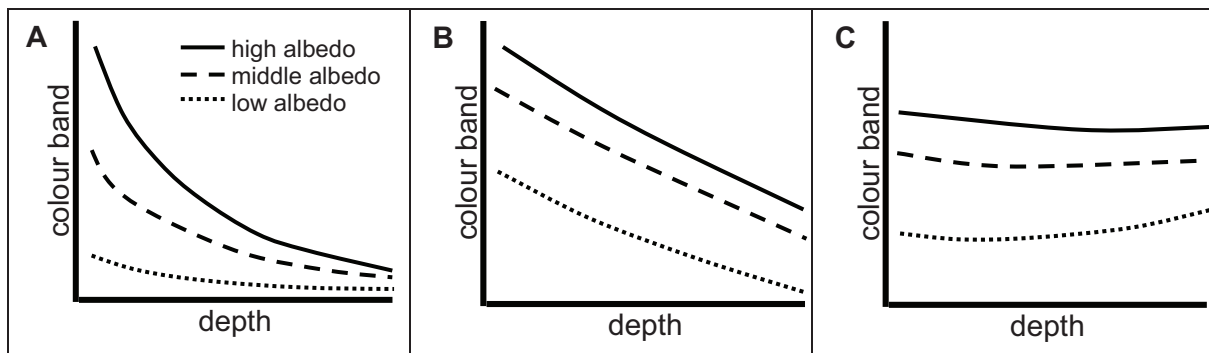


Figure 2-10: Conceptual model for de-correlating colour band data from depth. (a) Within a given waveband, the bottom-reflected radiance signal decreases approximately exponentially with depth. Deviations from exponential decay are due to scattering effects. The values shown here are modelled using the Hydrolight 4.1 forward radiative transfer model. (b) After subtracting the value for optically deep water, the natural logarithm of the bottom-reflected signal decreases approximately linearly with water depth. Different bottom albedos appear as parallel lines with the same slope. (c) Rotating the axes through the angle defined by the slope effectively de-correlates the colour band data from depth, while maintaining the relative intensities of the different bottom albedos (after Conger *et al.* 2006)

The most difficult aspect of the water depth remote sensing retrieval method is to distinguish the variations in water depth, bottom type, and scattering and absorption in the water column caused by chlorophyll, suspended sediments, coloured dissolved organic

matter, etc (Sandidge and Holyer 1998). As for the complex composition and their interactions in coastal water, attention should be paid to the elimination and reduction of environmental effects on the signals of water depth in current research (Wang *et al.* 2007).

For a given colour band, the remotely sensed signal (less atmospheric and water surface effects) can be modelled as a linear function of bottom albedo and an exponential function of water depth (Figure 2-10(a)). Variations from the exponential decay are due to backscattering in the water column. Taking the natural logarithm of the remotely sensed signal has the effect of (approximately) linearizing the colour band data with respect to depth (Figure 2-10(b)). Computing the model, a linear regression between the ln-transformed colour band and depth, and rotating the coordinate system about that regression line de-correlates the colour band data from water depth (Figure 2-10(c)). In other words, by rotating the ln-transformed colour band according to its linear relationship with depth, we are left with a colour band whose intensity no longer decreases with increasing depth. The de-correlated colour band data do not have physically meaningful units, but can be calibrated to absolute albedo using techniques such as the empirical line method. This model requires that bathymetry information exists for each pixel in the colour bands (Conger *et al.* 2006).

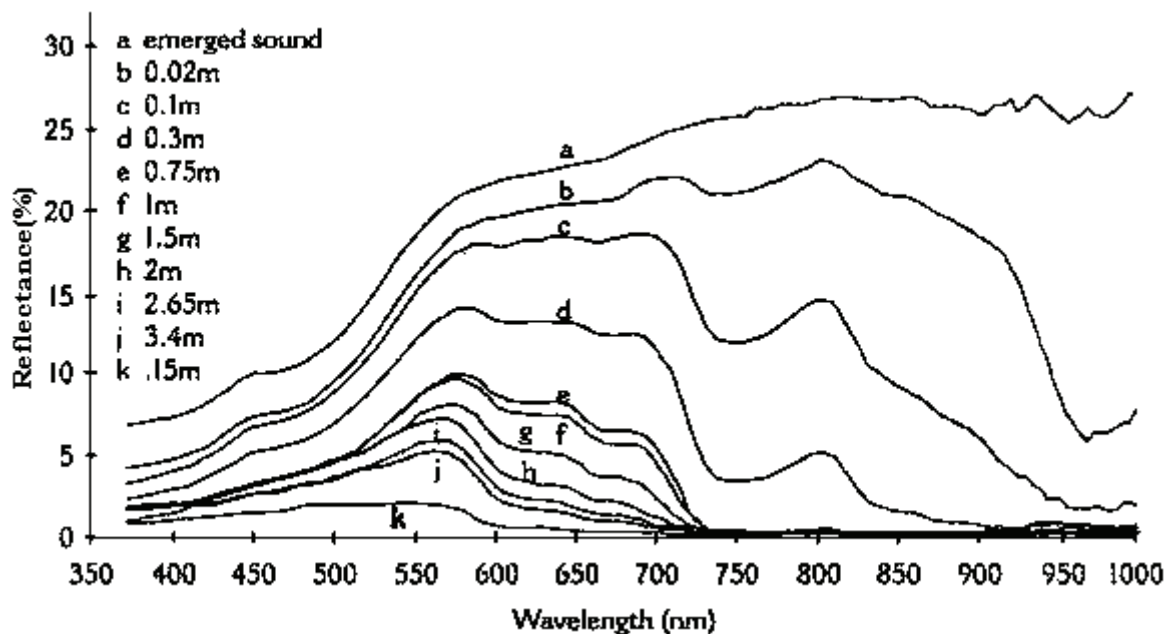


Figure 2-11: Reflectance spectra of water at depths ranging from 0.02 to 15 m (after Lafon *et al.* 2002)

The selection of the best spectral bands is governed by their capability of penetrating water, and the aquatic environment. Theoretically, the blue spectrum (0.45–0.52 μ m)

should be selected for optically sensing bathymetry due to its strong penetration capabilities. Spectral bands of short wavelengths are preferred in bathymetric mapping from space as there is low attenuation of electromagnetic radiation. However, this spectrum has not been universally accepted as the optimum. The optimal wavelength ranges for an estuary are 0.77–0.80 μm (Kumar *et al.* 1997).

The varied optimal wavelengths are explained by water clarity and the sensing environments. In pure and clear waters, little backscattering takes place and radiation is able to penetrate the deeper water. Nevertheless, the short wavelength algorithms advocated for bathymetric measurements in clear water cannot be applied to turbid productive waters. Turbid waters shift the optimum wavelength of sensing bathymetry towards longer radiation, away from the vicinity of 0.45 μm that tends to have the maximum penetration in clear waters (Jerlov 1976; Kirk 1994). In this environment, water depth is strongly correlated with the red band of the 0.746–0.759 μm range, but not the blue end of the spectrum (George 1997). The best way of determining the optimal wavelength for a water body is to measure the spectrum at different depths and select the wavelength ranges most sensitive to bathymetry (Figure 2-11) (Lafon *et al.* 2002).

2.5 Spectral range selection methods

2.5.1 Most sensitive spectral ranges

Several studies have shown that spectral bands that were found linked to water quality variables were in common spectral regions. However, a slight shift in wavelengths might occur due to the different nature of research (e.g., controlled laboratory settings versus natural conditions) and/or different conditions of water (e.g., high DOC and TSS). When Chlorophyll increased, the near-infrared peak often shifted to the longer wavelength as well. The spectral bands that were found to be significant from previous studies were used as a general guide in the optimal spectral band identification process in later sections.

Spectral wavebands that were successfully used in the reviewed researches are summarized in Table 2-1.

Table 2-1: Summary of wavebands from the literature review

Parameter	Wavelength (nm)	Optical properties	Reference
Chlorophyll- <i>a</i>	440-450	Distinct absorbance in blue range	Shafique <i>et al.</i> (2001)
	575	“Green peak” caused by minimum algae absorption	Subramaniam <i>et al.</i> (1999)
	650	Minimum absorbance	Dekker <i>et al.</i> (1992)
	670-680	Distinct maximum absorbance in red range	Kallio <i>et al.</i> (2003) Shafique <i>et al.</i> (2001) Dekker <i>et al.</i> (1992)
	705-720	Local peak due to maximum absorptions at 670	Kallio <i>et al.</i> (2003) Shafique <i>et al.</i> (2001)
TSS	705	Type of sediment	Shafique <i>et al.</i> (2001)
	580-690	Amount of sediment	Doxaran <i>et al.</i> (2002a)
(Secchi Disk) Depth	480-600	Clear water penetration	Gao <i>et al.</i> (2009)
	770-820	Peak due to suspended sediments	Wang <i>et al.</i> (2007)

2.5.2 Spectral derivative analysis

Spectroscopic derivatives are obtained by taking the difference between the reflectance of two bands and dividing that value by the difference between the wavelengths separating the two bands (Philpot 1991). When the two bands used in the calculation are adjacent to one another, the result is the first derivative (Shafique *et al.* 2001). Pepe *et al.* (2001) developed the chlorophyll-*a* model using a derivative method. The model based on the higher sensitivity of first derivative reflectance to concentrations of optically active in-water substances compare to the original radiance reflectance. Correlation analyses were carried out with a first derivative at each hand-held spectrometer band pass. The spectral band at 676 nm proved to be the best-correlating wavelength in most cases, corresponding with a peak in chlorophyll-*a* absorption (Han and Rundquist 1997). On the basis of those results, 676 nm as a sole wavelength was used to evaluate the applicability of the first

derivative spectra model to every lake condition. Considering the results of the first-derivative model over the complete acquired spectrum (380 – 780 nm), the result showed that higher correlation values were dependent on wavelength with respect to chlorophyll contents and sampling depths. In any case, 676 nm proved to be the most often correlated wavelength. The first derivative of reflectance at 676 was sufficiently reliable only when the average chlorophyll-*a* contents were higher than 2µg/l; and when the *Cyanophyceae* (bluegreen algae) presence was less than 20 percent in the phytoplankton biomass. The accuracy of the first derivative method and the near infrared/red reflectance ratio (NIR/red) were tested in the study. The NIR/red model was based on the contrast between a local reflectance peak feature at approximately 705 nm due to a minimum absorption by the pigment and the water, and a local reflectance minimum feature at approximately 670 nm due to the absorption maximum of chlorophyll-*a*. The results showed that the NIR/red model results were less satisfactory than the first derivative one.

Rencz (1999), and Huguenin and Jones (1986) examined a variety of higher order derivatives of spectra in an effort to identify the location of individual absorption regions. While assuming that each absorption range was symmetric around its band centre, the method did not require that absorptions have a specific shape. Band centres were identified where the second derivative of the spectrum was negative, the fourth derivative was positive, and the fifth derivative was zero. Like any derivative analysis, this method was highly sensitive to noise. Therefore, the Huguenin and Jones (1986) approach was critically dependent on an intelligent smoothing algorithm. Nonetheless, their approach was capable of resolving overlapping band centres separated by as little as 0.1 to 1.0 of the full width at half maximum (assuming Gaussia-shaped absorptions). Although the derivative technique was sensitive to noise, Tsai and Philpot (1998) concluded that an algorithm for derivative analysis of hyperspectral data was a tool that treated hyperspectral data as truly spectrally continuous data. Moreover, the approach could be used with no need to assume that the data were generated in highly controlled environments.

2.5.2 Spectral Band Ratio method

Certain band ratios could be used successfully for chlorophyll mapping in inland waters (Gitelson 1993; Koponen *et al.* 2002). Dekker (1993) and Gitelson *et al.* (1993) found that the optimum ratio of spectral radiance or reflectance at two wavelengths (λ_x) and (λ_y) is achieved where (λ_x) was in the range from approximately 680–710 nm (corresponding to

the chlorophyll-*a* fluorescence peak and volume scattering from particulate matter) and (λ_y) was at approximately 665–680 nm (the region of the chlorophyll-*a* absorption maximum):

$$\text{Chl } a(\mu\text{g} / L) = a_0 + a_1 \left(\frac{L(\lambda_x)}{L(\lambda_y)} \right) \quad [2.1]$$

Pulliainen *et al.* (2001) employed the wavelength ranges suggested by Gitelson *et al.* (1993) in their chlorophyll-*a* retrieval algorithms. The optimum channel ratio was selected empirically using a training dataset to determine the highest correlation with chlorophyll-*a* concentration. A linear regression model employing the channel ratio L702nm / L665nm yielded a maximum value of $R^2 = 0.94$. However, when the predicting waters were affected by various substrates besides chlorophyll (e.g., humic and high suspended sediment), application of Equation 2-1 with remote sensing data may encounter some problems, especially if other parameters in addition to chlorophyll-*a* affect the ratio $L(\lambda_x) / L(\lambda_y)$. This method might require the dataset to be pre-classified into different sub-groups, e.g., based on the shape of the measured radiance spectra, in order to increase the chlorophyll-*a* estimation accuracy.

Koponen *et al.* (2001) also used the AISA data to measure chlorophyll-*a* concentration in lakes. The study found that the ratio 702 nm/673 nm produced the best result. Their results confirmed that an airborne spectrometer was a useful tool for chlorophyll-*a* monitoring in lakes. The result corresponded well with the findings of other authors (e.g., Dekker *et al.* 1992 or Gitelson *et al.* 1993).

George and Malthus (2001) used an array of wavelength-specific correlation coefficients to determine the ‘single band.’ Low coefficient values indicated that the radiance values at these wavelengths were not influenced by the presence of phytoplankton. High positive or negative values indicated that the radiance values were strongly influenced by the concentration of phytoplankton. The strongest correlation between the two variables was recorded in the green and red portions of the spectrum where the R^2 values were positive and reached a maximum value of 0.86 ($P < 0.05$). Then, the correlation between all possible combinations and the measured concentration of chlorophyll-*a* was calculated. The results suggested that the most effective multi-band algorithm would contrast the amount of ‘green’ light reflected with that absorbed at the ‘blue’ end of the spectrum. The ratio of measurements centred at 550 nm and 440 nm (the ratio identical to the blue/green

ratio suggested by Clarke *et al.* 1970) was found to perform best for chlorophyll prediction, and the ratio of measurements at 685 nm and 745 nm (rather similar to the long-waveband ratio recommended by Dekker, 1993) performed well for waters containing high concentrations of dissolved organic matter.

2.5.3 Multivariate statistical methods

Multivariate statistics have been developed and applied successfully for spatial or spectral analysis of remote sensing data, usually derived from established methods in multivariate statistics (Richards and Jia 2006; Tsai and Philpot 1998). Giardino *et al.* (2001) adopted several statistical techniques to examine the relationship between *in situ* measured parameters (i.e., Secchi disk and chlorophyll-*a*) and remote sensing reflectance values from the Landsat Thematic Mapper (TM) sensor. These models included linear, exponential and log transformations. A few previous studies used nonlinear power models ($y=aX^b$) to address the curvilinear behaviour of this relationship (Cox *et al.* 1998; Lathrop 1992). Although a power model provided a strong correlation, residuals from it were not normally distributed. In contrast, the semi-log equation used by Kloiber *et al.* (2002) met the model assumptions. A similar result had been found by Pattiaratchi *et al.* (1994). Regression models were used to determine the relationship between the difference between reflectance values, the difference between TM bands 1 and 3 (TM1 – TM3), and the ratio between TM bands 1 and 2 (TM1/TM2). These models allowed the surface distribution of chlorophyll-*a* concentrations and Secchi disk depths to be determined with good confidence (the coefficients of determination were 0.99 and 0.85, respectively; Giardino *et al.* 2001).

Kloiber *et al.* (2002) took a further step to develop a standard model that used a consistent equation form for using satellite remote sensing data to estimate key variables related to lake management issues, such as trophic state condition and water clarity. Rather than using regression equations where the independent variables were different for each image, the feasibility of using a consistent equation form to relate ground observations and satellite data was examined. A Pearson correlation matrix was developed to examine the relative strength of correlation between Secchi disk transparency depth (SD) and various Landsat TM bands and band ratios. Results indicated that regressed log-transformed SD versus the TM1/TM3 ratio plus TM1 (TM1/TM3 + TM1) provided strong predictive relationships for multiple images over a 25-year period. However, the effect of increased scattering by suspended particles impacted much of the visible and near infrared portion of the spectrum from about 500 nm to about 850 nm. This scattering effect overwhelmed the

subtler influence of other features such as the chlorophyll-*a* minimum. Although a relationship between water clarity and Landsat-measured reflectance can be established, this should not be construed to imply that such relationships could be developed for other water quality variables such as chlorophyll-*a*.

Kloiber *et al.* (2002) noted the importance of radiometric calibration. The brightness values of the pixels in a satellite image were affected by sun angle, atmospheric interference, changes in detector response, and numerous other factors. If radiometric correction techniques accounted for these factors, then the coefficients for the models would be more consistent, and one set of coefficients would apply for different images across time and space.

All relevant publications on techniques that were used with hyperspectral data were reviewed and discussed, specifically what had been done, and what needed to be done in order to improve remote sensing of water quality for kettle holes. Although some of the spectral bands were identified in the previous studies, they were not universal due to the disadvantages of empirical methods that are data dependent. An empirical model was often derived based on the relationship between dependent and independent variables from a specific set of data. Spectral indicators based on correlations between local *in situ* measurements of water quality and spectral variables at one location may not represent the relationship between the same variables at different locations. Spectral indicators developed from wavebands that truly explain optical properties of the variables such as absorption and reflectance features are the potential solution. However, very few studies have been conducted on deriving the spectral features of water, such as spectral library development, when compared to those in mineral and vegetation sciences. In addition, the spectral bands identified by these derivative techniques were mostly derived from a specially controlled environment. Therefore, they may not be applicable in the real natural environment. A study to use spectral bands that were developed based on optical properties of water constitutes to quantify the relationship between water quality and spectral data within a natural biophysical condition needed to be conducted at large scales. However, this study shows that in order to implement a large-scale monitoring programme, precise investigation of small-scale processes is needed. This study attempts to access and develop algorithms that are spatially and temporally applicable for small shallow water bodies in order to create and maintain a full operational kettle holes' water quality monitoring programme.

3 Experimental design

3.1 *Study area*

The study area is located in state (Land) Mecklenburg-Vorpommern, Federal Republic of Germany. Therefore, biotic and abiotic components of the state are described briefly in the next section.

3.1.1 Geology and physiography

Mecklenburg-Vorpommern extends along the Baltic Sea coastal plain, from the Bay of Lübeck in the west, past the Darss Peninsula, to the Szczecinski Lagoon (Stettiner Haff) in the east. Its hinterland stretches southward to the lower Elbe River in the west and beyond the sources of the Havel River and nearly to the Oder River in the east. Most of Mecklenburg-Vorpommern drains into the Baltic. The region's landscape was largely shaped by glacial forces, which deposited materials that produced the beautiful hill country and low-lying lands that are now filled with wetlands, lakes, and meandering streams. Nearly two-thirds of the state is covered by farmland and about another one-fifth by forest (Britannica 2009).

There are chalk cliffs at Stubbenkammer's promontory on the island of Rügen, Germany, and Fishermen's huts on the west coast of Lake Müritz near Robel, Mecklenburg-Vorpommern. The central part of Mecklenburg-Vorpommern is traversed from west to east by a plateau of hilly country covered by fertile soil and beech forests. The state has more than 1,700 lakes (see Figure 3-1), including Lake Müritz in the south, the largest lake wholly within Germany's borders and the focus of a national park. The southwest, between the plateau and the Elbe, has poor sandy soils, pine forests, and marshy valleys. In the north the plateau has good clay soils. Along the coast, steep cliffs alternate with beaches and dunes. The north-eastern part of the state contains Germany's two largest islands, Rügen and Usedom, the former especially well known for dramatically high chalk cliffs on the Baltic Sea. Two national parks have been established on the coast, the West Pomeranian Boddenlandschaft National Park, largely on the Darss Peninsula and surrounding waters, and the Jasmund National Park, on the north-eastern end of Rügen. The state lies wholly within the North European Plain and has a moderate climate primarily influenced by the Atlantic Ocean and Baltic Sea (Britannica 2009).

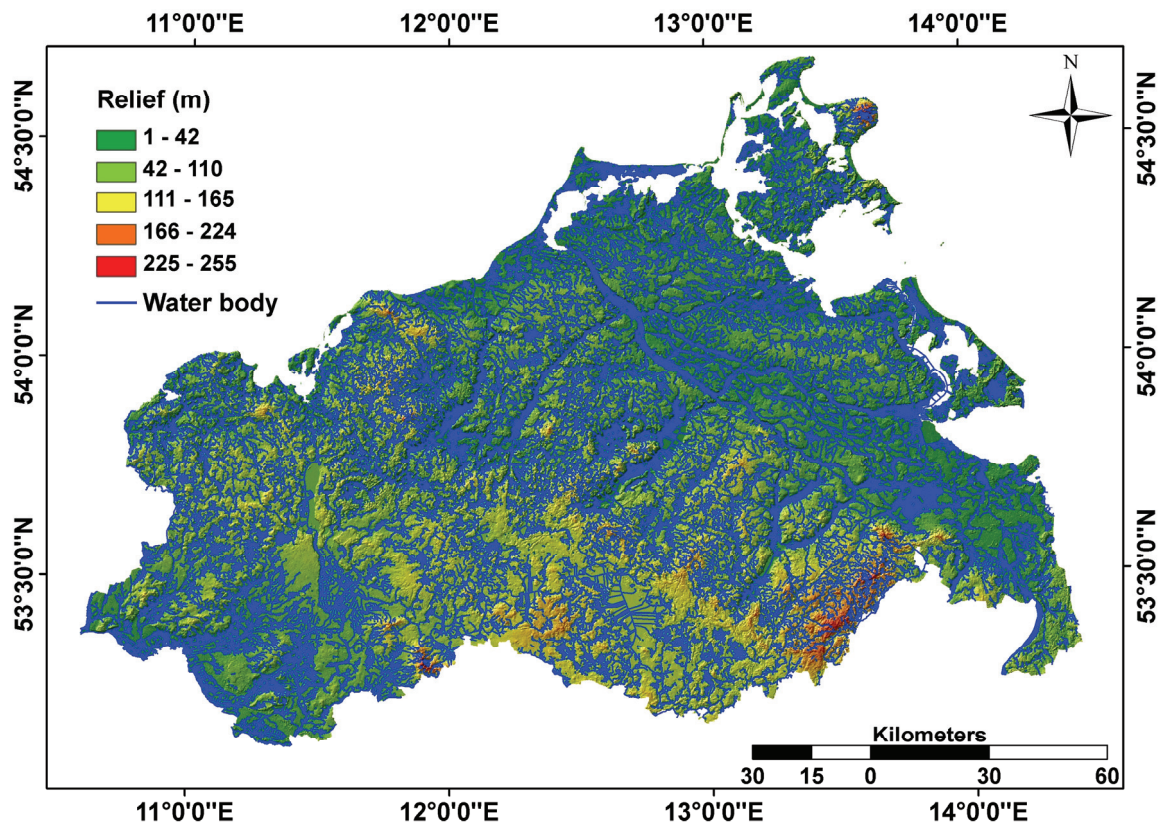


Figure 3-1: Relief map from SRTM (SRTM 2009) data overlaid with water bodies shapefile of Mecklenburg– Vorpommern (LUNG-MV 2009).

3.1.2 Land use and climate

Agriculture, once a relatively important economic activity in Mecklenburg-Vorpommern, is now most significant for its role in shaping the landscape. Agricultural output makes up only a small percentage of the state’s economic output and employment, though rural areas of Mecklenburg-Vorpommern depend more on agriculture as a way of life than most other parts of Germany. Because of its history of collectivized farming while it was part of German Democratic Republic (1945–90), Mecklenburg-Vorpommern has farm units that are large by German and western European standards. The chief crops are rye, wheat, barley, sugar beet, potatoes, and hay. Corn (maize) and peas are also grown, and the state is among Germany’s leading producers of rapeseed. The region’s pastures support herds of sheep, horses, and cattle, which supply milk for the production of butter and cheese. Fishing is carried out in the inland lakes and the Baltic Sea.

The yearly mean temperature for the state is about 9° C. During January, the coldest month, the average temperature is approximately 1.6°C. Average July’s temperatures are

between 16°C and 18°C. Annual precipitation varies between 400 millimetres and 600 millimetres (Britannica 2009; LUNG-MV 2009).

3.1.3 Selection of kettle holes

The test area is located close to the city of Demmin, about 150 km north of the city of Berlin, and covers approximately 10 km² (Figure 3-2). The first survey (May, 2007) showed that all kettle holes are within agricultural fields and have different shapes, sizes, water table depths, water regimes and trophic states. After elimination of permanently dry kettle holes, the primary monitoring programme included 9 sampling stations (Figure 1). However, some kettle holes dry out during summer, so the kettle holes K8 and K9 were excluded from further monitoring. Kettle hole K3 was entirely covered by duckweed (botanic *Lemna spp.*) and was also not considered in the study. Finally, field data were collected from 6 kettle holes in the period between June and October 2007 (a total of 7 datasets, 5 of which were with spectral data). Description of kettle holes is given in Appendix A.

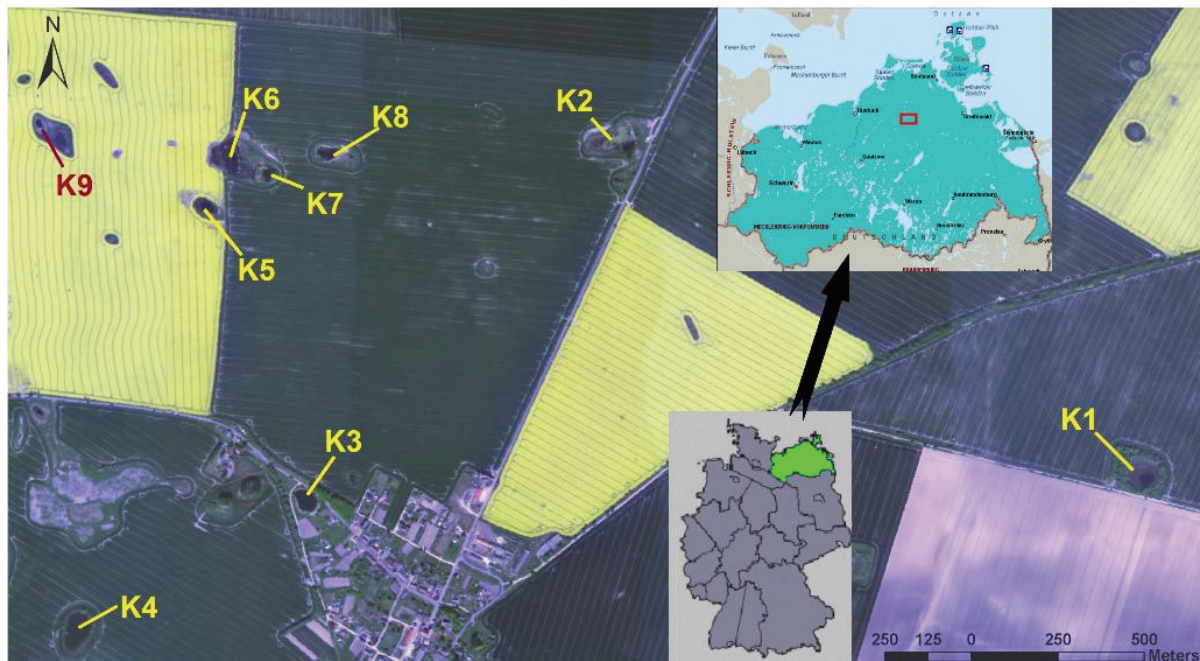


Figure 3-2: True colour composite ROSIS image (15 May 2008) of test area (close to the village Schmarsow, Demmin suburbs - FRG) with kettle holes numeration.

In summer 2008 kettle hole K2 dried out and it was also excluded from further monitoring. In 2008 ground truth data were collected in 10 field campaigns from 5 kettle holes in the period between May and September 2008. See Appendix B for a complete list of pigment concentrations of data from all campaigns. Overall, spectral ground truth collection

resulted from 15 datasets during 2007 and 2008, giving sufficient information for seasonal and annual analysis of water quality temporal dynamics.

3.1.4 Kettle holes' hydro-morphological characteristics

The basis for the characterization of the kettle holes was the investigation of hydro-morphological factors (length, width, water table depth, shore slope, water regime and algae content) and the application of the typology as described by Kalettka and Rudat (2006). Field research showed that all kettle holes belong to the 'storage type' with semi-permanent and permanent water regimes. Subtype categories and hydro-morphological characteristics are given in Table 3-1.

Table 3-1: Kettle holes' hydro-morphological characteristics

Name	Area (ha)	Depth (m)	Shore slope	Algae content	Water colour	Subtype	Remarks
K1	≈0.12	≈1÷1.5	Steep	Very High	Transparent	Big shallow	
K2	≈0.14	≈0.5÷1.0	Gentle	High	Transparent	Big shallow	
K4	≈0.80	≈2.5÷3.5	Steep	Very Low	Dark green	Big deep	
K5	≈0.10	≈0.3÷0.5	Steep	Very High	2007 - Light brown 2008 - Transparent	Small wadeable	
K6	≈0.25	≈0.6÷1.3	Gentle	Moderate	Transparent	Big shallow	Both kettle holes used to be one
K7	≈0.23	≈0.8÷1.2	Gentle	Low	Transparent	Big shallow	

3.2 Remote sensing data acquisition

Two sets of hyperspectral remote sensing data were used in the study. The two types of datasets were acquired from a hand-held ASD sensor and airborne sensors ROSIS (Reflective Optics System Imaging Spectrometer, German Aerospace Centre - DLR) and HyMap ('Hyperspectral Mapper' - HyVista, Australia).

3.2.1 Hand-held analytical spectral device (ASD)

Upwelling radiance data (for determination of reflectance spectra) were collected at the same time as water sampling from 6 lakes in 15 field campaigns (5 in 2007 and 10 in 2008) resulting in a total of 80 spectral datasets. Recorded radiance represented the vertical flux of energy upward from the water surface (primarily solar energy backscattered within the water column and emerging from the water surface). These nadir optical measurements were collected using a field spectroradiometer (ASD FieldSpec HH ultraviolet/visible and near-infrared (UV/ VNIR)). The instrument records a continuous spectrum with 25° FOV in 512 bands, ranging from 274 nm to 1,085 nm with 1.587 nm spectral resolution (ASDI 2009). Upwelling radiance from the water body is retrieved as relative reflectance in relation to the downwelling radiance spectrum measured from a reference panel (25-30 cm above the panel). This reference panel is made from sintered polytetrafluoroethylene that is a near-perfect Lambertian reflector. At each sampling station, the reference panel was scanned first. Depending on the depth and size of the kettle hole, the spectral measurement took place either on board a boat or at the shoreline.

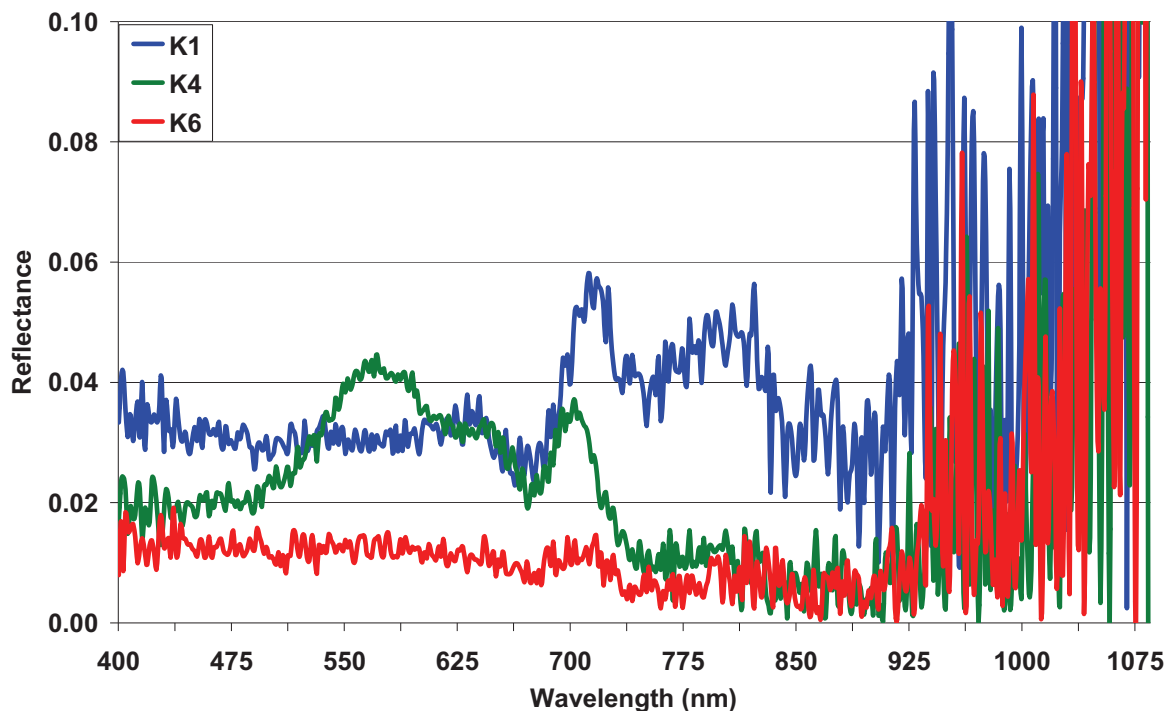


Figure 3-3: The variation of average upwelling radiance as measured from ASD from kettle holes K1, K4 and K6 acquired on 3 June 2008.

The measuring unit was oriented to the boat's side within the light propagation to minimize sun glint from waves, but far enough not to be affected by the boat's shadow. The same rules were applied for the shoreline measurements. In both cases data were collected at or

close to the central part of the kettle hole at a height of ≈ 30 cm in a vertical downward direction between 10 am and 2 pm. At least ten measurements were taken from each kettle hole repeatedly, which were afterwards averaged to minimize random effects and to enhance the signal to noise ratio. Figure 3-3 showed the variation of upwelling radiance of three kettle holes (field spectra) taken on 3 June 2008.

In summary, spectra collection performed at each sample site comprised: (1) the average of approximately 10 radiance spectra of the reference panel at the *beginning* of each measuring session; (2) the upwelling nadir radiance, where each measurement was an average of approximately 15 spectra collected at every sampling site; and (3) another average of approximately 10 spectra of the reflectance panel at the *end* of the measuring session.

The fraction of light reflected from the lake water was very small compared to other natural surfaces, such as soils and vegetation. Water-leaving radiances from natural water bodies are commonly less than 10% of the total radiance measured at the sensor. Most of them are even often less than 1% (Gordon 1987). Typically, in clear water, the radiance is maximal in the blue ($\lambda \approx 0.44 \mu\text{m}$), medium in the green ($\lambda \approx 0.55 \mu\text{m}$) and negligible in the near infrared ($\lambda \geq 0.75 \mu\text{m}$). Since the desired water-leaving radiance is only a small part of the signal recorded by the sensor, accurate radiometric correction is critical (Gordon 1987). To extract the true representative reflectance of substances in water column, the collected spectra needed to be transformed to reflectance values at different wavelengths that: (1) maximally relate to the concentration of the constituent of interest; and (2) minimize the effects of other optically active constituents and survey conditions.

3.2.2 Reflective optics system imaging spectrometer (ROSI)

ROSI (Reflective Optics System Imaging Spectrometer) is a compact airborne imaging spectrometer, which had been developed jointly by the former company MBB (now: Daimler-Chrysler Aerospace AG), the GKSS Research Centre (Institute of Hydrophysics) and the German Aerospace Centre, DLR (the former Institute of Optoelectronics, now Remote Sensing Technology Institute) based on an original design for a flight on ESA's EURECA platform (Gege *et al.* 2008). The first sensor was built in 1992, and after several modifications in 1994. It was completely re-designed and rebuilt by the company Erwin Schneider Systemtechnik in Germering, resulting in the current version - ROSIS-03. The main characteristics of the recent version of ROSIS are given in the following Table 3-2.

The driver for the design of ROSIS was its application for the detection of spectral fine structures especially in coastal and inland waters. This task determined the selection of the spectral range, bandwidth, and number of channels, radiometric resolution and its tilt capability for Sun glint avoidance. However, ROSIS can be used also for monitoring spectral features above land and within the atmosphere (DLR 2009).

The hyperspectral ROSIS imagery acquired on 15 May 2008, having a range from 389 to 845 nm and an interval of 4 nm in 115 bands, were recorded with full ground coverage at an altitude of about 3500 m resulting in a spatial resolution of 2×2 m.

Table 3-2: ROSIS sensor's specifications

Principle	Push-broom Grating Spectrometer
Spectral range	430 – 887 nm
Spectral sampling interval	4.0 nm
Total number of spectral channels	102 / 115
Pixel size at 3 km flight altitude	1.6 m x 1.6 m
Total field of view	±8°
Instantaneous field of view	0.56 mrad
Number of imaging elements	512
Max. scan frequency	62 Hz
Radiometric quantization	14 bit
Tilt capability along flight direction	±20°
Onboard calibration	Internal Hg lamp

3.2.3 Hyperspectral Mapper (HyMap)

HyMap (Hyperspectral Mapper) is a commercial hyperspectral sensor developed by Integrated Spectronics, Sydney, Australia, and operated by HyVista Corporation (Cox *et*

al. 1998). The system is a whiskbroom scanner with 126 spectral channels covering the 0.45 – 2.5 μm range over a 512-pixel swath. The HyMap uses real time altitude and differential global positioning system (DGPS) measurements to provide geo-coded imagery. The spectral and image information from the spectrometer is digitized and recorded on tape. To minimize distortion in the image by aircraft pitch, roll, and yaw motions, HyMap is mounted on a gyro-stabilized platform. While this platform minimizes the effect of aircraft motion, small image distortions remain, which are monitored using a three-axis accelerometer system (Pinnel 2007).

Table 3-3 provides some guidelines as to the configuration and operational bounds of the current HyMap sensor.

Table 3-3: HyMap sensor's specifications

Principle	Whisk-broom scanner with double mirror
Spectral range	400 – 2500 nm
Spectral sampling interval	13.0 – 17.0 nm
Bands	126
Pixel size at 3 km flight altitude	5 m x 5 m
Total field of view	$\pm 8^\circ$
Instantaneous field of view	2.5 mrad along track, 2.0 mrad across track
Number of imaging elements	512
Max. scan frequency	62 Hz
Radiometric quantization	14 bit
Onboard calibration	signal to noise ratio (>500:1)
Tilt capability along flight direction	$\pm 20^\circ$

The instrument offers a high signal-to-noise ratio (SNR) of more than 500:1 which is essential for mapping low reflecting targets such as submerged vegetation. These facts

make HyMap a very valuable instrument for the simulation of future spaceborne spectrometers which will also have a similar noise characteristic. This type of configuration is now finding an expanding role in environmental pollution monitoring, agriculture and forestry, soil mapping and the assessment of natural and introduced vegetation (Kruse *et al.* 2000).

Further specifications include: 3÷10m spatial resolution; 60 degrees swath width on-board radiometric and spectral calibration 3 axis gyros stabilized platform (Kruse *et al.* 2000). A HyMap image dataset was collected on 29 July 2008, providing datasets from an altitude of about 2000 m with a 4×4 m pixel size. Only the first 34 bands between 450 and 920 nm relevant for the determination of water constituents were used in this study.

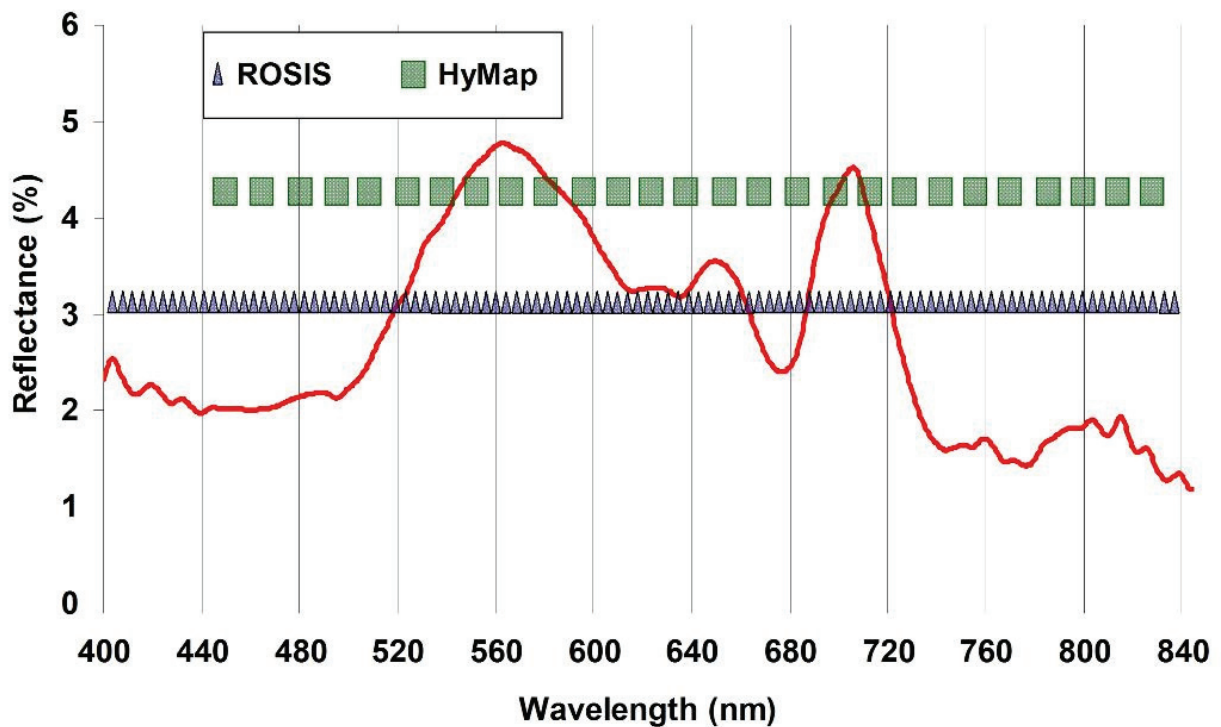


Figure 3-4: Central wavelengths of ROSIS and HyMap sensors in comparison with eutrophic water spectrum of K4 taken on 15 May 2008

Figure 3-4 gives descriptive information about the spectral resolution of sensors used in this research in comparison with surface reflectance from K4 taken on 15 May 2008.

3.2.4 Pre-processing of the airborne data

Both airborne datasets have been atmospherically corrected using the ATCOR4 software package for airborne data (Richter 1996). The radiative transfer in ATCOR4 is based on the MODTRAN-4 code (<http://www.rese.ch/atcor/atcor4/>). This software corrects at-sensor

radiance images for the solar illuminance, the Rayleigh and adjacency scattering in order to derive nadir-normalized ground reflectance. ATCOR4 also corrects the additional atmospheric signal due to scan angle variations and the adjacency effect which is especially relevant for water bodies. Key input parameters are flight altitude, ground elevation above sea level, zenith and azimuth angles of the sun, flight direction, and day of the year, as well as standard atmospheric condition. ATCOR4 data processing results in a ground reflectance image. Before processing, ATCOR4 was configured for the specific band settings of the ROSIS and HyMap sensors.

Geo-referencing of the ROSIS and HyMap images is based on data from a navigation system (IGI) which records simultaneously the flight attitude and position parameters. Both scanners were flown mounted on a stabilizing platform during clear sky weather conditions. Geo-coding was performed using special software which operates with flight parameters (i.e. sensor position, roll, pitch, true heading), and additional terrain information from a digital terrain model (DEM) for correction of the viewing geometry for each pixel. Geometric accuracy of the flight strips was checked using a number of ground control points from a topographic map (Gege *et al.* 2008). The overlay onto existing airborne image data with a ground sampling distance (GSD) of 20 cm shows good agreement of about 90% of the lake pixels with a position accuracy of less than 3 pixels (= 60 cm). According to existing specification at the German Aerospace Centre (DLR), both image datasets (ROSI and HyMap) were processed to L2 level, i.e. geo-referenced and atmospherically corrected spectral reflectance data. In order to enhance even the smallest changes in ground reflectance, the digital number (DN) values of both datasets were stretched to 10,000, e.g. 100 DN value on image corresponds to 1% of ground reflectance.

3.3 Laboratory analytical methods for water quality parameters

3.3.1 Water samples collection

Field activities at the sites included collection of water samples for laboratory analysis of chlorophyll-*a* (CHL), total chlorophyll (TCHL), total suspended sediments (TSS), water samples absorption at 750 nm, pH and electrical conductivity (EC). The water samples were collected in bottles of 1000 ml and were kept in the dark and analyzed at the end of the field day. Due to the fact that algae live primarily near the surface of a lake, chlorophyll samples were collected just below the surface.

Parameters pH and Electrical Conductivity were measured in the field using field kits and were checked again in a laboratory to get the most accurate data. Temperature at the spectrum measuring point was always measured at each station during sampling. Finally, complete lists of pigment concentrations and other water quality parameters sorted for each kettle hole are shown in Appendix B.

3.3.2 Chlorophyll

Chlorophyll was determined by using N,N'- dimethylformamide (DMF) extraction as described by Porra *et al.* (1989) . Samples were filtered using Whatman GF/F filters (0.7- μm pore size membrane) and incubated with 3 ml DMF for 12 h in darkness. Absorption was measured with a UV/VIS spectrophotometer (Lambda 2, Perkin Elmer) from 400 nm up to 750 nm. Pigment contents (chlorophyll-*a* and total in $\mu\text{g/L}$) were calculated from the absorbance spectra of the extracts using equations [3-1] and [3-2] according to Porra *et al.* (1989).

$$Chl\ a(\mu\text{g/L}) = \frac{(12.0 \times A_{667} - 3.11 \times A_{647}) \times 1000 \times e_v}{V \times d}, \quad [3-1]$$

$$Chl\ Total(\mu\text{g/L}) = \frac{(7.12 \times A_{667} + 17.67 \times A_{647}) \times 1000 \times e_v}{V \times d}, \quad [3-2]$$

Where:

A_x = absorbance at wavelength x

e_v = volume of DMF used in extraction (3 ml)

V = volume of filtered sample (ml)

d = diameter of the filter (1 cm)

3.3.3 Total suspended sediments

Before sampling, prepared glass fibre filters were soaked in distilled water and then dried at 103°C. Dried filters were weighed, their weights were recorded and then they were placed on a filtering flask. The sample bottles were shaken first and then poured in the water, and then the pump was turned on. The volumes of filtered water were recorded separately. The filters were dried at 103 to 105°C, placed to cool and their weights were recorded. TSS was calculated using the equation [3-3]:

$$TSS(mg / L) = ([A - B] * 1000) / C , \quad [3-3]$$

Where:

- A = End weight of the filter
 B = Initial weight of the filter
 C = Volume of water filtered

3.3.4 Water samples absorption at 750nm

For complete understanding of the connection between the water samples' optical properties and their pigment concentrations, the absorbance value at 750nm from the absorbance spectrum has to be measured (Bricaud and Stramski 1990). At this wavelength, phytoplankton absorption is negligible and the scattering is not wavelength-dependent (Tassan and Ferrari 1995). During extraction of chlorophyll concentrations, absorption values at 750 nm of each water sample were measured using the same UV/VIS spectrophotometer (Lambda 2, Perkin Elmer).

3.4 Methods for analysis of hand-held spectral data

The spectral analytical methodology for field and image datasets followed the flow diagram showed in Figure 3-5.

3.4.1 Data pre-processing

Reflectance is the percentage of light reflected by a target. It minimizes the effect of different illumination conditions, thus allowing a better quantitative measuring of the water colour. Radiance measurements from the field were converted to surface reflectance by using nearly coincident measurements over the Spectralon (Barium sulphate) panel (see equation [3-4]).

$$\rho_{in-situ}^a = E \uparrow_{in-situ} / E \uparrow_{spec} * \rho_{spec}^a \quad [3-4]$$

Where:

- $\rho_{in-situ}^a$ = *In situ* target percent reflectance
 $E \uparrow_{in-situ}$ = *In situ* radiance
 $E \uparrow_{spec}$ = Linearly interpolated reference panel radiance

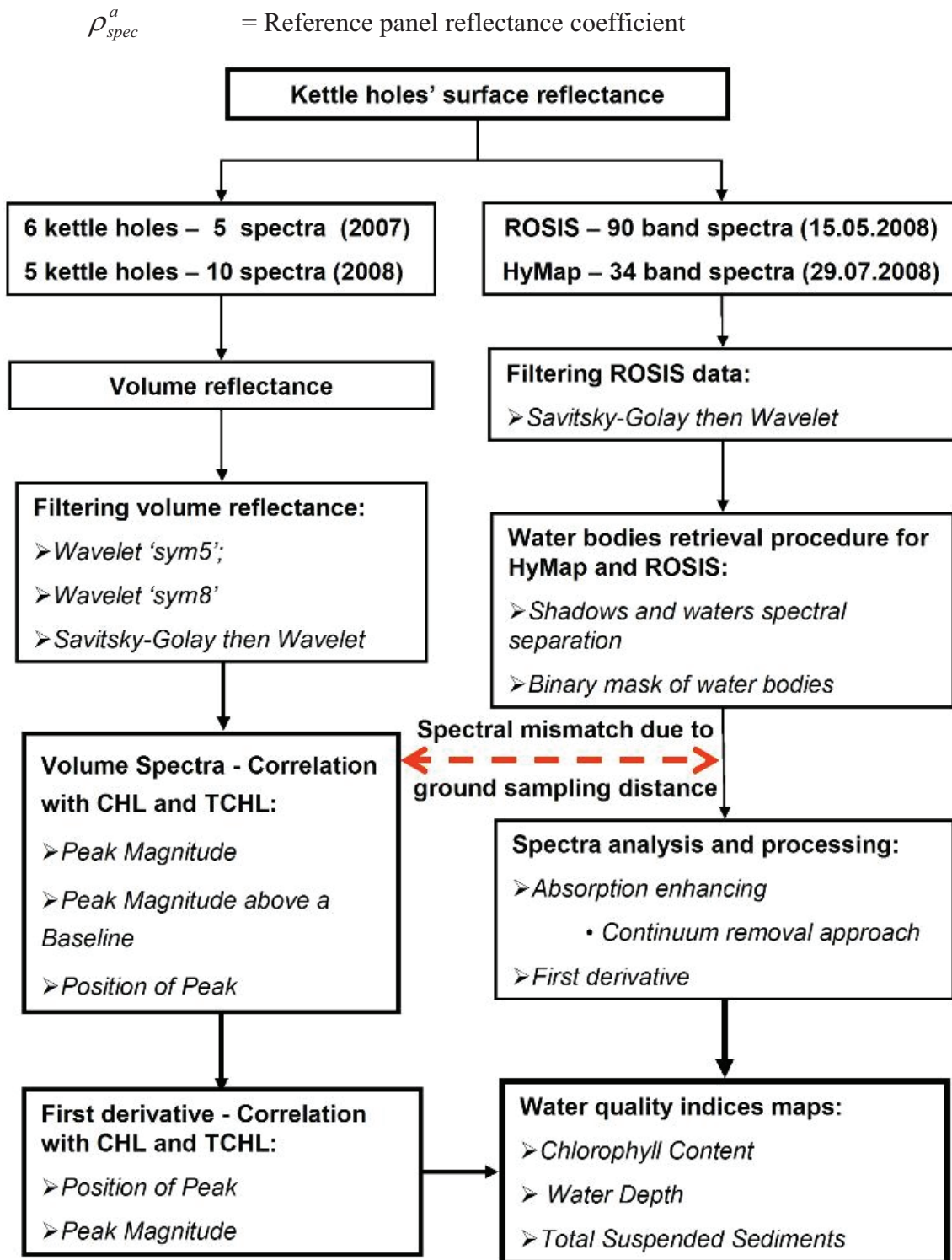


Figure 3-5: Spectral analytical procedure for field and airborne spectral data in the form of flow diagrams

These reflectance data represent the ratio of reflected energy to incident energy with values ranging from 0.0 to 1.0 (0.0 for no reflectance and 1.0 for 100% reflectance). The multiple spectra collected from each site were averaged to determine a mean spectral response for that lake.

The relatively small amounts of solar energy outside the 400 nm – 900 nm range result in data with comparatively high levels of noise (Liu *et al.* 2003). Therefore, further spectral processing and analysis in this research was based on the spectral data between 400 – 900 nm (Igamberdiev *et al.* In press). This range of wavelength has been used in a number of studies on inland waters (Dall'Olmo *et al.* 2005; Dekker *et al.* 2001c; Doxaran *et al.* 2005; Flink *et al.* 2001; Gitelson *et al.* 2007; Han 2005; Iluz *et al.* 2003; Shafique *et al.* 2001; Thiemann and Kaufmann 2002).

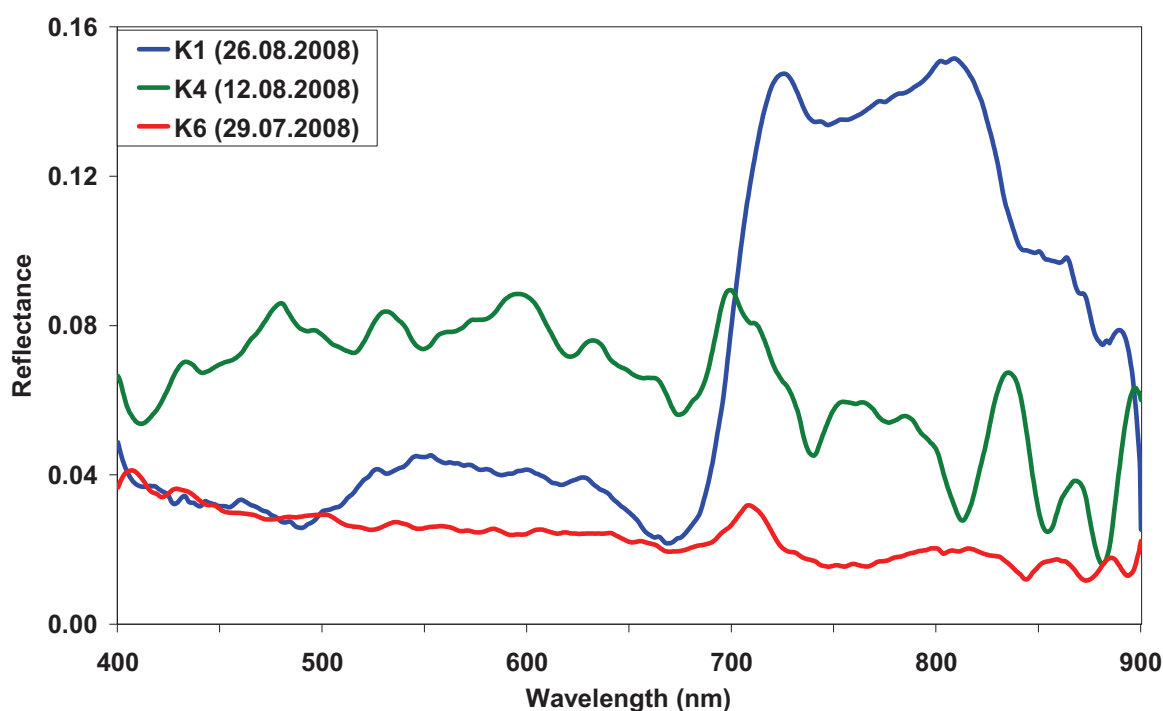


Figure 3-6: De-noised spectral signatures of kettle holes influenced by different biophysical dominants: K1 (CHL – 14.5 μ g/L, TSS – 2.5mg/L), K4 (CHL – 156 μ g/L, TSS – 12.0mg/L) and K6 (CHL – 3.0 μ g/L, TSS – 1.0mg/L)

De-noised reflectance from three kettles with various pigment concentration (CHL, TSS), acquired on different dates, are shown in Figure 3-6 (see reflectance de-noising techniques in Chapter 3.4.3). The magnitude of reflectance from kettle hole K1 in the range of 700÷900nm is the highest among the others. The influence on the spectral response from the algae-dominated bottom can be clearly seen. The spectral signature from hypereutrophic pond K4 refers to the so-called ‘classical lake reflection’. It is spectrally active in the green range (500÷600nm) and has clearly recognizable high absorption at 660÷680nm wavelength and the reflection peak near 700nm used for estimation of phytoplankton pigments in inland waters (Gitelson 1993; Thiemann 1999).

Kettle hole K6 has the lowest spectral response compared to the others. These types of spectral signatures are indicative of waters with low concentrations of suspended sediment. At the same time, despite the low CHL value ($3\mu\text{g/L}$) the peak reflectance at near-infrared wavelengths (near 700 nm) is detectable.

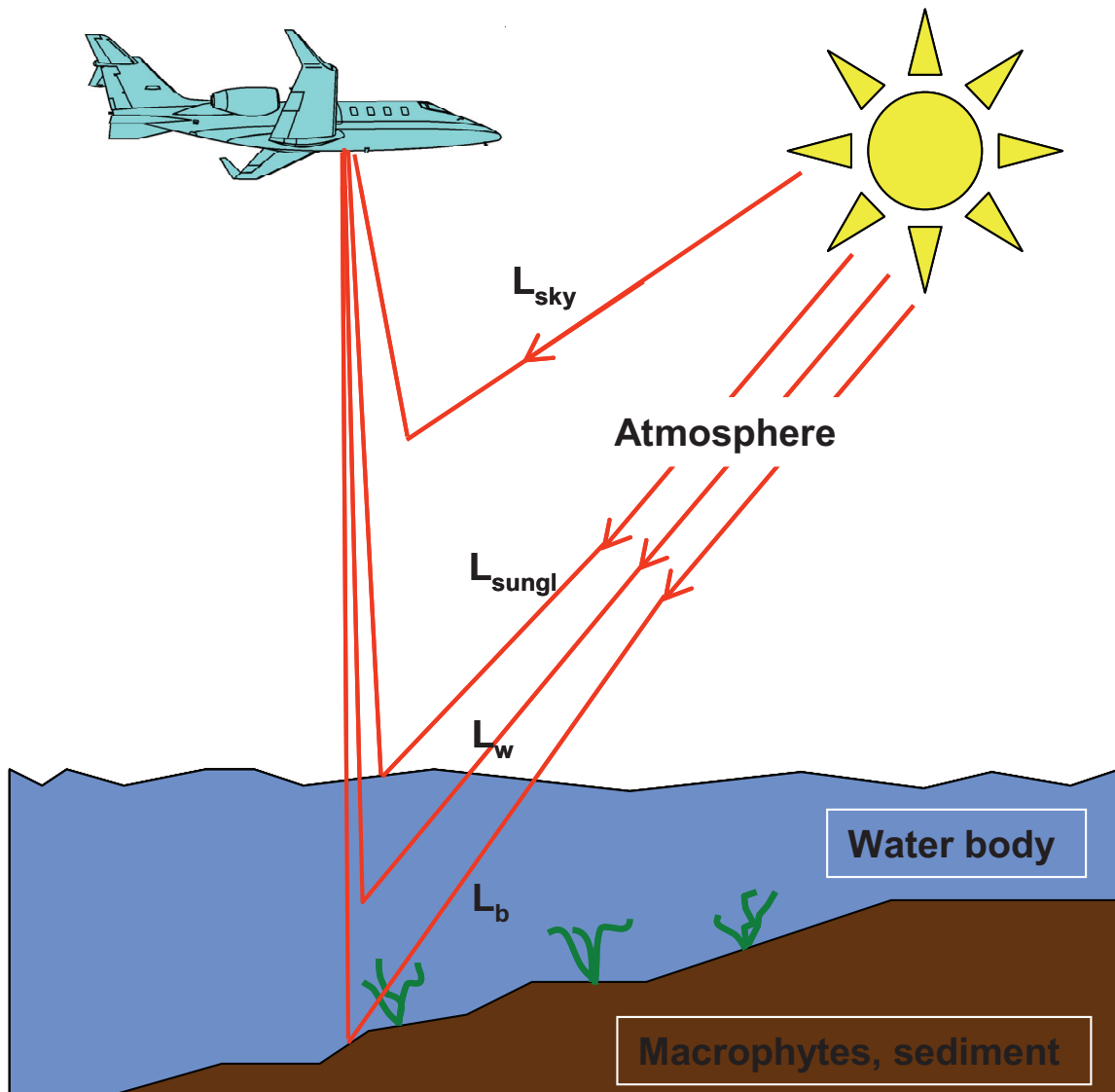


Figure 3-7: Schematic diagram of radiative transfer influenced by surface, phytoplankton, gelbstoff, suspended matter, and water molecules, as well as different bottom types that contribute to the signal as measured by a remote sensor in shallow water (adapted from Pinnel (2007))

3.4.2 Field spectra air-water correction

When direct and diffuse sunlight penetrates a lake surface, it may be absorbed or scattered by water molecules or by various suspended and dissolved materials present (see Figure

3.5). Only a fraction of the scattered and reflected photons find their way back to a remote sensor.

Following the pathway of light (known as the radiative transfer process) is paramount in understanding the various facets to remote sensing. The total radiance, (L_t) recorded by the remote sensor (Eq. [3.5]) is a function of the electromagnetic energy from the four sources (pathways) identified in Figure 3-7: first, incoming light can be scattered by the atmosphere back to a sensor (L_{sky}). Second, light can reach the water surface and be reflected back to the sensor. If this portion of light is reflected from direct sunlight it is called sunglint (L_{sungl}). Third, light can pass through the air-water interface, but be scattered back to the sensor by constituents within the water column (L_w), referred by the name *subsurface volumetric radiance* (or *volume reflectance*). This radiance value is related to the inherent optical properties (IOP) of the water.

A portion of this up-welling light is reflected down into the water body at the air water interface. Last, light can pass through the air-water interface, reaching a submersed substrate (macrophytes, bottom). Reflection occurs and light returns upwards through the water column exiting the air-water interface and reaching a sensor (L_b). This radiance value contains information on both water quality and substrate type (e.g. macrophytes, macroalgae, and sediment).

$$L_t = L_{sky} + L_{sungl} + L_w + L_b \quad [3-5]$$

Each remotely sensed signal from the surface water contains radiances from these four pathways. The atmospheric contribution, the air-water interface contribution, and the bottom substrate must be corrected in order to gain information on the water column component. To achieve the goal of identifying the optically active constituents in the water column, volumetric radiance L_w needs to be extracted from all the other radiance components being recorded by the sensor [Eq. 3-6]:

$$L_w = L_t - (L_{sky} + L_{sungl} + L_b) \quad [3-6]$$

The remote sensing analytical approach converts surface reflectance to volume reflectance. The volume reflectance is based on subsurface irradiance reflectance, which is nearly independent of atmospheric properties and is almost entirely determined by the optical properties of the water and its components (Lee *et al.* 1998; Turdukulov 2003; Wiangwang

2006). The equation [3-7] was originally suggested by Morel and Gentili (1993) and modified by Mobley (1994) for a description of remote sensing reflection:

$$R_{rs} = \frac{(1-p) * (1-p') * R(0-)}{1-r * R(0-) * n^2 * Q} + R_{surf} \quad [3-7]$$

Turdukulov (2003) derived the volume reflectance from equation [3-7] by developing the following equation [3-8]:

$$R(0-) = \frac{R_{rs} - R_{surf}}{\frac{(1-p) * (1-p')}{n^2} + r * Q * (R_{rs} - R_{surf})} \quad [3-8]$$

Where:

R_{rs} = is the remote sensing reflectance

$R(0-)$ = is the volume reflectance

R_{surf} = is a specular reflectance from the surface of the water body

Q = is a ratio of upwelling irradiance to upwelling radiance (5 sr^{-1})

p = is an internal Fresnel reflectance (0.03)

p' = is an air-water Fresnel reflection at the interface near nadir viewing angle (0.02)

n = is a refractive index of water (1.34)

r = is a water-air reflection (0.54)

Gege (2001) implemented this formula for calculating remote sensing reflectance in the WASI 2.0 (Water Colour Simulator) software. Values given in brackets are taken by default from the WASI 2.0 package (Gege *et al.* 2006). Equation [3-8] was successfully used by Lee *et al.* (1998) for calculating R_{rs} from simulated measured $R(0-)$ spectra. Turdukulov (2003) applied the abovementioned default values to River Sajo, Hungary and Wiangwang (2006) used these default values to obtain $R(0-)$ from field spectra taken from the Michigan inland lakes.

Sun glint from the water surface (specular reflectance, R_{surf}) can affect upwelling spectra measured above the water caused by waves or foam (Han and Rundquist 1998; Turdukulov 2003). In order to detect R_{surf} in the measured spectra, it was followed the assumption that the light absorption by pure water is predominant in NIR (970-1000 nm) and the water-leaving radiance in that region is close to zero (Ouillon *et al.* 1997). Contrary to this, Doxaran *et al.* (2002c) showed that this assumption can not be applied in highly turbid

waters and they proposed an averaging of the successive measurements. On the other hand, Han and Rundquist (1998) observed that the averaged reflectance spectra are still influenced by the specular reflectance. In this study the TSS range is moderately turbid (Figure 3-8b) and, therefore, it was followed the assumption of Ouillon *et al.* (1997).

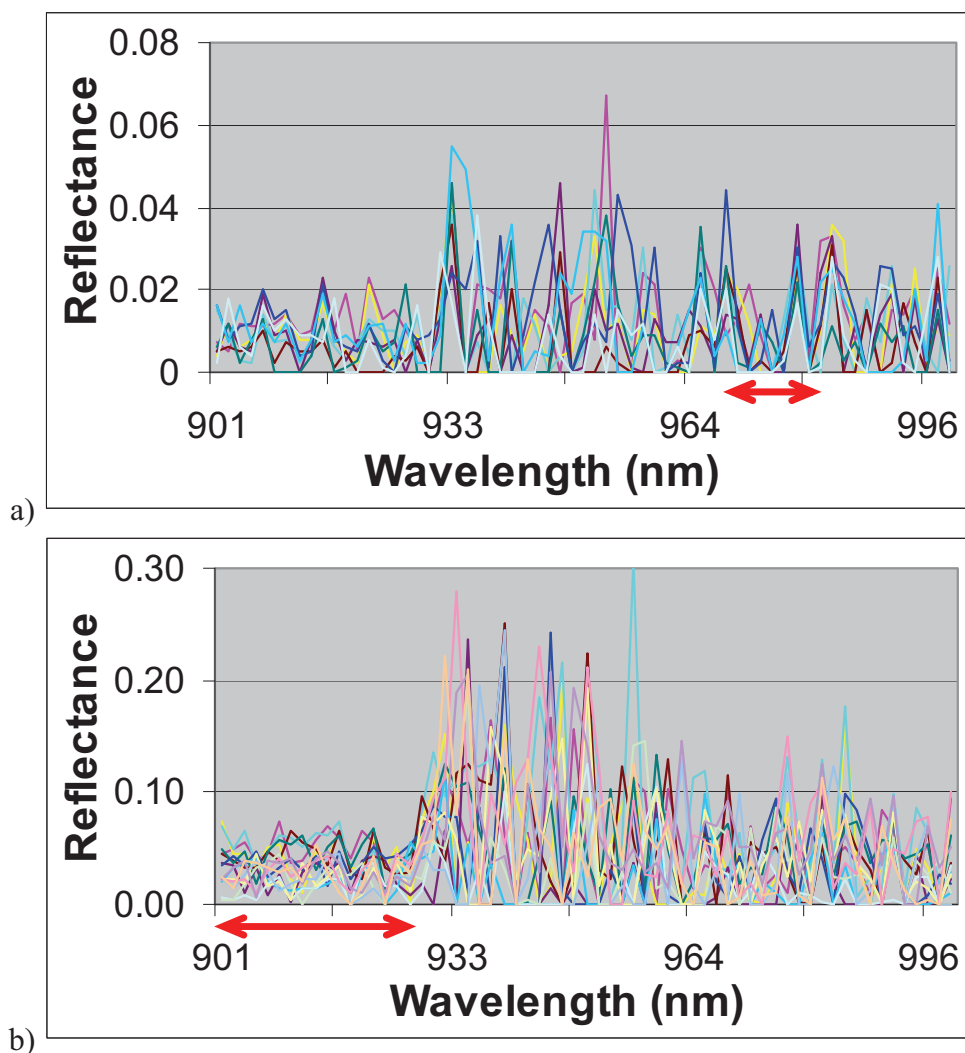


Figure 3-8: Spectra from K6. In low turbid water a) (TSS - 2.4 mg/L, on 23.08.2007) the spectra normalized between 970 nm and 980 nm. In moderately turbid water b) (TSS - 5.8 mg/L, on 06.09.2007) the spectra normalized at the minimum of 930 nm.

Taking into account the gradually increasing noise in the collected spectra, Turdukulov (2003) used minimum reflectance at 930 nm for volume reflectance calculations. Wiangwang (2006) applied the spectral range between 1,250 nm – 1,260 nm and found it more stable compared to other NIR regions.

In this study for low turbid lakes, the stabilized range between 970 nm and 980 nm was used (Ouillon *et al.* 1997), as shown in Figure 3-8a. For moderately turbid waters (Figure 3-8b), minimum reflectance at 930 nm was applied following the approach by Turdukulov

(2003). Only in a case of overcast skies (24.10.2007) was $R_{surf} = p'/\pi$ applied, according to Gege and Albert (2006).

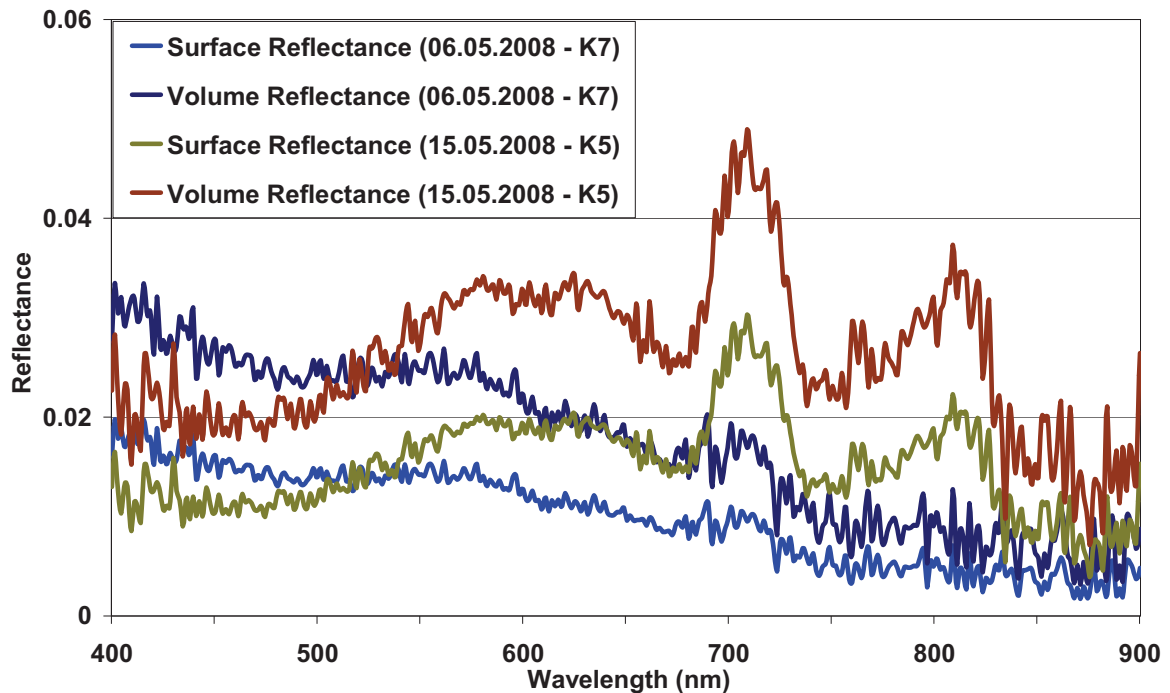


Figure 3-9: Comparison between remote sensing (surface) reflectance R_{rs} and volume (subsurface) reflectance $R(\theta_-)$ from two kettle holes.

Since all spectral data was always acquired at least ten times (in most cases 15-20 times) for low turbid waters (Figure 3-8a) the average minimum values in a range between 970 nm and 980 nm were used; for moderately turbid waters (Figure 3-8b) the average minimum reflectance values close to 930 nm were used (in the range of ± 1.5 nm). These average values were applied to remove specular reflectance and wave effects (assuming that they are wavelength independent) by subtracting them from the entire spectra. The calculated average minimum values of R_{surf} for clear sky conditions were between 0.005 and 0.0002.

Figure 3-9 shows the difference in the reflectance before and after the air-water interface was corrected. The corrected volume spectra are generally higher than the measured surface reflectance.

3.4.3 Reflectance filtering techniques

After using air-water correction the resulting volume reflectance spectra needed to be filtered to produce the data that are uncontaminated by noise from the atmosphere or the

sensor itself. Existing spectral analysis methods are based on the variation within the data (Gitelson *et al.* 2000; Kneubuehler *et al.* 2005); therefore, they are very sensitive to noise effects.

Noise can obscure important features such as peaks, valleys, or peak widths, or make the calculation of signal features such as slopes, areas and peak widths difficult (Wiangwang, 2006). The filter should maintain the sharpest absorption/reflectance features in the original signal. Mean and Savitzky-Golay filter (SGolay), Discrete Wavelet Transformation (DWT) and none-decimated DWT were used by Schmidt and Skidmore (2004) to smooth vegetation spectra. The same methods were applied by Wiangwang (2006) to the volumetric reflectance from Michigan inland lakes and it was found that the Savitzky-Golay filter proved to be best out of these approaches.

The application of the methods is based on the criteria that the selected model must smooth out high-frequency noise while maintaining the smallest features that could be associated with biophysical attributes (absorption troughs and reflectance peaks). We found that the higher polynomial do not provide more optical information than the lower ones; simple models were selected accordingly.

The ratio between the minimum near 670 nm and the maximum near 700 nm was successfully applied to the data obtained in highly diverse aquatic ecosystems dominated by different algal assemblages (Thiemann and Kaufmann 2002). The height of the peak above a baseline between 670 nm and 750 nm depends mainly on phytoplankton density and was used as its quantitative measure (Gitelson *et al.* 2000). Therefore, the region near 700 nm requires precise and accurate de-noising procedures.

Figure 3-10a shows that all smoothing filters in the range of 400nm and 800 nm performed well. This de-noising was done without a ‘noise decreasing’ procedure (see Appendix C) and the spectra were taken in normal weather conditions.

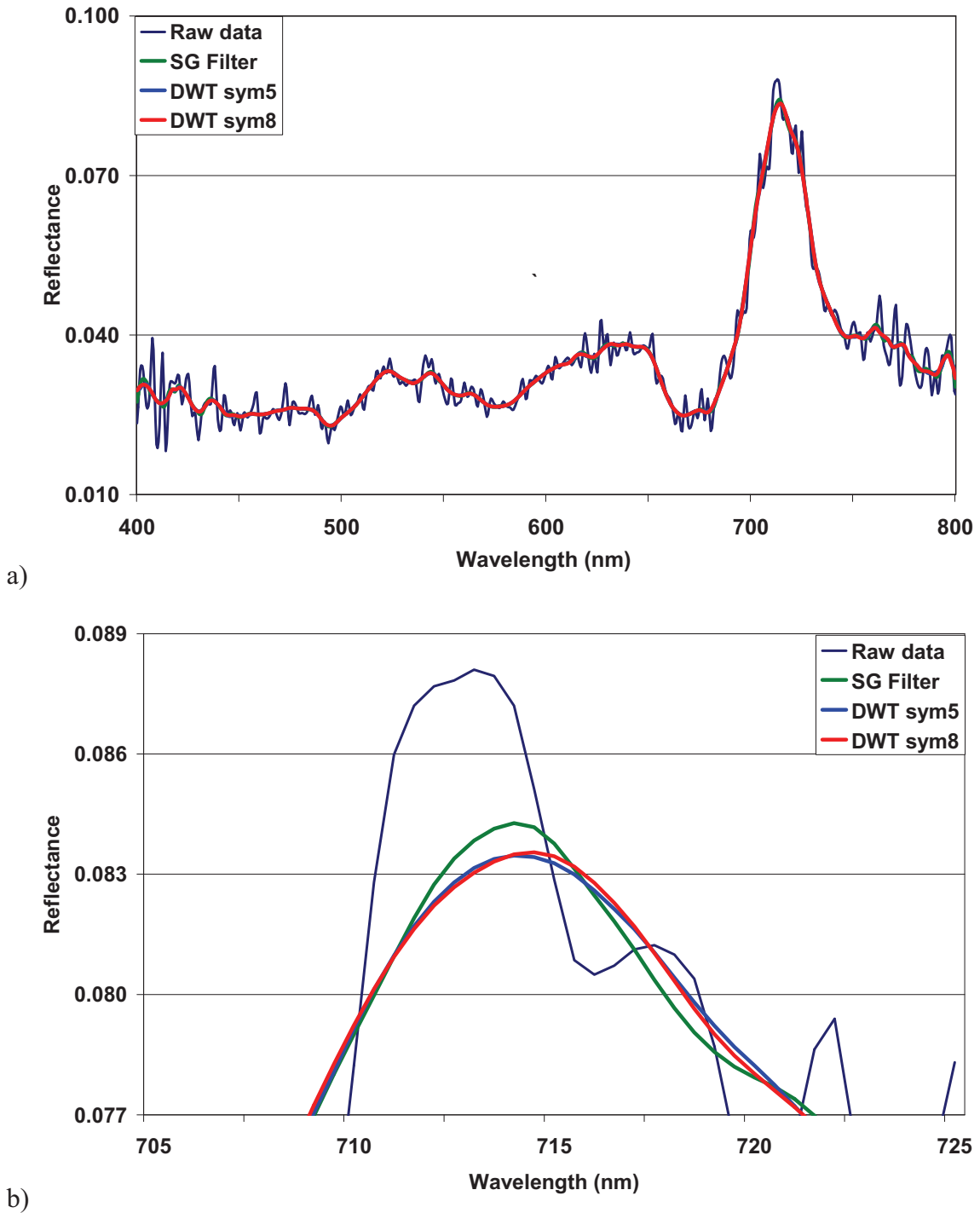


Figure 3-10: De-noised spectra taken from kettle hole K4 at 29.07.2008 (a). Result of de-noising algorithms in 705÷725nm region (b).

Figure 3-10b illustrates the results of filtering in 705÷725nm. Symlet *sym5* and especially Savitzky-Golay filters were shifted in the direction of the noised peak, whereas *sym8* Symlet preserved the exact position of the peak and height. Further calculation using the Position of Peak algorithm and first derivative analysis for all spectra from other dates showed that the performance of the *sym8* Symlet filter was correct.

All spectra were filtered using MATLAB R2008a software applying the Savitzky-Golay filter and Discrete De-noising Wavelets. In this study it was found that for clear sky conditions, it is best to use the DWT filter with a *sym5* or *sym8* Symlet wavelet depending on noise level.

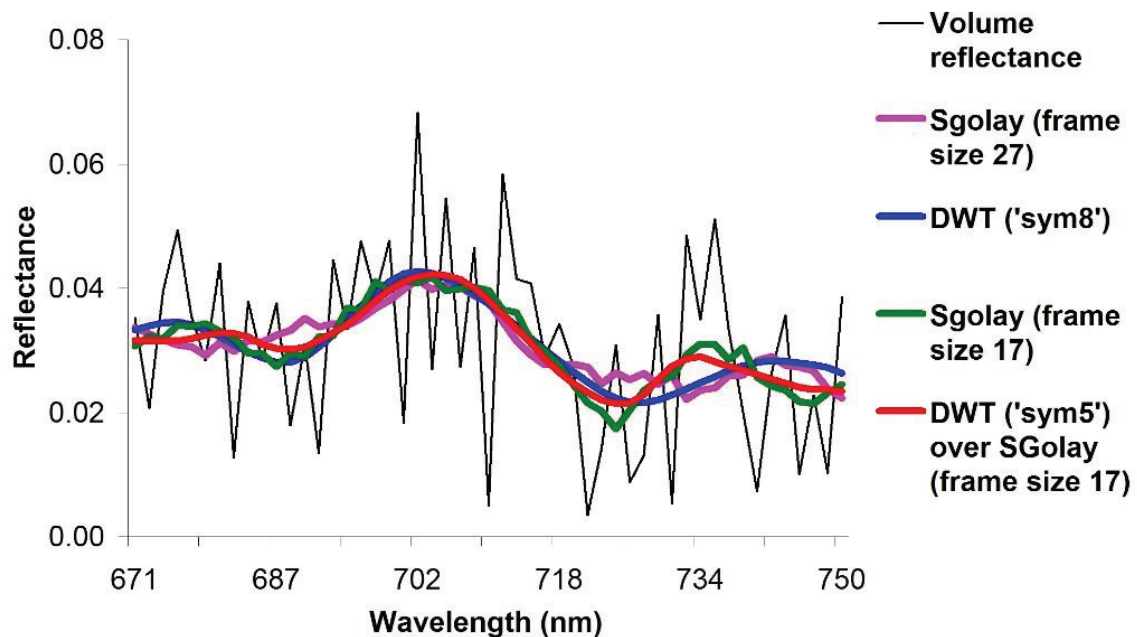


Figure 3-11: Noise removal filters comparison over volumetric reflectance as observed for K4 taken on 24.10.2007. The best performing filter is a combination of first the Savitzky-Golay Filter with a small frame size (e.g. 17) and then Discrete Wavelet Transformation with the *Sym5* de-noising wavelet.

Symlet *sym8* has a high filtering effect and was applied for filtering data from kettle hole K4. K4 is the largest investigated kettle hole and is situated in an open area where wind highly affects the reflection compared to the other kettle holes. We applied *sym8* only on data originating from kettle hole K4; for all others *sym5* was used. A Symlet wavelet seeks to preserve shapes of reflectance peaks and essentially performs a local polynomial regression to determine the smoothed value for each data point. This method is superior to adjacent averaging because it tends to preserve features such as peak height and width, which are usually ‘washed out’ by adjacent averaging. At the same time, in case of windy and overcast weather (Appendix D), the best performing filter was a combination of first the Savitzky-Golay filter with a small frame size (e.g. 17), and then Discrete Wavelet Transformation with the *sym5* wavelet (Figure 3-11). In all filters a polynomial degree of 3 best preserved the shape of the spectra and has been used for all data (Appendix C).

3.4.4 Spectral algebra

The semi-empirical algorithms applied in this work are all based on the use of reflectance data in the red and NIR range of the electromagnetic spectrum, since other portions of the spectrum are not suitable for chlorophyll estimation in Case II waters. Since pigment *in situ* data (Appendix B) indicated a eu- and hyper-trophic state of most of the sampled water bodies, the focus had to be laid on models which were already successfully tested in previous studies on water bodies with very high CHL content (Kneubuehler *et al.* 2005).

Peak Magnitude

Algal chlorophyll in water bodies has distinct absorption and reflectance features within reflectance spectra in the visible wavelength range (Gitelson 1992). One can distinguish the chlorophyll absorption bands near 435 nm and 675 nm and the distinct reflectance peak near 700 nm. The height of the reflectance peak near 700 nm in chlorophyll-laden waters is influenced by decreasing chlorophyll absorption and increasing absorption of pure water (Thiemann 1999). A graphical representation of the *Peak Magnitude* algorithm is shown in Figure 3-12a.

Peak Magnitude above a Baseline

The height of the mentioned peak above a baseline was related to CHL concentration for the first time by Neville and Gower (1977):

$$M_{Peak} = f(\lambda_m) - g(\lambda_m) \quad [3-9]$$

Where:

$f(\lambda_m)$ = the spectrum curve

$g(\lambda_m)$ = the baseline

M_{peak} = defines the wavelength of the maximum reflectance of the peak

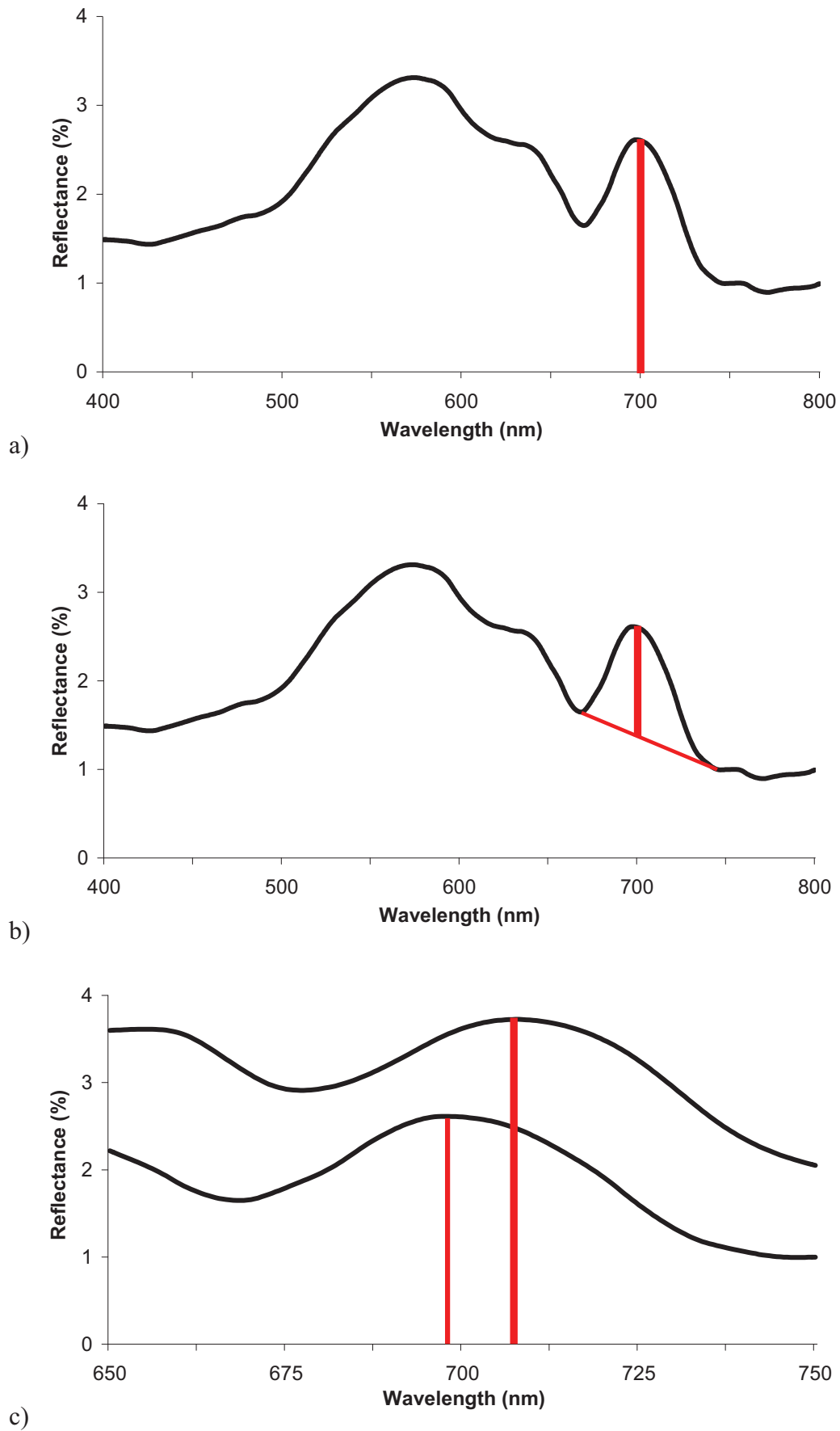


Figure 3-12: Semi-empirical algorithms for spectral signatures analysis: a) Peak Magnitude, b) Peak Magnitude above a Baseline and c) Position of Peak.

This algorithm correlates with chlorophyll concentration via the link between chlorophyll and algal biomass. According to Gitelson (2000), the magnitude of the peak depends on scattering by all suspended matter and thus increases with increase of phytoplankton biomass. An increase of the algal biomass leads to an increase of the active cell surface and thus to more scattering and higher reflectance values (Figure 3-12b).

Position of the Peak near 700 nm

The spectral position of the mentioned peak on the axis representing the wavelength is closely related to the chlorophyll content of the water body (Gitelson *et al.* 2000).

The increasing of absorption by chlorophyll leads to an offset of cell scattering at progressively higher wavelengths. Hence the position of the peak shifts toward longer wavelengths (Kneubuehler *et al.* 2005). This shift, measured in nm, can be used as a precise indicator for chlorophyll content. Unfortunately, the algorithm requires very narrow bands at a short sampling interval due to the short spectral range where the shift of the peak takes place. In an extensive study, Gitelson (2000) obtained R^2 values of over 0.9 and estimation errors of less than 2 nm for all water bodies (Figure 3-12c).

3.4.5 Spectral derivative analysis

The massive amount of hyperspectral data (the hundreds of spectral bands) may cause difficulties in traditional image processing and data handling techniques, although it provides information for analysis based on reflectance spectroscopic properties. Data used in spectroscopy are usually collected under controlled laboratory conditions with full control of the intensity and spectral distribution of the illumination as well as viewing geometry (Tsai and Philpot 1998). However, a well-defined spectrum and knowledge of spectral features provides sufficient information for a scientific interpretation of the real world features (Richards and Jia 2006). Absorption features are often observed in the reflectance spectra of specific substances. These features provide characteristics of the substrates of interest when a sufficient spectral resolution is obtained. Characterization, and thus automatic detection of such absorption features, is of particular interest in hyperspectral image recognition. Absorption features can be characterized by their locations (bands), relative depths and widths (full width at half the maximum depth). A complete spectrum can be divided into several regions and absorption features (Jensen 2006).

Derivative spectroscopy is a powerful tool that is commonly used in the analysis of hyperspectral remote sensing data from terrestrial environments (Tsai and Philpot 1998). Derivative techniques enhance minute fluctuations in reflectance spectra and separate closely related absorption features (Louchard *et al.* 2002). Derivative spectra indicate the rate of change of reflectance with wavelength ($dR(\lambda)/d\lambda$), which is the slope of the reflectance curve at wavelength λ . Derivative analysis allows one to correlate the shape of the reflectance pattern to chlorophyll concentrations. Derivative analysis has been applied by researchers in studying the spectral characteristics of chlorophyll and suspended sediments in water (Han 2005). Some major findings related to derivative analysis include: (1) the first-order derivative is able to remove pure water effects while the second derivative can remove suspended sediment effects (Goodin *et al.* 1993); (2) the first derivative at 690 nm is useful in estimating chlorophyll concentration in the presence of other water constituents (Han and Rundquist 1997); and (3) derivative spectra are an objective tool in isolating the absorption features of phytoplankton (Tsai and Philpot 1998).

Spectroscopic first derivatives were obtained by taking the difference between the reflectance of two bands and dividing that value by the difference between the wavelengths separating the two bands. The first step is to determine the slope of a line segment by simply dividing reflectance value differences by the wavelength interval separating them (rise/ run) as indicated by Equation [3-10]:

$$d^{1st} = (\rho_{n+1} - \rho_n) / (\lambda_{n+1} - \lambda_n) \quad [3-10]$$

Where:

- n = band number
- d^{1st} = 1st derivative (line segment slope)
- ρ = reflectance value
- λ = wavelength

Derivative analysis was applied to whole de-noised field spectral dataset and hyperspectral imagery for enhancing phytoplankton absorption features.

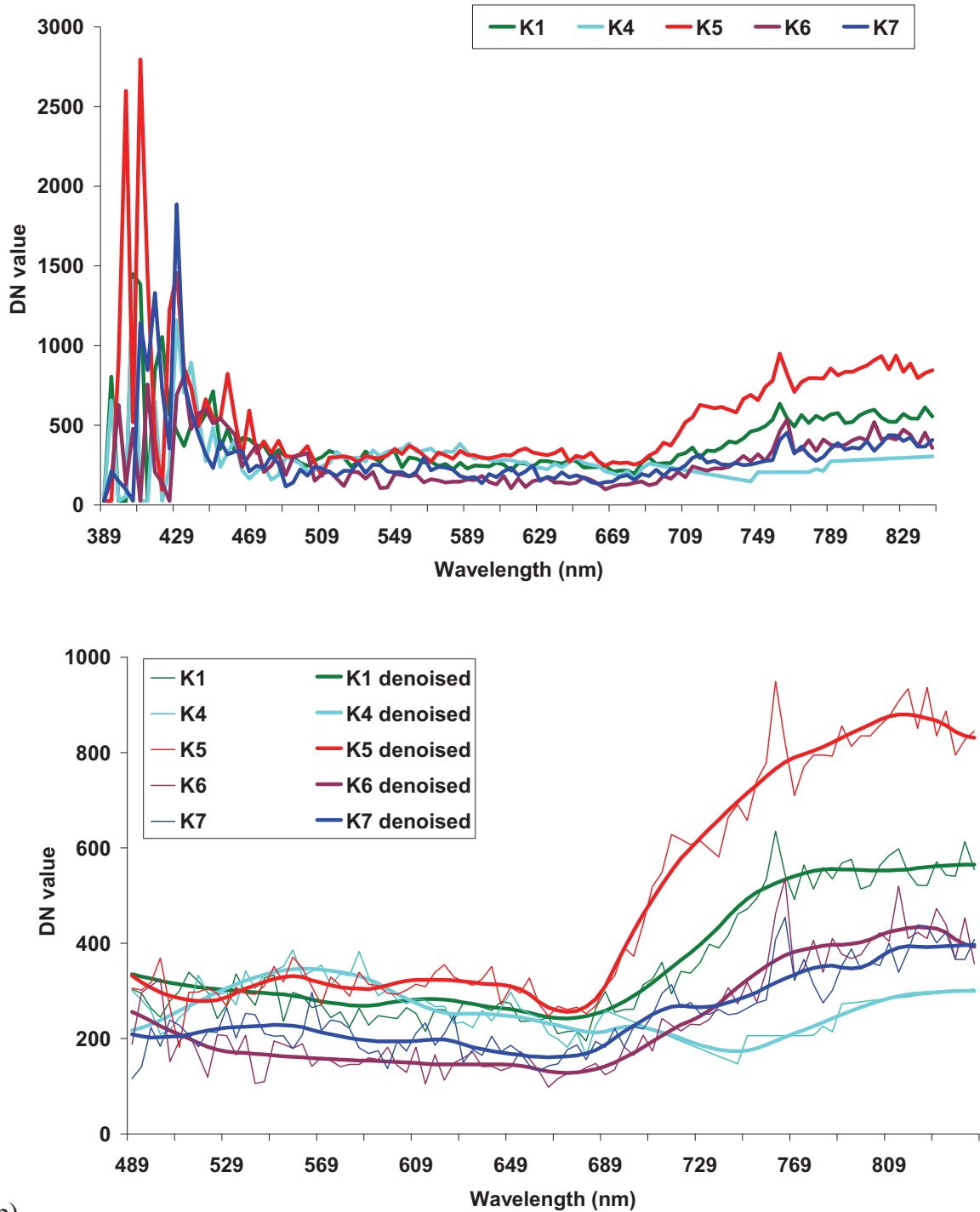
3.5 Methods for analysis of airborne images

Hyperspectral imagery analytical procedure in the form of flow diagrams is shown in Figure 3-5. The methodology of de-noising and derivative analysis is similar to field spectral processing. The water retrieval approach is based on spectral separation of water bodies and shadows.

3.5.1 De-noising of image spectra

The plot of kettle holes' spectral profiles in the ROSIS dataset illustrates that the range between 389nm and 480nm is highly noise influenced (Fig. 3-13a). This is mainly caused by the sensor performance in this range (Gege *et al.* 2008). Therefore, further processing of ROSIS data was focused on the range between 489nm and 845nm, i.e. 16÷115 bands which totals 90 bands. Analysis of spectral signatures of the lakes in that range showed that ground reflection of kettle holes is relatively noise contaminated (Fig. 3-13b). Atmospheric correction of low reflection (maximum DN values are less than 10,000, i.e. 10 %) and especially small targets like kettle holes is a very complex procedure and can not remove all noise effects from ground reflection (e.g. wind) especially with such high ground resolution of 2×2m. As mentioned above, even field spectra taken ≈30 cm above the water surface are still affected by noise. Consequently, the ROSIS image dataset has been smoothed using a combination of the Savitzky-Golay filter and Discrete Wavelet Transformation de-noising approach (Igamberdiev *et al.* In press). The resultant filtered spectral profiles of the studied kettle holes are shown in Fig. 3-13b.

The HyMap image dataset has a spectral interval of about 15nm with a ground resolution of 4×4m (which is almost 4 times coarser than the ROSIS resolution for both parameters) and the study of reflection profiles of kettle holes (see next chapter) showed that application of any filtering techniques can remove important absorption/reflectance features of the image spectrum, and thus, no smoothing methods were used.



b)

Figure 3-13: Spectral signatures of investigated kettle holes from ROSIS image on 15 May 2008; (a) Spectral profile of kettle hole in the range of 389 – 844nm (115 bands); (b) Noise removal filter comparison over kettle holes' reflections in the range of 489-844nm (90 bands)

3.5.2 Retrieval of water bodies from the airborne data

The existing spectral analysis methods of inland waters are based on the variation within the data (Dekker *et al.* 1996; Kneubuehler *et al.* 2005); therefore, spectral profiles of water

bodies have to be unique on the image in order to avoid any misclassifications with other land cover/use types. In reality, inland waters are mostly surrounded by different objects (e.g. trees) which are causing the effect of topographic shadows (Zhao *et al.* 2006). The confusion of topographic shadows and water bodies is very likely due to high spectral similarity in the 400÷900nm region (see Figure 6 a, b). Broadly, most of the proposed shadow removal approaches presented in the remote sensing field are either model based (use of 3D geometry and illumination of the scene) or image based (analysis of shadow properties) (Arevalo *et al.* 2008). These methods eliminate or remove the topographic shadow effects from all land use/cover types of the image (Sarabandi *et al.* 2004). In our study, we focused only on one land cover type (i.e. water); thus, we need an image mask containing just the studied kettle holes.

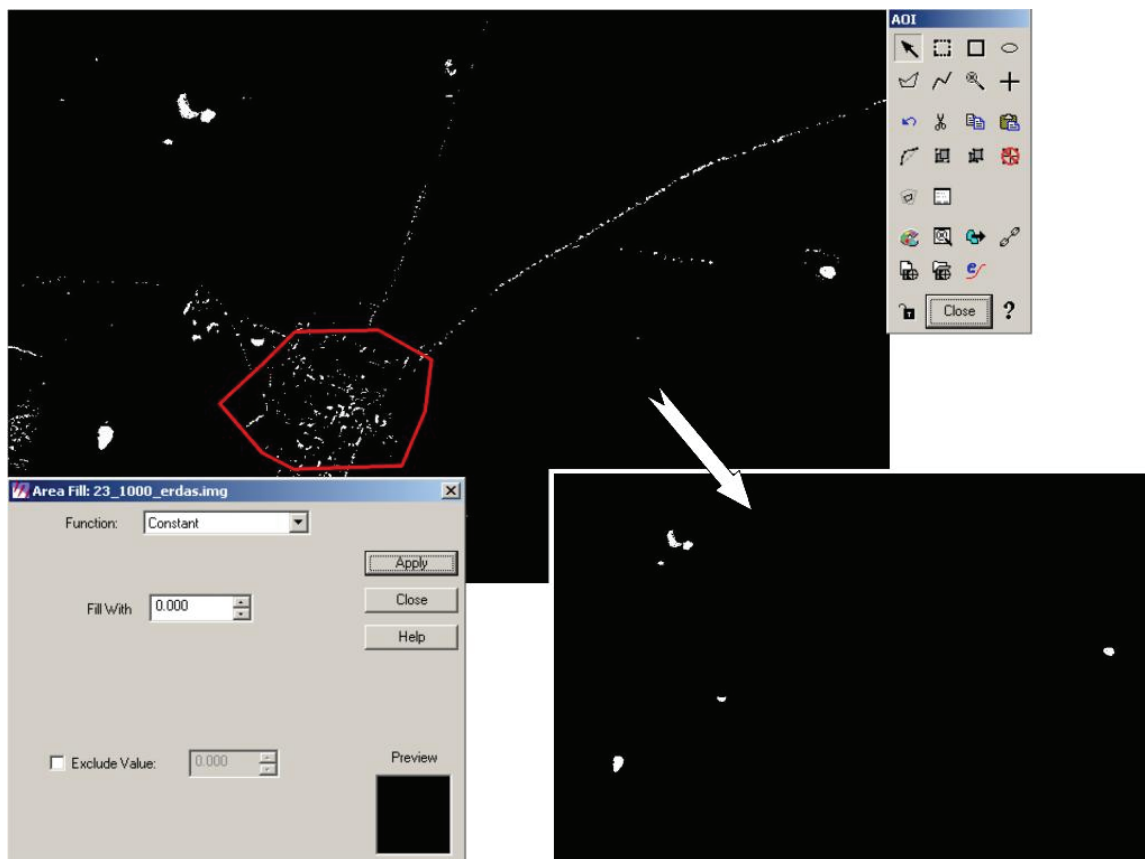


Figure 3-14: An image mask of water bodies created on band 23 of HyMap using 'Raster\Fill' and AOI tools of ERDAS Imagine Viewer (the red shows a polygon drawn using the AOI tool)

The analysis of the spectral signatures of the water bodies and shadows (see next chapter) shows that the reflectance near 770nm (83 band of ROSIS and 23 band of HyMap) over 10% belongs to another land cover type. Hence, it is simple to create a mask for both datasets with '1' value for all objects less than 10% (i.e. 1000DN) and '0' for the rest of

the image (Figure 3-14, upper image). On this image we can easily recognize interested water bodies (big circled white spots) and shadows (small dispersed dots). As is seen, the shadows mostly distributed within the settlement area or along the roads. The next step will be eliminating the shadows or other unnecessary objects like small ponds within the settlement area. First, a polygon needs to be carefully drawn over the shadow area using the AOI (Area of Interest) tool; then, '0' is applied to the mask over this area using the 'Raster\Fill' tool in ERDAS Imagine Viewer (Figure 3-14). These two procedures should be continued until the image mask of only the interested waters is created. The resulting raster map is applied as a binary mask to create water-only hyperspectral imagery of the original brightness from the airborne data.

3.5.3 Derivative analysis of image spectra

Received water-only hyperspectral imagery has been processed using equation [3-10] to a new imagery dataset based on the first derivative analysis. The creation process of the first derivative imagery dataset involves the use of ENVI 4.3 and MATLAB R2008a software packages. ENVI can export hyperspectral data to the binary file which can be easily imported to the MATLAB environment. MATLAB has powerful processing tools for technical computation and visualization of large binary datasets. A simple MATLAB routine developed for first derivative calculation using an imported hyperspectral binary file is shown in Appendix E. This routine calculates all non-zero elements using equation [3-10] and saves them to new datasets. The resulting first derivative datasets (i.e. matrixes) are imported to ENVI and saved with the same geo-referential and spectral parameters as the original ROSIS and HyMap imagery.

Examples of original and first derivative calculated spectra from kettle hole K6 are shown in Figure 3-15. It is clearly seen that derivative spectra have several peaks centenary to original curves. The biggest peak is in the 680÷687nm range. This peak represents the ascending side of the so-called '700 nm peak' and is considered as the important spectral range where the first derivatives are indicative of the concentration of chlorophyll-a (Han 2005). Note that the spectral position of the '700 nm peak' generally varies with chlorophyll concentrations (Gitelson 1992; Thiemann 1999). So the 680÷687nm may also vary in position accordingly. For example, a strong correlation between the first derivative and chlorophyll was found at 690nm for an inland water case (Han and Rundquist 1997).

Han (2005) found that the first derivative at 686nm produced the highest positive correlation with chlorophyll-a concentration ($R^2=0.858$).

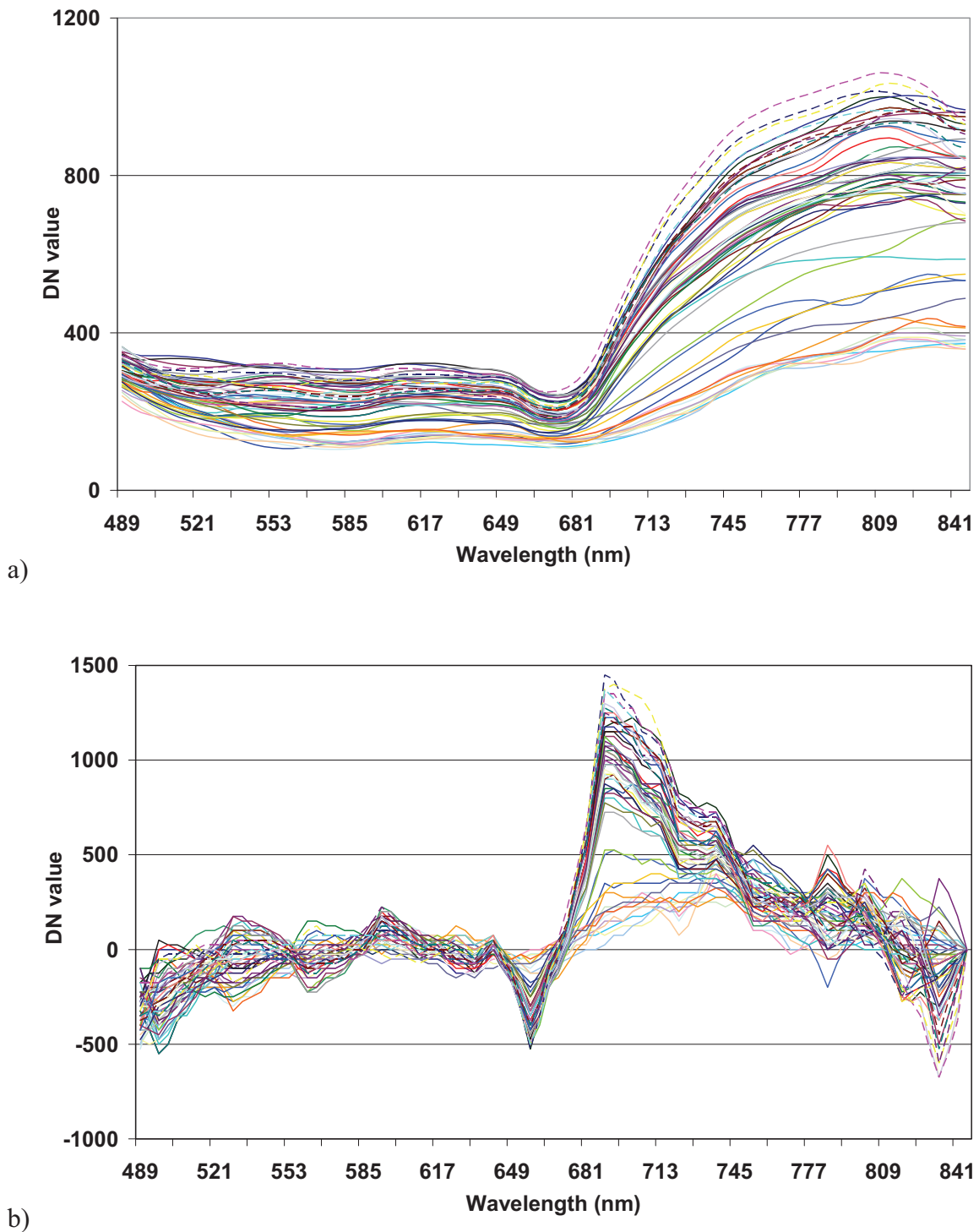


Figure 3-15: Original reflectance (a) and calculated first derivative (b) spectra on ROSIS image from kettle hole K6

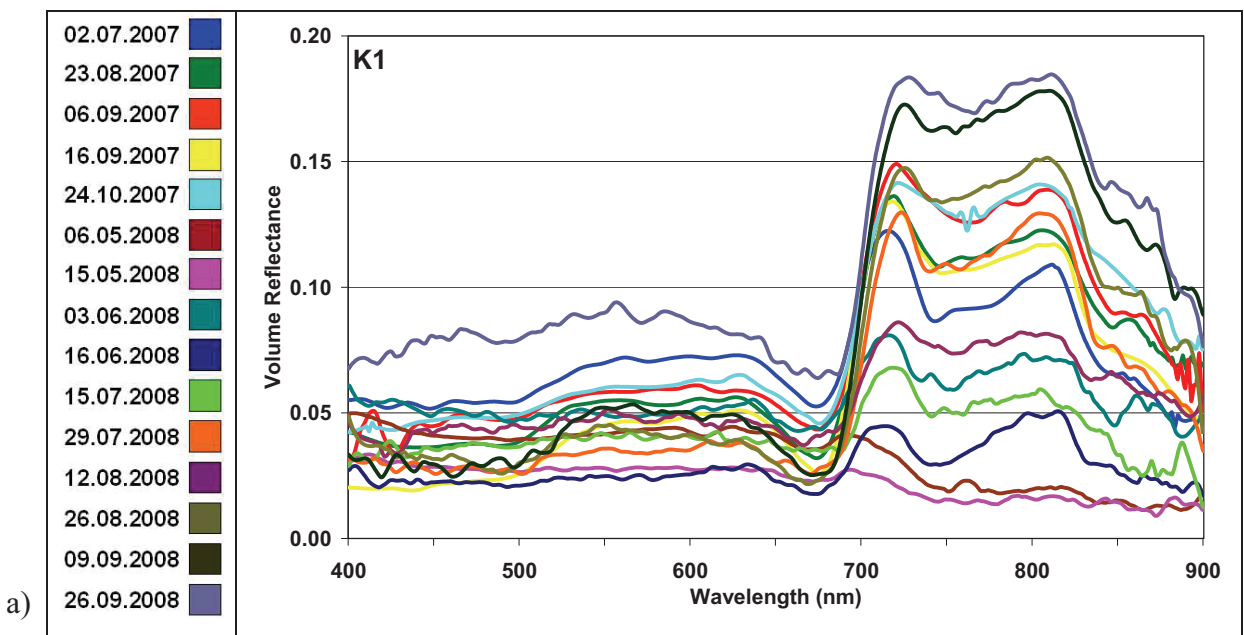
4 Results and discussions

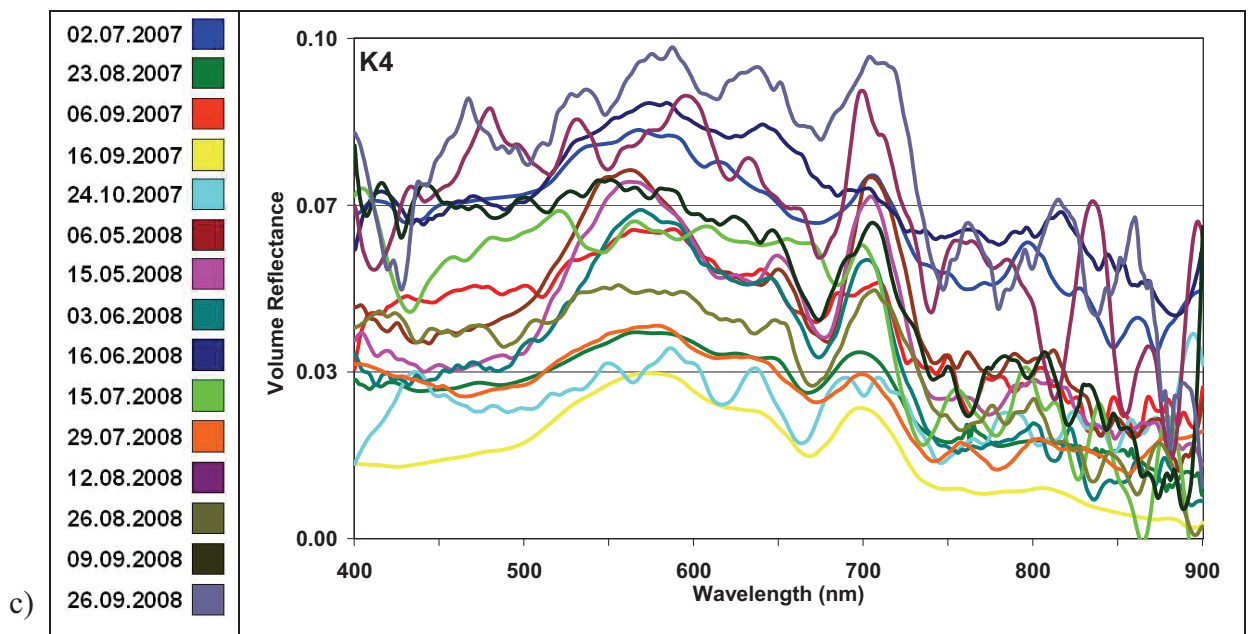
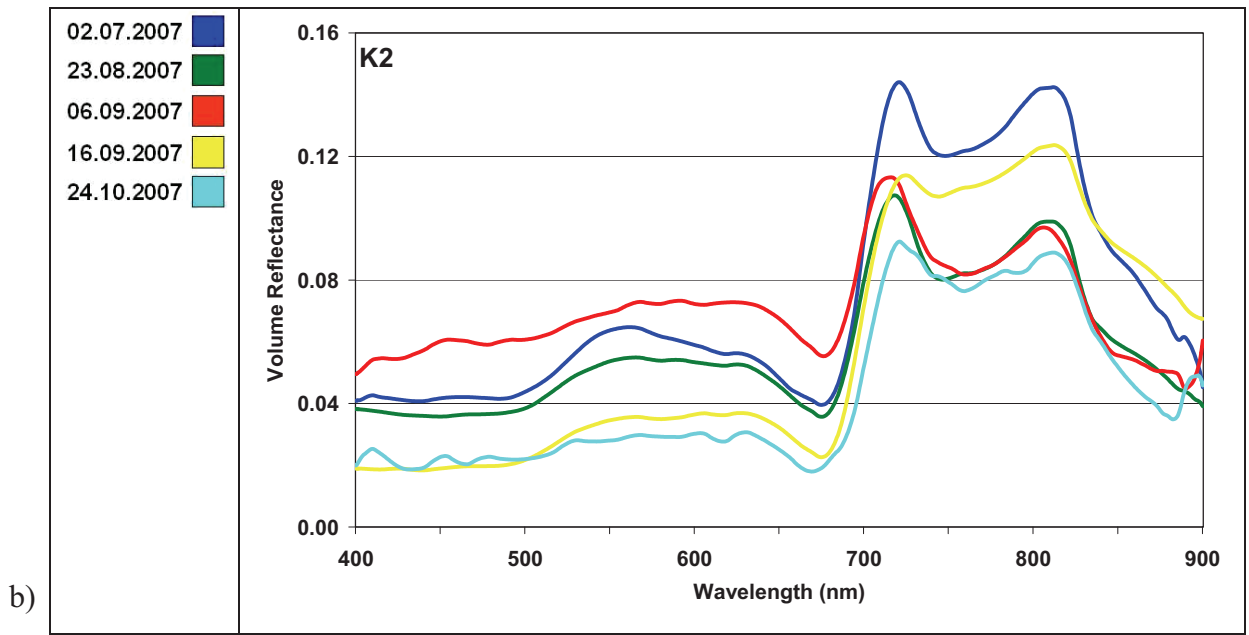
Broadly speaking, the results of this study can be divided into two sections: (1) seasonal and cross-seasonal analysis of normalized volume reflectance and derivative spectra from each kettle hole, application of semi-empirical algorithms for biomass estimations and accuracy assessment of these methods; (2) analysis of airborne hyperspectral imagery from ROSIS and HyMap sensors (acquired on 15 May and 29 July 2008 respectively) and field spectra for estimation of spatial and temporal variation of water quality parameters chlorophyll content, water depth (transparency) and total suspended sediment. Finally, at the end of this chapter the most sensitive spectral bands that are used for water quality parameters estimations in various types of kettle holes are discussed.

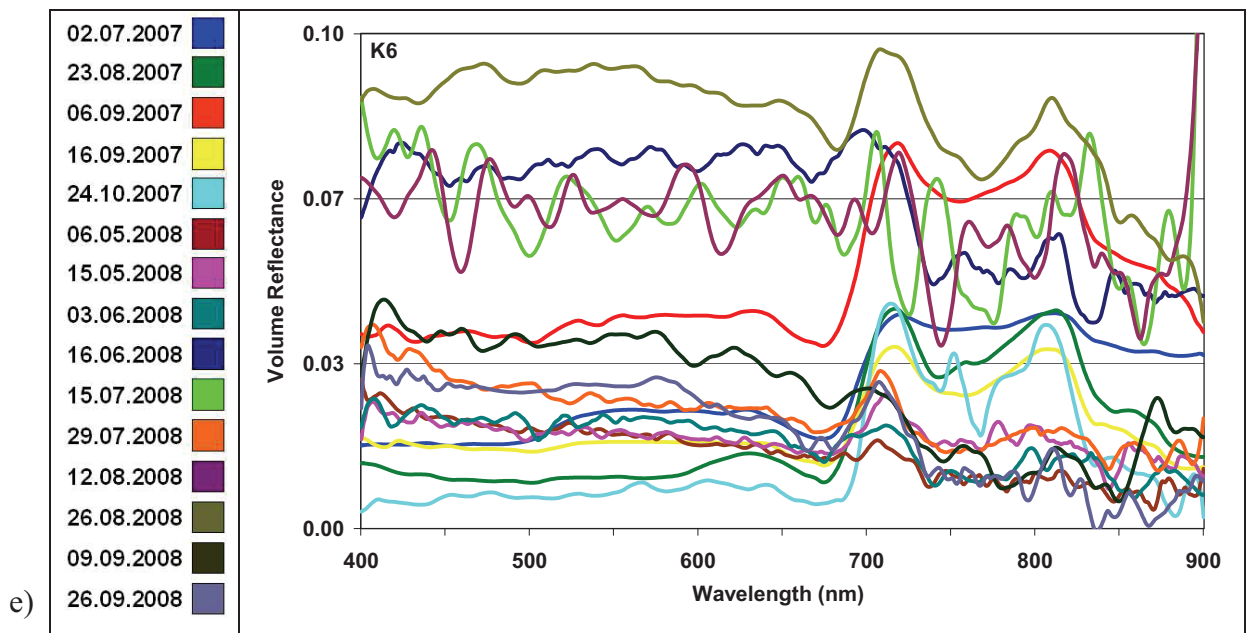
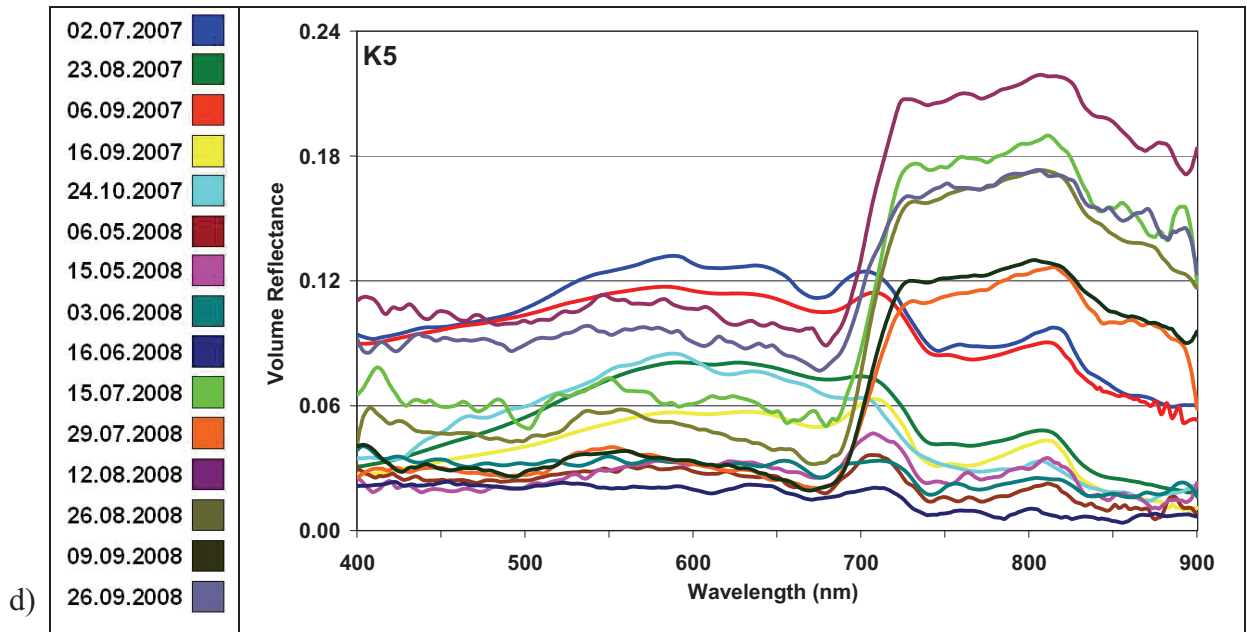
4.1 Analysis of handheld spectra

4.1.1 Spectral signatures of kettle holes

Spectral field data were collected in the agricultural seasons of 2007 and 2008 resulting in 15 datasets (5 in 2007, 10 in 2008). All field spectra were processed to volume reflectance using the methodology described in chapter 3.4.2. The spectral signatures of the kettle holes from fifteen field campaigns are shown in Figure 4-1.







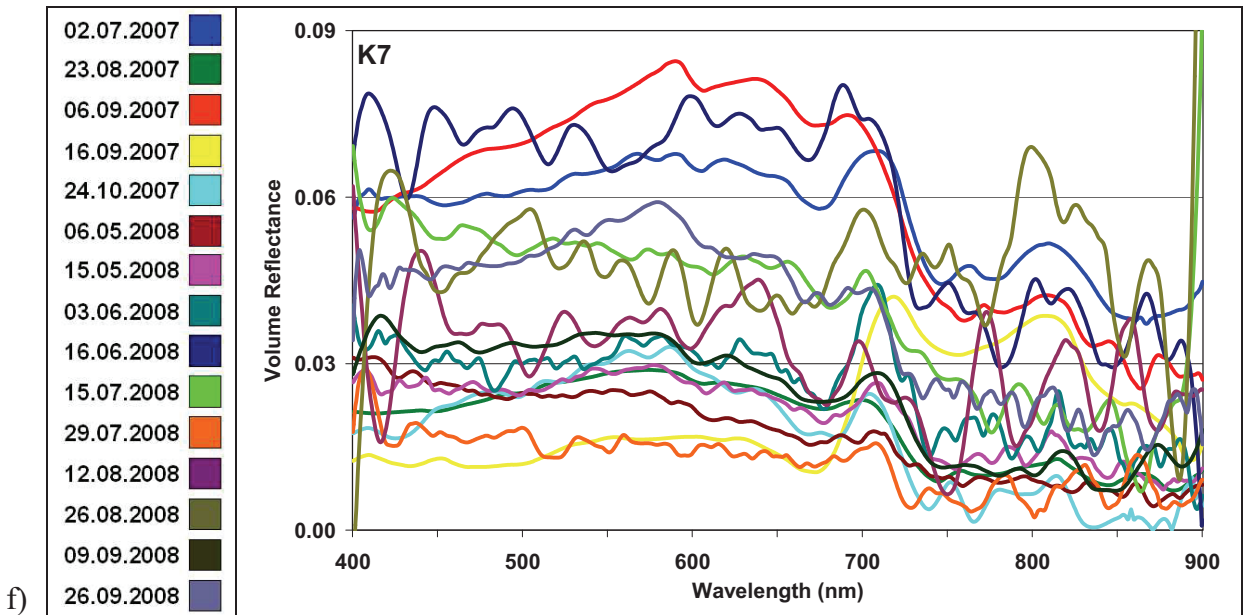


Figure 4-1: Kettle holes' volume reflectance collected in 2007 and 2008

4.1.2 Seasonal and cross-seasonal spectral response

The spectral curves from K1 in 2007-08 are comparable to reflection spectra from vegetation cover with a smaller magnitude. The signal is most likely caused by high algae content. In K1, algae plants grew almost to the surface. The reflectance in the Green electromagnetic spectrum (500÷600nm) is characterized by the first chlorophyll peak (i.e. the algae spectral response from the bottom). The Red/NIR range (650÷850nm) has the highest magnitude and two distinctive reflection peaks following one after another. The first Red/NIR range peak is higher than the second. At the same time, the two spectral curves from 06.05.2008 and 15.05.2008 have the lowest peaks (0.41 and 0.28 accordingly) compare to the others. This low reflection magnitude was mainly caused by two factors: high water level and low reflection of new growing algae at the beginning of the agricultural year. At low water levels and with maturely grown algae, the reflection curves have similar shapes with differences at the peak near 700nm which range between 0.44 and 0.18 (Figure 4-1a).

Overall, in this type of kettle hole (permanent water regime, 'big shallow', see typology in Table 3-1) the seasonal and cross-seasonal spectral curves are similar in the shape. The difference is only in the magnitude of reflection which was caused by water level, algae growth maturity and chlorophyll concentration. The differences caused by chlorophyll concentration are discussed in the next chapter.

Spectral signatures from K2 taken during the 2007 agricultural season are similar to K1 reflection spectra and are influenced by algae. In K1, algae plants grew almost to the water surface, whereas in K2 algae extended to 20-35cm below the surface. This depth difference is sensed by the spectrometer; overall the reflectance at K1 in 2007 and mostly in 2008 had values above 0.12, while K2's values were lower (0.09 - 0.11) at the 700 nm peak (Figure 4-1b). K2 in 2007 belonged to the 'big shallow' subtype with a semi-permanent water regime. In summer 2008, kettle hole K2 is dried out due to intensive agricultural activities at the shore line, and consequently it was excluded from further monitoring programmes.

K4 is the most turbid kettle hole (see Appendix B). K4 is around 3m deep, has a size of ≈ 0.8 ha and can be considered as a small lake; accordingly its spectral response is like a moderately turbid lake. The surface reflectance shapes of kettle hole K4 are comparable to the curves described by Dexoran *et al.* (2002a). The spectral response curves of K4 have a distinctive peak in the Green range caused by blue-green algae. The magnitude of this peak is comparable with the reflection peak at the Red/NIR region. The peak at 700nm is clearly seen in all spectral curves. This type of reflection peak at 700 nm is commonly used in remote sensing for chlorophyll concentration determination (Dekker 1993; Gitelson 1993). Two years of field observation of K4 revealed that it has a relatively stable water level and the highest variation in pigment concentration values (CHL ranges between 35 μ g/L and 225 μ g/L) compared to the other kettle holes (see Appendix B). Therefore, the seasonal and cross-seasonal variation of spectral curves has a similarity in shape, and the differences in magnitude depend on chlorophyll concentration (Figure 4-1c). For the received spectra, the range in 750÷900nm is characterized by high signal variation which consequently stabilized at 930nm or 970÷980nm regions (see Chapter 3.4.2 for reference).

Kettle hole K5 had the highest spectral magnitude and shape variation within the two years of field observations. In 2007 K5 had a brown water colour and consequently low transparency. In 2008 the situation changed due to a different amount of precipitation in the summer period. In the research area, the summer of 2007 provided less precipitation than the summer of 2008 which subsequently influenced the amount of water that reached all water bodies including kettle holes (DWD 2007; DWD 2008). The TSS values of 7 June and 2 July of 2007 were 100mg/L and 111mg/L accordingly, with an average value for the whole season of 36mg/L. In summer/autumn of 2008 the average TSS values were around 14-15mg/L (Appendix B). Therefore, the spectral signatures of K5 have two types of reflectance shapes: those influenced by turbid water and submerged vegetation. For the

whole field campaign of 2007 and the beginning of 2008, pond K5 had light brown (turbid) coloured water (Table 3-1). Consequently, the spectral response from moderately turbid water is described by Doxaran *et al.* (2002a). Starting from June-July 2008 the rain raised the water level and caused intensive growth of algae and subsequently changed the surface reflectance (Figure 4-1d). The analysis of spectral signatures of K5 shows how the changes take place in small shallow water bodies on a hyperspatial scale, and highlights their influence on the remote sensing signal.

Field investigations of the shape and size of K6 and K7 revealed that both water bodies used to be one kettle hole (see Figure 3-2). Gradually the water level lowered which split them up and caused intensive growing of grass at the edges. In terms of altitude, K6 is located lower than K7. The lower positioned K6 collects most of the surface runoff (consequently dissolved and particulate nutrients) from the surrounding catchments area which causes intensive algae growth. Therefore, the corresponding spectral response of K6 has various shapes mainly dominated by submerged vegetation reflection curves (Figure 4-1e). Contrary to other spectra, the volume reflectance signature calculated from up-welling radiance acquired on 15 July 2008 has the highest variation in shape. The calculated volume reflectance (which partially reduces the noise level) and subsequently the mean spectra are highly noise influenced (Appendix F). The main reason for this variation is the overcast and windy weather conditions on the collection date (Appendix B). Filtered spectra (see chapter 3.4.3) have several peaks in VIS/NIR ranges with the highest at 700nm. Overall, the spectral response of K6 shares a similarity with the reflectance from K1 or K2 but with a smaller magnitude.

Contrary to its neighbour, K7 has a sandy bottom and some small algae patches. The magnitude of reflectance is almost similar to K6, but the shape of the signal is different. The spectrum curves of K7 were similar to the reflection of low turbid waters as described by Ouillon *et al.* (1997) and Doxaran (2002a). The sand spectrum is more reflective in the longer wavelength and has a steeper visible NIR slope than the algae spectrum (Figure 4-1f). This implies that biomass estimation indices constructed from Red and NIR bands may be influenced by brightness, slope and nonlinear mixing effects associated with the differences of spectral signatures of sand and algae (Murphy *et al.* 2005). Overall, the reflectance shapes of K7 have a high peak at the Red range and a distinctive peak at 700nm.

Finally, analysis of the spectral response of investigated water bodies shows that the shape of the reflectance curves depends on hydro-morphological characteristics (shape, size, depth, bottom type and shore slope) of kettle holes, surface runoff, acquiring weather conditions and the level of algae distribution.

4.1.3 Spectral algebra algorithms and biomass concentrations

Seasonal and cross-seasonal de-noised volume reflectance from all kettle holes has been tested for with existing semi-empirical algorithms based on spectral algebra (see chapter 3.4.4) and first derivative analysis (see chapter 3.4.5).

Kneubuehler *et al.* (2005) analyzed all existing semi-empirical algorithms for spectrophotometric data collected from shallow lakes with a water depth of app. 1-2m. The *Magnitude of the Peak above a Baseline* and the *Position of the Peak* algorithms showed very good results when using a linear curve fit with a relative error of 8% and 6% accordingly. Figures 3-12a and 3-12c show graphs of both algorithms. The ratio between the minimum near 670 nm and the maximum near 700 nm was successfully applied to the data obtained in highly diverse aquatic ecosystems dominated by different algal assemblages (Gitelson *et al.* 2000; Thiemann and Kaufmann 2002).

The height of the peak above a baseline between 670 nm and 750 nm depends mainly on phytoplankton density and was used as its quantitative measure (Gitelson *et al.* 2000). In the case of K1, K2 and K6, spectral signatures are highly influenced by phytoplankton and correspond to the vegetation reflectance shape with lower magnitudes. From this type of curve, the maximum magnitude near 700 nm (Figure 3-12b) produces the best results (see the next chapter).

The effectiveness of derivative analysis in estimating chlorophyll-a concentration from coastal water has been tested by Han (2005). This study proved that the derivative spectra were more independent of wave effects and therefore continued to show the absorption features of chlorophyll under windy conditions. The spectral regions of derivative spectra 630–645 nm, 660–670 nm, 680–687nm and 700– 735nm were found to be potential regions where the first derivatives can be used to estimate chlorophyll concentration.

The theory of chlorophyll-laden waters showed that decreasing CHL absorption and increasing absorption of pure water is the major factor influencing the reflectance peak near 700 nm (Dekker *et al.* 1995; Thiemann and Kaufmann 2000). Thus, the vast majority

of investigations were dedicated to establishing correlations between CHL and remotely sensed data. At the same time, Kneubuehler *et al.* (2005) determined 0µg/L CHL concentration for two samples of the same lake, whereas received spectra showed presence of at least small contents of chlorophyll. However, the majority of algae in a water body are cyanobacteria that only contain CHL (Scheffer 1998), so laboratory measured TCHL was used for the regression analysis assuming that TCHL represents the concentration of CHL solely. By using TCHL the same assumption was followed. Therefore, algorithms based on spectral algebra and derivative analyses were applied for both biomass concentrations values, i.e. CHL and TCHL.

4.1.4 Application of spectral algebra algorithms for biomass estimation

Kettle hole K1

Figure 4-2 illustrates the first derivative spectra of kettle hole K1 calculated from the volume reflectance for the 2007 and 2008 datasets. The first derivatives for steeper slopes of reflectance curves tended to have higher absolute values. Note that the much greater variations among the spectra that appeared in figures 4-1a did not appear this time for their derivative spectra. The peak in the 680-700nm range which corresponds to the so-called ‘peak near 700nm’ can clearly be seen.

To test if the reflectance value at a specific wavelength can be used to estimate chlorophyll concentration, Pearson’s correlation coefficients (R) were calculated for volume and derivative spectra including seasonal (2007 and 2008) and cross-seasonal (2007-08) variations (Figure 4-3). As can be clearly seen, the reflectance value at 712nm wavelength has the best cross-seasonal correlations for CHL and TCHL, whereas values at 721nm and 751nm are most correlated for 2007 and 2008 seasons respectively (Figure 4-3a). Reflectance values at wavelength 712nm and 721nm clearly represent chlorophyll peak reflectance near 700nm while at 751nm it is chlorophyll absorption (see Figure 4-1a). Therefore, the volume reflectance values for these specific wavelengths were taken into the calculation procedure. Contrary to volume reflectance, the derivative spectra for the 2007 and 2008 seasons has only one specific wavelength at 711nm with the best correlation coefficients. However, cross-seasonal correlation between derivative spectra at the 697nm wavelength and biomass concentration produces the best result. Finally, it has to be noted that all correlations between biomass concentrations and volume reflectance and derivative

spectra have the best coefficients of determination from linear regression but with a negative slope.

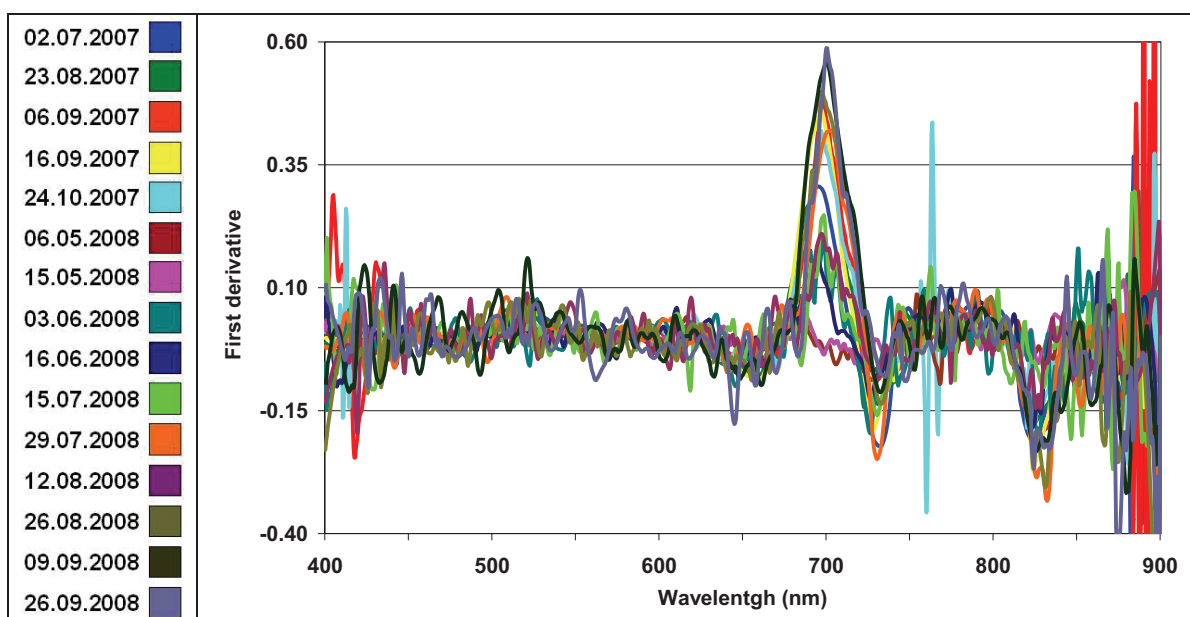


Figure 4-2: First derivative spectra of kettle hole K1 calculated from volume reflectance for 2007 and 2008 datasets

The reason for a negative relation between chlorophyll content and specific spectra criteria has been discussed by Scheffer (1998) with respect to the eutrophication of the shallow lakes. The available nutrients will either cause intensive algae growth or the cyanobacteria will benefit from the nutrient input and the lake will become turbid with a dark green colour. At a high water level chlorophyll is dissolved in the water column and the bottom reflectance has a low effect on the up-welling radiance. A low water level causes the ‘packaging effect’ (packed chlorophyll onto phytoplankton cells reduces light attenuation, Kirk 1994) and bottom reflectance contributes significantly to surface reflectance. However, K1 is completely covered with algae so that the water-leaving radiance above the surface has a low contribution from the bottom reflection. Therefore, it was not necessary to take explicitly into account the bottom reflection in the spectral analysis. At the beginning of June, K1 was characterized by a comparatively high water level and CHL values, as caused by fertilization, and a lower magnitude of spectral reflectance. Gradually the water level went down and the algae content increased, which altered the reflection.

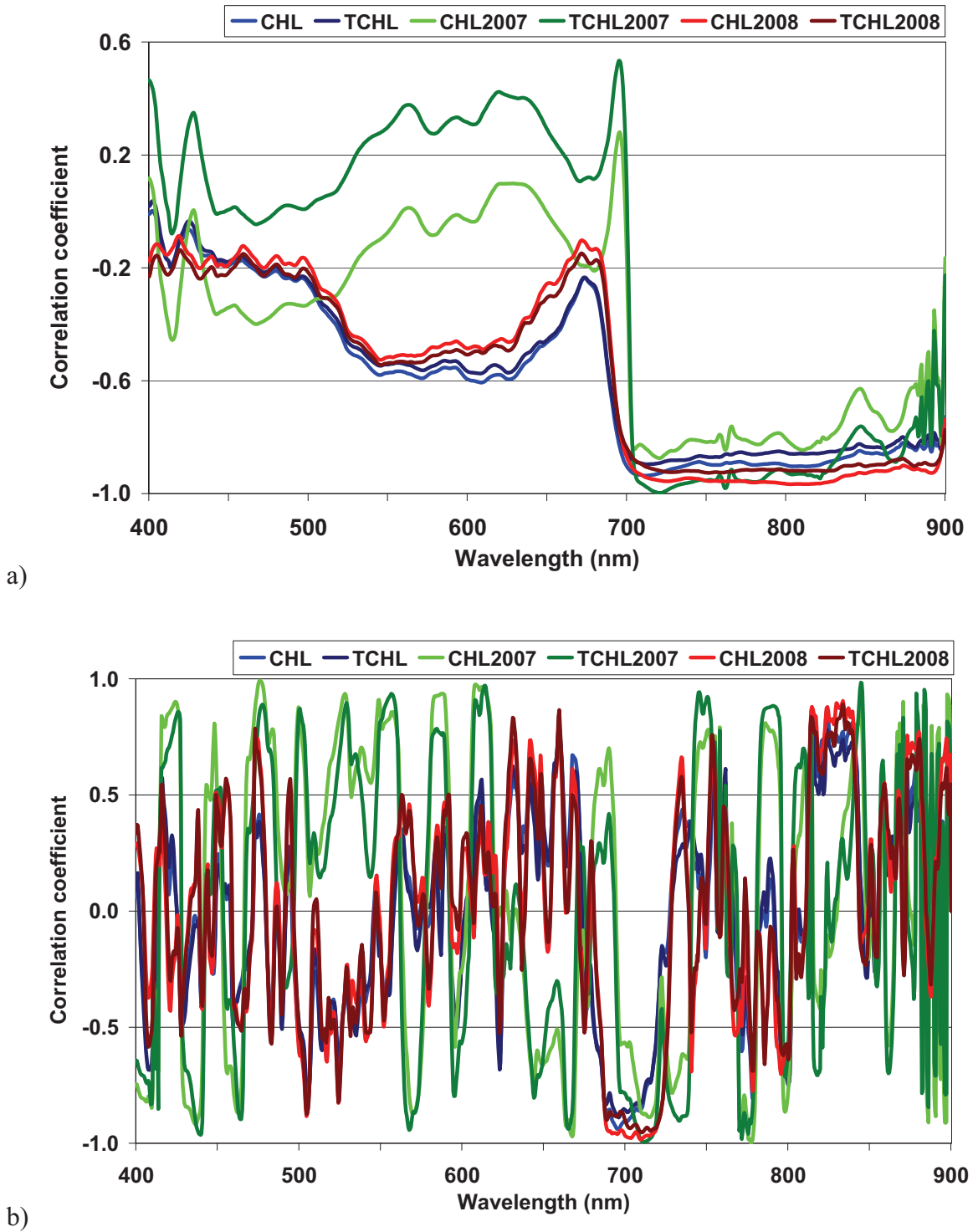


Figure 4-3: Pearson's correlation coefficients (R) for kettle hole K1 between volume reflectance, derivative spectra and biomass concentrations for seasonal (2007 and 2008) and cross-seasonal data (CHL and TCHL for 2007-08)

For example, for the season of 2007, the spectra of K1 had a magnitude of 0.1225 with a TCHL of 23 $\mu\text{g/L}$ on 02.07.2007 and a magnitude of 0.1490 with a TCHL of 16 $\mu\text{g/L}$ on 06.09.2007.

Table 4-1: Coefficients of determination from linear regression using various methods between normalized volume reflectance and biomass concentration for kettle hole K1 (n=15 in 2007-08, n=5 for 2007, n=10 for 2008)

	2007-08		2007		2008	
	CHL	TCHL	CHL	TCHL	CHL	TCHL
Magnitude at 712nm (721nm, 752nm)	0.8789	0.8030	0.7639	0.9959	0.9132	0.8583
Peak Magnitude	0.8591	0.8000	0.7749	0.9970	0.9169	0.8649
Position of Peak	0.4439	0.3210	0.5614	0.8720	0.5740	0.3755
Peak Magnitude above a Baseline	0.9302^a	0.8550	0.2691	0.5594	0.9306	0.8190
Magnitude at 697nm of 1 st derivative	0.8731	0.7814	0.7644	0.9861	0.9530	0.9037
Peak Magnitude of 1 st derivative	0.8482	0.7705	0.3309	0.6051	0.9379	0.8146
Position of Peak of 1 st derivative	0.31.86	0.2227	0.4883	0.7708	0.4578	0.3205

^a By bold showed best received correlations using volume reflectance and derivative spectra.

Table 4-1 gives coefficients for linear regressions using different algorithms between biomass concentration (CHL and TCHL) and normalized volume reflectance and derivative spectra.

The analysis of Table 4-1 shows that for the season of 2007 the best linear regression coefficients were between TCHL and the normalized and derivative spectra. The best correlation algorithms using normalized reflectance for season of 2007 were *Peak Magnitude* and *Magnitude at 721nm*, whereas for derivative spectra it is *Magnitude at 697nm*. In the season of 2008, correlation with TCHL still is very high; nevertheless the best linear regressions are with CHL values. Therefore, cross-seasonal correlation with CHL concentration produces higher linear regressions values compared with TCHL concentrations. This is probably caused by the differences in the number of samples in the season of 2007 (5 samples) and 2008 (10 samples). The best algorithms for the season of 2008, as well as for cross-seasonal correlations are a *Peak Magnitude above a Baseline* and *Magnitude at 697nm* for normalized reflectance and derivative spectra respectively.

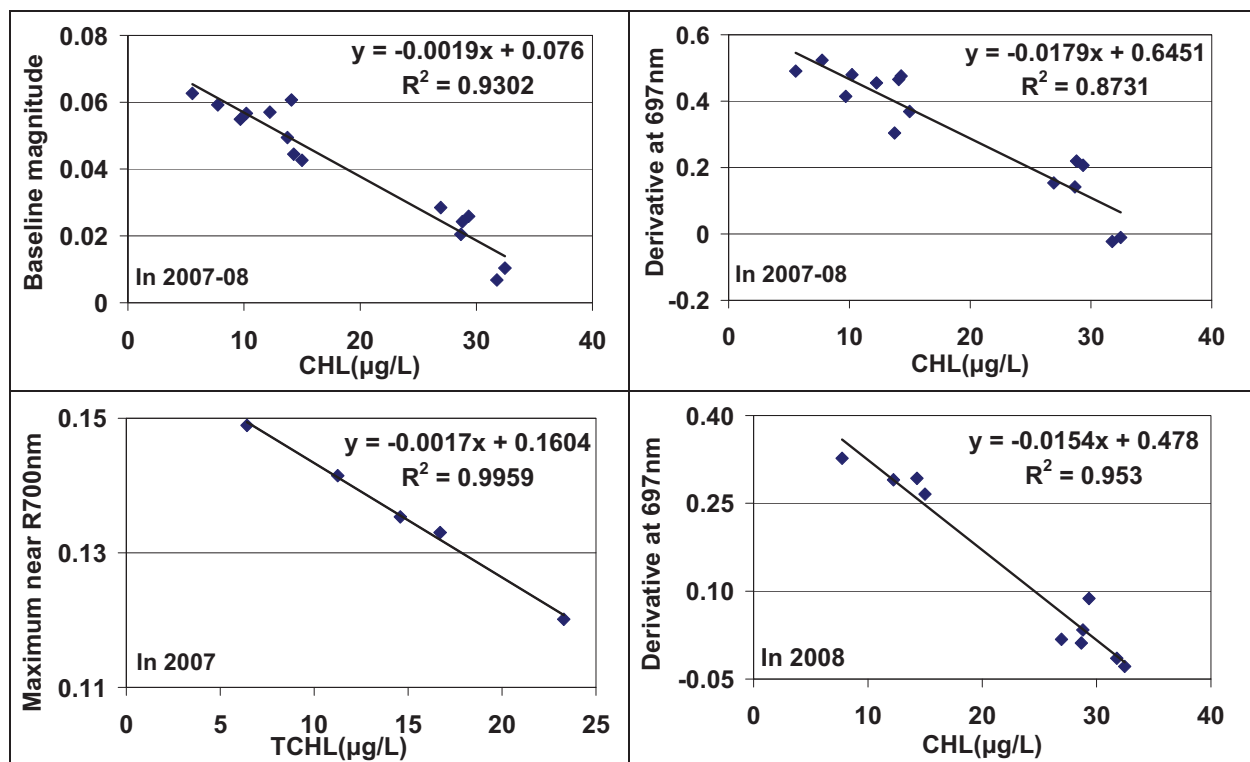


Figure 4-4: Received correlations between various algorithms and biomass concentration for kettle hole K1. Note scale, axes and algorithms differences.

Graphical presentations of the best received correlations are shown in Figure 4-4. All correlations (seasonal and cross-seasonal) have a negative slope caused by the packaging effect. The higher the chlorophyll and algae concentrations coupled with lowered water levels, the less chance there is of being totally dissolved (i.e. packed onto phytoplankton cells), and vice versa (high water and low chlorophyll content means more chances to be entirely dissolved).

Kettle hole K2

The monitoring programme and spectral analysis for kettle hole K2 were carried out only in 2007 (in 2008 it dried out). K2 had a constant water level throughout the year and exhibits a positive relation between spectra signals and biomass concentration.

Figure 4-5 illustrates the derivative spectra for the season derived from normalised reflectance in 2007. Similar to kettle hole K1, the derivative spectra of K2 had a high peak at 700nm.

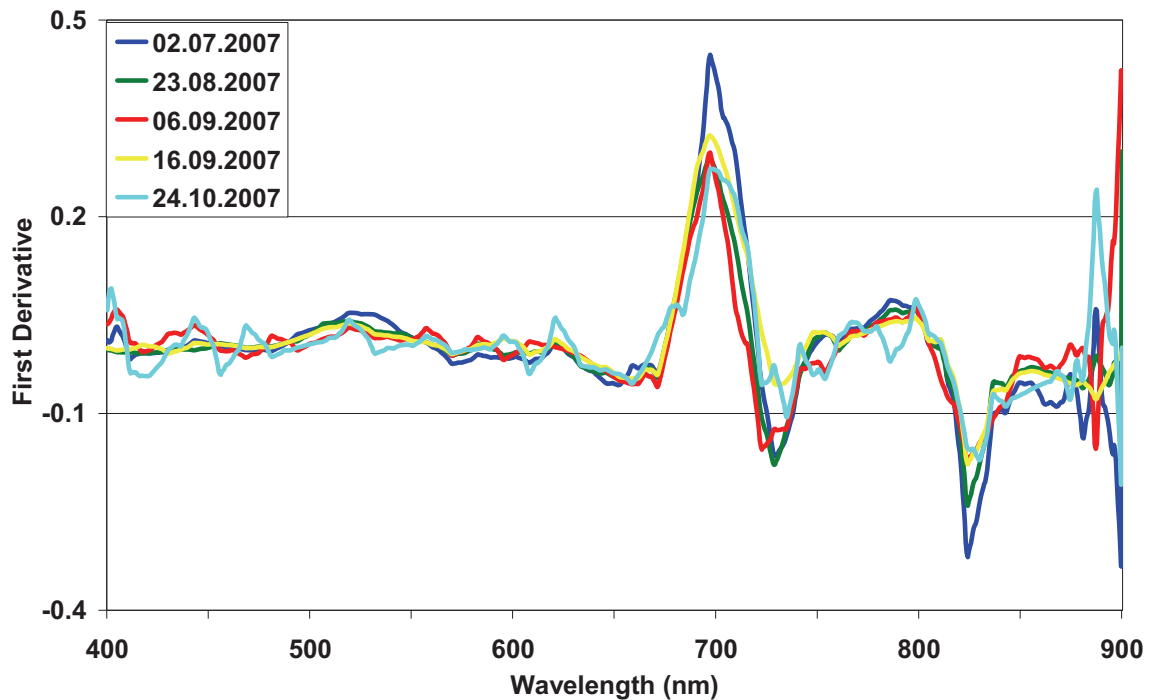


Figure 4-5: First derivative spectra of kettle hole K2 in the 2007 season

According to Pearson's correlation coefficients (R) calculated for volume reflectance and biomass concentrations (Figure 4-6a), the two reflectance values at 718nm and 743nm were closely correlated with CHL and TCHL respectively. The first reflectance represents solely the chlorophyll reflectance peak at 700nm and the second chlorophyll absorption (see Figure 4-1b). The correlation coefficients (R) between derivative spectra and biomass data produce the best result at 697nm (Figure 4-6b). Like in K1, this wavelength represents the chlorophyll reflectance peak near 700nm. These correlation relationships served as a reference for the selection of the most appropriate wavelengths in estimating chlorophyll from the remotely sensed data.

Table 4-2 shows the linear regression coefficients between biomass concentrations and various algorithms. The best correlation approach for CHL and normalized reflectance is a *Magnitude at 743nm* with R^2 value of 0.9753. The linear regression coefficients between TCHL as well as CHL and the *Peak Magnitude* algorithm also reveal good correlations. The algorithms *Position of Peak* and *Peak Magnitude above a Baseline* perform low correlation which is most likely caused by a strong influence to the chlorophyll peak reflection at 700nm by the high algae concentration.

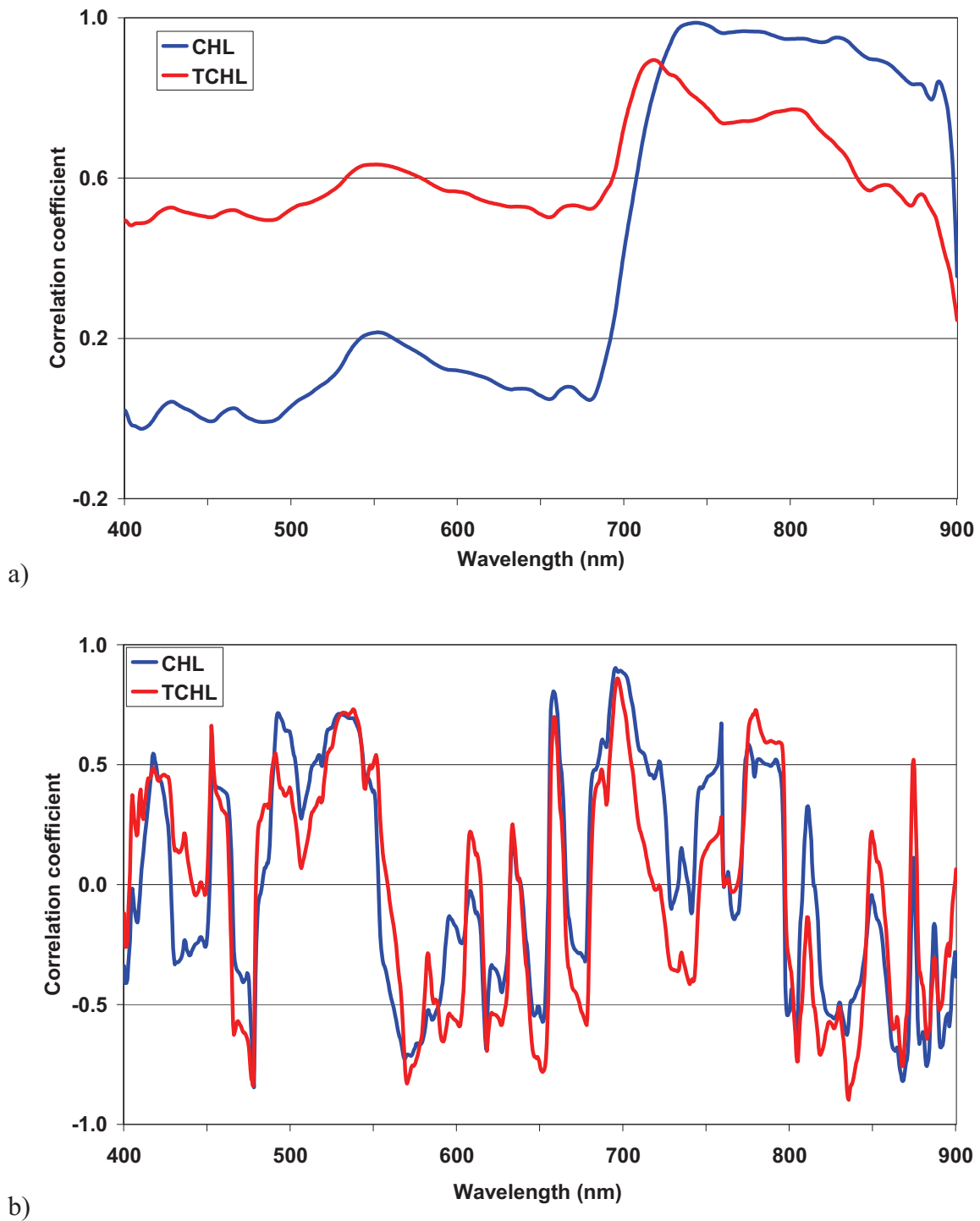


Figure 4-6: Pearson's correlation coefficients (R) between volume reflectance, derivative spectra and CHL, TCHL concentration in the 2007 season for kettle hole K2.

The linear regression coefficients between derivative spectra and biomass data resulted also in good correlations. Correlation between CHL produces slightly better results than TCHL. The best correlation algorithm for derivative is *a Magnitude at 696nm* for both biomass values. *Peak Magnitude* also gives acceptable coefficients of determination from

linear regression. The algorithm *Position of Peak* cannot be applied for derivative spectra since all reflectance values at peak magnitudes have the same wavelength.

Table 4-2: Linear regression coefficients using various methods between normalized volume reflectance and biomass concentration for kettle hole K2 in the season of 2007 (n=5)

	CHL	TCHL
Magnitude at 743nm (718nm)	0.9753	0.8002
Peak Magnitude	0.7268	0.8115
Position of Peak	0.2286	0.0014
Peak Magnitude above a Baseline	0,0286	0.2753
Magnitude at 697nm of 1 st derivative	0.8162	0.8002
Peak Magnitude of 1 st derivative	0.7850	0.7343
Position of Peak of 1 st derivative	N/A	N/A

Examples of the best received correlations between various algorithms and CHL concentration of kettle hole K2 are illustrated in figure 4-7.

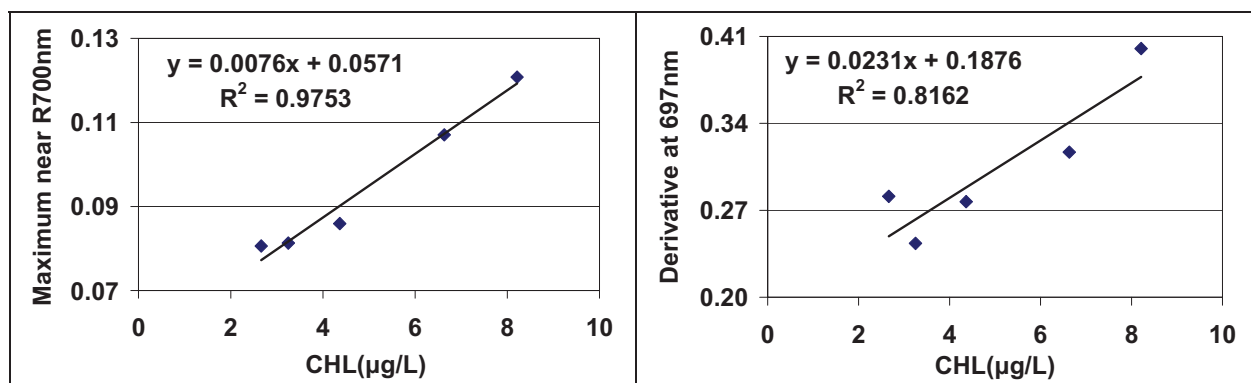


Figure 4-7: Received correlations between various algorithms and biomass concentration for kettle hole K2. Note the scale, axes and algorithms differences

Kettle hole K4

Figure 4-8 illustrates the first derivative spectra of kettle hole K1 extracted from normalized reflectance of 2007 and 2008 datasets. The kettle hole is the deepest and most turbid among the others and the surface reflectance shapes of kettle hole K4 are

comparable with the curves of the ‘classical spectral signatures’ described in the literature (Dekker *et al.* 1995; Doxaran *et al.* 2002a; Gitelson 1992; Thiemann 1999). K4 can be considered as a small lake; accordingly its surface reflectance (see figure 4-1c) and derivative spectra. The chlorophyll-laden peak at around 700nm is clearly recognizable. However, due to high suspended sediments concentration, the range starting from 800nm up to 900nm was gradually influenced by noise.

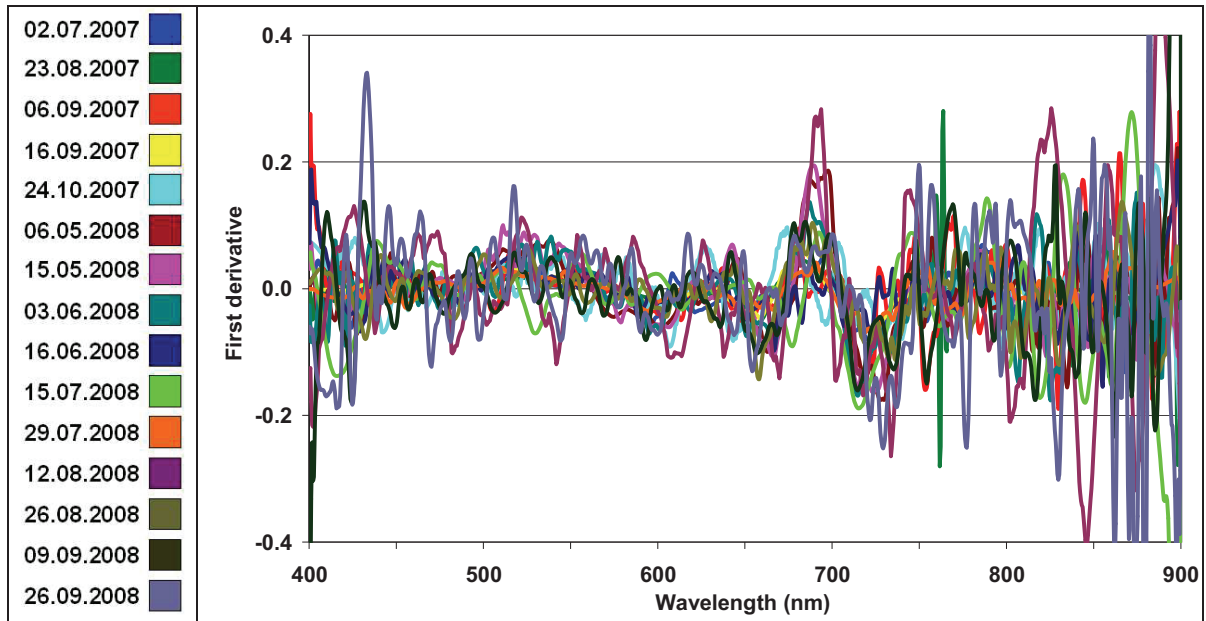


Figure 4-8: First derivative spectra of kettle hole K4 calculated from volume reflectance for 2007 and 2008 datasets

The results of seasonal and cross-seasonal Pearson’s correlation coefficients between volume reflectance, derivative spectra and CHL, and TCHL values are illustrated in Figure 4-8. Correlation between biomass and normalized reflectance produces no significant values except for TCHL in 2007. This correlation has the highest positive linear regression coefficient at 871nm wavelength (Figure 4-9a). The reason for this high correlation is due to the combination of absorptions from chlorophyll and suspended sediments which gradually normalize at the 850÷990nm range, especially in moderately and highly turbid waters (Doxaran *et al.* 2002b). A similar trend is seen with the spectra from 2008; it has a negative linear regression coefficient at 881nm wavelength. Since these wavelengths do not solely represent the correlation between chlorophyll content concentration and volume reflectance, they were omitted from further analysis.

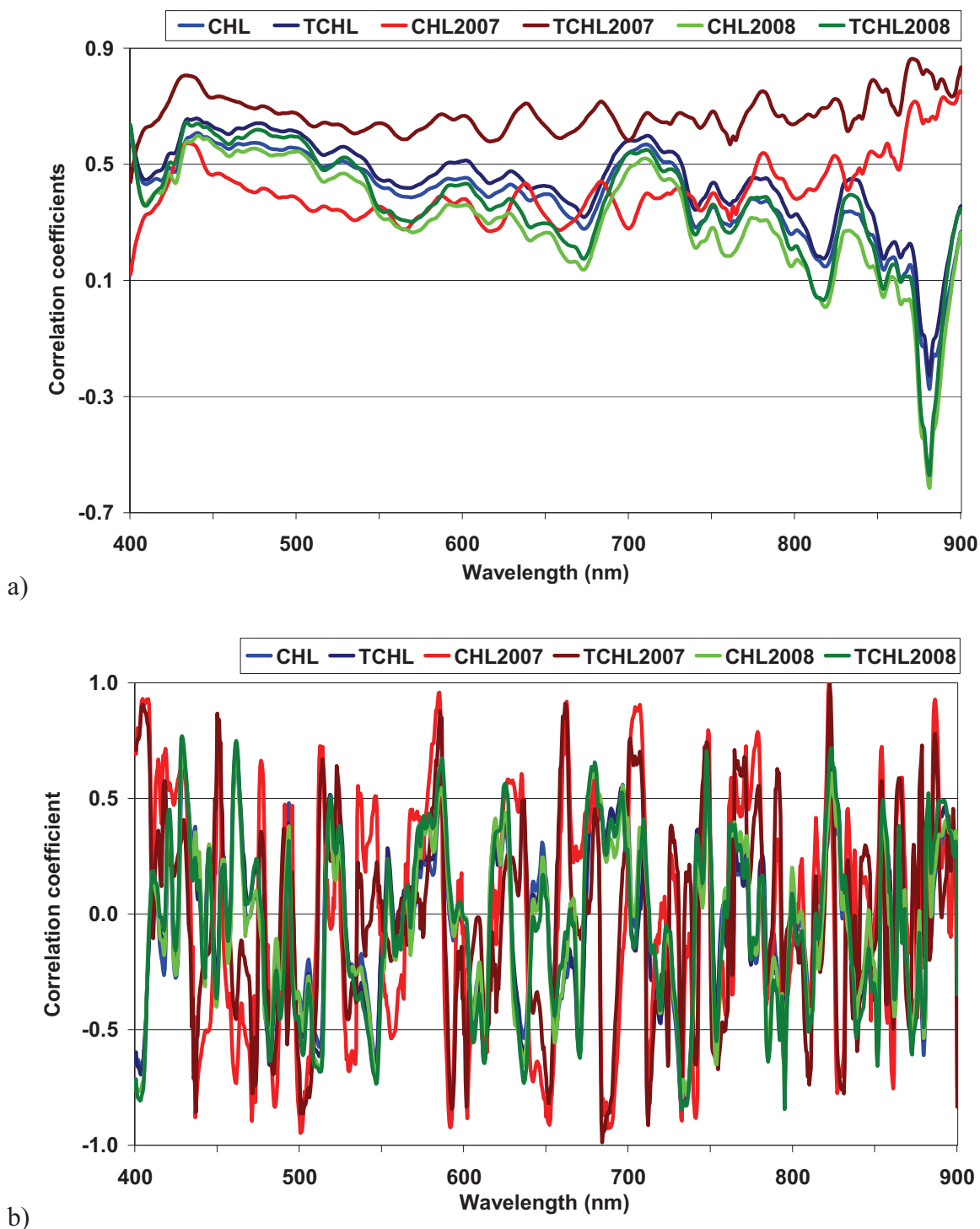


Figure 4-9: Pearson's correlation coefficients (R) for kettle hole K4 between volume reflectance, derivative spectra and biomass concentrations for seasonal (2007 and 2008) and cross-seasonal data (CHL and TCHL for 2007-08)

Seasonal and cross-seasonal correlations between derivative spectra and biomass concentration have high coefficients (R) for 2007 and low values for 2008. Similar to normalized reflectance, the difference in correlations for 2007 and 2008 seasons are most likely caused by suspended sediments (Figure 4-9b). The derivative spectra of 2007 with

relatively low-to-moderate TSS values (see Appendix B) are better correlated with biomass data, especially at wavelengths near 700nm. The season of 2008 had higher TSS values which consequently influenced the derivative spectra resulting in lower correlations coefficients. Taking these facts into account, the reflectance value at a specific wavelength approach was excluded from further calculations.

Table 4-3: Coefficients of determination from linear regression using various methods between normalized volume reflectance and biomass concentration for kettle hole K4 (n=15 in 2007-08, n=5 for 2007, n=10 for 2008)

	2007-08		2007		2008	
	CHL	TCHL	CHL	TCHL	CHL	TCHL
Peak Magnitude	0.3178	0.3607	0.1183	0.3988	0.2613	0.3121
Position of Peak	0.1105	0.0708	0.9760	0.8541	0.1309	0.0564
Peak Magnitude above a Baseline	0.5316	0.5071	0.8965	0.7911	0.4478	0.4540
Peak Magnitude of 1 st derivative	0.8380	0.8008	0.8965	0.5802	0.8354	0.8425
Position of Peak of 1 st derivative	0.0619	0.0642	0.1014	0.0005	0.0400	0.0336

Table 4-3 gives linear regressions coefficients using spectral algebra algorithms between biomass concentration (CHL and TCHL) and volume reflectance and derivative spectra.

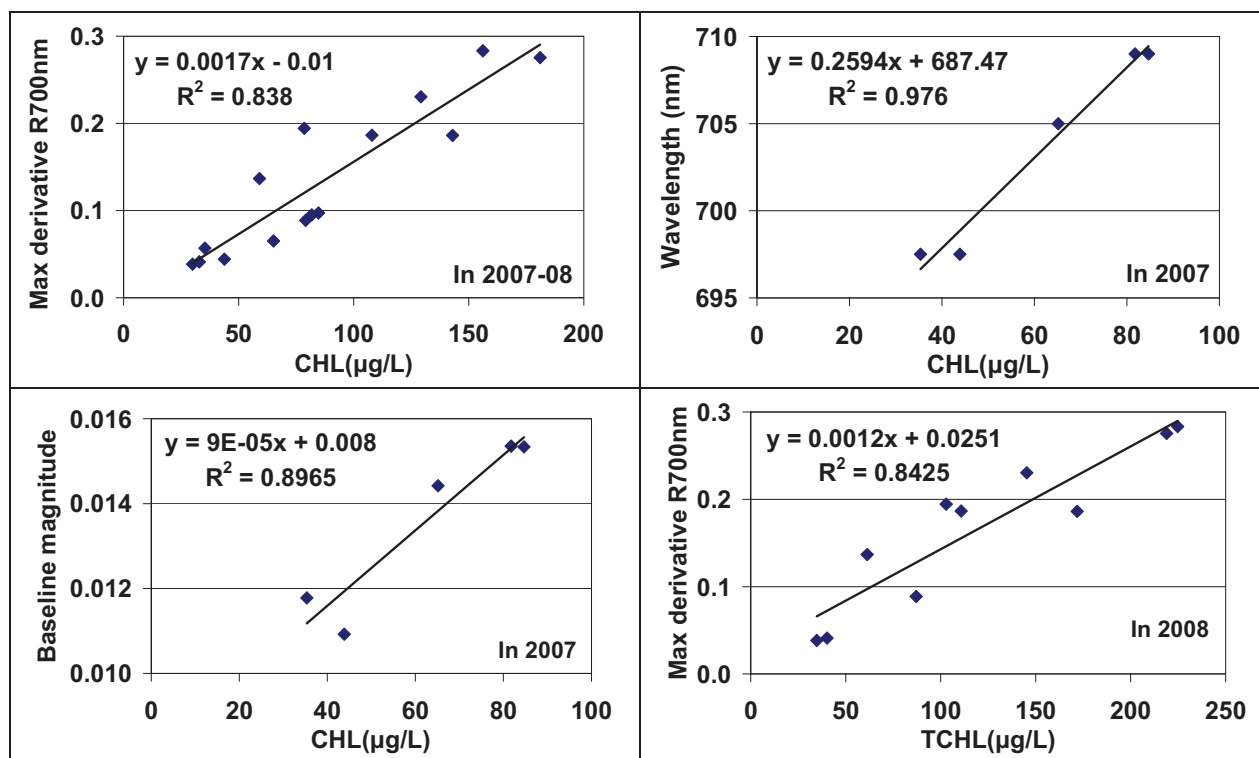


Figure 4-10: Received correlations between various algorithms and biomass concentration for kettle hole K4. Note scale, axes and algorithms differences

Therefore, for kettle hole K4, the determination of linear regression coefficients was concentrated on spectral algebra algorithms, as described in chapter 3.4.4.

Normalized volume reflectance of kettle holes K4 in 2007 is correlated best with CHL using the classical algorithms *Peak Magnitude above a Baseline* and *Position of Peak*. Derivative spectra of 2007 and biomass data perform the best correlation using the *Peak Magnitude* algorithm. For the season of 2008, the linear regression analyses between the derivative spectra and TCHL produces a high determination coefficient using the *Peak Magnitude* algorithm. Correlation for CHL is slightly lower than TCHL. Finally the best cross-seasonal correlation uses derivative spectra and the *Peak Magnitude* algorithm. This was expected because the hydro-morphological characteristics of this kettle hole compare to the shallow lakes with moderate chlorophyll and TSS concentrations, as described by Scheffer (1998). Han and Rundquist (1997) found that for such lakes, the application derivative analysis approach produces the best correlations. Figure 4-10 shows some of the best received seasonal and cross-seasonal correlations between various algorithms and biomass concentrations for kettle hole K4.

Kettle hole K5

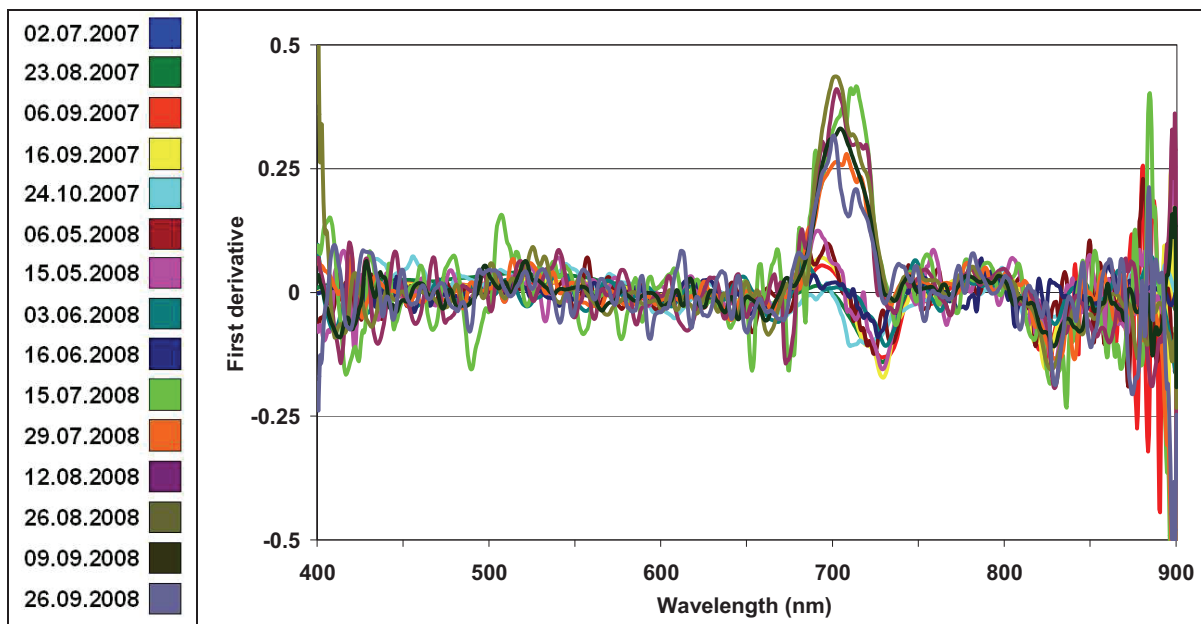


Figure 4-11: First derivative spectra of kettle hole K5 calculated from volume reflectance for 2007 and 2008 datasets

Kettle hole K5 was a very shallow kettle hole (30 – 50 cm) with high algae content. It had brown-coloured waters in season 2007 and was transparent in the next year.

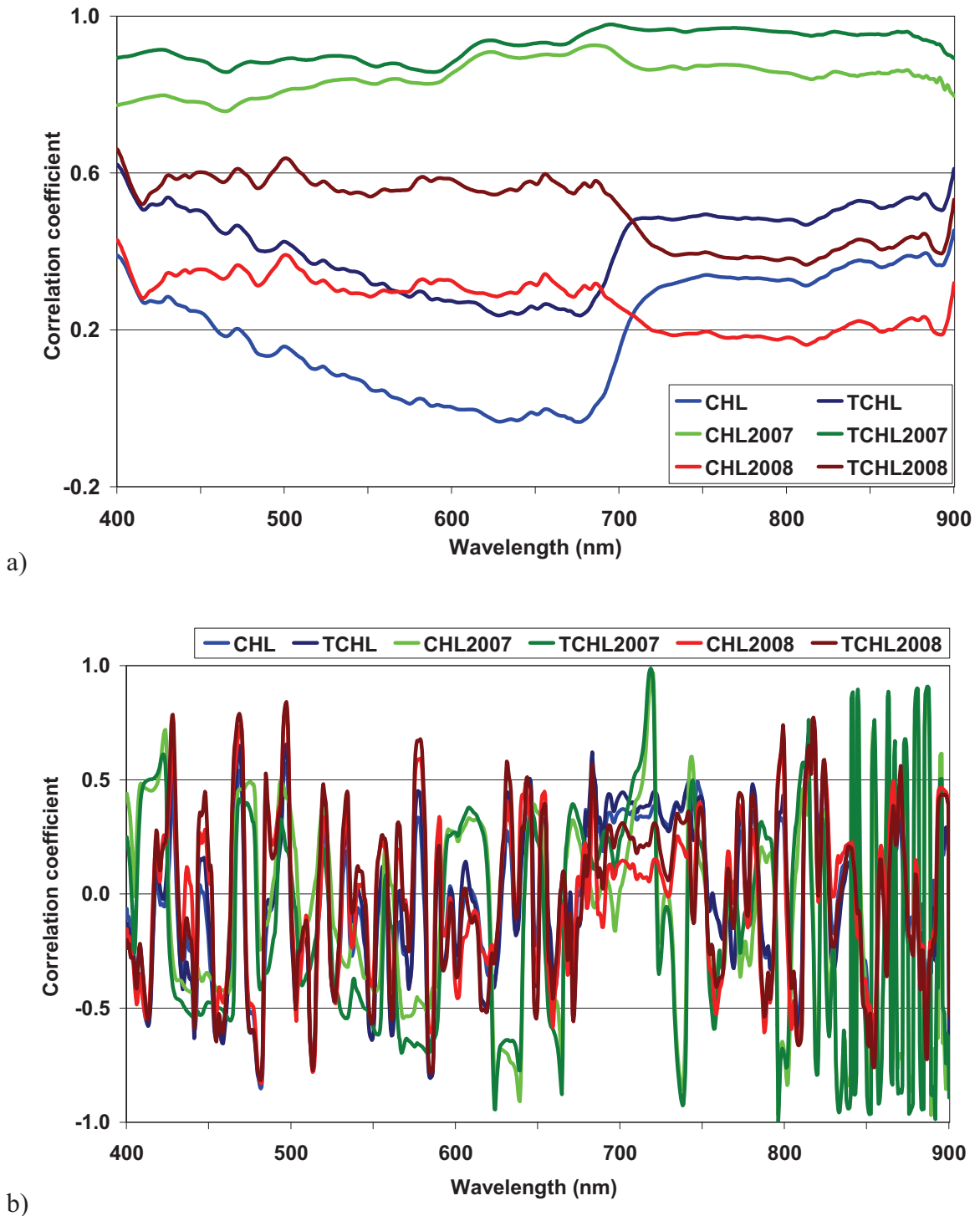


Figure 4-12: Pearson's correlation coefficients (R) for kettle hole K5 between volume reflectance, derivative spectra and biomass concentrations for seasonal (2007 and 2008) and cross-seasonal data (CHL and TCHL for 2007-08)

A different amount of precipitation in 2007 and 2008 combined caused different water colours in the first and second years of the field campaigns. These changes can be easily seen in the spectral signatures of both years. Consequently, the same types of change have affected the derivative spectra.

Figure 4-11 illustrates derivative spectra from K5 calculated from normalised reflectance. Two chlorophyll reflectance peaks near 700nm with different magnitudes can be observed in the derivative spectra: the first with a lower magnitude caused by turbid waters in 2007 and beginning of 2008; and the second with a higher magnitude influenced by algae-dominated shallow water.

Table 4-4: Coefficients of determination from linear and logarithmic regression using various methods between normalized volume reflectance and biomass concentration for kettle hole K5 (n=15 in 2007-08, n=5 for 2007, n=10 for 2008)

	2007-08		2007		2008	
	CHL	TCHL	CHL	TCHL	CHL	TCHL
Peak Magnitude	0.0696	0.2032	0.7751	0.9374	0.0301	0.1496
Position of Peak	0.1568	0.1698	0.1675	0.2696	0.0148	0.0518
Peak Magnitude above a Baseline	0.0125	0.0423	0.0572	0.1390	0.0002	0.0198
Magnitude at 482nm of 1 st derivative	0.7270	0.6707	0.0586	0.1084	0.6891	0.7216
Magnitude at 482nm of 1 st derivative	<i>0.8204^b</i>	<i>0.7677</i>	<i>0.0324</i>	<i>0.1384</i>	<i>0.8433</i>	<i>0.8767</i>
Peak Magnitude of 1 st derivative	0.1158	0.1623	0.0178	0.0098	0.0069	0.0611
Position of Peak of 1 st derivative	0.0001	0.006	0.1757	0.1004	0.0261	0.0010

^b By bold and italic showed best received logarithmic correlations using volume reflectance and derivative spectra.

Pearson's correlation coefficients have been calculated between biomass concentration and normalized reflectance, derivative spectra (Figure 4-12). As it expected, there is no high correlation for the season of 2008 and consequently for cross-seasonal combination. Only season of 2007 has stable and high correlation near chlorophyll absorption range of 680÷690nm (Figure 4-12a). It has to be separately mentioned that for season of 2007 biomass data from 2nd July were excluded from the calculation processes due to inconsistency caused by very high values (CHL = 62µg/L and TCHL = 101µg/L) compare with average concentrations of 3÷6µg/L.

Similar to volume reflectance correlations between chlorophyll content and derivative spectra produces are consistency only for 2007 (Figure 4-12b). Although the correlation with derivative spectra is better than with normalized reflectance, the cross-seasonal linear regression coefficients for the range of 660÷700nm are low. The only stable correlation is at 482nm. In derivative spectra this wavelength is an interaction zone in the visual region of light between Blue (400÷500nm) and Green (500÷600) ranges. In figure 4-1d it is seen that this part of the electromagnetic spectrum corresponds with the first chlorophyll absorption range, i.e. the visual reflection of (green coloured) algae.

Table 4-4 shows seasonal and cross-seasonal coefficients of determinations from linear and logarithmic regression between volume reflectance and biomass concentrations for kettle hole K5. The results of linear regression analysis in the *Magnitude at 482nm of 1st derivative* algorithm revealed that, contrary to other kettle holes, K5's derivative reflection at this wavelength has a higher correlation using logarithmic distribution.

The best linear and logarithmic correlations between derivative spectra and CHL, and derivative reflection distributions at 482nm wavelength, are shown in Figure 4-13.

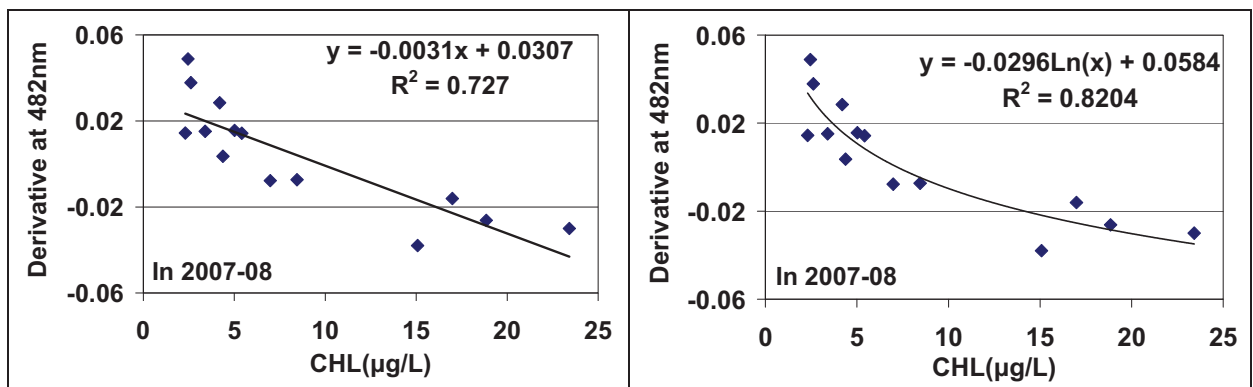


Figure 4-13: Received correlations between various algorithms and biomass concentrations for kettle hole K5. Note the scale, axes and algorithms differences.

The application of logarithmic and power functions is a part of the statistical analysis also used in regression models between *in situ* measured chlorophyll concentration and reflectance derived at various wavelengths (Jiao *et al.* 2006).

Kettle hole K6

Field research campaigns and analysis of airborne images (Figure 3-2) shows that kettle holes K6 and K7 used to be one kettle hole. K6 is located lower than K7, and, therefore, it

collects most of the surface runoff (i.e. nutrients) from the surrounding catchments area which is highly influential over the up-welling radiance. It has to be additionally mentioned that K6's bottom with partially sandy and algae covered parts causes also high variation in reflection.

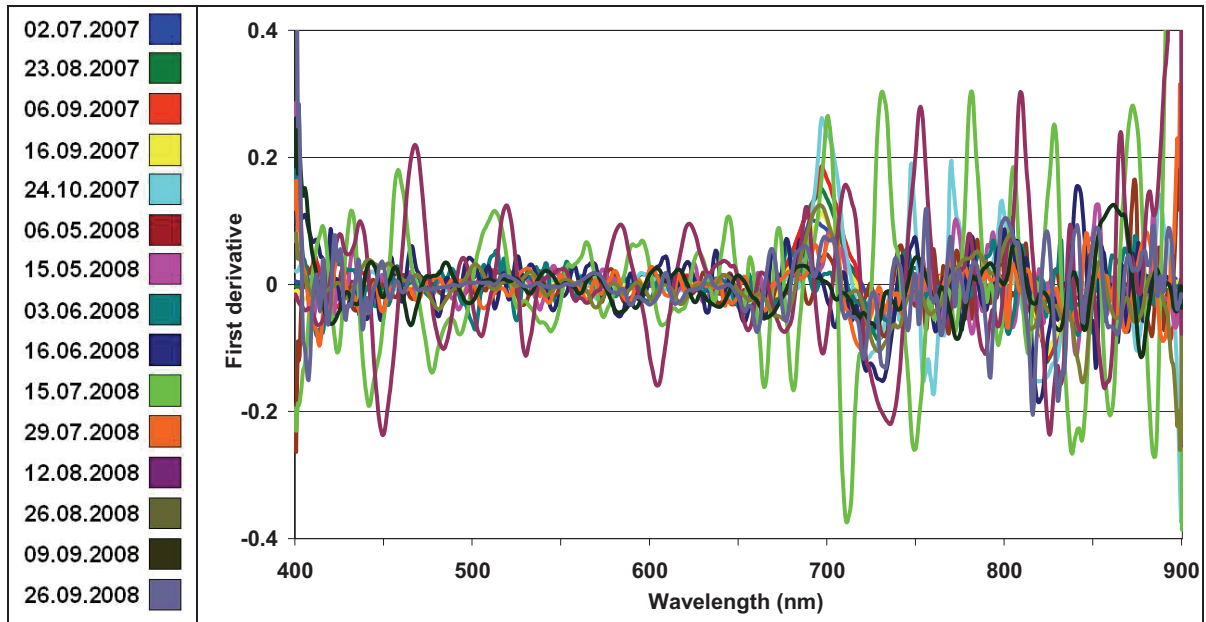
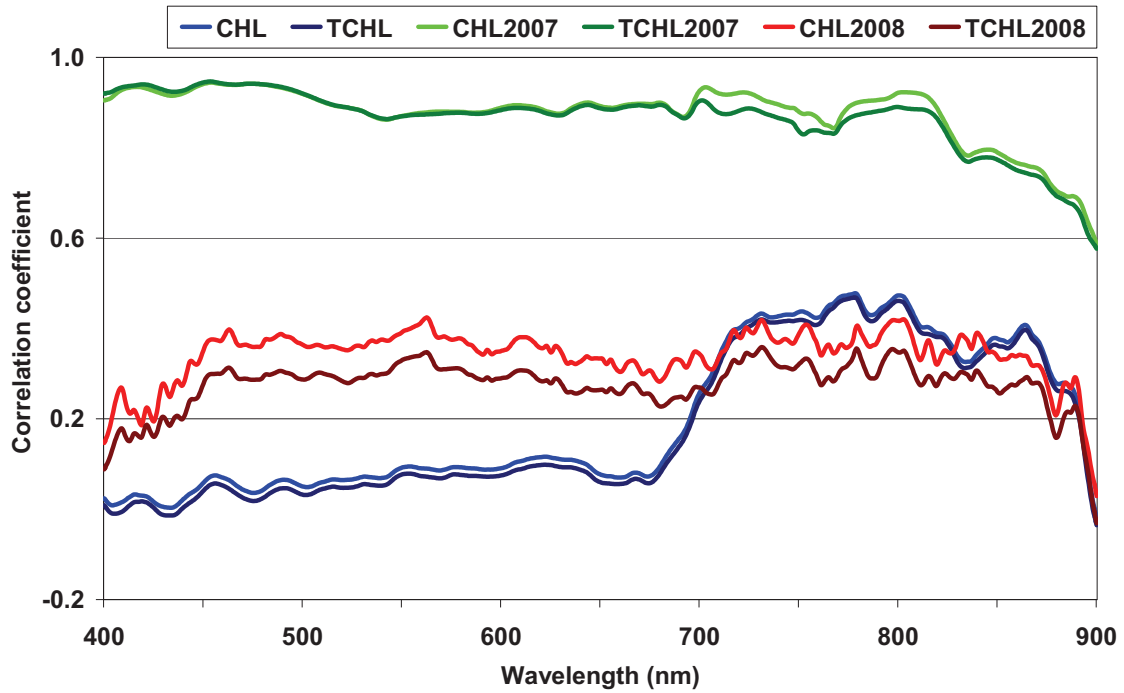


Figure 4-14: First derivative spectra of kettle hole K6 calculated from volume reflectance for 2007 and 2008 datasets

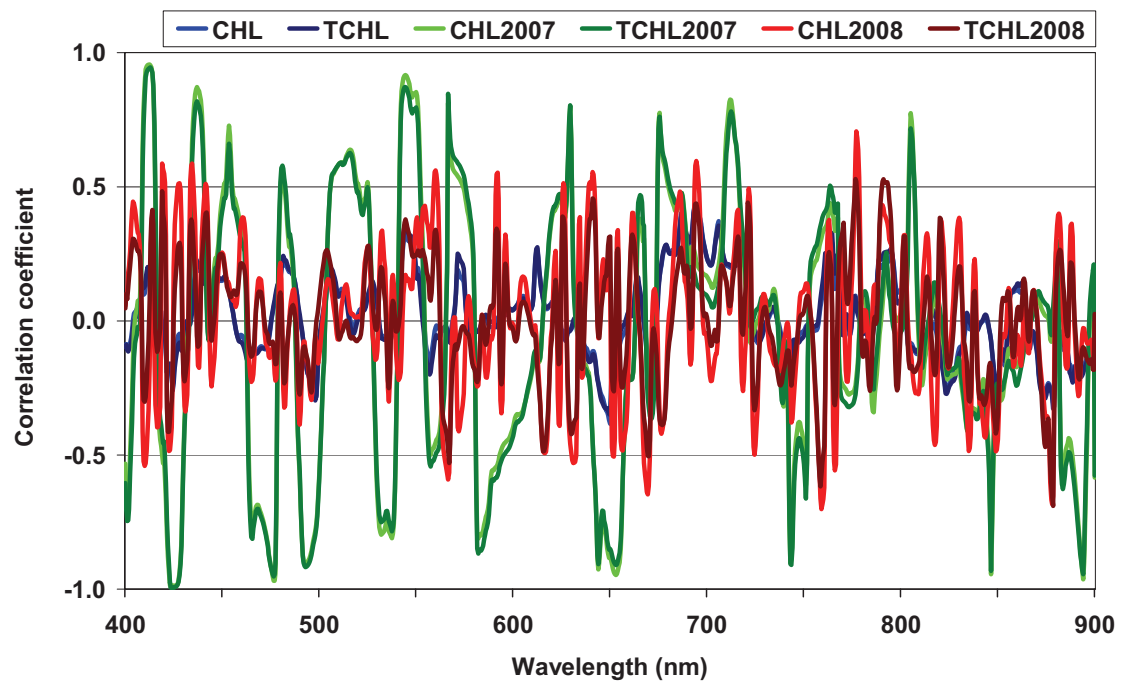
Analysis of the derivative spectra (Figure 4-14) similar to normalized reflectance shows that the spectra collected during overcast sky and windy conditions (e.g. 15 July and 12 August 2008 spectra – light green and cherry-coloured accordingly) have high variations.

The applicability results of volume reflectance and derivative spectra values at specific wavelengths for chlorophyll content estimation are illustrated in figure 4-15. Normalized reflectance is well correlated only for the 2007 season. The coefficients of linear determination for 2008 and consequently 2007-08 seasons are very low (Figure 4-15a).

This is most likely caused by two factors: (1) quick response of the kettle hole to (agricultural) activities in the surrounding catchments area which is reflected in the coming surface runoff, and (2) differences in weather conditions during remote sensing signal acquiring (i.e. clear or overcast skies).



a)



b)

Figure 4-15: Pearson's correlation coefficients (R) for kettle hole K6 between volume reflectance, derivative spectra and biomass concentrations for seasonal (2007 and 2008) and cross-seasonal data (CHL and TCHL for 2007-08)

Derivative spectra, like the normalized reflectance, have good correlation for 2007 but are low for 2008 and 2007-08 seasons (Figure 4-15b).

Analysis of linear regression coefficients between various algorithms and biomass concentrations revealed that correlations for 2008 and 2007-08 seasons are very low (less than 5%). Only the relation between CHL and derivative spectra using the *Peak Magnitude at 700nm* algorithm produces slightly better results (Figure 4-16a).

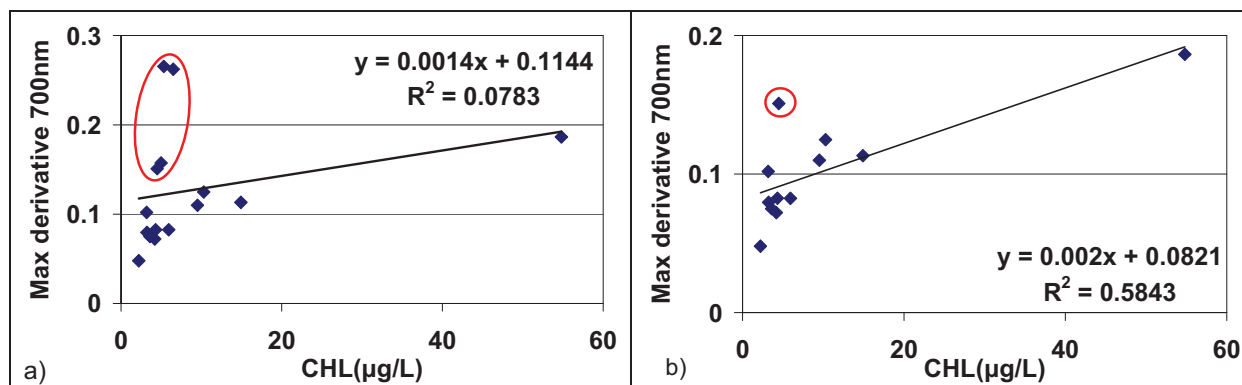


Figure 4-16: Correlation using Peak Magnitude at 700nm algorithm between derivative spectra and CHL concentrations for whole data in 2007-08 seasons (a) and without reflectance from overcast days

It is clearly seen that the majority of points fall into linear regression distribution. Only four points 'spoil' the correlation (Figure 4-16a - red oval). Three of these points (from 24 October 2007, 15 July and 12 August 2008) were collected on overcast and windy weather conditions (see Appendix D). Contrary to other kettle holes, remote sensing data collection from low positioned and oval-shaped K6 (see Figure 3-2) was the most difficult task. Changing light intensity coupled with high frequent waves caused by overcast skies and strong winds highly influenced the acquisition of a remote sensing signal from a handheld spectrometer (by shifting the device from the collecting point). Therefore, even de-noised and normalized reflectance from these dates constitutes many 'zigzag' curves, even with low chlorophyll concentrations which are also reflected in the derivative spectra.

Thus, for kettle hole K6 only, calculations of linear regression coefficients were performed without data from overcast days (Figure 4-16b). The result of the correlation coefficient ($\approx 60\%$) was significantly higher than the previous calculation ($\approx 8\%$). Only one point from 23 August 2007 had a high derivative reflectance at 700nm. The spectrum from this date was highly influenced by the high algae content bottom (see Appendix B) and low water level; the shape of this spectral signature was similar to the spectra of K1 but with a smaller magnitude - consequently its derivative reflectance value.

Table 4-5: Coefficients of determination from linear regression using various methods between normalized volume reflectance and biomass concentration for kettle hole K6 (without data from overcast days, n=15 in 2007-08, n=5 for 2007, n=10 for 2008)

	2007-08		2007		2008	
	CHL	TCHL	CHL	TCHL	CHL	TCHL
Peak Magnitude	0.1927	0.1796	0.8487	0.7827	0.1672	0.1203
Position of Peak	0.1835	0.2006	0.0036	N/A	0.3087	0.2171
Peak Magnitude above a Baseline	0.3239	0.3192	0.4876	0.4782	0.2227	0.1366
Peak Magnitude of 1 st derivative	0.5843	0.5922	0.6322	0.5898	0.8889	0.7255
Position of Peak of 1 st derivative	0.0038	0.0058	0.2415	0.2846	0.0025	0.0004

Table 4-5 shows the coefficients of determination linear regression using various algorithms between normalized reflectance and CHL, and TCHL concentration for kettle hole K6 without reflectance values from overcast days. For the season of 2007 with a low water level, kettle hole K6 spectra correlates best with *Peak Magnitude* and CHL ($R^2=0.85$). This can be explained by two aspects: (1) the high CHL values on the 06.09 and 16.09.2007 of 55 $\mu\text{g/L}$ and 15 $\mu\text{g/L}$ respectively (Figure 4-17a), while values of the other sampling dates are less than 8 $\mu\text{g/L}$, and (2) in season of 2007 water level was low so the response to agricultural activity in the catchment area was higher, causing intensive algae growth on the bottom. Therefore, the spectral signatures from that season, like in K1 and K2, are comparable with vegetation reflectance but with smaller magnitude.

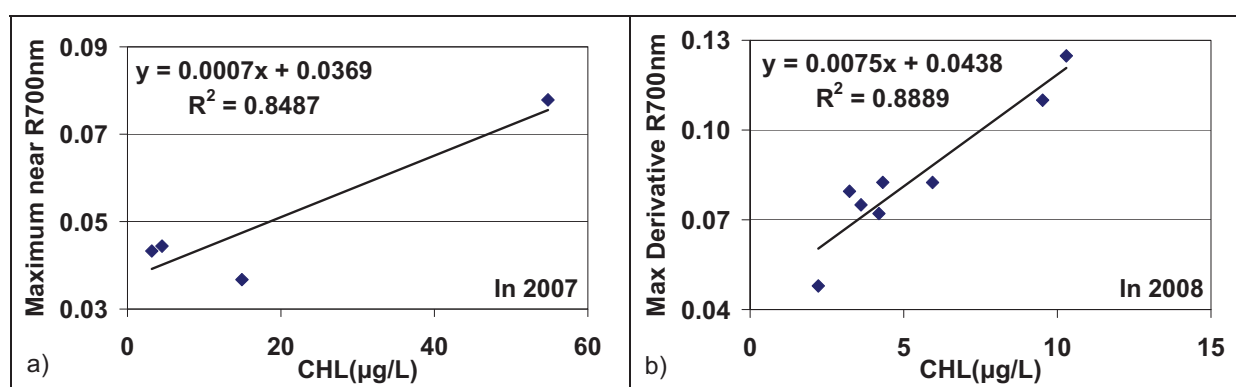


Figure 4-17: Received correlations between various algorithms and biomass concentration for kettle hole K6. Note the scale, axes and algorithms differences

The water level in the season of 2008 was higher than in 2007. Average CHL concentration is between 5 $\mu\text{g/L}$ and 6 $\mu\text{g/L}$ (Figure 4-17b). Thus, the spectral signatures for this year were influenced by the sandy and partially algae covered bottom.

Kettle hole K7

Kettle hole K7 has spectral signatures comparable with the reflectance curves of low turbid waters described by Doxaran (2002b). Seasonal and cross-seasonal spectra show high reflectance peaks on the 500÷700nm (i.e. the Green and Red part of the visual spectrum) range which is mainly caused by the sandy bottom. Almost the whole bottom of K7, especially the deepest part, is covered by sand. The reflectance of the sand spectrum increases gradually with the longer wavelength (Murphy *et al.* 2005). Similar to normalized reflectance, the derivative spectra have high variation in the Green and Red electromagnetic spectrum but peak near 700nm is distinctive (Figure 4-18).

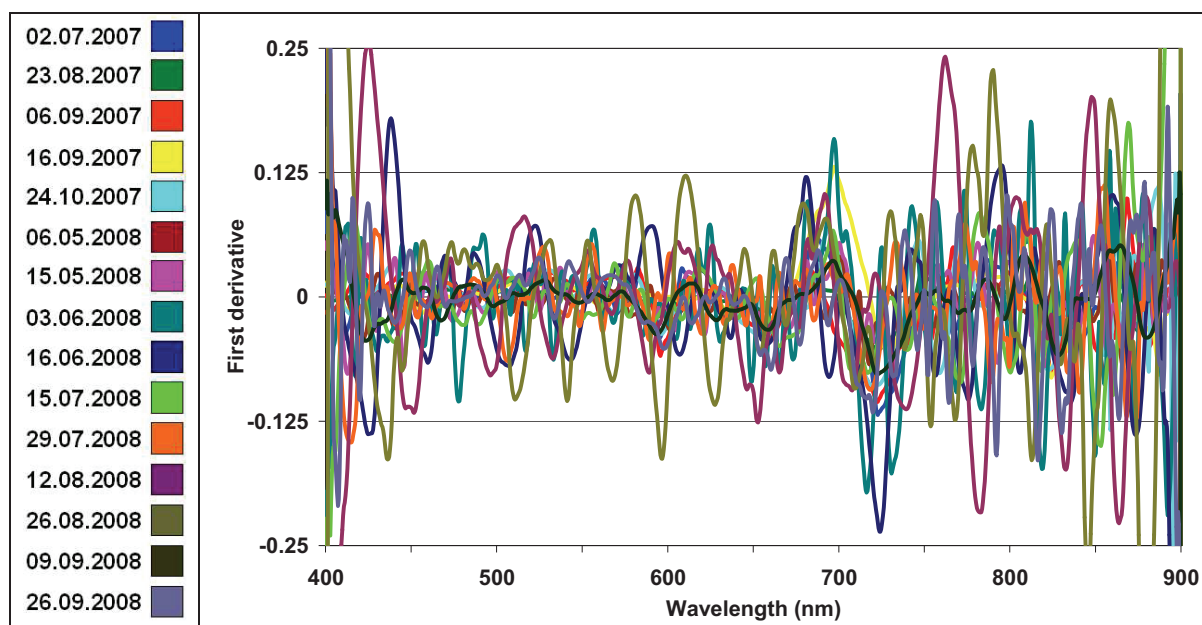


Figure 4-17: First derivative spectra of kettle hole K7 calculated from volume reflectance for 2007 and 2008 datasets. (Reference of colours with the dates is equivalent to Figure 4-1)

Pearson's correlation coefficients between biomass data and normalized reflectance clearly show relatively high values for season 2008 at 711nm wavelength compared to 2007 and 2007-08 seasons (Figure 4-18a). Calculation of correlation coefficients between derivative spectra and biomass concentrations reveals completely different values, especially for the season of 2007. Both CHL and TCHL of 2007 are highly correlated at 687nm wavelength. The CHL of 2008 and the TCHL for 2007-08 values have good correlation coefficients at the same wavelength (Figure 4-18b). Therefore, reflectance values of derivative spectra at 687nm have been used together with other algorithms.

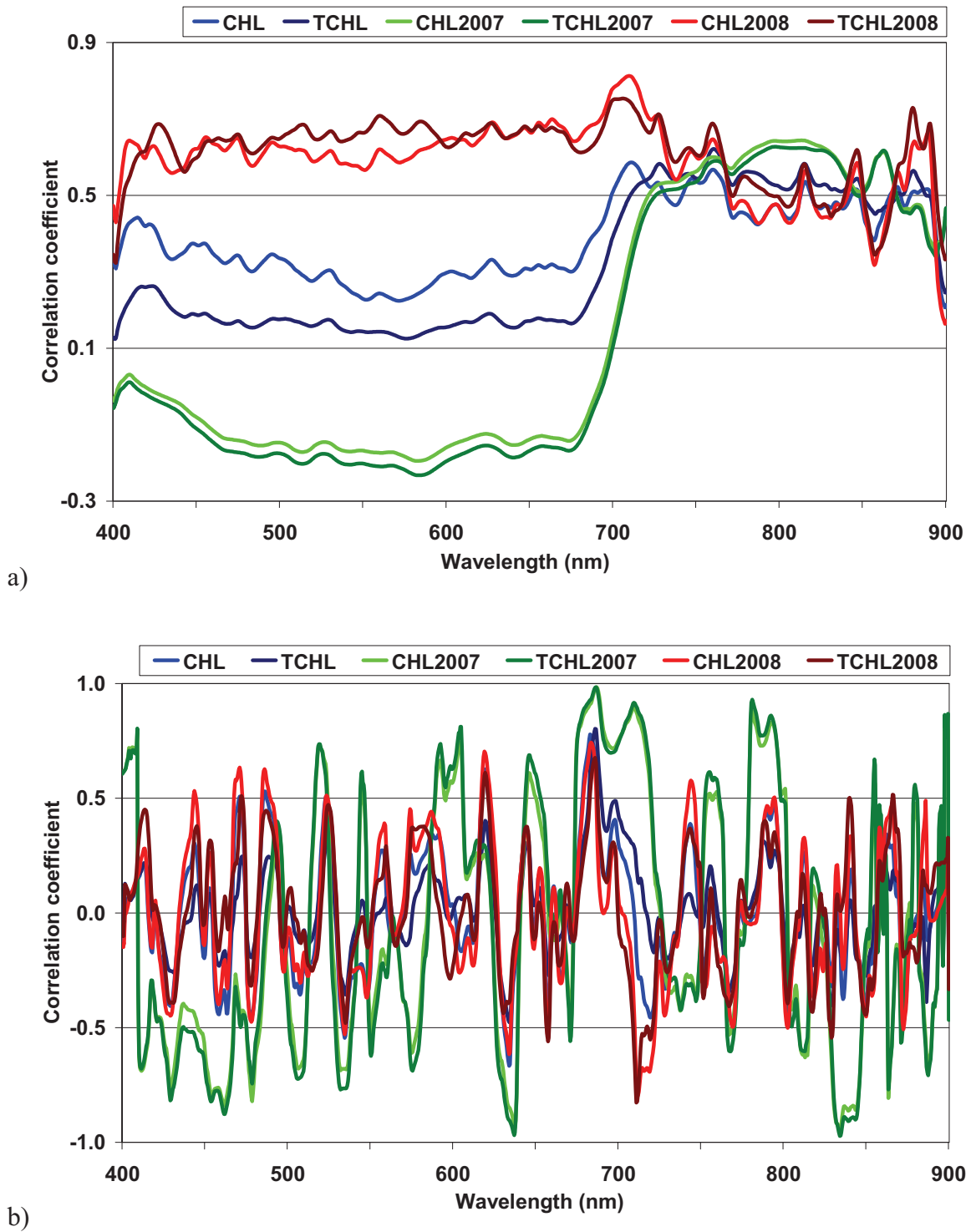


Figure 4-18: Pearson's correlation coefficients (R) for kettle hole K7 between volume reflectance, derivative spectra and biomass concentrations for seasonal (2007 and 2008) and cross-seasonal data (CHL and TCHL for 2007-08)

Calculations results of linear regression coefficients are give in Table 4-6.

Table 4-6: Coefficients of determination from linear regression using various methods between normalized volume reflectance and biomass concentration for kettle hole K7 (n=15 in 2007-08, n=5 for 2007, n=10 for 2008)

	2007-08		2007		2008	
	CHL	TCHL	CHL	TCHL	CHL	TCHL
Peak Magnitude	0.3253	0.2105	0.0750	0.0555	0.6398	0.5407
Position of Peak	0.0028	0.0966	0.7845	0.7858	0.1455	0.2073
Peak Magnitude above a Baseline	0.8516	0.5588	0.8947	0.8064	0.8505	0.5927
Magnitude at 687nm of 1 st derivative	0.5428	0.7478	0.9586	0.9655	0.5056	0.4734
Peak Magnitude of 1 st derivative	0.7634	0.4662	0.7082	0.6384	0.7863	0.3039
Position of Peak of 1 st derivative	0.0433	0.0236	0.1784	0.1359	0.2339	0.5180

Spectra of kettle holes K7 are best correlated with CHL using the classical algorithm *Peak Magnitude above a Baseline* (0.8516) for all seasonal and cross-seasonal reflectance values. *Magnitude at 687nm* performs best with both CHL and TCHL using derivative spectra. *Peak Magnitude* of derivative reflectance produces stable correlations with CHL in all seasonal and cross-seasonal datasets.

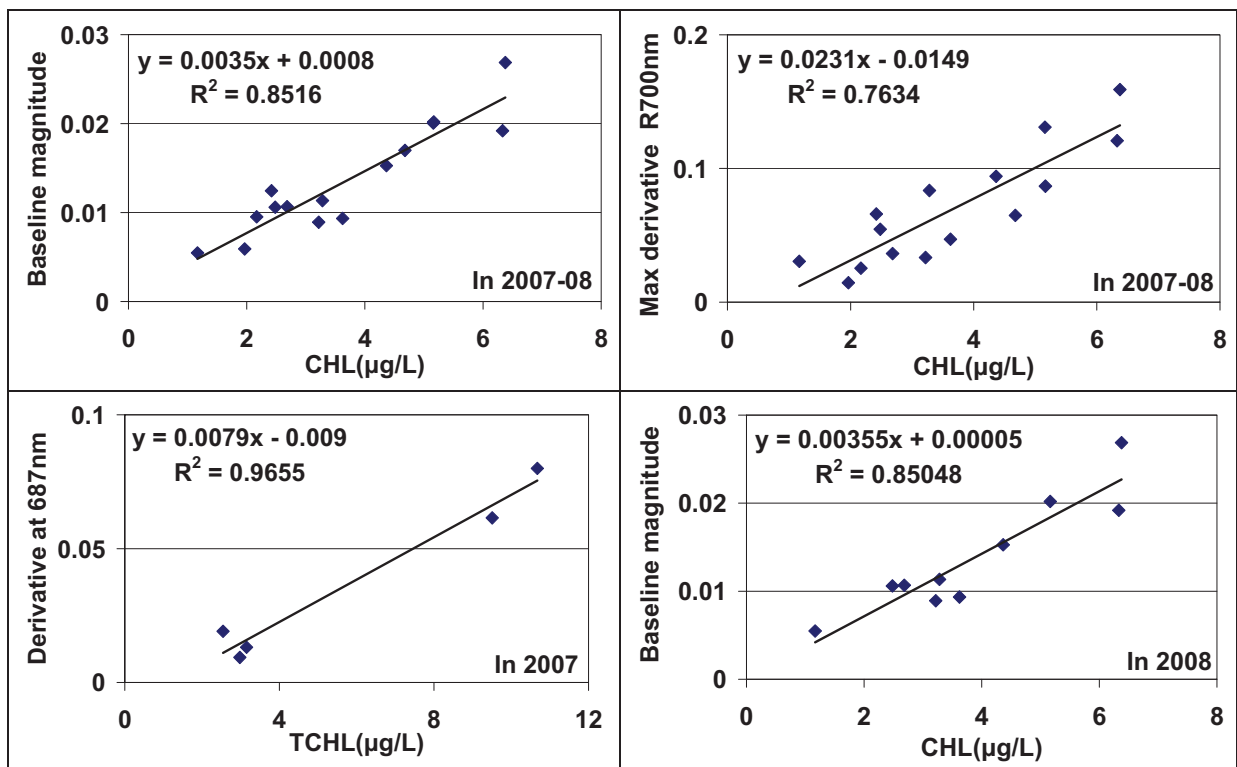


Figure 4-19: Received correlations between various algorithms and biomass concentration for kettle hole K7. Note the scale, axes and algorithms differences.

Finally, figure 4-19 shows some of the best received seasonal and cross-seasonal correlations between various algorithms and biomass concentrations for kettle hole K7.

4.1.5 Analysis of biomass estimation algorithms accuracy

Semi-empirical algorithms use optical and physical characteristics of the light in the water for the determination of the model but determination of the correlations coefficients is based on statistical analysis. All models used in this study are linked to the *in-situ* data by means of linear regression analysis to derive the semi-empirical correlation coefficients. In this way, the model is calibrated to the spatial and/or seasonal or cross-seasonal characteristics of kettle holes in the study area. In the literature, the Root Mean Square Error (RMSE) and the Standard Error of Estimate (SSE) are mostly taken to describe the quality of linear regressions (Kneubuehler *et al.* 2005; Wang *et al.* 2007). The RMSE and the SSE are calculated for better comparison with other research results in this field of science. Within these calculations, the residues become squared, which weights outlier stronger. Since in this study a few samples were available for each kettle hole, the absolute Mean Deviation (MD_a) and Mean Deviation as a Percentage ($MD\%$) are taken for analysis residues variations.

RMSE and SSE are defined in the case of linear regression analysis as:

$$RMSE = \sqrt{1/(n-2) \sum_{i=1}^n (y_i - y'_i)^2} \quad [4-1]$$

$$SSE = \sqrt{\frac{\sum_{i=1}^n (y_i - y'_i)^2}{n}} \quad [4-2]$$

where n is the total number of samples in the dataset, y_i is the measured *in situ* value and y'_i is the estimated value.

The RMSE is the distance, on average, of a data point from the fitted line, measured along a vertical line. The SSE is a measure of the accuracy of predictions made by a regression line, the smaller is SSE and the more accurate is the estimate.

The MD_a is defined as the mean of the absolute deviations of a set of data divided by the data's mean. For a number of samples n , the mean deviation is defined by:

$$MD_a = \frac{1}{n} \sum_{i=1}^n |y_i - y'_i| \quad [4-3]$$

To express the MD_%, the deviations are divided by the sum of the estimated values:

$$MD_{\%} = \frac{1}{n} \frac{\sum_{i=1}^n |y_i - y'_i|}{\sum_{i=1}^n y'_i} \times 100\% \quad [4-4]$$

Table 4-7 shows the accuracy of the best cross-seasonal algorithms for each kettle hole.

Table 4-7: Accuracy assessment of the best cross-seasonal algorithms for each kettle hole (n=15 for 2007-08)

Kettle hole	Algorithm	Biomass	R^2	RMSE (µg/L)	SSE (µg/L)	MD _a	MD _%
K1	Peak Magnitude above a Baseline	CHL	0.93	2.65	2.46	2.09	0.75
	Magnitude at 697nm of 1 st derivative	CHL	0.87	3.82	3.55	3.00	1.07
K2	Magnitude at 743nm	CHL	0.98	0.42	0.33	0.09	1.04
	Magnitude at 697nm of 1 st derivative	CHL	0.82	1.28	0.57	0.31	3.78
K4	Peak Magnitude of 1 st derivative	CHL	0.84	21.14	19.68	16.65	1.30
K5	Magnitude at 482nm of 1 st derivative (linear)	CHL	0.73	4.55	4.21	3.46	2.85
	Magnitude at 482nm of 1 st derivative (logarithmic)	CHL	0.82	3.81	3.53	2.39	1.93
K6	Peak Magnitude of 1 st derivative	TCHL	0.59	12.19	11.13	8.70	5.96
K7	Peak Magnitude above a Baseline	CHL	0.85	0.69	0.64	0.52	0.96
	Peak Magnitude of 1 st derivative	CHL	0.76	0.92	0.86	0.81	1.47

The results of accuracy assessment of the best cross-seasonal algorithms reveal that despite good and in some cases high seasonal correlations with TCHL (e.g. kettle hole K1 with $R^2=0.9970$ for *Peak Magnitude* algorithm in the season of 2007), application CHL as a

water quality parameter produces better results. In almost all kettle holes cross-seasonal correlations with parameter CHL have higher values than TCHL.

The study of spectral algebra algorithms based on normalized volume reflectance and derivative spectra shows that in spite of high variety of hydro-morphological, physical and bio-ecological factors influencing upwelling radiance from water bodies, the application of the derivative analysis approach produces stable correlations with chlorophyll concentrations. On the other hand, linear regression between CHL and the *Peak Magnitude* algorithm gives consistent correlation for high algae content kettle holes. At low algae content, *Peak Magnitude above a Baseline* algorithms give the best results, for example for kettle hole K7.

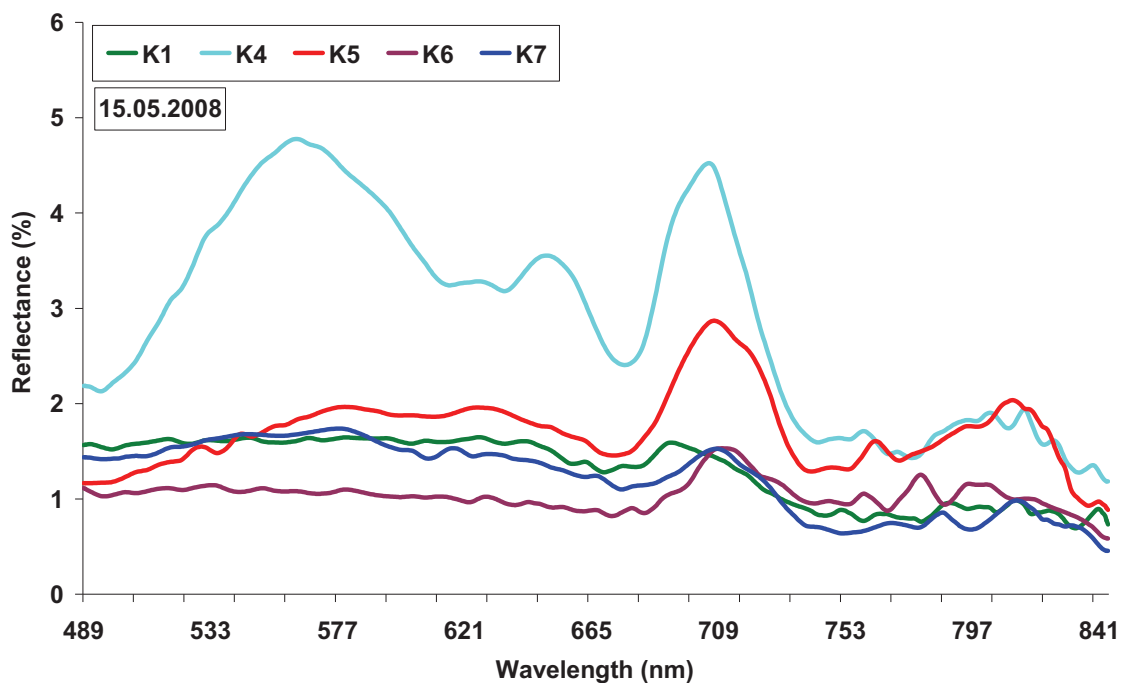
The methods based on the reflectance values at specific wavelength is the best applicable for high algae-dominated ponds, like for kettle holes K1, K2 and K5. For a ‘classical small lake’ with moderately turbid water K4 application of derivative analysis approach is the best methodology (the derivative analysis is able to remove pure water and suspended sediment effects – Han 2005).

Kettle hole K6 had the worst correlation coefficients out of all the ponds. Study of linear correlations coefficients from this kettle hole reveals that spectral data collection in overcast weather conditions is still noise affected despite the air-water correction and application of de-noising techniques. This type of kettle holes due to hydro-morphological characteristics (see Appendix A) has an immediate response from agricultural activities from surrounding areas (for example– the CHL value raised to 55 $\mu\text{g/L}$ on 06.09.2007 due to fertilization in surrounding fields, whereas the average CHL value is $\approx 10\mu\text{g/L}$). Nevertheless, the promising approach for this type of kettle hole is the application of derivative analysis (e.g. the results for the 2008 season – Table 4-5).

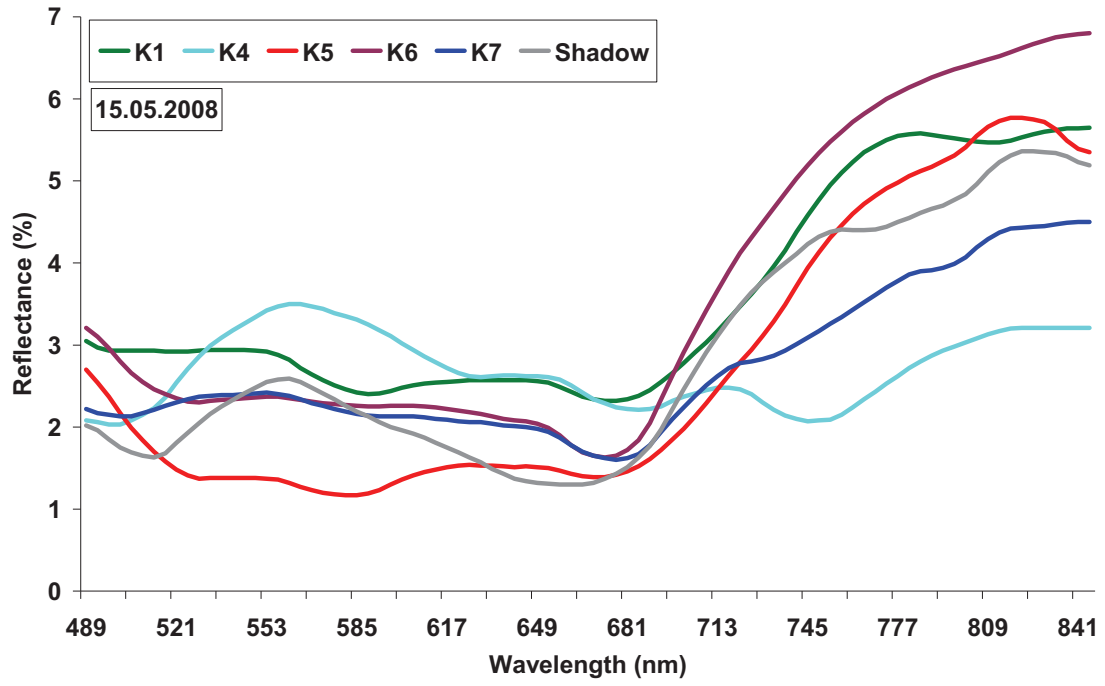
4.2 Analysis of airborne spectra

4.2.1 Analysis of field and airborne spectra

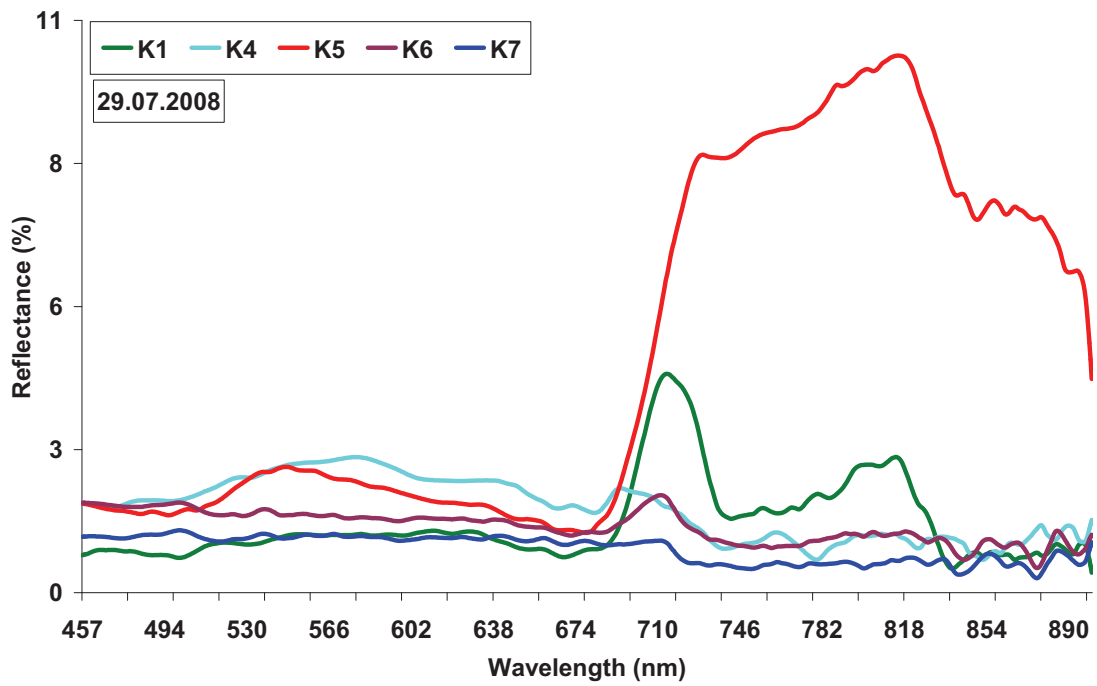
Spectral signatures from five kettle holes collected with Handheld Spectrometer and ROSIS and HyMap sensors on 15 May 2008 and 29 July 2008 respectively are shown in Figure 4-20. It is seen that field and airborne collected spectra for almost all kettle holes (except for K4) do not correspond to each other. Most likely the main reason for this spectral profiles mismatch is the difference in ground sampling distance. Field spectra was collected from so-called ‘pure objects’ and in the height of 30-35cm (i.e. area of $0.01\div 0.015\text{m}^2$) whereas each pixel of ROSIS and HyMap images have areas of 4 m^2 and 16 m^2 accordingly, and their spectra is highly influenced by algae or bottom properties of kettle holes (Scheffer 1998; Scheffer and van Nes 2007). Therefore, in field spectra the peak near 700nm is clearly seen (Figures 4-20a and 4-20c) whereas ROSIS and HyMap spectral profiles are comparable to vegetation reflection only with a smaller magnitude and peak shifted in the $740\div 820\text{nm}$ range (Figures 4-20b and 4-20d).



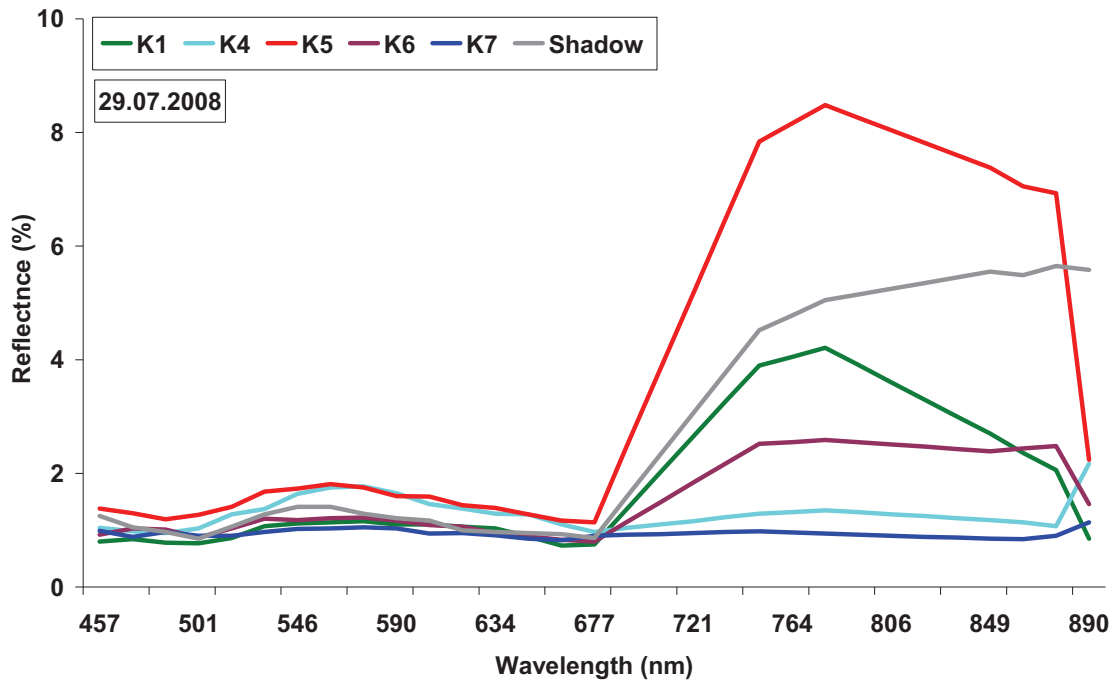
a)



b)



c)



d)

Figure 4-20: Average spectral signatures of kettle holes spectra taken on 15 May 2008 of ASD handheld field (a) and ROSIS (b), on 29 July 2008 ASD handheld field (c) and HyMap (d) respectively. X-axes of (a) and (c) are fitted for (b) and (d) accordingly

Only K4's field spectra and spectral profiles of airborne sensors are similar with respect to reflectance shape. This is mainly because of the special hydro-morphological characteristics of this kettle hole. K4 is $\approx 3\text{m}$ deep and has a size of ≈ 0.8 ha and it can be considered as a small lake; accordingly its spectral response is like a moderately turbid lake. For this type of kettle hole the linear relationship can be derived similarly to results received by Thiemann and Kaufmann, 2002. Nevertheless, for biomass mapping of all types of kettle holes, another classification methodology is needed.

4.2.2 Remote sensing data classification approach

Figure 4-21 illustrates observed CHL and TSS concentrations on flight campaign dates. On 15 May 2008 CHL and TSS concentrations for almost all kettle holes were relatively higher than on 29 July 2008. In the spring time, kettle holes were full of nutrients mostly due to land use practice within their respective catchment area (Igamberdiev et al. In press). The CHL values varied between $2.5\mu\text{g/L}$ and $32\mu\text{g/L}$ for both dates, except for K4, which had a value of $78\mu\text{g/L}$ on 15 May 2008. TSS was generally low (≈ 6 mg/L), only the water of K4 exceeded concentrations of more than 10 mg/L. In summary it can be concluded that on both flight dates the investigated kettle holes exhibited a low to moderate turbidity.

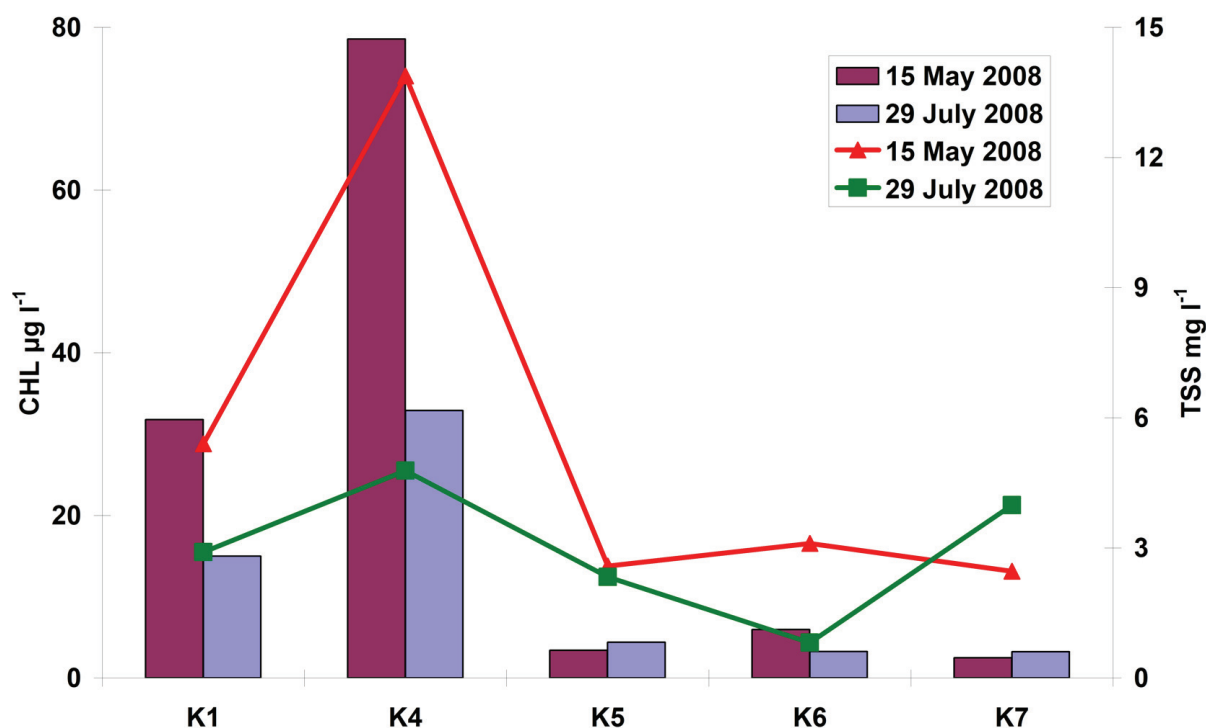


Figure 4-21: Observed CHL (bars) and TSS (lines) concentrations of the studied 5 kettle holes on the flight dates

Analysis of spectral signatures shows that the received correlations between biomass concentration and handheld spectra by Igamberdiev et al. (In press) cannot be applied to airborne spectral profiles. Application of recent methodologies like band ratio (Thiemann and Kaufmann 2002), derivative analysis (Han and Rundquist 1998; Han and Rundquist 1997), maximum reflectance (Jiao et al. 2006) and the semi-analytical model by Gitelson et al. (2008) to ROSIS and HyMap datasets did not give acceptable correlations due to high variability of hydro-morphological characteristics, algae content or different bottom types influencing water-leaving spectra and shifted chlorophyll reflection peaks for each kettle hole (Figures 4-20b and 4-20d). Nevertheless, analysis of airborne spectra revealed that the chlorophyll absorption peak near 677nm is the same for both datasets.

Several investigators studied the correlation between the chlorophyll absorption peaks (near 440nm and 678nm) and biomass concentration (Binding et al. 2008; Ma et al. 2006; Sydor 2006). In our case, the best results of direct correlation between absorption peak in airborne data and CHL concentration was still very low ($R^2=0.46$); therefore, for enhancing absorption properties both airborne spectral datasets were normalized by the Continuum Removal (CR) approach.

Continuum removal is widely used in geologic mapping and vegetation classification studies (Gomez et al. 2008; Schmidt and Skidmore 2003; Xu et al. 2008). CR normalizes reflectance spectra in order to allow comparison of individual absorption features from a common baseline (Xu et al. 2008). The continuum is a convex hull fitted over the top of a spectrum to connect local spectrum maxima (Mutanga and Skidmore 2003). The continuum-removed reflectance $R'_{(\lambda)}$ is obtained by dividing the reflectance value $R_{(\lambda)}$ for each waveband by the reflectance level of the continuum line (convex hull) $Rc_{(\lambda)}$ at the corresponding wavelength:

$$R'_{(\lambda_i)} = \frac{R_{(\lambda_i)}}{Rc_{(\lambda_i)}} \quad [4-4]$$

The first and last spectral data values are on the hull and therefore the first and last values of continuum removed spectrum are equal to '1'. The output curves have values between '0' and '1', in which the absorption troughs are enhanced (Kokaly and Clark 1999; Mutanga et al. 2005; Schmidt and Skidmore 2001). Enhancement of bands by continuum removal is done by correcting the apparent shifts in the band minimum caused by wavelength dependent scattering, which imparts a slope to the spectrum. Removal of the continuum slope corrects the band minimum to that of the true band centre (Clark and Roush 1984).

4.2.3 Chlorophyll content mapping

Figure 4-22 shows continuum-removed average absorption features of kettle holes for ROSIS and HyMap datasets. Continuum-removed reflectance clearly shows spectral characteristics of the lakes and the absorption peak at 677nm. This peak corresponds to 48 (676.6nm) and 16 (677.3nm) bands for ROSIS and HyMap datasets accordingly. Based on absorption peak data and sensor-specific characteristics, different regression approaches were tested to determine the CHL concentration from the ROSIS and HyMap reflectance spectra. Linear regression algorithms of ROSIS (formula [4-5]) and HyMap (formula [4-6]) with the best correlation coefficients (ROSI $R^2=0.81$; HyMap $R^2=0.74$) and the least mean standard error of CHL (ROSI $\pm 7.9\mu\text{g/L}$; HyMap $\pm 11.4\mu\text{g/L}$) were derived from average airborne spectra of each kettle hole:

$$\text{ROGIS: CHL} = (\text{RCR} - 0.3612) / 0.003 \quad [4-5]$$

$$\text{HyMap: CHL} = (\text{RCR} - 0.1714) / 0.012 \quad [4-6]$$

where RCR= continuum removed absorption peak image band.

Chlorophyll mapping of kettle holes using continuum-removed absorption peak bands of ROSIS and HyMap is shown in Figure 4-23. It is clearly seen that on 15 May 2008 (the beginning of cropping season), ROSIS image contained more water bodies compared to HyMap image on 29 July 2008 (midterm of cropping season). The classification of kettle holes revealed heterogeneous distribution of chlorophyll within water bodies except the small lake K4. Such large variability of algal chlorophyll concentration within one day for small and shallow water bodies is unlikely (Scheffer 1998), so the main reason for diverse biomass distribution within kettle holes is a variety of optically active in-water constituents.

From the handheld reflectance analysis results (Igamberdiev et al. In press) and field survey data, it is known that kettle hole K1 was completely covered with algae and the ‘packaging effect’ strongly modified the water-leaving radiance. The packaging of the pigments within the phytoplankton cells reduced light attenuation when compared with the same quantity of pigment dissolved in the water column (Kirk 1994). Therefore, alteration of water reflection by the packaging effect led to underestimation of biomass concentration in classification. Consequently, on 15 May 2008 the classified image K1 had the values of two classes (CHL variation from 6 to 30 $\mu\text{g/L}$) whereas the actual biomass concentration was 30 $\mu\text{g/L}$. It is seen that the central part of the kettle hole caused light attenuation and, as a result, underestimation of chlorophyll concentration. On 29 July 2008 classified scene is almost similar mapping results with ROSIS image. A few black points correspond with the above water surface vegetation and were excluded by pre-processing from further classification. The central part of the small lake corresponded to the low CHL concentration (actual is 14 $\mu\text{g/L}$) whereas the shore line biomass values varied from 11 to 35 $\mu\text{g/L}$.

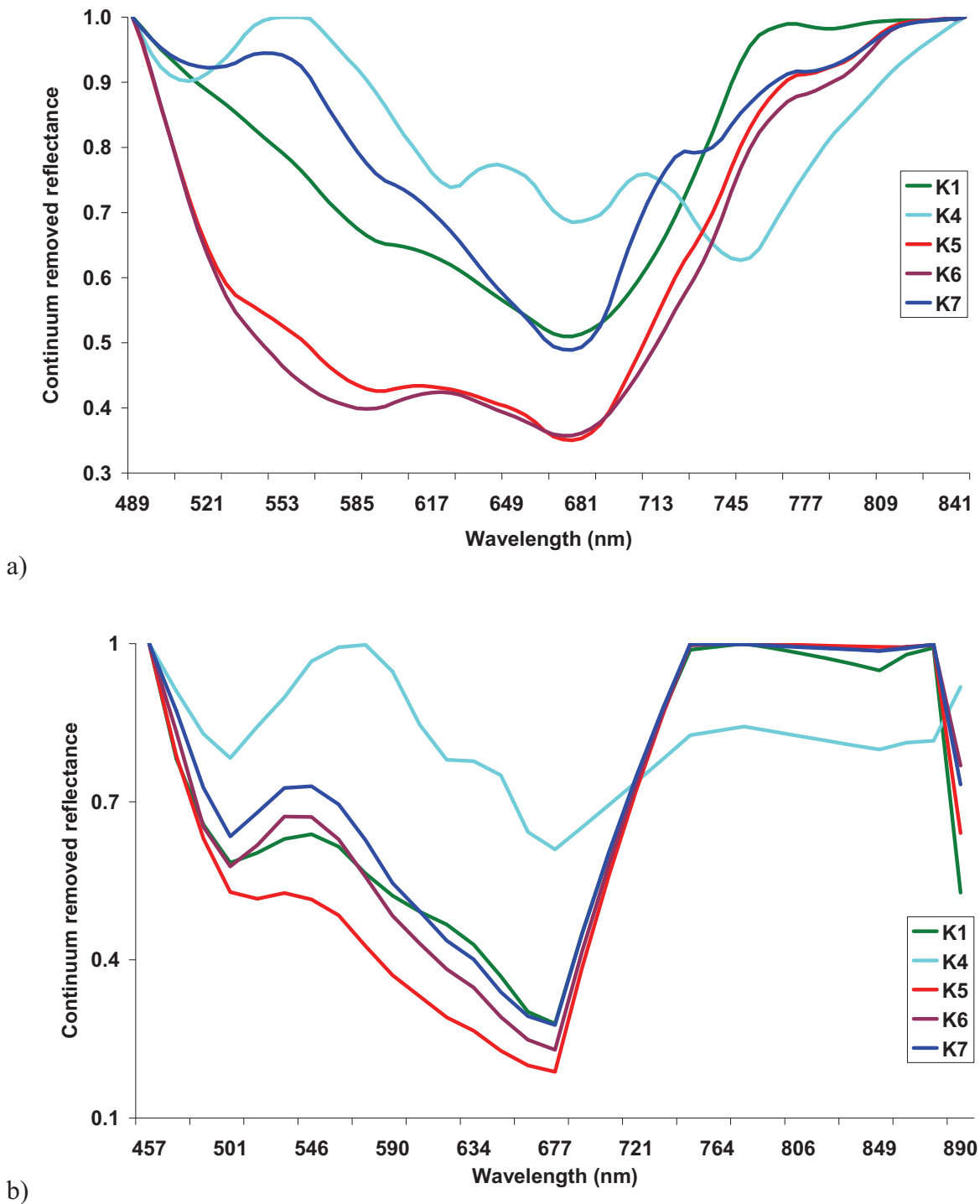


Figure 4-22: Continuum-removed average reflectance of kettle holes for ROSIS (a) and HyMap (b) datasets

High absorption values at the shore line are likely caused by a combination of two factors: HyMap pixel size ($4 \times 4\text{m}$) and submerged vegetation.

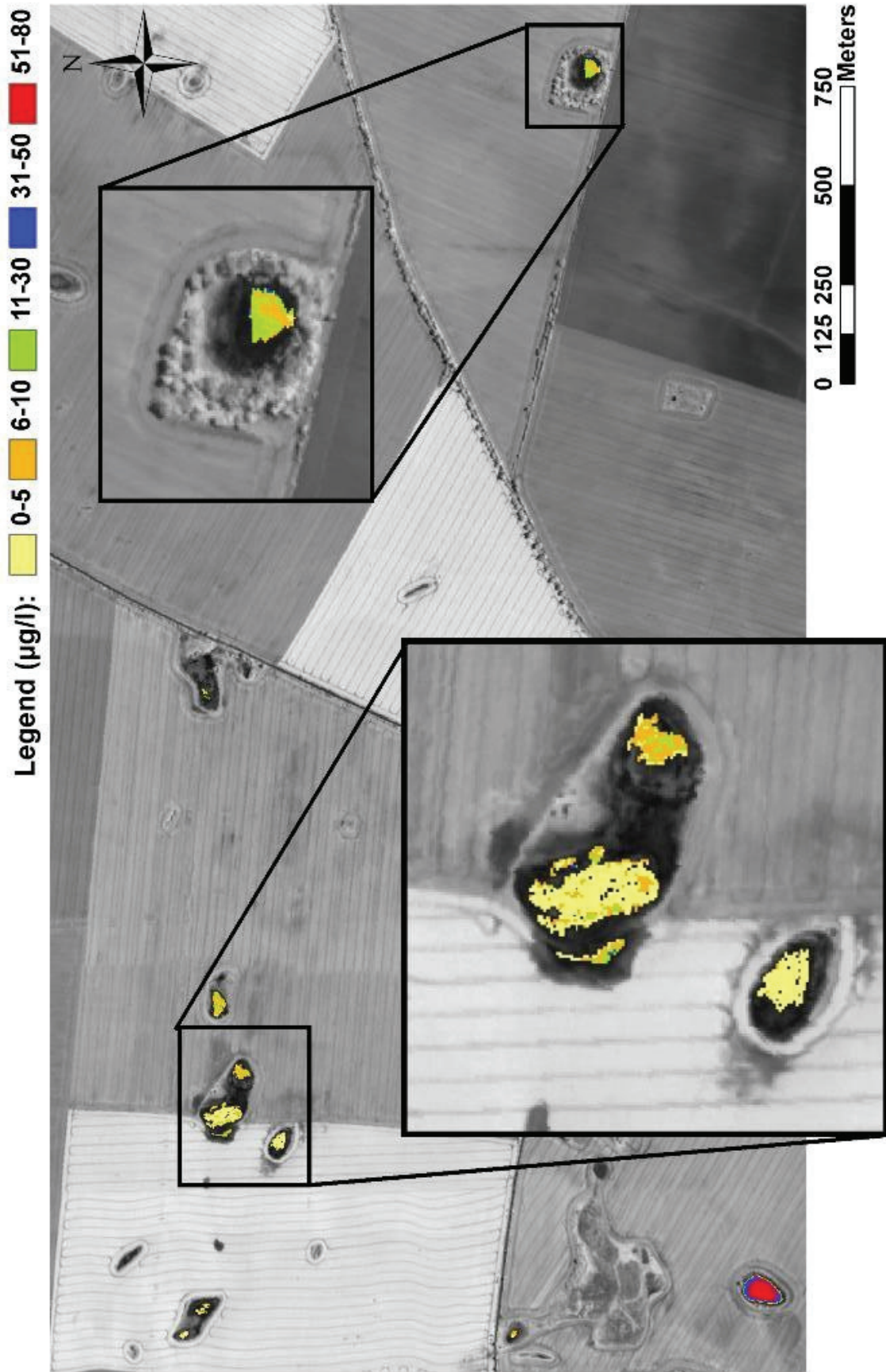




Figure 4-23: Chlorophyll spatial variations retrieved from ROSIS (a) and HyMap (b) data with enlargement of kettle holes

Classification of K4 for both datasets gave the best results and biomass mapping showed homogenous distribution. It was expected, since field and airborne spectra were matching each other: it had the highest chlorophyll and absorption values (Figure 4-22 and Figure 4-23). From the literature review we can conclude that K4 is a ‘classical’ eutrophic small

shallow lake and the existing CHL mapping algorithms (Gitelson *et al.* 2008; Kneubuehler *et al.* 2005; Thiemann and Kaufmann 2002) are most suitable for such types of water bodies.

K5 is very shallow (30-40 cm) and the smallest among the investigated kettle holes with low biomass concentration. On 15 May and 29 July 2008 CHL values were 3 μ g/L and 4 μ g/L respectively, so in both datasets the classification showed an even biomass distribution.

Table 4-8: Accuracy assessment of CHL mapping from the ROSIS dataset

Classes of CHL (μ g/L)	0 - 5	6 - 10	11 - 30	31 - 50	51 - 80	Total
0 - 5	778	110	40	8	0	936
6 - 10	325	36	56	0	0	417
11 - 30	92	0	98	0	0	190
31 - 50	0	0	0	154	80	234
51 - 80	0	0	0	147	1008	1155
Total	1195	146	194	309	1088	2932
Overall accuracy						70.74%

Table 4-9: Accuracy assessment of CHL mapping from the HyMap dataset

Classes of CHL (μ g/L)	0 - 5	6 - 10	11 - 20	21 - 35	Total
0 - 5	280	28	0	0	308
6 - 10	68	23	0	0	91
11 - 20	115	92	47	8	262
21 - 35	0	0	21	250	271
Total	463	143	68	258	932
Overall accuracy					64.38%

On the ROSIS image (Figure 4-23a) K6 is overflowed (small water strip nearby) and has almost no surface vegetation. It is mostly correctly classified and only some pixels have higher reflection. Contrary to K6 kettle hole, K7 is completely misclassified. The CHL values of K6 and K7 on 15 May 2008 were 5 μ g/L and 4 μ g/L respectively. The main reason for K7's and K6's partial misclassification is their hydro-morphological characteristics. The shallower K7 has a flat bottom almost all over, whereas the bottom of the K6 is trapezium-shaped with the deepest part situated near K7 (it is clearly seen on Figure 4-23b). The whole bottom of K6 as well as the K7's deepest part is covered by sand. The reflectance of the sand spectrum increases gradually with the longer wavelength and the

spectrum reveals higher reflection values compared with other water constituents (e.g. mud, algae). An absorption trough of sand has a slight dip in reflectance at 677nm and is consistent with absorption by CHL (Murphy *et al.* 2005). Therefore, in ROSIS and HyMap in average spectra of K7 absorption peak has relatively high values (Figure 4-23).

Finally, the overall accuracy of classification for the ROSIS dataset was 71% (Table 4-8), and for HyMap it was 64% (Table 4-9). Classification accuracy tables of both airborne datasets show that low and especially very high CHL concentrations have less errors of mapping compared to moderate CHL values. The reflection and absorption peaks of chlorophyll particularly with moderate concentration (approximately between 10 and 25µg/L) were highly influenced by high variations of in-water constituents of kettle holes. So for the implementation of any kettle holes' biomass monitoring programme, the following factors needed to be taken into account: hydro-morphological characteristics, bottom type and packaging effect.

Low classification accuracy caused as it is described above due to high variability of optically active in-water constituents. Overall, ROSIS with 2×2m spatial and 4nm spectral resolutions is more preferable for small water bodies' biomass concentration mapping compared to HyMap with a GSD of 4m.

4.2.4 Suspended sediment concentration mapping

It is relatively easy to remotely sense suspended sediments in a water body because of their strong backscattering of incident radiation (Liu *et al.* 2003). A water body with suspended sediment in it would generally appear brighter in imagery (Jensen 2006). Reflectance in the 580 - 690nm region increases as more sediment is added to the water bodies (see Figure 2-9). Taking into account the fact that for both flight dates the TSS values exhibited from a low to moderate (i.e. between 1mg/L and 14mg/L), the estimation of sediment concentrations from airborne spectra is focused on the 480÷680nm range.

Pearson's correlation coefficients were calculated between average normalized reflectance, derivative spectra and TSS concentrations from all kettle holes for ROSIS and HyMap datasets (Figure 4-24). Correlation coefficients calculated from normalized reflectance are lower than from derivative reflectance, especially for HyMap. Derivative correlation curves from both datasets are similar in shape and have three high correlation peaks at wavelengths of 550÷560nm (positive), 580÷590nm (negative) and 620÷630nm (positive).

This proves again (similar to research results of Han, 2005) that a derivative approach is a potentially powerful methodology for analysis of in-water constituents like suspended sediments and chlorophyll content.

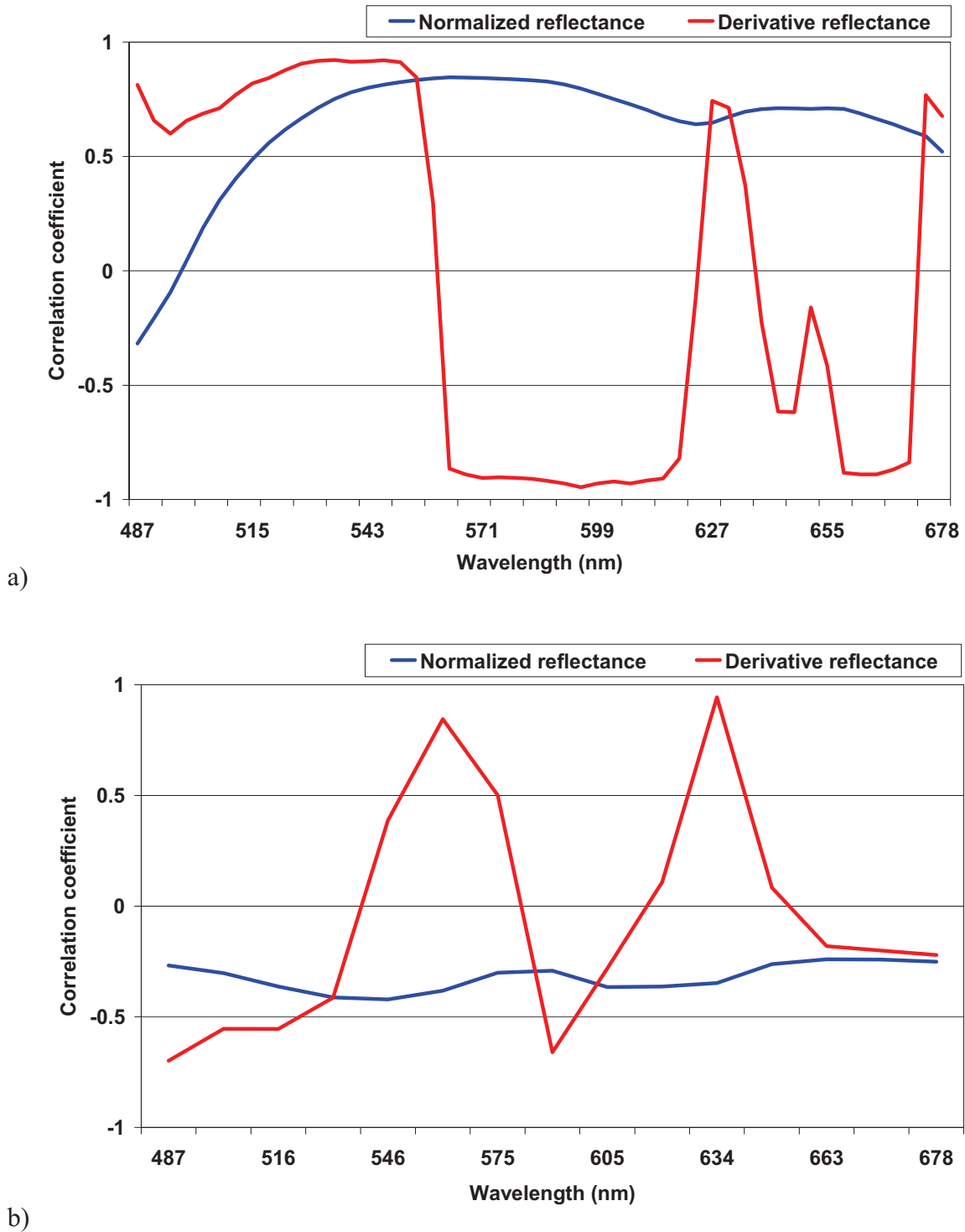


Figure 4-24: Pearson's correlation coefficients (R) between average normalized reflectance, derivative spectra and TSS concentrations from all kettle holes for ROSIS (a) and HyMap datasets

Analysis of derivative correlation spectra (Figure 4-24) shows that the best correlation between TSS concentrations and ROSIS spectra is at 596nm (-0.95) and for HyMap is at 630nm (0.94). Graphical illustrations of linear regressions between suspended sediments concentrations and derivative reflection values at these wavelengths from ROSIS and HyMap hyperspectral imagery are shown in Figure 4-25.

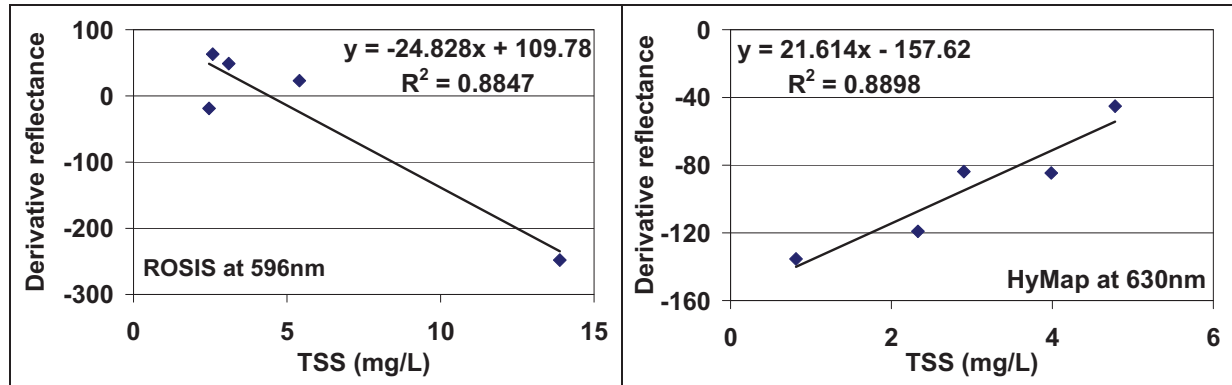


Figure 4-25: Received linear regression correlations between TSS concentrations from investigated kettle holes and derivative reflection values at 596nm and 630nm wavelengths from ROSIS and HyMap datasets accordingly

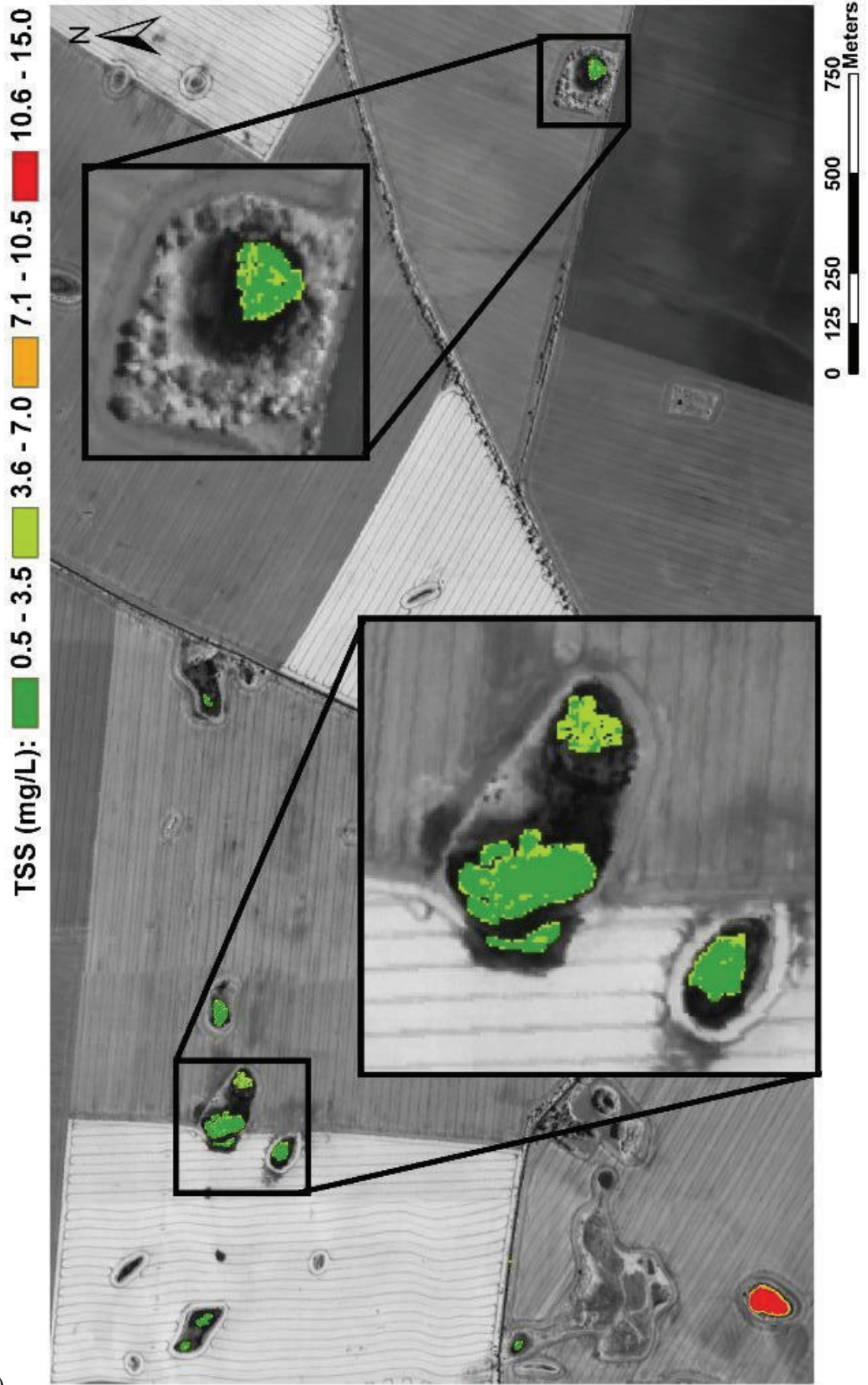
Based on the results shown in Figure 4-25, the linear regression algorithms of ROSIS (formula [4-7]) and HyMap (formula [4-8]) for TSS concentrations estimation were derived from average derivative reflectance at 596nm and 630nm wavelengths accordingly of each kettle hole:

$$\text{ROSIS: TSS} = (109.8 - \text{DR}_{596}) / 24.8 \quad [4-7]$$

$$\text{HyMap: TSS} = (\text{DR}_{630} + 157.6) / 21.6 \quad [4-8]$$

where DR_n – derivative reflectance at n wavelength.

Results of TSS concentrations mapping with the least mean standard error (ROSIS \pm 2.6mg/L; HyMap \pm 1.9mg/L) from ROSIS and HyMap derivative spectra are shown in Figure 4-26.



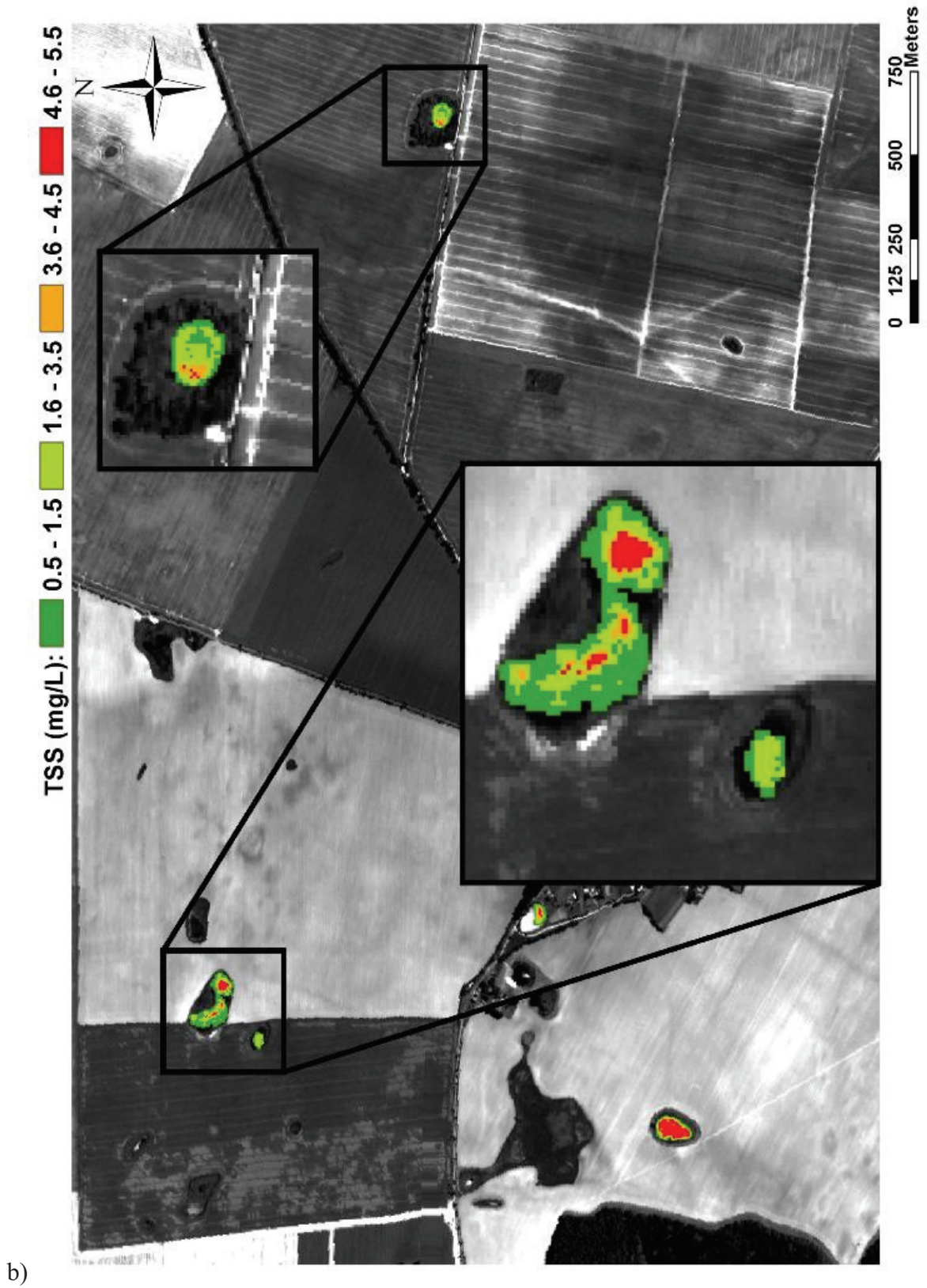


Figure 4-26: Suspended sediment concentrations spatial variations retrieved from ROSIS (a) and HyMap (b) data with enlargement of kettle holes

Table 4-10: Accuracy assessment of TSS mapping from ROSIS dataset

Classes of TSS (mg/L)	0.5-3.5	3.6-7.0	7.1-10.5	10.6-15.0	Total
0.5-3.5	1021	77	37	0	1135
3.6-7.0	276	283	56	36	651
7.1-10.5	22	0	74	0	96
10.6-15.0	0	0	0	1049	1049
Total	1319	360	167	1085	2931
Overall accuracy					82.80%

Classified map from ROSIS data (Figure 4-26a) shows good results of TSS mapping with overall accuracy of 83% (Table 4-10). Similar to CHL, mapping low (K5 and K6) and very high (K4) TSS values are classified with fewer errors. Absorption at 596nm from green algae bottom of K1 influences derivative spectra by causing underestimation of TSS values. TSS concentration on 15 May 2008 was 5.4 mg/L and only the deepest part with shoreline is in this range, the rest is underestimated. On the other hand, K7 with TSS of 2.5mg/L is overestimated which is caused by high reflectance from sandy bottom. Correlation analysis on Figure 4-25a shows that these two TSS values of K1 and K7 are staying slightly apart from the main regression line. Taking into account that this correlation is based on average spectra, this kind of misclassification was expected.

Table 4-11: Accuracy assessment of TSS mapping from HyMap dataset

Classes of TSS (mg/L)	0.5-1.5	1.6-3.5	3.6-4.5	4.6-6.5	Total
0.5-1.5	206	18	0	0	224
1.6-3.5	58	157	0	10	225
3.6-4.5	41	29	147	8	225
4.6-6.5	12	28	21	197	258
Total	317	232	168	215	932
Overall accuracy					75.86%

Suspended sediment concentrations mapping from a HyMap dataset produces relatively good results with overall accuracy of 76% (Table 4-11). Contrary to 15 May, the TSS values variation was almost two times less than on 29 July 2008 (i.e. from 1mg/L to 5mg/L). More than half of K1 is correctly classified due to lower TSS and CHL values (see Figure 4-21). Only the deepest areas with high algae content and shallow parts are wrongly estimated. K4 and K5 are mostly correctly classified; only shoreline values are calculated slightly lower due to depth differences with the central area. K6 is mostly correctly classified. Almost all of K7 and the deepest part of K6 are wrongly estimated, due to sandy bottom.

4.2.5 Water depth mapping

For complete understanding of the relationship between airborne spectra and the trophic status of kettle holes, additionally to the parameters described in chapter 3.3 and listed in the Appendix B, only on the flight dates the water depth values from measurement sites of each kettle hole were also collected. Limited human resources during field campaigns and the distant between measuring laboratory and the sampling sites made it difficult to collect the water depth values on all dates of monitoring. The values of water depth from both flight dates are illustrated in figure 4-27.

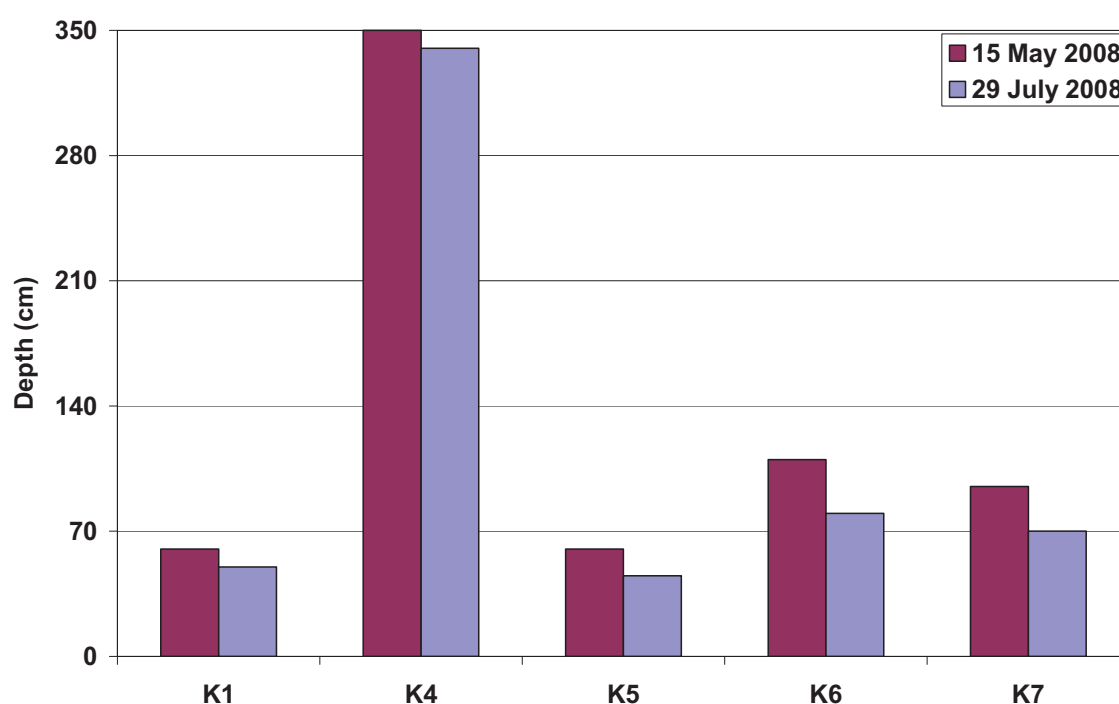


Figure 4-27: Observed water depth values of the 5 studied kettle holes on the flight dates

The most difficult aspect of the water depth remote sensing retrieval method is the tendency for variations to arise from changes in water depth, bottom type, and scattering and absorption in the water column (by chlorophyll, suspended sediments, coloured dissolved organic matter, etc.). As for the complex composition and their interactions in coastal and inland waters, there is a rare general model even in the same region. More attention should be paid to the elimination and reduction of environmental effects on the signals of water depth in the research (Conger *et al.* 2006). Correlation between derivative reflectance and depth was successfully adopted by Wang (2007) and it was proved to be useful to reduce the influence of substances in the coastal waters.

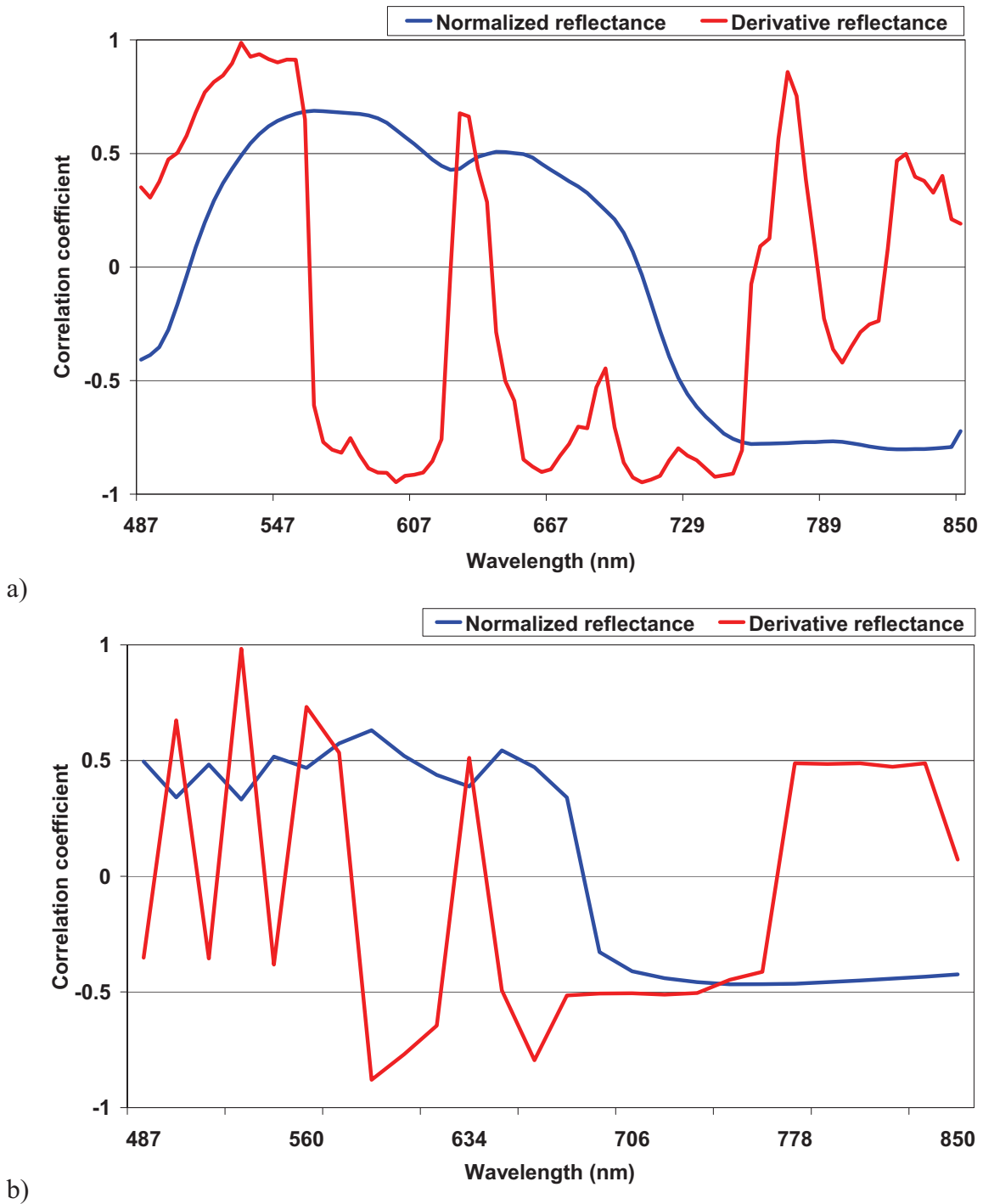


Figure 4-28: Pearson's correlation coefficients (R) between average normalized reflectance, derivative spectra and depth from all kettle holes for ROSIS (a) and HyMap datasets

Pearson's correlation coefficients between average normalized reflectance, derivative spectra of airborne datasets and water depth values are shown in Figure 4-28. Correlation curves of normalized reflectance and derivative spectra from ROSIS and HyMap are similar to each other in shape. At the same time, the derivative correlation curves are best correlated with water depth values. Similar to TSS correlations, derivative correlation

curves from both datasets are similar in shape and have three high correlation peaks at wavelengths of 520÷530nm (positive), 580÷590nm (negative) and 620÷630nm (positive). The ROSIS dataset also has a high peak at 772nm. Among all peaks the derivative reflectance values from 530nm are best correlated with water depth.

Correlation coefficients between water depth and derivative reflectance values at 530nm are 0.97 and 0.98 for ROSIS and HyMap respectively. Graphical illustrations of linear regressions between water depth and derivative reflection values at 530nm wavelength from ROSIS and HyMap hyperspectral imagery are shown in Figure 4-29.

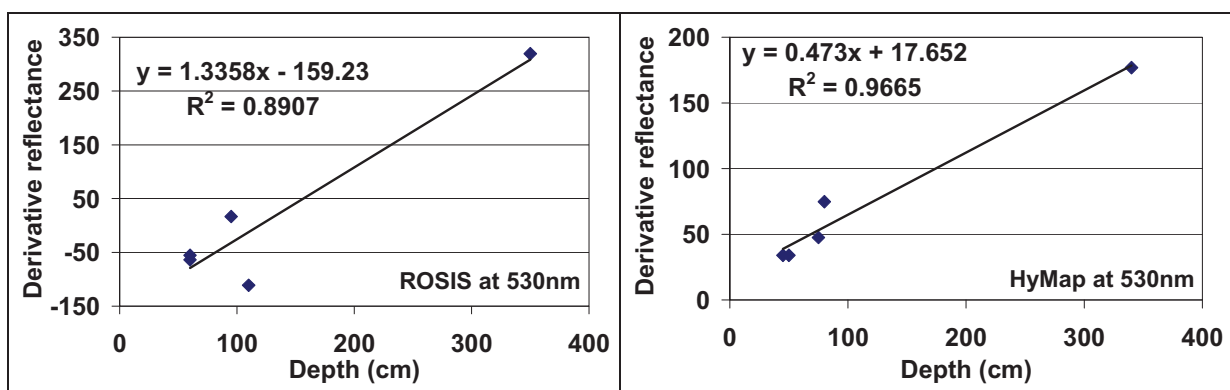


Figure 4-29: Received linear regression correlations water depth from investigated kettle holes and derivative reflection values at 530nm wavelength from ROSIS and HyMap datasets

Based on the results shown in Figure 4-29 the linear regression algorithms of ROSIS (formula [4-9]) and HyMap (formula [4-10]) for water depth estimation were derived from average derivative reflectance at 530nm wavelength of each kettle hole:

$$\text{ROGIS: TSS} = (\text{DR}_{530} + 159.2) / 1.3 \quad [4-9]$$

$$\text{HyMap: TSS} = (\text{DR}_{530} - 17.7) / 0.47 \quad [4-10]$$

where DR_{530} is the derivative reflectance at 530nm wavelength.

Results of water depth mapping with the least mean standard error (ROGIS $\pm 22\text{cm}$; HyMap $\pm 24\text{cm}$) from ROSIS and HyMap derivative spectra are shown in Figure 4-30.

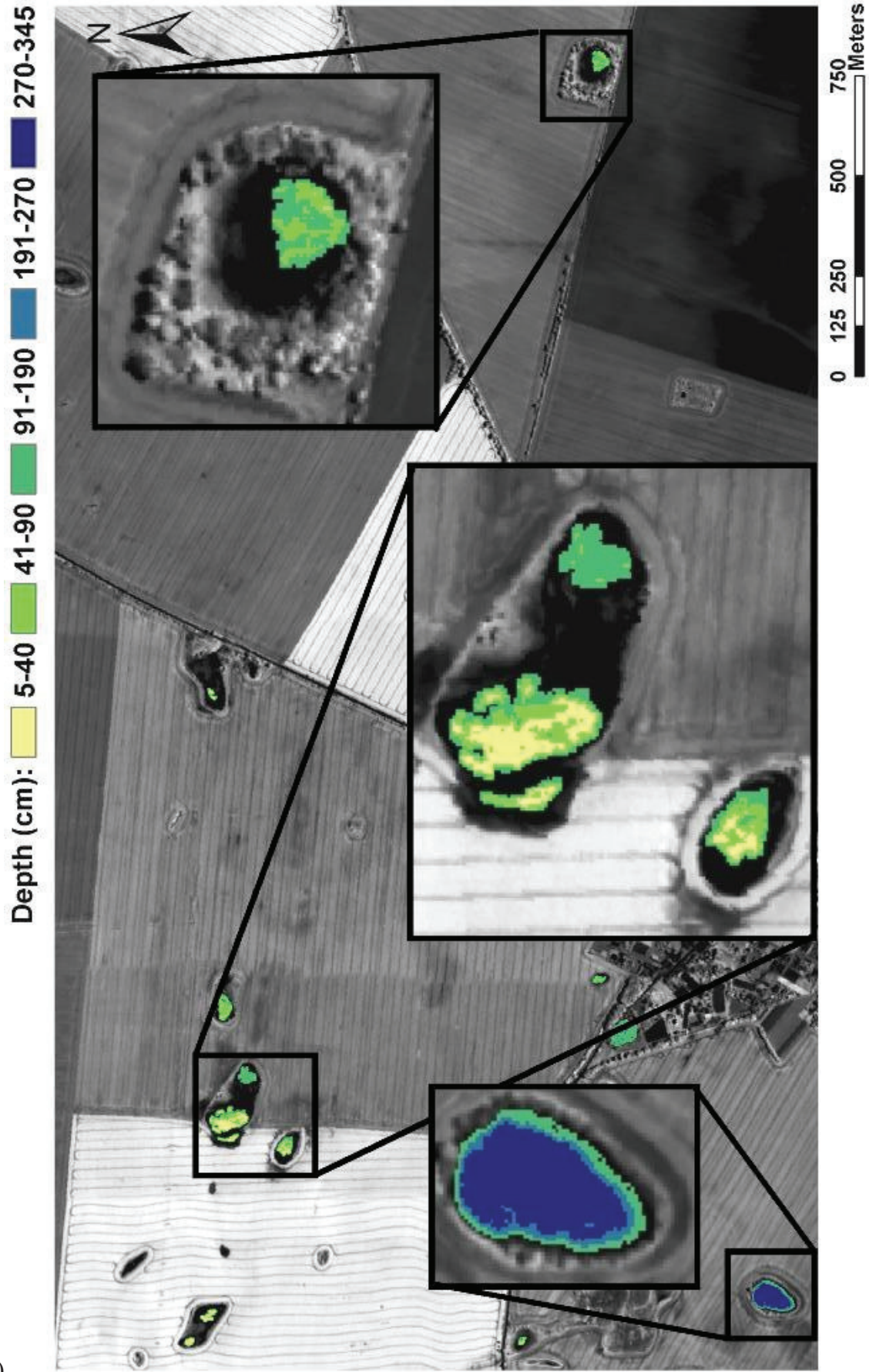




Figure 4-30: Water depth spatial variations retrieved from ROSIS (a) and HyMap (b) data with enlargement of kettle holes

Accuracy assessments of water depth mapping from ROSIS and HyMap datasets are given in tables 4-11 and 4-12. Contrary to other parameters, water depth is not a constant value within one water body on a time of RS image acquisition. Thus, accuracy assessment is

based on water depth data collected on flight days and field survey analysis of hydro-morphological characteristics of each water body collected during monitoring.

Table 4-12: Accuracy assessment of water depth mapping from ROSIS dataset

Classes of Depth (cm)	5-40	41-90	91-190	191-270	270-345	Total
5-40	571	39	14	11	0	635
41-90	113	393	35	0	0	541
91-190	41	0	492	0	0	533
191-270	0	0	0	103	80	183
270-345	0	0	0	54	987	1041
Total	725	432	541	168	1067	2933
Overall accuracy						86.81%

The classified water depth map (Figure 4-30a) retrieved from the ROSIS dataset shows very good results with an overall accuracy of 87% (Table 4-12). More than half of kettle hole K1 is correctly classified. Misclassification of K1 (a shallow strip in the middle) is mostly caused by the high influence of the green algae reflection peak at 530nm. Almost the whole of K4's classification is correct. The shoreline values are gradually and smoothly changed from low to deepest depth class. Similar to K1, kettle hole K5 has the wrong depth classification value at the shoreline caused by green algae reflection. Nevertheless, the most part of K5 is properly classified. K6 and K7 are classified with very good accuracy. The shallower K7 has a flat bottom almost all over, whereas the bottom of the K6 is trapezium-shaped with the deepest part situated near K7. At the same time there are some misclassifications with high depth values at the shoreline between K6 and K7 caused by submerged algae.

Table 4-13: Accuracy assessment of water depth mapping from HyMap dataset

Classes of Depth (cm)	5-40	41-110	111-190	191-270	Total
5-40	189	17	0	0	206
41-110	58	264	0	0	322
111-190	37	29	53	11	130
191-270	8	13	16	237	274
Total	292	323	69	248	932
Overall accuracy					79.72%

The overall accuracy of water depth mapping (Figure 4-30b) from HyMap imagery is 80% (Table 4-13). Almost all of K1 is properly classified except for two small patches from the deepest part of the kettle hole. The relatively correct classification of K1 was caused by

low values of CHL and TSS on HyMap flight day. K4 is also mostly classified with very good accuracy. K5 is classified completely correctly due to its small and shallow size and its low biomass concentration on 29 July 2008 (Appendix B). Almost half of K6 is wrongly classified. Analysis of the hydro-morphological characteristics of K6 revealed that at low algae and CHL concentrations (i.e. $3\mu\text{g/L}$), the sandy part of the bottom had a significant influence on the water-leaving radiance. It is most likely that misclassification of the deepest part of K6 is caused by the influence of sand reflection. K7 also has a sandy bottom but as shown in figure 4-30b it is correctly classified. The reason for this classification difference is the amount of sand at the bottom. Low-positioned K6 collects at its deepest part all sediments from the surrounding area. Consequently, at low CHL concentrations the reflection from this part is very high, and at high biomass values the water-leaving radiance is influenced by algae content (like in CHL mapping on 15 May 2008). Contrary to K6, the bottom of K7 is flat and the sand is distributed evenly. Therefore, using the derivative analysis approach for K7 reduces influences from the sandy bottom reflection.

Finally, accuracy of water depth classification is higher than CHL and TSS concentrations mapping.

4.3 Optimal spectral ranges

The summary of the most sensitive spectral ranges (bands) from handheld and airborne spectra based on normalized reflectance and derivative analysis that were used for water quality parameters (CHL, TSS and water depth) estimations in various types of kettle holes are given in Table 4-14.

Analysis of Table 4-14 shows that generally the derivative spectra are relatively better correlated with water quality parameters acquired either from handheld or airborne sensors. Only in the case of CHL mapping using airborne datasets does the application of continuum removal produce the best correlation results.

Table 4-14: Identified optimal spectral wavebands for water quality parameters

Water quality parameter	Reflectance type	Dominated in-water parameter	Spectral range (nm)	Biophysical characteristics
Chlorophyll- <i>a</i> (CHL)	Handheld normalized	Algae	710 – 750	Chlorophyll reflection peak
	Handheld derivative approach	Algae	696 – 698	Chlorophyll reflection peak
	Handheld derivative approach	Suspended sediments, turbidity	680 – 698	Chlorophyll reflection peak
	Handheld derivative approach	Low water level, high variation turbidity	480 – 490	GREEN reflectance of electromagnetic spectrum
	Handheld normalized	Transparent waters, sandy bottom	690 – 715	Chlorophyll reflection peak
	Handheld derivative approach	Transparent waters, sandy bottom	678 – 690	Chlorophyll reflection peak
	Airborne CR reflection	All types	677	Chlorophyll absorption peak
TSS	Airborne derivative approach	For most types, except for sandy bottoms	550 – 560 580 – 590 620 – 630	Amount of sediment
Depth	Airborne derivative approach	For most types, except for very sandy bottoms	520 – 530 580 – 590 620 – 630	Rate of transparency

5 Conclusions and future research

5.1 Water quality assessment based on handheld spectra

The acquisition of inland water quality (WQ) data is an important but tedious task due to the pronounced spatial and temporal variability of most in-water constituents, especially for small shallow water bodies. Hyperspectral remote sensing can provide useful information for water quality monitoring in agricultural young moraine landscapes in North-Eastern Germany. This research aimed to make a first attempt at presenting the ability of hyperspectral remote sensing (two-years field spectrometry data, HyMap and ROSIS sensors imagery) for kettle holes' water quality parameters (chlorophyll, water depth, total suspended sediments) mapping in agricultural young moraine landscapes in North-Eastern Germany.

The test area is located close to the city of Demmin, about 150 km north of the city of Berlin, and covers approximately 10km². The first survey (May, 2007) showed that all the kettle holes are within agricultural fields and have different shapes, sizes, water table depths, water regimes and trophic states. After elimination of the permanently dry kettle holes, the primary monitoring programme included 9 sampling stations. However, some kettle holes dried out during summer, so the kettle holes K8 and K9 were excluded from further monitoring. Kettle hole K3 was entirely covered by duckweed (botanic *Lemna spp.*) and was also not considered in the study. Finally, the field data were collected from 6 kettle holes in the period between June and October 2007 (a total of 7 datasets, 5 of which were with spectral data). In summer 2008 kettle hole K2 dried out and it was also excluded from further monitoring. Between May and September 2008, ground truth data were collected in 10 field campaigns from 5 kettle holes. Overall, spectral and pigment ground truth collection resulted in 15 datasets during 2007 and 2008, giving sufficient information for seasonal and annual analysis of water quality temporal dynamics. Field activities at the sites included the collection of water samples for laboratory analysis of chlorophyll-*a* (CHL), total chlorophyll (TCHL), total suspended sediments (TSS), water samples absorption at 750 nm, pH and electrical conductivity (EC).

Upwelling radiance data (for determination of reflectance spectra) were collected at the same time as water sampling from 6 lakes in 15 field campaigns (5 in 2007 and 10 in 2008) resulting in a total of 80 spectral datasets. Recorded radiance represented the vertical flux

of energy upward from the water. These nadir optical measurements were collected using a field spectroradiometer (ASD FieldSpec HH ultraviolet/visible and near-infrared (UV/VNIR)). The instrument records a continuous spectrum with 25° FOV in 512 bands, ranging from 274 nm to 1,085 nm with 1.587 nm spectral resolution. Upwelling radiance from the water body is retrieved as relative reflectance in relation to the downwelling radiance spectrum measured from a reference panel (25-30 cm above the panel). Depending on the depth and size of the kettle hole, the spectral measurement took place either on board a boat or at the shoreline.

An analytical approach for water quality retrieval relates the subsurface irradiance reflectance (or volume reflectance) to the water constituent concentrations. Volume reflectance is nearly independent of atmospheric properties and entirely determined by the optical properties of the water and its constituents. Therefore, all received field spectra were processed using air-water correction formulae volume reflectance.

After using air-water correction, the resulting volume reflectance spectra needed to be filtered to produce the data that are uncontaminated by noise from the atmosphere or the sensor itself. The volume spectra were filtered using MatLab 7.0 software applying the Savitzky-Golay filter and Discrete De-noising Wavelets. It was found that for clear sky conditions it is best to use the DWT filter with the 'sym5' or 'sym8' Symlet wavelet, depending on noise level. The Symlet wavelet seeks to preserve the shapes of reflectance peaks and essentially performs a local polynomial regression to determine the smoothed value for each data point. This method is superior to adjacent averaging because it tends to preserve features such as peak height and width, which are usually 'washed out' by adjacent averaging. At the same time in case of windy weather, the best performing filter was a combination of first the Savitzky-Golay filter with a small frame size (e.g. 17) and then Discrete Wavelet Transformation with 'sym5' wavelet. In all filters, a polynomial degree of 3 best preserved the shape of the spectra and has been used for all data.

The study of spectral algebra algorithms based on normalized volume reflectance and derivative spectra shows that in spite of the high variety of hydro-morphological, physical and bio-ecological factors influencing upwelling radiance from the water body, the application of the derivative analysis approach produces stable correlations with chlorophyll concentrations. For example, for a 'classical small lake' with moderately turbid water K4 application of derivative analysis approach is the best methodology. The

method based on the reflectance values at a specific wavelength is the best applicable for high-algae-dominated ponds, such as kettle holes K1, K2 and K5.

Kettle hole K6 has the worst correlation coefficients out of all the ponds. The study of the linear correlations coefficients from this kettle hole reveals that spectral data collection during overcast weather conditions is still noise-affected, despite the air-water correction and application of de-noising techniques. This type of kettle holes due to its hydro-morphological characteristics has an immediate response to the agricultural activities from the surrounding area. The promising approach for this type of kettle hole is the application of derivative analysis.

The results of the accuracy assessment of the best cross-seasonal algorithms reveal that application as a biomass indicator the water quality parameter CHL produces best results. In almost all of the kettle holes, the cross-seasonal correlations with parameter CHL have higher values than with TCHL. The spectral signatures of the water bodies are kettle holes' type specific and depend on the agricultural activity and respective nutrient status in a catchment area. The packaging effect significantly influences the water-leaving reflectance and can lead to underestimating the biomass concentration in RS signal analysis and image classification. The correlation between the spectral signals and the chlorophyll concentration is stable over one season as long as the 'type of kettle hole' does not change.

5.2 Water quality assessment based on airborne spectra

A multi-temporal database was built including the data of the ROSIS (Reflective Optics System Imaging Spectrometer, German Aerospace Centre - DLR) and HyMap ('Hyperspectral Mapper' - HyVista, Australia) airborne hyperspectral sensors. The collected ROSIS image spectra (15 May 2008), having a range from 389 to 845nm and an interval of 4nm in 115 bands, were recorded with full ground coverage at an altitude of about 3500m resulting in a spatial resolution of 2×2 m.

HyMap is a whisk-broom scanner with 126 bands between 450 and 2500nm and provided a dataset of 29 July 2008 from an altitude of about 2000m with 4×4m pixel size and about 15nm bandwidth and spectral intervals. Only the first 34 bands between 450 and 920nm relevant for the determination of water constituents were used in this study.

Water samples at a depth between 0 and 0.2 m for chlorophyll content analysis and *in situ* reflectance data at the height of ≈ 30 cm in a vertical downward direction were taken between 10 am and 2 pm during two flight campaigns on 15 May 2008 and 29 July 2008.

All airborne data sets have been atmospherically corrected using the ATCOR4 software package for airborne data. This software corrects at-sensor radiance images for the solar illuminance, the Rayleigh and adjacency scattering in order to derive nadir-normalized ground reflectance. Geo-referencing of the ROSIS and HyMap images is based on data from a navigation system (IGI) which records simultaneously the flight altitude and position parameters. Both scanners were flown mounted on a stabilizing platform during clear sky weather conditions. The overlay onto an existing airborne image data with a ground sampling distance (GSD) of 20 cm shows good agreement of about 90% of the lake pixels with a position accuracy of less than 3 pixels (= 60 cm).

According to current specification at the German Aerospace Centre (DLR) both image datasets (ROSI and HyMap) were processed to L2 level, i.e. geo-referenced and atmospherically corrected spectral reflectance data. In order to enhance even the smallest changes in ground reflectance the digital number (DN) values of both datasets have been stretched to 10,000, e.g. 100 DN value on an image corresponds to 1% of ground reflectance.

The plot of kettle holes' spectral profiles in the ROSIS dataset illustrated that the range between 389nm and 480nm is highly noise influenced. Therefore, further processing of ROSIS data was focused on the range between 489nm and 845nm, i.e. 16÷115 bands – a total of 90 bands. Analysis of spectral signatures in that range showed that ground reflection of kettle holes is relatively noise contaminated. Consequently, the ROSIS image dataset has been smoothed using a combination of the Savitzky-Golay filter and Discrete Wavelet Transformation de-noising approach.

The HyMap image dataset has a spectral interval of about 15nm with a ground resolution of 4×4m (which is almost 4 times higher than the ROSIS resolution for both parameters) and the study of the reflection profiles of kettle holes showed that application of any filtering techniques can remove important absorption/reflectance features of the image spectrum; thus, no smoothing methods were used.

Existing spectral analysis methods of inland waters are based on the variation within the data; therefore, spectral profiles of water bodies have to be unique on the image in order to avoid any misclassifications with other land cover/use types. In reality, inland waters are mostly surrounded by different objects (e.g. trees) which cause topographic shadows. Analysis of spectral signatures of water bodies and shadows in airborne datasets shows that with reflectance near 770nm, over 10 % belongs to other land cover types. Hence, it was simple to create a binary mask for both datasets with '1' value for all objects less than 10 % (i.e. with 1000 DN values) and '0' for the rest of the image. Finally, the received images were easy to aggregate into shadows and water classes using standard image processing tools. The resulting raster map is applied as a binary mask to create water-only images of the original brightness from airborne hyperspectral data.

Field and airborne spectra for almost all kettle holes do not correspond to each other due to differences in the ground sampling distance (as opposed to earlier studies). The chlorophyll reflection peak for all water bodies is situated in the 740÷820nm range. Application of recent biomass estimation algorithms did not give acceptable correlations due to the high variability of the factors (e.g. hydro-morphological characteristics, algae or bottom types) influencing the chlorophyll reflection peak. In addition, field spectra from the height of 30-35cm (i.e. an area of 0.01 – 0.015m²) were collected. Airborne pixels of ROSIS and HyMap imagery have an area of 4m² and 16m² accordingly, and their spectra are highly influenced by algae or the bottom properties of kettle holes. Analysis of airborne spectra revealed that chlorophyll absorption near 677nm is the same for both datasets. In order to enhance absorption properties, both airborne hyperspectral datasets were normalized by the continuum removal approach. Linear regression algorithms for ROSIS and HyMap datasets were derived using normalized average chlorophyll absorption spectra for each kettle hole. Overall accuracy of biomass mapping for ROSIS data is 71% and 64 % for HyMap and with the least mean standard error of CHL for ROSIS is ± 7.9µg/L and for HyMap ± 11.4µg/L.

For estimation of water depth and total suspended sediment (TSS) the derivative analysis approach has been applied to the airborne image datasets. Derivative airborne spectra show best correlation for TSS at 596nm and at 630nm with overall classification accuracy of 83% and 86% with the least mean standard error of ±2.6mg/L and ± 1.9mg/L for ROSIS and HyMap datasets accordingly.

For complete understanding of the relation between airborne spectra and the trophic status of kettle holes, in addition to the parameters listed in Appendix B on flight dates, the values of water depth were also collected. Correlation between water depth and derivative reflectance at 530nm of ROSIS and HyMap hyperspectral imagery reveals high linear regressions coefficients with classification accuracy of 87% and 80% and the least mean standard error of $\pm 22\text{cm}$ and $\pm 24\text{cm}$ respectively.

The results of this study show that hyperspectral remote sensing can provide useful information for water quality monitoring in agricultural young moraine landscapes in North-Eastern Germany. However, biomass mapping results showed that, depending on the type of kettle hole, the ‘packaging effect’ and bottom reflection can lead to miscalculation of chlorophyll content.

Overall, ROSIS with $2\times 2\text{m}$ spatial and 4nm spectral resolutions is preferable for small water bodies’ biomass concentration mapping compared to HyMap with a GSD of 4m .

5.3 Future research

The future research can be followed in two directions: (1) integration of the water quality parameters mapping based on received algorithms and methods to the land use/ land cover monitoring programmes; (2) improvement of established methodology by investigating the subsurface spectral properties of kettle holes.

5.3.1 Water quality parameters mapping as a part of land use/ land cover maps

Lakes’ and streams’ ecosystems around the world are being impacted by eutrophication, especially for small water bodies. Most water quality models simulate increases in eutrophication based on initial conditions of the water body, therefore demanding comprehensive water quality sampling programmes. However, the conventional measurement of water quality requires *in situ* sampling and expensive and time-consuming laboratory work. Remote sensing can overcome these constraints by providing an alternative means of water quality monitoring over a range of temporal and spatial scales. Remote sensing has been increasingly used for determining and monitoring trophic status of inland water bodies especially over the past 30 years. A number of studies have shown that applications of remote sensing can meet the demand for the large sample sizes required of water quality studies conducted on the watershed scale. Imagery from satellite

and aircraft remote sensing systems has been used in the assessment of water quality parameters such as temperature, chlorophyll content, turbidity, and total suspended sediment (TSS) for lakes and reservoirs.

Hyperspectral remote sensing is more advantageous than multispectral remote sensing in that the radiation reflected from a target is recorded in extremely narrow wavebands (e.g. a few nanometres). In this way the subtle radiometric variation of the target can be detected and even quantified from remotely sensed data.

However, previous studies have focused on the discovery of the relationship between remote sensing data and *in-situ* measurements. To make remote sensing tools useful for practical applications to kettle holes, water quality modelling must be incorporated with land use/land cover quality monitoring programmes in their catchment areas. Moreover, integrating a geographic information system (GIS) allows for the display of refined monitoring simulation results, rather than the use of traditional numerical figures. This provides a means by which trophic status modelling data can be presented in a way that is practical for water quality management.

The suggestions for specific objectives of future studies are to: 1) establish a model to process remote sensing data and provide a rapid and efficient monitoring technique for agricultural activities in kettle holes' catchment areas; 2) present predicted water quality conditions temporally and spatially on a geo-referenced map(s); and 3) display sequential (temporal) images of agricultural activities and water quality predictions to provide decision makers with easily understandable information.

However, these study results show that in order to implement a large-scale kettle holes' water quality monitoring programme, precise investigations of small-scale processes are needed.

5.3.2 Investigation of subsurface spectral properties of kettle holes

The fast yet accurate determination of water quality of inland surface water bodies is most critical for the evaluation of climate and land use change impact. Hyperspectral remote sensors have proven to be best suited to eutrophication monitoring for large water bodies. However, no method is at hand allowing quantifying chlorophyll content, as a proxy for nutrient loading and trophic state, for small water bodies such as kettle holes. Thus, future research should tackled an investigation into bottom reflection and packaging effects as the

two main factors restricting the derivation of clear relations between spectral signal intensity and CHL for ponds. In order to derive reliable semi-empirical/analytical models, a series of field campaigns covering multiple kettle holes and therewith a broad variety of size-classes, hydro-morphologies and pigmentation types of phytoplankton, as well as background conditions, have to be initiated. Obtained spectra and ground truth data including specific parameters such as phytoplankton pigments and size distribution of phytoplankton will serve as a basis for algorithm development for the correction of bottom reflection and packaging effect from remote sensed spectra.

The overall idea of the proposed studies is to develop algorithm(s) allowing the application of remote sensing data for the detection of water quality parameters of shallow water bodies with high coloured dissolved organic matter (CDOM) content and/or covered partially by macrophytes – a situation common for kettle holes. Two main problems have been identified during this research work which need to be solved: 1) large water-leaving irradiance variability, caused by water level changes and variability of inherent optical properties of the water body itself; and 2) an inconsistent relation between extractive and RS-based chlorophyll content determination caused most probably by i) variability of the effective packaging in the phytoplankton organisms and ii) variability of the CDOM materials content of the water body.

Therefore, in order to improve the accuracy of kettle holes' biomass classification using high spatial and spectral resolution remote sensing data, future research should be focused on:

1. Packaging effect and bottom type.

- 1.1. Investigation of the processes of light attenuation (absorption and scattering) in small water bodies (kettle holes) influenced by packaging effect and different bottom types:

- Collection of spectral (remote sensing reflectance above water surface in a range of 400 – 1000 nm) and pigment (Chlorophyll, CDOM, TSS and others) information from 20-30 kettle holes
- Underwater absorption measurements using a dual probe spectrometer
- Testing the influence of different bottom types (clay, sand, algae) on water leaving reflectance

1.2. Development of an algorithm for correcting the packaging effect:

- Analysis of collected data and identification of possible packaging effects on the remote signal
- Stepwise derivation of correction algorithm(s)

2. Ground sampling distance. Investigated field and airborne spectra for almost all kettle holes do not correspond to each other due to a mismatch in the sampling distance ($0.01\div 0.015\text{m}^2$ versus 4m^2 and 16m^2). For understanding this phenomena, the seasonal upwelling radiance from the water body has to be collected over different types of kettle holes at different heights (e.g. 30cm, 50cm, 1m and 2m). Received spectra and further studied differences in surface reflection coupled with biomass concentration data will help in analyzing field and airborne ground reflection

The combined research results of these two components offer the opportunity to ‘upscale’ observations to larger spatial scales.

6 References

- ALLABY, M., 2006, *A Dictionary of Ecology* pp. 480 (Oxford: Oxford University Press).
- AREVALO, V., GONZALEZ, J. and AMBROSIO, G., 2008, Shadow detection in colour high-resolution satellite images. *International Journal of Remote Sensing*. **29**(7), pp. 1945-1963.
- ASDI, 2009, Analytical Spectral Devices Inc. Available online at: www.asdi.com (accessed 01 September 2009)
- ATTILA, J., PYHALAHTI, T., HANNONEN, T., KALLIO, K., PULLIALNEN, J., KOPONEN, S., HARMA, P. and ELOHELMO, K., 2008, Analysis of turbid water quality using, airborne spectrometer data with a numerical weather prediction model-aided atmospheric correction. *Photogrammetric Engineering and Remote Sensing*. **74**(3), pp. 363-374.
- BINDING, C.E., JEROME, J.H., BUKATA, R.P. and BOOTY, W.G., 2008, Spectral absorption properties of dissolved and particulate matter in Lake Erie. *Remote Sensing of Environment*. **112**(4), pp. 1702-1711.
- BRANDO, V.E. and DEKKER, A.G., 2003, Satellite hyperspectral remote sensing for estimating estuarine and coastal water quality. *IEEE Transactions on Geoscience and Remote Sensing*. **41**(6), pp. 1378-1387.
- BRICAUD, A. and STRAMSKI, D., 1990, Spectral absorption coefficients of living phytoplankton and nonalgal biogenous matter: A comparison between the Peru upwelling area and the Sargasso Sea. *Limnology and Oceanography*. **35**(3), pp. 562-582.
- BRITANNICA, 2009, Encyclopedia Britannica. Available online at: <http://www.britannica.com> (accessed 01 December 2009)
- BUKATA, R.P., JEROME, J.H., KONDRATIEV, K.Y. and POZDNYAKOV, D.V., 1995, *Optical Properties and Remote Sensing of Inland and Coastal Waters* (New York: CRC Press), pp. 362.
- BUKATA, R.P., JEROME, J.H., KONDRATYEV, K.Y., POZDNYAKOV, D.V. and KOTYKHOV, A.A., 1997, Modelling the radiometric color of inland waters: Implications to a) remote sensing and b) limnological color scales. *Journal of Great Lakes Research*. **23**(3), pp. 254-269.
- CANNIZZARO, J.P. and CARDER, K.L., 2006, Estimating chlorophyll-a concentrations from remote-sensing reflectance in optically shallow waters. *Remote Sensing of Environment*. **101**(1), pp. 13-24.
- CARLSON, R.E. and SIMPSON, J., 1996, *A Coordinator's Guide to Volunteer Lake Monitoring Methods*. Available online at: http://dipin.kent.edu/trophic_state.htm (accessed 18.11.2009)
- CARPENTER, S.R., CARACO, N.F., CORRELL, D.L., HOWARTH, R.W., SHARPLEY, A.N. and SMITH, V.H., 1998, Nonpoint pollution of surface waters with phosphorus and nitrogen. *Ecological Applications*. **8**(3), pp. 559-568.
- CLARK, C.D., RIPLEY, H.T., GREEN, E.P., EDWARDS, A.J. and MUMBY, P.J., 1997, Mapping and measurement of tropical coastal environments with hyperspectral and high spatial resolution data. *International Journal of Remote Sensing*. **18**(2), pp. 237-242.
- CLARK, R.N. and ROUSH, T.L., 1984, Reflectance Spectroscopy - Quantitative-Analysis Techniques for Remote-Sensing Applications. *Journal of Geophysical Research*. **89**(Nb7), pp. 6329-6340.

- CLARKE, G.L., EWING, G.C. and C. J. LORENZEN, 1970, Spectra of backscattered light from the sea obtained from aircraft as a measure of chlorophyll concentration *Science*. **167**(3921), pp. 1119-1121.
- CONGER, C.L., HOCHBERG, E.J., FLETCHER, I., CHARLES H. and ATKINSON, M.J., 2006, Decorrelating remote sensing color bands from bathymetry in optically shallow waters. *IEEE Transactions on Geoscience and Remote Sensing*. **44**(6), pp. 1655-1660.
- COX, R.M., FORSYTHE, R.D., VAUGHAN, G.E. and OLMSTED, L.L., 1998, Assessing water quality in the Catawba river reservoirs using Landsat Thematic Mapper satellite data. *Lake and Reservoir Management*. **14**(4), pp. 405-416.
- DALL'OLMO, G. and GITELSON, A., 2005, Effect of bio-optical parameter variability on the remote estimation of chlorophyll-a concentration in turbid productive waters: experimental results. *Applied Optics*. **44**(3), pp. 412-422.
- DALL'OLMO, G., GITELSON, A.A. and RUNDQUIST, D.C., 2003, Towards a unified approach for remote estimation of chlorophyll-a in both terrestrial vegetation and turbid productive waters. *Geophysical Research Letters*. **30**(18), pp. HLS 1-1 - 1-4.
- DALL'OLMO, G., GITELSON, A.A., RUNDQUIST, D.C., LEAVITT, B., BARROW, T. and HOLZ, J.C., 2005, Assessing the potential of SeaWiFS and MODIS for estimating chlorophyll concentration in turbid productive waters using red and near-infrared bands. *Remote Sensing of Environment*. **96**(2), pp. 176-187.
- DEKKER, A., BRANDO, V.E., ANSTEE, J., PINNEL, N., KUTSER, T., HOOGENBOOM, H., PASTERKAMP, R., PETERS, S., VOS, R., OLBERT, C. and MALTHUS, T., 2001a, Applications of imaging spectrometry in inland, estuarine, coastal and ocean waters. In: F. van der Meer and S.M. de Jong (Editors), *Imaging Spectrometry: Basic principles and prospective applications* (Dordrecht: Kluwer Academic Publishers).
- DEKKER, A., BRANDO, V.E., ANSTEE, J.M., PINNEL, N., KUTSER, T., HOOGENBOOM, H.J., PETERS, S., PASTERKAMP, R., VOS, R., OLBERT, C. and MALTHUS, T.J., 2001b, Imaging spectrometry of water. In: F.D.v.d. Meer and S.M.d. Jong (Editors), *Imaging Spectrometry*, pp. 307-359 (The Netherlands: Kluwer Academic Publishers).
- DEKKER, A., VOS, R. and PETERS, S., 2001c, Comparison of remote sensing data, model results and in situ data for total suspended matter (TSM) in the Southern Frisian lakes. *The Science of the Total Environment*. **268**(pp. 197-214).
- DEKKER, A.G., 1993, Detection of optical water quality parameters for eutrophic waters by high resolution remote sensing. *PhD-thesis. Vrije Univecsiteit, Amsterdam, The Netherlands*.
- DEKKER, A.G., MALTHUS, T.J. and HOOGENBOOM, H.J., 1995, The Remote Sensing of Inland Water Quality. *Advances in Environmental Remote Sensing*, pp. 123-142.
- DEKKER, A.G., MALTHUS, T.J., WIJEN, M.W. and SEYHAN, 1992, The Effect of Spectral Bandwidth and Positioning on the Spectral Signature Analysis of Inland Waters. *Remote Sensing of Environment*. **41**(2/3), pp. 211-225.
- DEKKER, A.G., ZAMUROVIC-NENAD, Z., HOOGENBOOM, H.J. and PETERS, S.W.M., 1996, Remote sensing, ecological water quality modelling and in situ measurements: A case study in shallow lakes. *Hydrological Sciences Journal-Journal Des Sciences Hydrologiques*. **41**(4), pp. 531-547.
- DLR, 2009, German Aerospace Center (DLR). Available online at: <http://www.opairs.aero/media/download/pdf/rosis-description.pdf> (accessed 01 September 2009)

- DOXARAN, D., CHERUKURU, R.C.N. and LAVENDER, S.J., 2005, Use of reflectance band ratios to estimate suspended and dissolved matter concentrations in estuarine waters. *International Journal of Remote Sensing*. **26**(8), pp. 1763-1769.
- DOXARAN, D., FROIDEFOND, J.M. and CASTAING, P., 2002a, A reflectance band ratio used to estimate suspended matter concentrations in sediment-dominated coastal waters. *International Journal of Remote Sensing*. **23**(23), pp. 5079-5085.
- DOXARAN, D., FROIDEFOND, J.M. and CASTAING, P., 2003, Remote-sensing reflectance of turbid sediment-dominated waters. Reduction of sediment type variations and changing illumination conditions effects by use of reflectance ratios. *Applied Optics*. **42**(15), pp. 2623-2634.
- DOXARAN, D., FROIDEFOND, J.M., LAVENDER, S. and CASTAING, P., 2002b, Spectral signature of highly turbid waters - Application with SPOT data to quantify suspended particulate matter concentrations. *Remote Sensing of Environment*. **81**(1), pp. 149-161.
- DOXARAN, D., FROIDEFOND, J.M., LAVENDER, S. and CASTAING, P., 2002c, Spectral signature of highly turbid waters. Application with SPOT data to quantify suspended particulate matter concentrations. *Remote Sensing of Environment*. **81**(1), pp. 149-161.
- DUAN, H., MA, R., ZHANG, Y. and ZHANG, B., 2009, Remote-sensing assessment of regional inland lake water clarity in northeast China. *Limnology*. **10**(2), pp. 135-141.
- DWD, 2007, DEUTSCHER WETTER DIENST (German Weather Service). Climate data from Anklam, Greifswald and Trollenhagen weather stations from 1.4.2007 to 30.10.2007.
- DWD, 2008, DEUTSCHER WETTER DIENST (German Weather Service). Climate data from Anklam, Greifswald and Trollenhagen weather stations from 1.11.2007 to 30.11.2008.
- FISHER, S.G., 1994, Pattern, process and scale in freshwater systems: some unifying thoughts. In: P.S. Giller, A.G. Hildrew and D.G. Raffaelli (Editors), *Aquatic ecology -scale, pattern and process*, pp. 575-591 (Oxford: Blackwell).
- FLINK, P., LINDELL, T. and OSTLUND, C., 2001, Statistical analysis of hyperspectral data from two swedish lakes. *The Science of the Total Environment*. **268**(1-3), pp. 155-169.
- GAO, J., 2009, Bathymetric mapping by means of remote sensing: methods, accuracy and limitations. *Progress in Physical Geography*. **33**(1), pp. 103-116.
- GEGE, P., 2001, The water colour simulator WASI: A software tool for simulation and analysis of optical in-situ spectra. In *Geoscience and Remote Sensing Symposium, IGRASS*. Proceedings of IEEE International, 9-13 July 2001, Sydney, Australia, pp. 2743-2745.
- GEGE, P. and ALBERT, A., 2006, A tool for inverse modelling of spectral measurements in deep and shallow water. In: L.L. Richardson and E.F. LeDrew (Editors), *Remote Sensing of Aquatic Coastal Ecosystems Processes: Science and Management Applications* (the Netherlands: Springer).
- GEGE, P., BACHMANN, M. and HOLZWARTH, S., 2008, ROSIS Bonn 2008. Summary Report).
- GEORGE, D.G., 1997, Cover Bathymetric mapping using a Compact Airborne Spectrographic Imager (CASI). *International Journal of Remote Sensing*. **18**(10), pp. 2067 - 2071.
- GEORGE, D.G. and MALTHUS, T.J., 2001, Using a compact airborne spectrographic imager to monitor phytoplankton biomass in a series of lakes in North Wales *The Science of the Total Environment*. **268**(1-3), pp. 215-226.

- GIARDINO, C., BRANDO, V.E., DEKKER, A.G., STRÖMBECK, N. and CANDIANI, G., 2007, Assessment of water quality in Lake Garda (Italy) using Hyperion. *Remote Sensing of Environment*. **109**(2), pp. 183-195.
- GIARDINO, C., PEPE, M., BRIVIO, P.A., GHEZZI, P. and ZILIOI, E., 2001, Detecting chlorophyll, Secchi disk depth and surface temperature in a sub-alpine lake using Landsat imagery. *Science of the Total Environment*. **268**(1-3), pp. 19-29.
- GITELSON, A., 1992, The peak near 700 nm on radiance spectra of algae and water: relationships of its magnitude and position with chlorophyll concentration. *International Journal of Remote Sensing*. **13**(17), pp. 3367-3373.
- GITELSON, A., SZILAGYI, F. and MITTENZWEY, K.H., 1993, Improving quantitative remote sensing for monitoring of inland water quality. *Water Research*. **27**(7), pp. 1185-1194.
- GITELSON, A., YACOBI, Y., RUNDQUIST, D.C., STARK, R., HAN, L. and ETZION, D., 2000, Remote estimation of chlorophyll concentration in productive waters: Principals, algorithm development and validation. In *National Water Quality Monitoring Conference Proceedings of Advisory Committee on Water Information* (www.acwi.gov), Austin, Texas, pp. 149-160.
- GITELSON, A.A., 1993, Nature of the peak near 700-nm on the radiance spectra and its application for remote estimation of phytoplankton pigments in inland waters. *Proceedings of SPIE - The International Society for Optical Engineering*. **1971**(1), pp. 170-179.
- GITELSON, A.A., DALL'OLMO, G., MOSES, W., RUNDQUIST, D.C., BARROW, T., FISHER, T.R., GURLIN, D. and HOLZ, J., 2008, A simple semi-analytical model for remote estimation of chlorophyll-a in turbid waters: Validation. *Remote Sensing of Environment*. **112**(9), pp. 3582-3593.
- GITELSON, A.A., SCHALLES, J.F. and HLADIK, C.M., 2007, Remote chlorophyll-a retrieval in turbid, productive estuaries: Chesapeake Bay case study. *Remote Sensing of Environment*. **109**(4), pp. 464-472.
- GOMEZ, C., LAGACHERIE, P. and COULOUMA, G., 2008, Continuum removal versus PLSR method for clay and calcium carbonate content estimation from laboratory and airborne hyperspectral measurements. *Geoderma*. **148**(2), pp. 141-148.
- GOODIN, D., HAN, L., FRASER, R., RUNDQUIST, D. and STEBBINS, W., 1993, Analysis of suspended solids in water using remotely sensed high resolution derivative spectra. *Photogrammetric Engineering and Remote Sensing*. **59**(4), pp. 505-510.
- GORDON, H.R., 1987, Calibration Requirements and Methodology for Remote Sensors Viewing the Ocean in the Visible. *Remote Sensing of Environment*. **22**(1), pp. 103-126.
- HAN, L., 1997, Spectral reflectance with varying suspended sediment concentrations in clear and algae-laden waters. *Photogrammetric Engineering and Remote Sensing*. **63**(6), pp. 701-705.
- HAN, L., 2005, Estimating chlorophyll-a concentration using first-derivative spectra in coastal water. *International Journal of Remote Sensing*. **26**(23), pp. 5235-5244.
- HAN, L. and RUNDQUIST, D.C., 1998, The impact of a wind-roughened water surface on remote measurements of turbidity. *International Journal of Remote Sensing*. **19**(1), pp. 195-201.
- HAN, L.H. and RUNDQUIST, D.C., 1997, Comparison of NIR/RED ratio and first derivative of reflectance in estimating algal-chlorophyll concentration: A case study in a turbid reservoir. *Remote Sensing of Environment*. **62**(3), pp. 253-261.
- HARMA, P., VEPSALAINEN, J., HANNONEN, T., PYHALAHTI, T., KAMARI, J., KALLIO, K., ELOHEIMO, K. and KOPONEN, S., 2001, Detection of water quality using simulated

- satellite data and semi-empirical algorithms in Finland. *Science of the Total Environment*. **268**(1-3), pp. 107-121.
- HOWARTH, R.W., 2008, Coastal nitrogen pollution: A review of sources and trends globally and regionally. *Harmful Algae*. **8**(1), pp. 14-20.
- HUGUENIN, R.L. and JONES, J.L., 1986, Intelligent Information Extraction from Reflectance Spectra: Absorption Band Positions. *Journal of Geophysical Research*. **91**(B9), pp. 9585-9598.
- IGAMBERDIEV, R., LENNARTZ, B., GRENZDOEFFER, G., BILL, R. and SCHUBERT, H., In press, Analysis of spectral signatures of small water bodies (kettle holes) in the agricultural young moraine landscape of North-Eastern Germany. *International Journal of Remote Sensing*.
- ILUZ, D., YACOBI, Y.Z. and GITELSON, A., 2003, Adaptation of an algorithm for chlorophyll-a estimation by optical data in the oligotrophic Gulf of Eilat. *International Journal of Remote Sensing*. **24**(5), pp. 1157-1163.
- ISLAM, A., WANG, L., SMITH, C., REDDY, S., LEWIS, A. and SMITH, A., 2007, Evaluation of satellite remote sensing for operational monitoring of sediment plumes produced by dredging at Hay Point, Queensland, Australia. *Journal of Applied Remote Sensing*. **1**(1).
- JENSEN, J.R., 2006, Remote sensing of the environment: An Earth resource perspective (Upper Saddle River, New Jersey: Prentice Hall), pp. 592.
- JERLOV, N.G., 1976, Matine optics (Amsterdam: Elsevier Scientific), pp. 231.
- Ji, W., CIVCO, D.L. and KENNARD, W.C., 1992, Satellite remote bathymetry: A new mechanism for modeling. *Photogrammetric Engineering and Remote Sensing*. **58**(5), pp. 545-549.
- JIAO, H.B., ZHA, Y., GAO, J., LI, Y.M., WEI, Y.C. and HUANG, J.Z., 2006, Estimation of chlorophyll-a concentration in Lake Tai, China using in situ hyperspectral data. *International Journal of Remote Sensing*. **27**(19), pp. 4267-4276.
- KAHLE, P., TIEMEYER, B. and LENNARTZ, B., 2009, Methodische Aspekte zum Monitoring der Wasserqualität künstlich entwässertertiefelandeinzugsgebiete (Methodological aspects of water-quality monitoring in artificially drained lowland catchments). *Hydrologie und Wasserbewirtschaftung*. **53**(4), pp. 228-235.
- KALETKA, T., BERGER, M., PFEFFER, H. and RUDAT, C., 2005, Integrated Conservation and Management of Kettle Holes in Young Moraine Agricultural Landscapes of Northeast Germany. In *Integrated land and water resources management : towards sustainable rural development* Proceedings of 21st European Regional Conference of the International Commission on Irrigation and Drainage, 15-19 May 2005, Frankfurt (Oder) and Slubice, Germany and Poland, pp. 1-4.
- KALETKA, T. and RUDAT, C., 2006, Hydrogeomorphic types of glacially created kettle holes in North-East Germany. *Limnologica*. **36**(1), pp. 54-64.
- KALLIO, K., ATILA, J., HARMA, P., KOPONEN, S., PULLIAINEN, J., HYYTIAINEN, U.M. and PYHALAHTI, T., 2008, Landsat ETM+ images in the estimation of seasonal lake water quality in boreal river basins. *Environmental Management*. **42**(3), pp. 511-522.
- KALLIO, K., KOPONEN, S. and PULLIAINEN, J., 2003, Feasibility of airborne imaging spectrometry for lake monitoring – A case study of spatial chlorophyll-a distribution in two meso-eutrophic lakes. *International Journal of Remote Sensing*. **24**(19), pp. 3771-3790.
- KIRK, J.T.O., 1994, Light and photosynthesis in aquatic ecosystems (Cambridge: University Press), pp. 401.

- KLOIBER, S.M., BREZONIK, P.L., OLMANSON, L.G. and BAUER, M.E., 2002, A procedure for regional lake water clarity assessment using Landsat multispectral data. *Remote Sensing of Environment*. **82**(1), pp. 38-47.
- KNEUBUEHLER, M., GEMPERLI, C., SCHLAPFER, D., ZAH, R. and ITTEN, K., 2005, Determination of water quality parameters in Indian ponds using remote sensing methods. In *EARSel 4th Workshop on Imaging Spectroscopy*. Proceedings of Warsaw University, 27-29 April, Warsaw, Poland, pp. 301-315.
- KOKALY, R.F. and CLARK, R.N., 1999, Spectroscopic determination of leaf biochemistry using band-depth analysis of absorption features and stepwise multiple linear regression. *Remote Sensing of Environment*. **67**(3), pp. 267-287.
- KOPONEN, S., PULLIAINEN, J., KALLIO, K. and HALLIKAINEN, M., 2002, Lake water quality classification with airborne hyperspectral spectrometer and simulated MERIS data. *Remote Sensing of Environment*. **79**(1), pp. 51-59.
- KOPONEN, S., PULLIAINEN, J., SERVOMAA, H., ZHANG, Y., HALLIKAINEN, M., KALLIO, K., VEPSALAINEN, J., PYHALAHTI, T. and HANNONEN, T., 2001, Analysis on the feasibility of multi-source remote sensing observations for Chlorophyll a monitoring in Finnish lakes. *The Science of the Total Environment*. **268**(1-3), pp. 95-106.
- KRUSE, F.A., BOARDMAN, J.W., LEFKOFF, A.B., YOUNG, J.M., KIERSIN-YOUNG, K.S., COCKS, T.D., JENSSEN, R. and COCKS, P.A., 2000, HyMap: An Australian Hyperspectral Sensor Solving Global Problems – Results from USA HyMap Data Acquisitions. In *10th Australasian Remote Sensing and Photogrammetry Conference*. Proceedings of Causal Productions, 21-25 August 2000, Adelaide, Australia, pp. published on CD-ROM.
- KUMAR, K.V., PALIT, A. and K., B.S., 1997, Bathymetric mapping in Rupnarayan-Hooghly river confluence using IRS data. *International Journal of Remote Sensing*. **18**(11), pp. 2269 – 2270.
- LAFON, V., FROIDEFOND, J.M., LAHET, F. and CASTAING, P., 2002, SPOT shallow water bathymetry of a moderately turbid tidal inlet based on field measurements. *Remote Sensing of Environment*. **81**(1), pp. 136-148.
- LATHROP, R.G., 1992, Landsat Thematic Mapper monitoring of turbid inland water quality. *Photogrammetric Engineering and Remote Sensing*. **58**(4), pp. 465-470.
- LEE, Z.P., CARDER, K.L., MOBLEY, C.D., STEWARD, R.G. and PATCH, J.S., 1998, Hyperspectral remote sensing for shallow waters. I. A semi-analytical model. *Applied Optics*. **37**(27), pp. 6329–6338.
- LILLESAND, T.M., KIEFER, R.W. and CHIPMAN, J.W., 2007, *Remote Sensing and Image Interpretation* (Hoboken, New Jersey: Wiley), pp. 1164.
- LIU, Y.S., ISLAM, M.A. and GAO, J., 2003, Quantification of shallow water quality parameters by means of remote sensing. *Progress in Physical Geography*. **27**(1), pp. 24-43.
- LODHI, M.S., RUNDQUIST, D.C., HAN, L. and JUZILA, M.S., 1997, The potential for remote sensing of loess soils suspended in surface waters *Journal of the American Water Resources Association*. **33**(1), pp. 111-127.
- LOUCHARD, E.M., REID, R.P. and STEPHENS, C.F., 2002, Derivative analysis of absorption features in hyperspectral remote sensing data of carbonate sediments. *Optics Express*. **10**(26), pp. 1573-1584
- LUNG-MV, 2009, Landesamt für Umwelt, Naturschutz and Geologie - Mecklenburg-Vorpommern. Available online at: <http://www.lung.mv-regierung.de> (accessed 01 December 2009)
- LYZENGA, D.R., 1978, Passive Remote-Sensing Techniques for Mapping Water Depth and Bottom Features. *Applied Optics*. **17**(3), pp. 379-383.

- MA, R., DUAN, H., GU, X. and ZHANG, S., 2008, Detecting aquatic vegetation changes in Taihu lake, China using multi-temporal satellite imagery. *Sensors*. **8**(6), pp. 3988-4005.
- MA, R., TANG, J., DAI, J., ZHANG, Y. and SONG, Q., 2006, Absorption and scattering properties of water body in Taihu Lake, China: Absorption. *International Journal of Remote Sensing*. **27**(19), pp. 4277-4304.
- MATHER, P., 2004, Computer Processing of Remotely-Sensed Images: An Introduction (John Willey and Sons Ltd: West Sussex, England), pp. 442.
- MERBACH, W., KALETTKA, T., RUDAT, C. and AUGUSTIN, J., 2002, Trace gas emissions from riparian areas of small eutrophic inland waters in Northeast-Germany. *Wetlands in Central Europe*, pp. 235-244.
- MITSCH, W. and GOSSELINK, J., 2007, Wetlands (Hoboken, New Jersey: Wiley), pp. 600.
- MOBLEY, C.D., 1994, Light and Water: Radiative Transfer in Natural Waters (San Diego, California: Academic Press), pp. 592.
- MOREL, A. and GENTILI, B., 1993, Diffuse reflectance of oceanic waters: II. Bidirectional aspects. *Applied Optics*. **32**(33), pp. 6864-6879.
- MURPHY, R.J., TOLHURST, T.J., CHAPMAN, M.G. and UNDERWOOD, A.J., 2005, Estimation of surface chlorophyll-a on an emerged mudflat using field spectrometry: Accuracy of ratios and derivative-based approaches. *International Journal of Remote Sensing*. **26**(9), pp. 1835-1859.
- MURPHY, R.J., UNDERWOOD, A.J., TOLHURST, T.J. and CHAPMAN, M.G., 2008, Field-based remote-sensing for experimental intertidal ecology: Case studies using hyperspatial and hyperspectral data for New South Wales (Australia). *Remote Sensing of Environment*. **112**(8), pp. 3353-3365.
- MUTANGA, O. and SKIDMORE, A.K., 2003, Continuum - removed absorption features estimate tropical savanna grass quality in situ. In *Workshop on imaging spectroscopy*. Proceedings of 3rd EARSeL workshop 13-16 May 2003, Herrsching, Germany, pp. 543-558.
- MUTANGA, O., SKIDMORE, A.K., KUMAR, L. and FERWERDA, J., 2005, Estimating tropical pasture quality at canopy level using band depth analysis with continuum removal in the visible domain. *International Journal of Remote Sensing*. **26**(6), pp. 1093-1108.
- NEVILLE, R.A. and GOWER, J.F.R., 1977, Passive remote sensing of phytoplankton via chlorophyll-a fluorescence. *Journal of Geophysical Research*. **82**(C24), pp. 3487-3493.
- OUILLOIN, S., FORGET, P., FROIDEFOND, J.M. and NAUDIN, J.J., 1997, Estimating suspended matter concentrations from SPOT data and from field measurements in the Rhone river plume. *Marine Technology Society Journal*. **31**(2), pp. 15-20.
- PATTIARATCHI, C., LAVERY, P., WYLLIE, A. and HICK, P., 1994, Estimates of water quality in coastal waters using multi-date Landsat Thematic Mapper data *International Journal of Remote Sensing*. **15**(8), pp. 1571-1584.
- PENUELAS, J., GAMON, J.A., FREDEEN, A.L., MERINO, J. and FIELD, C.B., 1994, Reflectance Indexes Associated with Physiological-Changes in Nitrogen-Limited and Water-Limited Sunflower Leaves. *Remote Sensing of Environment*. **48**(2), pp. 135-146.
- PEPE, M., GIARDINO, C., BORSANI, G., CARDOSO, A.C., CHIAUDANI, G., PREMAZZI, G., RODARI, E. and ZILIOLI, E., 2001, Relationship between apparent optical properties and photosynthetic pigments in the sub-alpine Lake Iseo. *Science of the Total Environment*. **268**(1-3), pp. 31-45.
- PHILPOT, W.D., 1991, The derivative ratio algorithm: avoiding atmospheric effects in remote sensing. *IEEE Transactions on Geoscience and Remote Sensing*. **29**(3), pp. 350-357.

- PINNEL, N., 2007, A method for mapping submerged macrophytes in lakes using hyperspectral remote sensing. PhD Thesis, Department of Ecology, Technical University, Munich.
- PORRA, R.J., THOMPSON, W.A. and KRIEDEMANN, P.E., 1989, Determination of Accurate Extinction Coefficients and Simultaneous-Equations for Assaying Chlorophyll-a and Chlorophyll-B Extracted with 4 Different Solvents - Verification of the Concentration of Chlorophyll Standards by Atomic-Absorption Spectroscopy. *Biochimica Et Biophysica Acta*. **975**(3), pp. 384-394.
- POZDNYAKOV, D.V., KONDRATYEV, K.Y., BUKATA, R.P. and JEROME, J.H., 1998, Numerical modelling of natural water colour: implications for remote sensing and limnological studies. *International Journal of Remote Sensing*. **19**(10), pp. 1913-1932.
- PULLIAINEN, J., KALLIO, K., ELOHEIMO, K., KOPONEN, S., SERVOMAA, H., HANNONEN, T., TAURIAINEN, S. and HALLIKAINEN, M., 2001, A semi-operative approach to lake water quality retrieval from remote sensing data. *The Science of the Total Environment*. **268**(1-3), pp. 79-93.
- RENCZ, A.N., 1999, Remote Sensing for the Earth Sciences (Manual of Remote Sensing) (Hoboken, New Jersey: Wiley), pp. 728.
- RICHARDS, J.A. and JIA, X., 2006, Remote Sensing Digital Image Analysis: An Introduction (Berlin: Springer),
- RICHTER, R., 1996, Atmospheric correction of DAIS hyperspectral image data. *Computers & Geosciences*. **22**(7), pp. 785-793.
- RIJKEBOER, M., DEKKER, A. and GONS, H., 1998, Subsurface irradiance reflectance spectra of inland waters differing in morphometry and hydrology. *Aquatic Ecology*. **31**(pp. 313-323).
- RUNDQUIST, D.C., HAN, L.H., SCHALLES, J.F. and PEAKE, J.S., 1996, Remote measurement of algal chlorophyll in surface waters: The case for the first derivative of reflectance near 690 nm. *Photogrammetric Engineering and Remote Sensing*. **62**(2), pp. 195-200.
- SANDIDGE, C.J. and HOLYER, J.R., 1998, Coastal bathymetry from hyperspectral observations of water radiance. *Remote Sensing of Environment*. **65**(pp. 341-352).
- SARABANDI, P., YAMAZAKI, F., MATSUOKA, M. and KIREMIDJIAN, A., 2004, Shadow detection and radiometric restoration in satellite high resolution images. *IEEE International Geoscience and Remote Sensing Symposium Proceedings*, pp. 3744-3747.
- SATHYENDRANATH, S., 2000, Remote sensing of ocean colour in coastal and other optically complex waters. International Ocean-Colour Coordinating Group (IOCCG). Technical Report 3, Institute of Oceanography, Bedford, Canada.
- SCHEFFER, M., 1998, Ecology of shallow lakes (Berlin: Springer), pp. 384.
- SCHEFFER, M. and VAN NES, E.H., 2007, Shallow lakes theory revisited: various alternative regimes driven by climate, nutrients, depth and lake size. *Hydrobiologia*. **584**(1), pp. 455-466.
- SCHMIDT, K.S. and SKIDMORE, A.K., 2001, Exploring spectral discrimination of grass species in African rangelands. *International Journal of Remote Sensing*. **22**(17), pp. 3421-3434.
- SCHMIDT, K.S. and SKIDMORE, A.K., 2003, Spectral discrimination of vegetation types in a coastal wetland. *Remote Sensing of Environment*. **85**(1), pp. 92-108.
- SEEHAUSEN, O., VANALPHEN, J.J.M. and WITTE, F., 1997, Cichlid fish diversity threatened by eutrophication that curbs sexual selection. *Science*. **277**(5333), pp. 1808-1811.
- SHAFIQUE, N.A., BRADLEY, A.C., FULK, F. and CORMIER, S.M., 2001, The Selection of Narrow Wavebands for Optimizing Water Quality Monitoring on the Great Miami

- River, Ohio using Hyperspectral Remote Sensor Data. *Journal of Spatial Hydrology*. **1**(1), pp. 1-22.
- SRTM, 2009, The Shuttle Radar Topography Mission (SRTM). Available online at: <http://www2.jpl.nasa.gov/srtm/> (accessed 30 December 2009)
- SUBRAMANIAM, A., CARPENTER, E.J., KARENTZ, D. and FALKOWSKI, P.G., 1999, Optical Properties of the Marine Diazotrophic Cyanobacteria *Trichodesmium*; I. Absorption and Spectral Photosynthetic Characteristics. *Limnology and Oceanography*. **44**(3), pp. 608-617.
- SVAB, E., TYLER, A.N., PRESTON, T., PRESING, M. and BALOGH, K.V., 2005, Characterizing the spectral reflectance of algae in lake waters with high suspended sediment concentrations. *International Journal of Remote Sensing*. **26**(5), pp. 919-928.
- SYDOR, M., 2006, Use of hyperspectral remote sensing reflectance in extracting the spectral volume absorption coefficient for phytoplankton in coastal water: Remote sensing relationships for the inherent optical properties of coastal water. *Journal of Coastal Research*. **22**(3), pp. 587-610.
- TASSAN, S. and FERRARI, G.M., 1995, An alternative approach to absorption measurements of aquatic particles retained on filters. *Limnology and Oceanography*. **40**(8), pp. 1358-1368.
- TEODORO, A.C., MARCAL, A.R.S. and VELOSO-GOMES, F., 2007, Correlation analysis of water wave reflectance and local TSM concentrations in the breaking zone with remote sensing techniques *Journal of Coastal Research*. **23**(6), pp. 1491-1497.
- THIEMANN, S., 1999, The origin of the reflectance peak near 700 nm in chlorophyll-aladen waters-an experiment. In *Geoscience and Remote Sensing Symposium*. Proceedings of IEEE International, Hamburg, pp. 1146 - 1148.
- THIEMANN, S. and KAUFMANN, H., 2000, Determination of chlorophyll content and trophic state of lakes using field spectrometer and IRS-1C satellite data in the Mecklenburg lake district, Germany. *Remote Sensing of Environment*. **73**(2), pp. 227-235.
- THIEMANN, S. and KAUFMANN, H., 2002, Lake water quality monitoring using hyperspectral airborne data - a semiempirical multisensor and multitemporal approach for the Mecklenburg Lake District, Germany. *Remote Sensing of Environment*. **81**(2-3), pp. 228-237.
- TIEMEYER, B., KAHLE, P. and LENNARTZ, B., 2006, Nutrient losses from artificially drained catchments in North-Eastern Germany at different scales. *Agricultural Water Management*. **85**(1-2), pp. 47-57.
- TIEMEYER, B., KAHLE, P. and LENNARTZ, B., 2009, Phosphorus losses from an artificially drained rural lowland catchment in North-Eastern Germany. *Agricultural Water Management*. **96**(4), pp. 677-690.
- TIEMEYER, B., LENNARTZ, B. and KAHLE, P., 2008, Analysing nitrate losses from an artificially drained lowland catchment (North-Eastern Germany) with a mixing model. *Agriculture, Ecosystems and Environment*. **123**(1-3), pp. 125-136.
- TIEMEYER, B., MOUSSA, R., LENNARTZ, B. and VOLTZ, M., 2007, MHYDAS-DRAIN: A spatially distributed model for small, artificially drained lowland catchments. *Ecological Modelling*. **209**(1), pp. 2-20.
- TRIPATHI, N.K. and RAO, A.M., 2002, Bathymetric mapping in Kakinada Bay, India, using RS-1D LISS-III data. *International Journal of Remote Sensing*. **23**(6), pp. 1013-1025.
- TSAI, F. and PHILPOT, W., 1998, Derivative analysis of hyperspectral data. *Remote Sensing of Environment*. **66**(1), pp. 41-51.

- TSAI, F. and PHILPOT, W.D., 2002, A derivative-aided hyperspectral image analysis system for land-cover classification. *Ieee Transactions on Geoscience and Remote Sensing*. **40**(2), pp. 416-425.
- TURDUKULOV, U., 2003, Determination of water quality parameters using imaging spectrometry (case study for the Sajó floodplain, Hungary). Master of Science Thesis, ITC, Enschede, The Netherlands.
- WANG, J., TIANA, Q., FUA, W., WANG, X. and DUA, X., 2007, Hyperspectral models of coastal water depth extraction. In *Geoinformatics 2007: Remotely Sensed Data and Information* Proceedings of Society of Photo-Optical Instrumentation Engineers, 25-27 May 2007, Nanjing, China pp. 675219.1-675219.10.
- WATZNAUER, A., 1989, Wörterbuch der Geowissenschaften Deutsch-Englisch (Frankfurt/M.: Deutsch (Harri)).
- WETZEL, R.G., 1992, Clean Water - a Fading Resource. *Hydrobiologia*. **243**(pp. 21-30.
- WIANGWANG, N., 2006, Hyperspectral data modelling for water quality studies in Michigan's inland lakes. PhD Thesis, Dept. of Geography, Michigan State University., East Lansing.
- WRIGLEY, R.C. and HORNE, A.J., 1974, Remote-Sensing and Lake Eutrophication. *Nature*. **250**(5463), pp. 213-214.
- XU, Y., ZHANG, X., HU, G. and YANG, H., 2008, Continuum removal improved with slope extremum and its application to spectrum classification of field objects. *Journal of Computational Information Systems*. **4**(2), pp. 693-698.
- ZHAO, H.M., CHEN, X.L. and TIAN, L.Q., 2006, A New Method to Retrieve Topographic shadow Based on Multi-spectral Operation. *IEEE International Geoscience and Remote Sensing Symposium*, pp. 2761-2764.

Appendix A

Kettle holes description



Kettle hole K1 – has oval shape with steep banks and ≈ 40 m length, ≈ 30 m width and depth is $\approx 1-1.5$ m. It is full of algae which come almost up to surface of the water. The water appears more or less clear. Banks are full of rush.



Kettle hole K2 – is a very flat with the shape irregular rectangle. It has ≈ 48 m length, ≈ 24 m width and depth is $\approx 0.5 \div 1.0$ m. It is fully fulfilled by algae which come out of the water surface. Water is very muddy and turbid. Banks are full of rush. In season of 2008 kettle hole K2 dried up.



Kettle hole K4 – one of the very nicely preserved kettle holes with the size close to lakes. It has very steep banks and ≈ 100 m length, ≈ 60 m width and depth is $\approx 2.5 \div 3.5$ m. From the normal eyes view there is no any sign of algae. Most probably they are very small and very few. It is due to the water which is moderately turbid and water column is deep, so sunlight almost doesn't reach the bottom. Banks are full of rush.



Kettle hole K5 – has oval shape with small steep banks and ≈ 40 m length, ≈ 30 m width and depth is $\approx 0.3 \div 0.5$ m. It is fully fulfilled by algae which come out of the water surface. Water is very muddy and turbid. Banks are full of different type of grass.



Kettle hole K6 – is a flat and has almost oval shape with small steep banks and ≈ 100 m length, ≈ 30 m width and depth is $\approx 0.6 \div 1.3$ m. Nearly 30-45% of it are covered by algae which comes up to the surface. Despite that the central part of it is open and water is moderately turbid. Banks are full of different type of grass.



Kettle hole K7 – is a flat and has almost oval shape with small steep banks and ≈ 60 m length, ≈ 40 m width and depth is $\approx 0.8 \div 1.2$ m. It is seen from the airborne image that Sch6 and Sch7 used to be connected by surface flow now this path is completely covered by grass. The water in most of the part is clear. Only near by banks there are algae which come to the surface.

Appendix B

Pigment concentrations data from 2007 and 2008 field campaigns

Kettle hole - K1

Date	CHL, $\mu\text{g/L}$	TCHL, $\mu\text{g/L}$	TSS, mg/L	Absorption at 750 nm	Ph	EC, μS at 25C°
24 May 2007	14.68	23.97	-999.00	0.0037	7.98	398.85
07 June 2007	15.84	19.97	5.67	0.0053	9.19	283.37
02 July 2007	13.41	23.09	0.77	0.0277	7.99	303.38
23 August 2007	10.06	14.50	4.17	0.0141	7.57	355.02
06 September 2007	5.49	6.39	2.32	0.0044	7.89	443.08
16 September 2007	13.90	16.60	6.80	0.0131	8.09	444.31
24 October 2007	9.56	11.18	1.95	0.0028	8.20	405.21
06 May 2008	32.46	36.41	5.50	0.0094	7.43	639.27
15 May 2008	31.76	35.71	5.40	0.0136	7.28	616.18
03 June 2008	26.93	33.52	4.46	0.0107	7.66	648.67
16 June 2008	28.67	42.04	3.63	0.0067	7.91	646.58
15 July 2008	28.80	38.43	3.80	0.0069	7.84	455.88
29 July 2008	14.99	18.87	2.90	0.0087	8.31	480.89
12 August 2008	29.33	33.48	2.70	0.0089	8.26	545.17
26 August 2008	14.28	20.97	2.32	0.0044	8.79	425.89
09 September 2008	7.74	10.75	1.54	0.0075	8.26	462.56
26 September 2008	12.23	17.70	1.03	0.0047	8.11	518.38

Kettle hole – K2

Date	CHL, $\mu\text{g/L}$	TCHL, $\mu\text{g/L}$	TSS, mg/L	Absorption at 750 nm	Ph	EC, μS at 25C°
24 May 2007	9.91	16.57	-999.00	0.0043	7.84	387.19
07 June 2007	7.69	10.83	5.91	0.0053	9.79	384.78
02 July 2007	8.03	12.49	7.00	0.0246	9.39	359.61
23 August 2007	2.60	3.97	1.73	0.0019	7.98	412.58
06 September 2007	4.32	9.26	8.56	0.0020	7.67	476.21
16 September 2007	6.54	7.22	2.80	0.0081	8.03	468.12
24 October 2007	3.20	4.37	1.47	0.0023	7.53	489.59

Kettle hole – K4

Date	CHL, $\mu\text{g/L}$	TCHL, $\mu\text{g/L}$	TSS, mg/L	Absorption at 750 nm	Ph	EC, μS at 25C°
24 May 2007	37.04	43.55	-999.00	0.0043	8.64	378.70
07 June 2007	33.35	41.71	2.31	0.0114	7.70	340.14
02 July 2007	64.55	95.28	13.75	0.0322	7.63	327.78
23 August 2007	43.24	62.66	3.87	0.0144	7.35	322.88
06 September 2007	80.88	109.89	6.00	0.0150	7.39	355.45
16 September 2007	34.95	42.25	12.00	0.0159	7.60	352.43
24 October 2007	83.74	93.01	10.40	0.0194	7.59	349.75

06 May 2008	107.97	110.78	5.18	0.0408	8.88	322.15
15 May 2008	78.55	102.87	13.88	0.0446	8.57	300.29
03 June 2008	59.04	61.30	17.35	0.0355	8.35	312.79
16 June 2008	30.00	34.75	5.94	0.0069	7.52	320.11
15 July 2008	79.18	87.08	7.18	0.0176	7.30	296.24
29 July 2008	32.89	40.18	4.78	0.0158	8.91	364.32
12 August 2008	156.14	224.72	11.65	0.0463	7.74	404.88
26 August 2008	129.23	145.27	11.60	0.0280	7.72	396.35
09 September 2008	181.03	218.88	13.28	0.0336	7.69	384.84
26 September 2008	143.02	171.86	8.83	0.0319	8.28	358.15

Kettle hole – K5

Date	CHL, µg/L	TCHL, µg/L	TSS, mg/L	Absorption at 750 nm	Ph	EC, µS at 25C°
24 May 2007	14.09	18.96	-999.00	0.0148	7.36	433.86
07 June 2007	94.28	111.43	21.29	0.0513	7.38	340.56
02 July 2007	62.01	100.58	12.29	0.0268	6.17	249.28
23 August 2007	4.20	6.76	8.67	0.0147	9.40	254.67
06 September 2007	5.02	11.00	7.40	0.0083	9.40	263.74
16 September 2007	2.31	3.48	11.76	0.0157	9.74	257.47
24 October 2007	2.62	3.43	7.00	0.0107	7.84	243.58
06 May 2008	6.98	6.98	3.20	0.0028	7.50	441.82
15 May 2008	3.40	4.56	2.58	0.0042	7.38	407.11
03 June 2008	16.99	18.63	5.28	0.0074	7.50	405.09
16 June 2008	8.45	9.35	2.17	0.0108	7.84	404.73
15 July 2008	2.46	3.27	9.21	0.0078	9.88	333.53
29 July 2008	4.38	6.15	2.33	0.0029	9.35	319.54
12 August 2008	18.85	33.63	6.50	0.0095	9.14	358.65
26 August 2008	5.41	6.06	4.91	0.0024	8.96	325.52
09 September 2008	23.41	28.50	6.04	0.0132	8.96	364.77
26 September 2008	15.07	24.14	8.39	0.0221	8.74	373.36

Kettle hole – K6

Date	CHL, µg/L	TCHL, µg/L	TSS, mg/L	Absorption at 750 nm	Ph	EC, µS at 25C°
24 May 2007	7.47	13.06	-999.00	0.0055	7.07	333.09
07 June 2007	17.27	19.37	9.40	0.0124	7.40	272.67
02 July 2007	3.18	5.52	6.00	0.0155	6.03	232.31
23 August 2007	4.50	7.28	2.40	0.0031	7.53	194.67
06 September 2007	54.81	54.96	5.80	0.0170	7.53	219.66
16 September 2007	14.92	20.90	2.42	0.0039	7.99	228.15
24 October 2007	6.51	6.88	2.80	0.0002	7.35	230.85

06 May 2008	2.22	3.23	1.68	0.0142	7.80	398.27
15 May 2008	5.94	10.21	3.10	0.0067	7.40	371.84
03 June 2008	9.52	10.23	2.31	0.0099	8.58	370.24
16 June 2008	4.20	6.14	1.49	0.0045	7.43	402.93
15 July 2008	5.33	7.09	1.40	0.0093	7.43	384.00
29 July 2008	3.24	3.97	0.81	0.0041	8.97	370.98
12 August 2008	4.99	6.99	1.44	0.0062	8.44	464.93
26 August 2008	10.29	12.17	3.90	0.0070	7.88	468.17
09 September 2008	4.32	8.67	0.83	0.0023	7.74	473.50
26 September 2008	3.61	5.21	0.87	0.0103	8.60	388.02

Kettle hole – K7

Date	CHL, µg/L	TCHL, µg/L	TSS, mg/L	Absorption at 750 nm	Ph	Ec, µS at 25C°
24 May 2007	3.86	7.01	0.00	0.0025	8.60	400.98
07 June 2007	1.91	2.99	2.00	0.0013	7.85	349.00
02 July 2007	4.64	9.48	2.00	0.0100	7.48	319.30
23 August 2007	1.94	3.13	1.60	0.0023	7.17	294.50
06 September 2007	2.12	2.51	1.73	0.0016	7.39	318.50
16 September 2007	5.10	10.63	1.70	0.0048	7.81	317.16
24 October 2007	2.35	2.93	4.67	0.0022	7.38	293.04
06 May 2008	1.17	1.60	2.14	0.0058	8.53	393.03
15 May 2008	2.48	3.16	2.46	0.0042	8.73	344.63
03 June 2008	6.38	7.46	1.89	0.0058	7.87	361.69
16 June 2008	6.33	6.81	4.28	0.0063	7.32	405.98
15 July 2008	5.17	7.07	4.41	0.0068	7.41	407.33
29 July 2008	3.22	4.26	3.99	0.0060	8.92	398.57
12 August 2008	3.28	4.93	2.97	0.0073	7.85	510.57
26 August 2008	4.36	6.56	1.06	0.0032	7.84	480.79
09 September 2008	2.68	5.31	1.33	0.0013	8.37	442.91
26 September 2008	3.62	6.75	1.81	0.0058	8.17	412.72

On 24 May 2008 due to technical difficulties water samples for TSS were not collected. In the tables these values are shown as -999.00.

Appendix C

MATLAB routine for reflectance de-noising and graphical visualization

% Step 1 – Loading spectra (ASCII format)

```
clear all
input=load('-ascii', 'temp.txt');
clc
a=size(input);
whos
```

% Step 2 – De-noising using Savitzky-Golay and Discrete Wavelet Transformation Filters

```
xx=27; % Note the number should be odd
for i=1:a(2)-1 ...
temp(:,i) = sgolayfilt(input(:,i+1),3,17);    % Decreasing noise level (omitted for spectra
                                              taken in normal weather condition)

sg_sred(:,i)=sgolayfilt(temp(:,i),3,xx);
[thr,sorh,keepapp] = ddencmp('den','wv',temp(:,i));...
dwt_sred1(:,i) = wdencmp('gbl',temp(:,i),'sym5',3,thr,sorh,keepapp);
dwt_sred2(:,i) = wdencmp('gbl',temp(:,i),'sym8',3,thr,sorh,keepapp);
end;
```

% Step 3 – visualization of raw (noised) and de-noised spectra

```
for i=1:a(2)-1 ...
plot (input(:,1), input(:,i+1),'-k')
hold on
plot (input(:,1), sg_sred(:,i),'-r','LineWidth',2)
plot (input(:,1), dwt_sred1(:,i),'-g','LineWidth',2)
plot (input(:,1), dwt_sred2(:,i),'-b','LineWidth',2)
title(['Graph #- ',num2str(i)])
pause
clf
end
```

% Example of visualization one of the received results, i.e. dwt_sred1

```
for i=1:a(2)-1 ...
plot (input(:,1), dwt_sred1(:,i),'-b','LineWidth',2)
title(['Graph #- ',num2str(i)])
pause
clf
end
```

%Step 4 – Saving results

```
save('dwt_temp_den.txt','dwt_sred1','-ascii');
save('dwt_temp_den1.txt','dwt_sred2','-ascii');
save('sg_temp_den.txt','sg_sred','-ascii');
```

Appendix D

Data from a nearby weather station (Greifswald) during sampling

№	Date of field trip	Atmospheric pressure (hPa)	Mean of air temperature (°C)	Maximum wind speed (m/s)	Daily sum of sunshine hours
	02 July 2007	1005.8	19.3	5.0	2.5
	23 August 2007	1014.5	17.6	6.0	11.3
	06 September 2007	1021.6	12.7	8.5	3.4
	16 September 2007	1013.2	14.6	11.9	8.7
	24 October 2007	1028.4	9.7	13.5	0.0
	06 May 2008	1027.0	12.5	6.0	12.5
	15 May 2008	1009.4	11.1	7.0	14.8
	03 June 2008	1013.9	16.5	16.6	15.7
	16 June 2008	1007.5	14.5	10.6	9.6
	15 July 2008	1019.4	18.7	10.1	0.4
	29 July 2008	1019.4	21.3	12.3	14.7
	12 August 2008	998.4	17.3	9.3	0.0
	26 August 2008	1018.1	17.3	9.1	2.4
	09 September 2008	1017.1	16.5	9.0	8.8
	26 September 2008	1034.9	12.5	7.8	5.4

Appendix E

MATLAB routine and subroutine for processing of the hyperspectral imagery to the first derivative dataset

Main routine for data processing

```
function [output]=derv_proc(input)
tic
a1=size(input);
output=zeros(a1(1),a1(2));
bb=955;      % number of rows
for a=1:1727 % number of columns
for aa=1:bb
for ab=0:89 %number of bands
i(ab+1)=input(aa+bb*ab,a);
end;
if (i(1)==0)
    i2=i;
else
i2=my_derv(i);
end;
for ab=0:47
output(aa+bb*ab,a)=i2(ab+1);
end;
end;
end;

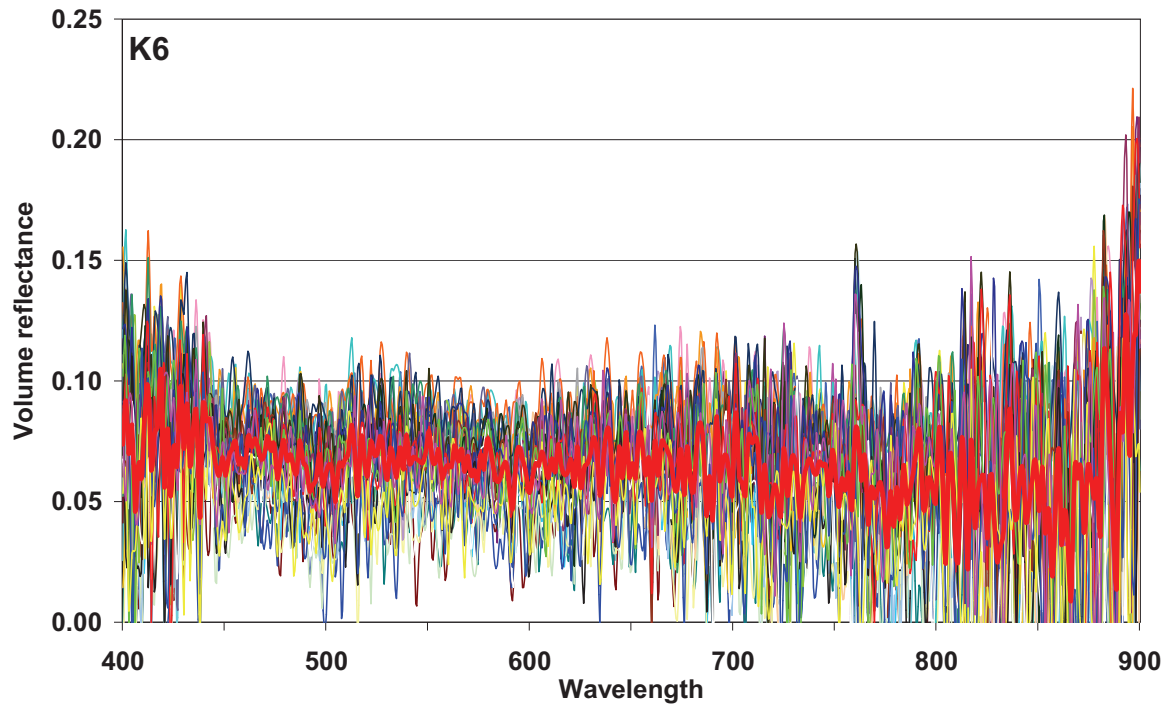
for ab=0:47
    i(ab+1)=output(222+bb*ab,322);
end;
plot (i);
toc
```

Subroutine for first derivative calculation

```
function [output]=my_derv(input)
a=size(input);
output=zeros(a(1),a(2));
for i=1:a(2)-1
    if input(i)>0
        output(i)=(input(i+1)-input(i))/0.04; % Wavelength of 4µm/100
                                                % in order to have similar range of values
    end;
end;
```


Appendix F

Volume reflectance calculated from field spectra collected on overcast weather



Field spectra collected in 15 July 2008 from kettle hole K6. Bold red line is mean value.

Selbständigkeitserklärung

Ich erkläre, dass ich die hier vorgelegte Arbeit selbständig und ohne fremde Hilfe verfasst, andere als die von mir angegebenen Quellen und Hilfsmittel nicht benutzt und die den benutzten Werken wörtlich oder inhaltlich entnommenen Stellen als solche kenntlich gemacht habe.

Rostock, den 09.02.2010

Rahmatulla Igamberdiev

Curriculum Vitae

Name: Rahmatulla Mamirovich Igamberdiev
Date of birth: 01.03.1978
Place of birth: Osh, Kyrgyz Republic
Nationality: Kyrgyz Republic

EDUCATION

Oct. 2006 – present DAAD scholarship for PhD thesis research at Faculty for Agricultural and Environmental Sciences, University of Rostock, Germany.

Jan.-May 2006 Michigan State University, Institute of Water Research (www.iwr.msu.edu). Junior Faculty Development Program fellow (www.jfdp.org) funded by Department of State, USA

December 04-16, 2005 Istanbul, NATO-ASI – Advanced Modeling Techniques for Rapid Diagnosis and Assessment of CBRN Agents Effects on Water Resources, Kumburgaz, Istanbul, Turkey.

Oct 2004- Jun 2005 PG courses on RS&GIS, CSSTEAP (affiliated to UN), Indian Institute of Remote Sensing, Dehradun, India (www.cssteap.org)

Jan 2001 – Jul. 2005 Postgraduate [aspirant] courses in water chemistry, water management, ecology of water resources, Osh Technological University, Osh, Kyrgyzstan

Aug. 1995-Jun. 2000 Diploma of Higher Education with Highest Honors, Engineer Computer Science, Osh Technological University [5 Technical degree program], Osh, Kyrgyzstan

PROFESSIONAL SERVICE

Jul. – Dec. 2005 Head of Department of External Affairs, Osh TU
 Jun. 2004 – Sep. 2004 In charge of Head of Department of External Affairs
 Sep. 2003 – present Senior Lecturer
 Sep 2000 – Aug. 2003 Lecturer, Department of Cybernetics and Informational Technologies, Osh TU

AWARDS

1997-1999 Outstanding student recognition, Osh TU
 1999-2000 Presidential grant «Umut» as a best student, Osh TU
 2004– 2005 National foundation “Meerim” grant as best aspirant (PhD student) of Osh Technological University, Osh

LANGUAGES

Uzbek (native), Kyrgyz, highly proficient in Russian, proficient in English and German, Arabic (basic level).

SCHOOL EDUCATION

1985-1995 Gymnasium #5, Osh, Kyrgyz Republic

Theses for the dissertation entitled:

WATER QUALITY MONITORING OF THE KETTLE HOLES BY MEANS OF HYPERSPECTRAL REMOTE SENSING IN MECKLENBURG-VORPOMMERN STATE, GERMANY

submitted by Rahmatulla Igamberdiev

09.02.2010

- Kettle holes are small digressional lentic waters or wetlands (<1 ha) often glacially shaped within the depressions of catchments. In North-Eastern Germany more than 150,000 kettle holes can be found mostly within arable land and forest. However, kettle holes are subject to pollution, drainage, and structural alteration by intensive land use practices. The agricultural activity embraces artificial drainage measures which strongly alter the sites' hydrology including the hydro period of the kettle holes. The temporal development of the chlorophyll content of kettle holes somehow reflects the land use patterns and fertilization practice within the respective catchment. Furthermore, shores of kettle holes are a source for enhanced greenhouse gas emissions due to eutrophication.
- In Germany, kettle holes are protected by law, but there is still a need to develop effective conservation and management strategies. Especially the fast yet efficient and precise determination of the water quality and the temporal development in kettle holes are required to assess the sustainability of agricultural and conservation measures.
- The acquisition of inland water quality (WQ) data is an important but tedious task due to the pronounced spatial and temporal variability of most in-water constituents, especially for small shallow water bodies. Hyperspectral remote sensing (HRS) can provide useful information for WQ monitoring in agricultural young moraine landscapes in North-Eastern Germany. This research aimed to make a first attempt at presenting the ability of hyperspectral remote sensing (two-years field spectrometry data, HyMap and ROSIS sensors imagery) for kettle holes' water quality parameters (chlorophyll, water depth, total suspended sediment) mapping in agricultural young moraine landscape in North-Eastern Germany.
- The test area is located close to the city of Demmin, about 150 km north of the city of Berlin, and covers approximately 10km². After elimination of kettle holes that

were permanently dry and entirely covered by duckweed, the monitoring programme in 2007 included 6 sampling stations. In summer 2008, kettle hole K2 dried out and it was also excluded from further monitoring. In this year ground truth data were collected in 10 field campaigns from 5 kettle holes in the period between May and September 2008. Overall, spectral and pigment ground truth collection resulted in 15 datasets during 2007 and 2008, giving sufficient information for seasonal and annual analysis of water quality temporal dynamics. Field activities at the sites included collection of water samples for laboratory analysis of Chlorophyll *a* (CHL), Total Chlorophyll (TCHL), Total Suspended Sediments (TSS), water samples absorption at 750 nm, pH and Electrical Conductivity (EC).

- Upwelling radiance data were collected at the same time as water sampling from 6 lakes in 15 field campaigns (5 in 2007 and 10 in 2008) resulting with a total of 80 spectral datasets. Recorded radiance represented the vertical flux of energy upward from the water. These nadir optical measurements were collected using a field spectroradiometer (ASD FieldSpec HH ultraviolet/visible and near-infrared (UV/VNIR)). The instrument records a continuous spectrum with 25° FOV in 512 bands, ranging from 274 nm to 1085 nm with 1.587 nm spectral resolution. Upwelling radiance from the water body was retrieved as relative reflectance in relation to downwelling radiance spectrum measured from a reference panel (25-30 cm above the panel). Depending on the depth and size of the kettle hole, the spectral measurement took place either on board a boat or at the shoreline.
- An analytical approach for WQ parameters retrieval relates the subsurface irradiance reflectance (or volume reflectance) to the water constituent concentrations. Volume reflectance is nearly independent of atmospheric properties and entirely determined by the optical properties of the water and its constituents. Therefore, all received field spectra were processed using air-water correction formulae volume reflectance.
- After using air-water correction the resulting volume reflectance spectra needed to be filtered to produce data that are uncontaminated by noise from the atmosphere or the sensor itself. The volume spectra were filtered using MatLab 7.0 software applying Savitzky-Golay filter and Discrete De-noising Wavelets. It was found that for clear sky conditions it is best to use the DWT filter with ‘sym5’ or ‘sym8’ Symlet wavelet depending on the noise level. At the same time, in case of windy

weather, the best performing filter was a combination of first the Savitzky-Golay filter with a small frame size (e.g. 17) and then Discrete Wavelet Transformation with a 'sym5' wavelet. In all filters a polynomial degree of 3 best preserved the shape of the spectra and has been used for all data.

- The study of spectral algebra algorithms based on normalized volume reflectance and derivative spectra shows that in spite of high variety of hydro-morphological, physical and bio-ecological factors influencing upwelling radiance from the water body, the application of the derivative analysis approach produces stable correlations with chlorophyll concentrations.
- The results of accuracy assessment of the best cross-seasonal algorithms reveal that application as a biomass indicator the WQ parameter CHL produces best results. The spectral signatures of the water bodies are kettle holes' type specific and depend on the agricultural activity and respectively nutrient status in a catchments area. Packaging effect significantly influences the water leaving reflectance and can lead to underestimating the biomass concentration in RS signal analysis and image classification. The correlation between the spectral signals and the chlorophyll concentration is stable over one season as long as the 'type of kettle hole' does not change.
- A multi-temporal database was built including data of the ROSIS and HyMap airborne hyperspectral sensors. The collected ROSIS image spectra, having a range from 389 to 845nm and an interval of 4nm in 115 bands, were recorded in a spatial resolution of 2×2 m. HyMap is a whisk-broom scanner with 126 bands between 450 and 2500nm and provided data with 4×4m pixel size and about 15nm bandwidth. Only the first 34 bands between 450 and 920nm relevant for the determination of water constituents were used in this study.
- All airborne data sets have been atmospherically corrected using the ATCOR4 software package for airborne data. This software corrects at-sensor radiance images for the solar illuminance, the Rayleigh and adjacency scattering in order to derive nadir-normalized ground reflectance. Geo-referencing of the ROSIS and HyMap images is based on data from a navigation system (IGI) which records simultaneously the flight attitude and position parameters.
- ROSIS data was focused on the range between 489nm and 845nm, i.e. 16÷115 bands – total 90 bands. Analysis of spectral signatures in that range showed that ground reflection of kettle holes is relatively noise contaminated. Thus, the ROSIS

image dataset has been smoothed using a combination of Savitzky-Golay filter and Discrete Wavelet Transformation de-noising approach. The study of HyMap reflection profiles of kettle holes showed that application of any filtering techniques can remove important absorption/reflectance features of image spectrum, so no smoothing methods were used.

- Analysis of spectral signatures of water bodies and shadows in airborne datasets shows that reflectance near 770nm over 10 % belongs to other land cover types. Hence, it was simple to create a binary mask for both datasets with '1' value for all object less than 10 % and '0' for the rest of the image. Received images were easy to aggregate into shadows and water classes using standard image processing tools. The resulting raster map was applied as a binary mask to create water-only images of the original brightness from airborne hyperspectral data.
- Field and airborne spectra for almost all kettle holes did not correspond to each other due to differences in ground sampling distance. Application of recent biomass estimation algorithms did not give acceptable correlations due to high variability of the factors influencing chlorophyll reflection peak. In addition, field spectra from the height of 30-35cm (i.e. area of 0.01 – 0.015m²) were collected. Airborne pixels of ROSIS and HyMap imagery have an area of 4m² and 16m² accordingly and their spectra are highly influenced by algae or bottom properties of kettle holes.
- Analysis of airborne spectra revealed that chlorophyll absorption near 677nm is the same for both datasets. In order to enhance absorption properties, both airborne hyperspectral datasets were normalized by the continuum removal approach. Linear regression algorithms for ROSIS and HyMap datasets were derived using normalized average chlorophyll absorption spectra for each kettle hole. Overall accuracy of biomass mapping for ROSIS data is 71% and 64 % for HyMap.
- For estimation of water depth and TSS derivative analysis approach was applied to the airborne image datasets. Derivative airborne spectra show best correlation for TSS at 596nm and at 630nm with overall classification accuracy of 83% and 76% for ROSIS and HyMap datasets accordingly. For complete understanding of the relation between airborne spectra and trophic status of kettle holes, the values of water depth were also collected on flight dates. Correlation between depth and derivative reflectance at 530nm of ROSIS and HyMap hyperspectral imagery reveals high linear regressions coefficients with classification accuracy of 87% and 80% respectively.

- The results of this study show that HRS can provide useful information for WQ monitoring in agricultural young moraine landscapes in North-Eastern Germany. However, biomass mapping results showed that, depending on the type of kettle hole, the ‘packaging effect’ and bottom reflection could lead to miscalculation of chlorophyll content. Overall, ROSIS with 2×2m spatial and 4nm spectral resolutions is preferable for small water bodies’ biomass concentration mapping over HyMap with a GSD of 4m.
- The future research can be followed in two directions: (1) integration of the WQ parameters mapping based on received algorithms and methods to the land use/land cover monitoring programmes; (2) improvement of established methodology by investigating the subsurface spectral properties of kettle holes.
- (1) Previous studies have focused on the discovery of the relationship between remote sensing data and *in-situ* measurements. To make remote sensing tools useful for practical applications to kettle holes, WQ modelling must be incorporated with land use/land cover quality monitoring programmes of their catchment areas. Moreover, integrating a geographic information system (GIS) allows for the display of refined monitoring simulation results, rather than the use of traditional numerical figures. This provides a means by which trophic status modelling data can be presented in a way that is practical for WQ management.
- (2) In order to improve the accuracy of kettle holes’ biomass classification using high spatial and spectral resolution remote sensing data, future research should be focused on: i) packaging effect and bottom type (investigation of the processes of light attenuation influenced by packaging effect and different bottom types and development of an algorithm for correcting the packaging effect); ii) ground sampling distance (seasonal upwelling radiance from various types of kettle holes has to be collected at different heights to study distinctions in surface reflection coupled with biomass concentration).
- Precise investigations of the influence to water-leaving reflectance from the packaging effect, bottom types and differences due to ground sampling distance can offer the opportunity to ‘upscale’ observations to larger spatial scales.